

MIN3P-THCm

A Three-dimensional Numerical Model for
Multicomponent Reactive Transport in Variably
Saturated Porous Media

Validation report

(draft)

Mingliang Xie, Danyang Su and K. Ulrich Mayer
University of British Columbia
Department of Earth, Ocean and Atmospheric Sciences
Vancouver, BC, Canada V5T 2M1

Kerry MacQuarrie
University of New Brunswick
Department of Civil Engineering
Fredericton, N.B., Canada E3B 5A3

July 20, 2018

COPYRIGHT NOTICE AND USAGE LIMITATIONS

All rights are reserved. The MIN3P-THCm model and User's Guide are copyright. The documentation, executable, source code, or any part thereof, may not be reproduced, duplicated, translated, or distributed in any way without the express written permission of the copyright holder. The MIN3P-THCm program must be specifically licensed for inclusion in software distributed in any manner, sold commercially, or used in for-profit research/consulting. Distribution of source code is expressly forbidden.

DISCLAIMER

Although great care has been taken in preparing MIN3P-THCm and its documentation, the authors cannot be held responsible for any errors or omissions. As such, this code is offered `as is'. The authors make no warranty of any kind, express or implied. The authors shall not be liable for any damages arising from a failure of this program to operate in the manner desired by the user. The authors shall not be liable for any damage to data or property which may be caused directly or indirectly by use of this program. In no event will the authors be liable for any damages, including, but not limited to, lost profits, lost savings or other incidental or consequential damages arising out of the use, or inability to use, this program. Use, attempted use, and/or installation of this program shall constitute implied acceptance of the above conditions. Authorized users encountering problems with the code, or requiring specific implementations not supported by this version, are encouraged to contact the authors for possible assistance.

ACKNOWLEDGEMENTS

The author would like to thank Shawn G. Benner (University of Waterloo, now at Idaho State University, Boise, ID), Frederic Gerard (Eco&Sols, UMR1222, INRA/IRD/SupAgro, Montpellier, France), Sergio Andres Bea (UBC, now at CONICET, IHLLA-Large Plains Hydrology Institute, Buenos Aires, Argentina), and Tom Henderson (UBC, now at Montana Department of Environmental Quality, Helena, MT) for their contributions to earlier versions of the User's Guide.

ABSTRACT

This report documents the representative validation and verification examples of the reactive transport code MIN3P-THCm including problem definition, model set up, material properties, simulated results and the location of the input file(s) and databases. Most examples are primarily developed to test, verify and/or validate the new functions added to the code using analytical methods (if available), comparison against other reactive transport codes and hand calculations. More examples are added with other validation activities such as participation in international benchmarking, comparison of simulated results to laboratory and in situ experiments through related projects. Consequently, a collection of 125 benchmarks are accumulated and maintained to ensure the functionality of the corresponding code over the course of the code development in compliance with the NWMO Technical Computing Software procedures (Document No.: NWMO-PROC-EN-0002, Revision: R0002). A selection of the representative examples are documented in this report.

Contents

1	Introduction.....	1-35
2	Validation examples.....	2-35
2.1	BATCH REACTIONS.....	2-36
2.1.1	<i>Surface complexation of arsenate.....</i>	2-36
2.1.1.1	Problem definition	2-36
2.1.1.2	Model setup.....	2-36
2.1.1.3	Parameters	2-37
2.1.1.4	Results	2-37
2.1.1.5	File locations.....	2-38
2.1.2	<i>pH-dependent anion surface complexation</i>	2-38
2.1.2.1	Problem definition	2-38
2.1.2.2	Model setup.....	2-38
2.1.2.3	Results	2-39
2.1.2.4	File locations.....	2-40
2.1.3	<i>pH-dependent cation surface complexation.....</i>	2-40
2.1.3.1	Problem definition	2-40
2.1.3.2	Model setup.....	2-41
2.1.3.3	Results	2-41
2.1.3.4	File locations.....	2-42
2.1.4	<i>Pitzer equation – Chemical speciation of Dead Sea water.....</i>	2-42
2.1.4.1	Problem definition	2-42
2.1.4.2	Model setup.....	2-43
2.1.4.3	Parameters	2-43
2.1.4.4	Results	2-43
2.1.4.5	File locations.....	2-43
2.2	GROUNDWATER FLOW AND WATER VAPOR TRANSPORT.....	2-46
2.2.1	<i>1D gravity drainage in soil column.....</i>	2-46
2.2.1.1	Problem definition	2-46
2.2.1.2	Model setup.....	2-46
2.2.1.3	Parameters	2-46
2.2.1.4	Results	2-47
2.2.1.5	File locations.....	2-47
2.2.2	<i>1D infiltration in soil column</i>	2-48
2.2.2.1	Problem definition	2-48
2.2.2.2	Model setup.....	2-48
2.2.2.3	Parameters	2-48

Validation report-page# 1-6

2.2.2.4	Results	2-48
2.2.2.5	File locations.....	2-49
2.2.3	<i>1D drainage problem in sand column</i>	2-49
2.2.3.1	Problem definition	2-49
2.2.3.2	Model setup.....	2-49
2.2.3.3	Parameters	2-50
2.2.3.4	Results	2-50
2.2.3.5	File locations.....	2-50
2.2.4	<i>2D transient water table mounding</i>	2-51
2.2.4.1	Problem definition	2-51
2.2.4.2	Model setup.....	2-52
2.2.4.3	Parameters	2-52
2.2.4.4	Results	2-53
2.2.4.5	File locations.....	2-53
2.2.5	<i>1D water vapor movement</i>	2-54
2.2.5.1	Problem definition	2-54
2.2.5.2	Model setup.....	2-54
2.2.5.3	Parameters	2-54
2.2.5.4	Results	2-54
2.2.5.5	File locations.....	2-55
2.3	DENSITY DEPENDENT FLOW AND CONSERVATIVE SOLUTE TRANSPORT	2-55
2.3.1	<i>Elder problem</i>	2-56
2.3.1.1	Problem definition	2-56
2.3.1.2	Model setup.....	2-56
2.3.1.3	Parameters	2-57
2.3.1.4	Results	2-57
2.3.1.5	File locations.....	2-58
2.3.2	<i>Modified Henry problem</i>	2-59
2.3.2.1	Problem definition	2-59
2.3.2.2	Model setup.....	2-59
2.3.2.3	Parameters	2-59
2.3.2.4	Results	2-60
2.3.2.5	File locations.....	2-60
2.4	ENERGY BALANCE	2-61
2.4.1	<i>Radial flow with energy transport (analytical solution)</i>	2-61
2.4.1.1	Problem definition	2-61
2.4.1.2	Model setup.....	2-61
2.4.1.3	Parameters	2-61
2.4.1.4	Results	2-62

Validation report-page# 1-7

2.4.1.5	File locations	2-63
2.4.2	<i>Aquifer thermal energy storage (2D Radial)</i>	2-64
2.4.2.1	Problem definition	2-64
2.4.2.2	Model setup	2-64
2.4.2.3	Parameters	2-64
2.4.2.4	Results	2-65
2.4.2.5	File locations	2-67
2.4.3	<i>Density dependent flow with heat and solute transport (Henry-Hilleke problem)</i>	2-68
2.4.3.1	Problem definition	2-68
2.4.3.2	Model setup	2-68
2.4.3.3	Problem definition	2-68
2.4.3.4	Results	2-69
2.4.3.5	File locations	2-69
2.4.4	<i>Thermo-haline convection</i>	2-70
2.4.4.1	Problem definition	2-70
2.4.4.2	Model setup	2-71
2.4.4.3	Parameters	2-71
2.4.4.4	Results	2-71
2.4.4.5	File locations	2-73
2.4.5	<i>Salt dome problem</i>	2-73
2.4.5.1	Problem definition	2-73
2.4.5.2	Model setup	2-74
2.4.5.3	Parameters	2-74
2.4.5.4	Results	2-74
2.4.5.5	File locations	2-74
2.5	MULTICOMPONENT REACTIVE TRANSPORT	2-77
2.5.1	<i>Steady-state diffusion - radial coordinates</i>	2-78
2.5.1.1	Problem definition	2-78
2.5.1.2	Model setup	2-78
2.5.1.3	Parameters	2-78
2.5.1.4	Analytical solution	2-79
2.5.1.5	Results	2-80
2.5.1.6	File locations	2-80
2.5.2	<i>Transient diffusion - radial coordinates</i>	2-80
2.5.2.1	Problem definition	2-80
2.5.2.2	Model setup	2-81
2.5.2.3	Parameters	2-81
2.5.2.4	Analytical solution	2-81
2.5.2.5	Results	2-82

Validation report-page# 1-8

2.5.2.6	File locations	2-83
2.5.3	<i>Transient advective-dispersive transport – radial coordinates</i>	2-83
2.5.3.1	Problem definition	2-83
2.5.3.2	Model setup.....	2-83
2.5.3.3	Parameters	2-84
2.5.3.4	Analytical solution.....	2-84
2.5.3.5	Results	2-85
2.5.3.6	File locations.....	2-86
2.5.4	<i>Gas diffusion with constant moisture content - dry conditions</i>	2-86
2.5.4.1	Problem definition	2-86
2.5.4.2	Model setup.....	2-86
2.5.4.3	Parameters	2-87
2.5.4.4	Results	2-87
2.5.4.5	File locations.....	2-88
2.5.5	<i>Gas diffusion with variable moisture content</i>	2-88
2.5.5.1	Problem definition	2-88
2.5.5.2	Model setup.....	2-89
2.5.5.3	Parameters	2-89
2.5.5.4	Results	2-89
2.5.5.5	File locations.....	2-89
2.5.6	<i>Gas diffusion with constant moisture content – wet conditions</i>	2-90
2.5.6.1	Problem definition	2-90
2.5.6.2	Model setup.....	2-90
2.5.6.3	Parameters	2-91
2.5.6.4	Results	2-91
2.5.6.5	File locations.....	2-92
2.5.7	<i>Cation Exchange – Example 1</i>	2-92
2.5.7.1	Problem definition	2-92
2.5.7.2	Model setup.....	2-92
2.5.7.3	Parameters	2-92
2.5.7.4	Results	2-93
2.5.7.5	File locations.....	2-93
2.5.8	<i>Cation exchange – Example 2</i>	2-94
2.5.8.1	Problem definition	2-94
2.5.8.2	Model setup.....	2-94
2.5.8.3	Parameters	2-94
2.5.8.4	Results	2-95
2.5.8.5	File locations.....	2-95
2.5.9	<i>Trace metal mobility and surface complexation</i>	2-96

Validation report-page# 1-9

2.5.9.1	Problem definition	2-96
2.5.9.2	Model setup.....	2-96
2.5.9.3	Parameters	2-97
2.5.9.4	Results	2-97
2.5.9.5	File locations.....	2-98
2.5.10	<i>Dedolomitization – Dissolution-precipitation reactions</i>	2-99
2.5.10.1	Problem definition.....	2-99
2.5.10.2	Parameters	2-99
2.5.10.3	Results.....	2-99
2.5.10.4	File locations	2-100
2.5.11	<i>Pyrite oxidation and gas diffusion in the vadose zone</i>	2-100
2.5.11.1	Problem definition.....	2-100
2.5.11.2	Model setup	2-101
2.5.11.3	Parameters	2-101
2.5.11.4	Results.....	2-103
2.5.11.5	File locations	2-103
2.5.12	<i>Porosity-permeability enhancement due to mineral dissolution</i>	2-103
2.5.12.1	Problem definition.....	2-103
2.5.12.2	Model setup	2-104
2.5.12.3	Parameters	2-104
2.5.12.4	Results.....	2-105
2.5.12.5	File locations	2-106
2.5.13	<i>Clogging due to mineral dissolution/precipitation – Simple chemistry</i>	2-106
2.5.13.1	Problem definition.....	2-106
2.5.13.2	Model setup	2-106
2.5.13.3	Parameters	2-107
2.5.13.4	Results.....	2-107
2.5.13.5	File locations	2-108
2.5.14	<i>Clogging due to mineral dissolution/precipitation – Complex chemistry</i>	2-109
2.5.14.1	Problem definition.....	2-109
2.5.14.2	Model setup	2-109
2.5.14.3	Parameters	2-110
2.5.14.4	Results.....	2-110
2.5.14.5	File locations	2-111
2.5.15	<i>Linear retardation of PCE and benzene</i>	2-113
2.5.15.1	Problem definition.....	2-113
2.5.15.2	Model set-up.....	2-113
2.5.15.3	Parameters	2-113
2.5.15.4	Analytical solution	2-114

Validation report-page# 1-10

2.5.15.5	Results.....	2-115
2.5.15.6	File locations	2-116
2.5.16	<i>Aerobic degradation of toluene.....</i>	2-116
2.5.16.1	Problem definition.....	2-116
2.5.16.2	Model set-up.....	2-116
2.5.16.3	Results.....	2-117
2.5.16.4	File locations	2-118
2.5.17	<i>Reactive transport in highly saline solution.....</i>	2-118
2.5.17.1	Problem definition.....	2-118
2.5.17.2	Model set-up.....	2-118
2.5.17.3	Parameters	2-118
2.5.17.4	Results.....	2-119
2.5.17.5	File locations	2-120
2.5.18	<i>Multisite ion exchange (ionx-2m)</i>	2-121
2.5.18.1	Problem definition.....	2-121
2.5.18.2	Model set up	2-121
2.5.18.3	Parameters	2-122
2.5.18.4	Results.....	2-123
2.5.18.5	Data location.....	2-125
2.5.19	<i>Multicomponent diffusion</i>	2-126
2.5.19.1	Problem definition.....	2-126
2.5.19.2	Model setup	2-126
2.5.19.3	Parameters	2-126
2.5.19.4	Results.....	2-126
2.5.19.5	File location	2-127
2.5.20	<i>Multicomponent diffusion in radial coordinate</i>	2-128
2.5.20.1	Problem definition.....	2-128
2.5.20.2	Model setup	2-128
2.5.20.3	Parameters	2-128
2.5.20.4	Results.....	2-128
2.5.20.5	File location	2-128
2.5.21	<i>Microbially mediated chromium reduction.....</i>	2-129
2.5.21.1	Problem definition.....	2-129
2.5.21.2	Model setup	2-130
2.5.21.3	Parameters	2-131
2.5.21.4	Results.....	2-131
2.5.21.5	File location	2-134
2.5.22	<i>Salinity dependent sulfate reduction – option 1</i>	2-134
2.5.22.1	Problem definition.....	2-134

Validation report-page# 1-11

2.5.22.2	Model setup	2-134
2.5.22.3	Parameters	2-135
2.5.22.4	Results.....	2-136
2.5.22.5	File location	2-140
2.5.23	<i>Salinity dependent sulfate reduction – option 2</i>	2-140
2.5.23.1	Problem definition.....	2-140
2.5.23.2	Model setup	2-140
2.5.23.3	Parameters	2-140
2.5.23.4	Results.....	2-141
2.5.23.5	File location	2-146
2.6	HYDROMECHANICAL COUPLING.....	2-146
2.6.1	<i>Verification of vertical stress</i>	2-146
2.6.1.1	Problem definition	2-146
2.6.1.2	Model set-up	2-146
2.6.1.3	Results	2-146
2.6.1.4	File locations.....	2-147
3	Demonstration examples	3-148
3.1	BATCH REACTIONS.....	3-148
3.1.1	<i>Kinetic dissolution of calcite and albite in a batch reactor</i>	3-148
3.1.1.1	Problem definition	3-148
3.1.1.2	Model setup.....	3-148
3.1.1.3	Parameters	3-149
3.1.1.4	Results	3-149
3.1.1.5	File locations.....	3-150
3.1.2	<i>Kinetic dissolution of calcite in a batch reactor</i>	3-150
3.1.2.1	Problem definition	3-150
3.1.2.2	Model setup.....	3-150
3.1.2.3	Parameters	3-151
3.1.2.4	Results	3-151
3.1.2.5	File locations.....	3-152
3.1.3	<i>pH-dependent speciation of chromium</i>	3-152
3.1.3.1	Problem definition	3-152
3.1.3.2	Model setup.....	3-152
3.1.3.3	Results	3-153
3.1.3.4	File locations.....	3-153
3.1.4	<i>pH-dependent speciation of iron</i>	3-154
3.1.4.1	Problem definition	3-154
3.1.4.2	Model setup.....	3-154
3.1.4.3	Results	3-154

Validation report-page# 1-12

3.1.4.4	File locations	3-155
3.1.5	<i>Dissolution and sorption of PCE - linear isotherm</i>	3-155
3.1.5.1	Problem definition	3-155
3.1.5.2	Model setup.....	3-155
3.1.5.3	Results	3-156
3.1.5.4	File locations.....	3-157
3.1.6	<i>pH-dependent anion surface complexation with implicit method</i>	3-157
3.1.6.1	Problem definition	3-157
3.1.6.2	Results	3-158
3.1.6.3	File locations.....	3-158
3.1.7	<i>pH dependent cation surface complexation with implicit method</i>	3-159
3.1.7.1	Problem definition	3-159
3.1.7.2	Results	3-160
3.1.7.3	File locations.....	3-160
3.2	GROUNDWATER FLOW	3-161
3.2.1	<i>2D steady state fully-saturated flow</i>	3-161
3.2.1.1	Problem definition	3-161
3.2.1.2	Model setup.....	3-161
3.2.1.3	Parameters	3-161
3.2.1.4	Results	3-161
3.2.1.5	File locations.....	3-162
3.2.2	<i>2D steady state variably-saturated flow</i>	3-162
3.2.2.1	Problem definition	3-162
3.2.2.2	Model setup.....	3-163
3.2.2.3	Parameters	3-163
3.2.2.4	Results	3-163
3.2.2.5	File locations.....	3-164
3.2.3	<i>2D transient fully-saturated flow</i>	3-164
3.2.3.1	Problem definition	3-164
3.2.3.2	Model setup.....	3-164
3.2.3.3	Parameters	3-165
3.2.3.4	Results	3-165
3.2.3.5	File locations.....	3-166
3.2.4	<i>2D transient variably-saturated flow</i>	3-166
3.2.4.1	Problem definition	3-166
3.2.4.2	Model setup.....	3-166
3.2.4.3	Parameters	3-166
3.2.4.4	Results	3-166
3.2.4.5	File locations.....	3-167

Validation report-page# 1-13

3.2.5	<i>2D variably-saturated steady state flow with seepage</i>	3-167
3.2.5.1	Problem definition	3-167
3.2.5.2	Model setup.....	3-167
3.2.5.3	Parameters	3-168
3.2.5.4	Results	3-168
3.2.5.5	File locations.....	3-169
3.2.6	<i>2D variably-saturated transient flow with seepage</i>	3-169
3.2.6.1	Problem definition	3-169
3.2.6.2	Model setup.....	3-169
3.2.6.3	Parameters	3-170
3.2.6.4	Results	3-170
3.2.6.5	File locations.....	3-170
3.2.7	<i>3D variably-saturated flow</i>	3-171
3.2.7.1	Problem definition	3-171
3.2.7.2	Model setup.....	3-171
3.2.7.3	Parameters	3-171
3.2.7.4	Results	3-172
3.2.7.5	File locations.....	3-172
3.3	DENSITY DEPENDENT FLOW AND CONSERVATIVE SOLUTE TRANSPORT	3-173
3.3.1	<i>Box problems – Hydrostatic box test (Diersch)</i>	3-173
3.3.1.1	Problem definition	3-173
3.3.1.2	Model setup.....	3-173
3.3.1.3	Parameters	3-173
3.3.1.4	Results	3-174
3.3.1.5	File locations.....	3-175
3.3.2	<i>Hydrostatic box problem (Voss)</i>	3-176
3.3.2.1	Problem definition	3-176
3.3.2.2	Model set-up	3-176
3.3.2.3	Results	3-176
3.3.2.4	File locations.....	3-177
3.4	MULTICOMPONENT REACTIVE TRANSPORT	3-178
3.4.1	<i>1D advective-dispersive transport with aqueous complexation</i>	3-178
3.4.1.1	Problem definition	3-179
3.4.1.2	Model setup.....	3-179
3.4.1.3	Parameters	3-179
3.4.1.4	Results	3-180
3.4.1.5	File locations.....	3-180
3.4.2	<i>2D advective-dispersive transport with aqueous complexation</i>	3-180
3.4.2.1	Problem definition	3-180

Validation report-page# 1-14

3.4.2.2	Model setup	3-180
3.4.2.3	Parameters	3-182
3.4.2.4	Results	3-182
3.4.2.5	File locations	3-182
3.4.3	<i>Spatial averaging methods for diffusion coefficients</i>	3-183
3.4.3.1	Problem definition	3-183
3.4.3.2	Model setup	3-183
3.4.3.3	Parameters	3-183
3.4.3.4	Averaging methods for effective diffusion coefficient	3-183
3.4.3.5	Results	3-183
3.4.3.6	File locations	3-184
3.4.4	<i>1D advective-dispersive transport with transient boundary conditions</i>	3-185
3.4.4.1	Problem definition	3-185
3.4.4.2	Model setup	3-185
3.4.4.3	Parameters	3-185
3.4.4.4	Results	3-187
3.4.4.5	File locations	3-187
3.4.5	<i>1D advective-dispersive transport with aqueous complexation and mineral dissolution-precipitation</i>	3-187
3.4.5.1	Problem definition	3-187
3.4.5.2	Model setup	3-187
3.4.5.3	Parameters	3-188
3.4.5.4	Results	3-188
3.4.5.5	File locations	3-188
3.4.6	<i>2D advective-dispersive transport with aqueous complexation and mineral dissolution-precipitation</i>	3-189
3.4.6.1	Problem definition	3-189
3.4.6.2	Model setup	3-189
3.4.6.3	Parameters	3-190
3.4.6.4	Results	3-190
3.4.6.5	File locations	3-191
3.4.7	<i>Mineral weathering in a soil column</i>	3-191
3.4.7.1	Problem definition	3-191
3.4.7.2	Model setup	3-191
3.4.7.3	Parameters	3-192
3.4.7.4	Results	3-193
3.4.7.5	File locations	3-193
3.4.8	<i>1D advective-dispersive transport with binary mono-valent ion exchange</i>	3-194
3.4.8.1	Problem definition	3-194
3.4.8.2	Model setup	3-194

Validation report-page# 1-15

3.4.8.3	Parameters	3-195
3.4.8.4	Results	3-195
3.4.8.5	File locations.....	3-196
3.4.9	<i>1D advective-dispersive transport including Monod kinetics, degradation of organic contaminants.....</i>	3-197
3.4.9.1	Problem definition	3-197
3.4.9.2	Model setup.....	3-197
3.4.9.3	Parameters	3-197
3.4.9.4	Results	3-198
3.4.9.5	File locations.....	3-198
3.4.10	<i>1D advective-dispersive transport - Degassing from a hydrocarbon spill</i>	3-201
3.4.10.1	Problem definition.....	3-201
3.4.10.2	Model setup	3-201
3.4.10.3	Parameters	3-201
3.4.10.4	Results.....	3-202
3.4.10.5	File locations	3-202
3.4.11	<i>Dissolution and volatilization of an organic contaminant mixture in the vadose zone.....</i>	3-204
3.4.11.1	Problem definition.....	3-204
3.4.11.2	Model setup	3-204
3.4.11.3	Parameters	3-205
3.4.11.4	Results.....	3-205
3.4.11.5	File locations	3-205
3.4.12	<i>1D-advective-dispersive transport with anionic surface complexation reactions</i>	3-207
3.4.12.1	Problem definition.....	3-207
3.4.12.2	Model setup	3-207
3.4.12.3	Parameters	3-208
3.4.12.4	Results.....	3-209
3.4.12.5	File locations	3-209
3.4.13	<i>1D-advective-dispersive transport with cationic surface complexation reactions.....</i>	3-209
3.4.13.1	Problem definition.....	3-209
3.4.13.2	Model setup	3-209
3.4.13.3	Parameters	3-210
3.4.13.4	Results.....	3-211
3.4.13.5	File locations	3-211
3.4.14	<i>Groundwater remediation by a permeable reactive barrier.....</i>	3-211
3.4.14.1	Problem definition.....	3-211
3.4.14.2	Model setup	3-212
3.4.14.3	Parameters	3-213
3.4.14.4	Results.....	3-213

Validation report-page# 1-16

3.4.14.5	File locations	3-213
3.4.15	<i>Acid rock drainage generation and attenuation</i>	3-215
3.4.15.1	Problem definition.....	3-215
3.4.15.2	Model setup	3-216
3.4.15.3	Parameters	3-216
3.4.15.4	Results.....	3-216
3.4.15.5	File locations	3-217
3.4.16	<i>Isotope fractionation</i>	3-219
3.4.16.1	Problem definition.....	3-219
3.4.16.2	Model setup	3-219
3.4.16.3	Parameters	3-221
3.4.16.4	Results.....	3-222
3.4.16.5	File locations	3-223
3.4.17	<i>1D salinity dependent SRB reaction</i>	3-223
3.4.17.1	Problem definition.....	3-223
3.4.17.2	Model setup	3-224
3.4.17.3	Parameters	3-224
3.4.17.4	Results.....	3-225
3.4.17.5	File locations	3-226
4	Validation examples against experiments.....	4-227
4.1	MONT TERRI IN-SITU DIFFUSION EXPERIMENTS	4-227
4.1.1	<i>In-situ diffusion experiment in clay</i>	4-228
4.1.1.1	Problem definition	4-228
4.1.1.2	Model setup.....	4-228
4.1.1.3	Experimental data	4-229
4.1.1.4	Parameters	4-231
4.1.1.5	Results	4-232
4.1.1.6	File location.....	4-232
4.1.2	<i>In-situ diffusion experiment in clay (MIE Model)</i>	4-233
4.1.2.1	Problem definition	4-233
4.1.2.2	Model setup.....	4-233
4.1.2.3	Parameters	4-233
4.1.2.4	Results	4-234
4.1.2.5	File location.....	4-235
4.1.3	<i>Effect of chemical perturbation on diffusion and retardation in clay</i>	4-236
4.1.3.1	Problem definition	4-236
4.1.3.2	Model setup.....	4-236
4.1.3.3	Experimental data	4-237
4.1.3.4	Parameters	4-239

Validation report-page# 1-17

4.1.3.5	Results	4-239
4.1.3.6	File location.....	4-240
4.1.4	<i>Effect of chemical perturbation on diffusion and retardation in clay (MIE)</i>	4-241
4.1.4.1	Problem definition	4-241
4.1.4.2	Model setup.....	4-241
4.1.4.3	Experimental data	4-241
4.1.4.4	Parameters	4-241
4.1.4.5	Results	4-242
4.1.4.6	File location.....	4-246
4.1.5	<i>Back diffusion during overcoring</i>	4-246
4.1.5.1	Problem definition	4-246
4.1.5.2	Model setup.....	4-246
4.1.5.3	Parameters	4-246
4.1.5.4	Results	4-247
4.1.5.5	File location.....	4-248
4.1.6	<i>Back diffusion during overcoring (MIE)</i>	4-248
4.1.6.1	Problem definition	4-248
4.1.6.2	Model setup.....	4-248
4.1.6.3	Parameters	4-248
4.1.6.4	Results	4-248
4.1.6.5	File location.....	4-249
4.2	EBS-TF EXPERIMENTS.....	4-250
4.2.1	<i>diffusion through compacted Ca-montmorillonite</i>	4-251
4.2.1.1	Problem definition	4-251
4.2.1.2	Model setup.....	4-251
4.2.1.3	Parameters	4-251
4.2.1.4	Results	4-252
4.2.1.5	File location.....	4-252
4.2.2	<i>Gypsum dissolution and diffusion through Ca-montmorillonite</i>	4-253
4.2.2.1	Problem definition	4-253
4.2.2.2	Model setup.....	4-254
4.2.2.3	Parameters	4-254
4.2.2.4	Results	4-254
4.2.3	<i>Gypsum dissolution, diffusion and ion exchange through Na-montmorillonite</i>	4-256
4.2.3.1	Problem definition	4-256
4.2.3.2	Model setup.....	4-256
4.2.3.3	Parameters	4-256
4.2.3.4	Results	4-257
4.2.3.5	File location.....	4-258

Validation report-page# 1-18

4.2.4	<i>Multicomponent transport through a compacted and saturated MX-80 bentonite.....</i>	4-258
4.2.4.1	Problem definition	4-258
4.2.4.2	Model setup.....	4-258
4.2.4.3	Parameters	4-260
4.2.4.4	Results	4-261
4.2.4.5	File location.....	4-262
5	SSBench benchmarking.....	5-262
	References.....	5-263
	Appendix I: PITZER VIRIAL COEFFICIENTS DATA BASE FOR MODEL VERIFICATION.....	5-267
	Appendix II: List of benchmarking papers	5-270

Validation report-page# 1-19

LIST OF TABLES

	<u>Page</u>
<i>Table 2.1: List of batch reaction benchmarks</i>	<i>2-36</i>
<i>Table 2.2: Initial geochemical conditions for benchmark As(V)_surfx.....</i>	<i>2-37</i>
<i>Table 2.3: Physical parameters of surface site for verification problem As(V)_surfx..</i>	<i>2-37</i>
<i>Table 2.4: Reaction stoichiometries of surface complexion reactions for benchmark As(V)_surfx</i>	<i>2-37</i>
<i>Table 2.5: Initial geochemical conditions for benchmark surfa.....</i>	<i>2-39</i>
<i>Table 2.6: Physical parameters for the surface for verification problem surfa (Stumm and Morgan 1996)</i>	<i>2-39</i>
<i>Table 2.7: Initial geochemical conditions for benchmark surfme</i>	<i>2-41</i>
<i>Table 2.8: Physical parameters for the surface for verification problem surfme (Stumm and Morgan 1996)</i>	<i>2-41</i>
<i>Table 2.9: Speciation of Dead Sea water – Model input (Bea et al., 2011)</i>	<i>2-43</i>
<i>Table 2.10: Speciation of Dead Sea Water – Aqueous Speciation (Bea et al., 2011) ...</i>	<i>2-44</i>
<i>Table 2.11: Speciation of Dead Sea Water – Mineral Saturation Indices (Bea et al., 2011)</i>	<i>2-45</i>
<i>Table 2.12: List of flow and evaporation benchmarks</i>	<i>2-46</i>
<i>Table 2.13: Physical parameters for benchmark drain1</i>	<i>2-46</i>
<i>Table 2.14: Physical parameters for benchmark infil1</i>	<i>2-48</i>
<i>Table 2.15: Physical parameters for benchmark haverk.....</i>	<i>2-50</i>
<i>Table 2.16: Physical parameters for benchmark clement</i>	<i>2-53</i>
<i>Table 2.17: Physical parameters for benchmark verif-evap</i>	<i>2-54</i>
<i>Table 2.18: List of density dependent flow benchmarks.....</i>	<i>2-56</i>
<i>Table 2.19: Parameters for Elder Convection Problem (Bea et al., 2011).....</i>	<i>2-57</i>
<i>Table 2.20: Parameters for Modified Henry Saltwater Intrusion Problem (Bea et al., 2011)</i>	<i>2-59</i>
<i>Table 2.21: List of energy balance benchmarks</i>	<i>2-61</i>
<i>Table 2.22: Parameters for Radial Flow Problem with Energy Transport (Bea et al., 2011)</i>	<i>2-62</i>
<i>Table 2.23: Parameters for aquifer thermal energy storage problem (density-dependent Flow and energy transport) (Bea et al., 2011)</i>	<i>2-65</i>
<i>Table 2.24: Parameters for Henry-Hilleke problem (density-dependent flow, heat and</i>	

Validation report-page# 1-20

<i>solute transport) (Bea et al., 2011).....</i>	2-68
<i>Table 2.25: Parameters for thermo-haline convection problems (Bea et al., 2011).....</i>	2-72
<i>Table 2.26: Parameters for Salt-Dome Problem (Bea et al., 2011).....</i>	2-75
<i>Table 2.27: List of reactive transport benchmarks.....</i>	2-77
<i>Table 2.28: Initial and boundary conditions for reactive transport.....</i>	2-78
<i>Table 2.29: Initial and boundary conditions for reactive transport.....</i>	2-81
<i>Table 2.30: Initial and boundary conditions for flow and reactive transport.....</i>	2-84
<i>Table 2.31: Initial and boundary conditions for flow and reactive transport.....</i>	2-87
<i>Table 2.32: Physical parameters for benchmark diffdry.....</i>	2-87
<i>Table 2.33: Initial and boundary conditions for flow and reactive transport.....</i>	2-89
<i>Table 2.34: Initial and boundary conditions for flow and reactive transport.....</i>	2-91
<i>Table 2.35: Initial and boundary conditions (IC & BC)</i>	2-92
<i>Table 2.36: Composition of Initial and Boundary Waters and Chemical Parameters of the Domain (Cation Exchange Problem).....</i>	2-94
<i>Table 2.37: Parameters of the porous media (Cation Exchange Problem)</i>	2-94
<i>Table 2.38: Initial and boundary conditions for flow and reactive transport.....</i>	2-96
<i>Table 2.39: Physical parameters for benchmark surfx.....</i>	2-97
<i>Table 2.40: Reaction stoichiometries of surface complexation reactions</i>	2-97
<i>Table 2.41: Composition of initial and boundary waters (dedolomization) (Bea et al., 2011)</i>	2-99
<i>Table 2.42: Initial and boundary conditions for flow and reactive transport.....</i>	2-101
<i>Table 2.43: Physical parameters for benchmark pyrox.....</i>	2-101
<i>Table 2.44: The shrinking core reaction parameters for pyrite oxidation</i>	2-103
<i>Table 2.45: Initial and boundary conditions for flow and reactive transport.....</i>	2-104
<i>Table 2.46: Thermodynamic mineral reaction parameters</i>	2-104
<i>Table 2.47: Kinetic parameters for minerals.....</i>	2-104
<i>Table 2.48: Initial and boundary conditions for flow and reactive transport.....</i>	2-106
<i>Table 2.49: Mineral reaction parameters.....</i>	2-107
<i>Table 2.50: Kinetic parameters of minerals</i>	2-107
<i>Table 2.51: Initial and boundary conditions for flow and reactive transport.....</i>	2-109
<i>Table 2.52: Mineral reaction parameters.....</i>	2-110
<i>Table 2.53: Kinetic parameters of minerals</i>	2-110
<i>Table 2.54: Initial and boundary conditions for flow and reactive transport.....</i>	2-113

Validation report-page# 1-21

<i>Table 2.55: Physical parameters for benchmark raoult.....</i>	2-114
<i>Table 2.56: Toluene Degradation Problem: Composition of Initial and Boundary Waters (Bea et al., 2011).....</i>	2-117
<i>Table 2.57: Replacement of gypsum by polyhalite: composition of initial and boundary waters of the domain (Bea et al., 2011).....</i>	2-118
<i>Table 2.58: Composition of initial and boundary pore waters.....</i>	2-122
<i>Table 2.59: Physical and chemical parameters for benchmark</i>	2-123
<i>Table 2.60: Ion exchange reactions used in the simulation.....</i>	2-123
<i>Table 2.61: Selected model parameters used for the simulation of nitric acid diffusion in saltwater.....</i>	2-126
<i>Table 2.62: Stoichiometry of Microbially Mediated Reactions (Based on Molins et al. 2014).....</i>	2-130
<i>Table 2.63: Replacement of gypsum by polyhalite: composition of initial and boundary waters of the domain (Molins et al., 2014).....</i>	2-131
<i>Table 2.64: Rate Constant and Kinetic Parameters for Microbially Mediated Reactions (Based on Molins et al. 2014).....</i>	2-132
<i>Table 2.65: Initial and boundary conditions (IC & BC) of the aqueous and mineral compositions for the example sulpqc</i>	2-134
<i>Table 3.1: List of geochemical batch reaction test examples</i>	3-148
<i>Table 3.2: Initial geochemical conditions for demonstration example albite</i>	3-149
<i>Table 3.3: Geometric update model parameters for calcite and albite for demonstration example albite</i>	3-149
<i>Table 3.4: Initial geochemical conditions for demonstration example appelo</i>	3-151
<i>Table 3.5: Geometric update model parameters for calcite</i>	3-151
<i>Table 3.6: Initial geochemical condition for demonstration example Cr(III).....</i>	3-153
<i>Table 3.7: Initial geochemical condition for demonstration example Fe(III).....</i>	3-154
<i>Table 3.8: NAPL reaction parameter – demonstration example linsorb.....</i>	3-155
<i>Table 3.9: Kinetic parameters of C₂Cl₄(n)</i>	3-156
<i>Table 3.10: Initial geochemical conditions - demonstration example linsorb</i>	3-156
<i>Table 3.11: List of flow test examples.....</i>	3-161
<i>Table 3.12: Physical parameters for demonstration example stedfs.....</i>	3-161
<i>Table 3.13: Physical parameters for demonstration example stedvs</i>	3-163
<i>Table 3.14: Physical parameters for demonstration example transf.....</i>	3-165
<i>Table 3.15: Physical parameters for demonstration example tranvs</i>	3-166
<i>Table 3.16: Physical parameters for demonstration example shlomo</i>	3-168

Validation report-page# 1-22

Table 3.17: Physical parameters for the demonstration example shlomot	3-170
Table 3.18: Physical parameters for demonstration example clem3d	3-172
Table 3.19: Parameters for Hydrostatic Box Problem (Bea et al., 2011).....	3-174
Table 3.20: Parameters for Hydrodynamic Box Problem (Bea et al., 2011).....	3-176
Table 3.21: List of reactive transport test examples.....	3-178
Table 3.22: Initial and boundary conditions (IC & BC) for demonstration example complex	3-179
Table 3.23: Initial and boundary conditions for flow and reactive transport.....	3-181
Table 3.24: Initial and boundary conditions (IC & BC) for tracer HTO	3-183
Table 3.25: Initial & boundary hydraulic and reactive transport conditions for benchmark transrc	3-185
Table 3.26: Physical parameters for demonstration example transrc	3-186
Table 3.27: Initial and boundary hydraulic and reactive transport conditions for demonstration example dissol.....	3-187
Table 3.28: Geometric update model parameters for calcite dissolution	3-188
Table 3.29 Initial and boundary conditions for flow and reactive transport – demonstration example het_2d	3-190
Table 3.30: Geometric update model parameters for calcite for benchmark het_2d..	3-190
Table 3.31: Initial and boundary conditions for flow and reactive transport for demonstration example weather	3-192
Table 3.32: Physical parameters for benchmark transrc	3-192
Table 3.33: Geometric update model parameters for calcite and albite	3-193
Table 3.34: Initial and boundary conditions of solutions for demonstration example ion-binary	3-195
Table 3.35: Initial and boundary conditions for aqueous solutions and minerals for demonstration example comprtran.....	3-197
Table 3.36: Initial and boundary conditions (IC & BC) for solutions and minerals ..	3-201
Table 3.37: Intra-aqueous kinetic reactions and effective ate coefficients for benchmark degassing.....	3-202
Table 3.38: Initial and boundary conditions for flow and reactive transport – demonstration example raoult	3-204
Table 3.39: Physical parameters for demonstration example raoult	3-205
Table 3.40: Initial and boundary conditions for flow and reactive transport – demonstration example - benchmark surfa2.....	3-207
Table 3.41: Physical parameters for benchmark surfa2	3-207
Table 3.42: Initial and boundary conditions for flow and reactive transport –	

Validation report-page# 1-23

<i>demonstration example surfme2</i>	3-209
<i>Table 3.43: Reaction stoichiometries of reduction-corrosion reactions (Mayer, 1999) ...</i>	<i>3-211</i>
<i>Table 3.44: Initial and boundary conditions for flow and reactive transport – demonstration example prb.....</i>	<i>3-212</i>
<i>Table 3.45: Physical parameters for demonstration example prb</i>	<i>3-213</i>
<i>Table 3.46: Initial and boundary conditions for reactive transport – demonstration example amd_ex.....</i>	<i>3-215</i>
<i>Table 3.47: Physical parameters for demonstration example amd_ex.....</i>	<i>3-216</i>
<i>Table 3.48: Mineral reaction and kinetic parameters for demonstration example amd_ex</i>	<i>3-217</i>
<i>Table 3.49: Initial concentrations [mg/L] of the aqueous components in the domain</i>	<i>3-220</i>
<i>Table 3.50: Time dependent boundary concentrations [mg/L] of the aqueous components representing eight replacements of injection solutions</i>	<i>3-220</i>
<i>Table 3.51: Mineral reaction and kinetic parameters for demonstration example waybrant</i>	<i>3-221</i>
<i>Table 3.52: General parameters for the circulation chamber, filter, gap and OPA ...</i>	<i>3-221</i>
<i>Table 3.53: Initial and boundary conditions (IC & BC) of the aquous and mineral compositions for the example sulfur</i>	<i>3-224</i>
<i>Table 4.1: List of validation cases in Mont Terri in-situ diffusion experiments.....</i>	<i>4-227</i>
<i>Table 4.2: Calculated Equivalent Outer Radius of Circulation Chamber ($r' iBH$), Filter ($r' F$), and Gap ($r' Gap$) and Borehole Capacity of the Circulation Chamber (α').....</i>	<i>4-229</i>
<i>Table 4.3: Composition of the Synthetic OPA Porewater Used in the DR-A Diffusion and Sorption Experiment - Phase I (van Loon et al. 2003)</i>	<i>4-229</i>
<i>Table 4.4: Measured Tracer Concentrations [$mol\ L^{-1}$] during the DR-A In-situ Diffusion Experiment - Phase I (Xie et al. 2014).....</i>	<i>4-230</i>
<i>Table 4.5: General parameters for the circulation chamber, filter, gap and OPA</i>	<i>4-231</i>
<i>Table 4.6: Free aqueous phase diffusion coefficients (D_0) (Lide et al., 1994), correction factors $f_{\phi,jc}$ and $f_{\tau,jc}$ (Xie et al. 2014).....</i>	<i>4-231</i>
<i>Table 4.7: Parameters for the Generalized Cs^+ Cation Exchange Model for Illite (van Loon et al. 2009; as Modified by Gimmi 2012)</i>	<i>4-233</i>
<i>Table 4.8: Composition of the Synthetic OPA Porewater Used in the DR-A Diffusion and Sorption Experiment - Phase II (Xie et al. 2014).....</i>	<i>4-236</i>
<i>Table 4.9: Measured Major Ion Concentrations [$mol\ L^{-1}$] in the Circulation Solution during the DR-A In-situ Diffusion Experiment Phase II until Overcoreing (Xie et al. 2014).....</i>	<i>4-237</i>

Validation report-page# 1-24

<i>Table 4.10: Measured Tracer Concentrations [mol L⁻¹] in the Circulation Solution during the DR-A In-situ Diffusion Experiment - Phase II until Overcoring (Xie et al. 2014)</i>	4-238
<i>Table 4.11: General parameters for the circulation chamber, filter, gap and OPA ...</i>	4-239
<i>Table 4.12: Free aqueous phase correction factors f_φ, j_c and f_τ, j_c</i>	4-239
<i>Table 4.13: Measured Cs⁺ Concentrations [mol L⁻¹] in the Circulation Solution during the DR-A In-situ Diffusion Experiment - Phase II until Overcoring (Calculated Based on NAGRA 2012)</i>	4-241
<i>Table 4.14: General parameters for the circulation chamber, filter, gap and OPA ...</i>	4-246
<i>Table 4.15: List of validation cases in EBS-TF experiments.....</i>	4-250
<i>Table 4.16: Sample dimensions and soil properties for Benchmark II (Birgersson, 2011)</i>	4-250
<i>Table 4.17: Experimental data and simulated results for the accumulated mass of CaSO₄ for case B2.1</i>	4-253
<i>Table 4.18: Experimental data and simulated results for the accumulated mass of CaSO₄ for case B2.2a</i>	4-255
<i>Table 4.19: Experimental data and simulated results for the averaged accumulated CaSO₄ and Na₂SO₄ mass in [mol] for case B2.2b.....</i>	4-257
<i>Table 4.20: Components (i.e. primary species) and minerals used in the Benchmark IV simulations.....</i>	4-259
<i>Table 4.21: Composition of the infiltrating fluid (left-hand reactive transport boundary condition) and the initial conditions</i>	4-260
<i>Table 4.22: Selectivity coefficients for ion exchange reactions (from Bradbury and Baeyens 2003)</i>	4-260

Validation report-page# 1-25

LIST OF FIGURES

	<u>Page</u>
Figure 2.1 Comparison of concentrations of surface complexes vs pH simulated by MIN3P-THCm and PHREEQC (benchmark As(V)_surfx)	2-38
Figure 2.2 Comparison of simulated results for the ligand binding by a hydrous oxide from a 10^{-7} M solution by MIN3P-THCm and reported by Stumm and Morgan (1996) (benchmark surfa).....	2-40
Figure 2.3 Comparison of simulated results for the binding of a metal (Me^+) by a hydrous oxide from a 10^{-7} M solution by MIN3P-THCm (lines) and calculated data by Stumm and Morgan (1996) (symbols) (benchmark surfme)	2-42
Figure 2.4 Comparison of Water Content Calculated by MIN3P-THCm vs Experimental Observation (drain1).....	2-47
Figure 2.5: Comparison of Saturation Calculated by MIN3P-THCm vs HYDRUS (infil1)	2-49
Figure 2.6 Comparison of Saturation Calculated by MIN3P-THCm vs HYDRUS and Experimental Observation (haverk).	2-51
Figure 2.7 (a) Schematic diagram of the flow domain. (b) Experimental details and numerical simulation domain (Vauclin et al., 1979)	2-52
Figure 2.8 Comparison of hydraulic head contours after 8 hours calculated by MIN3P-THCm vs experimental observation.....	2-53
Figure 2.9 Comparison of Water Content Calculated by MIN3P-THCm vs Experimental Observation	2-55
Figure 2.10 Elder problem domain and boundary conditions (Bea et al., 2011)	2-57
Figure 2.11 Solute concentration results for the Elder problem simulated by MIN3P-THCm (left) and d^3f (right). The relative concentration contours are, from top to bottom, 0.8, 0.6, 0.4 and 0.2 of the saltwater source concentration (Bea et al., 2011) 2-58	
Figure 2.12 The modified Henry problem for lateral saltwater intrusion. (A) Simulation domain with flow and transport boundary conditions. (B) Relative solute concentration results at 0.833 d for MIN3P-THCm (solid lines) and the semi-analytical solution of Simpson and Clement (2004) (dashed lines) (Bea et al., 2011) 2-60	
Figure 2.13 Temperature profiles at 10.5, 21, 42 and 84 days (from left to right) for the radial flow with energy transport benchmark. A) MIN3P-THCm results (solid lines) are compared with the analytical solution (dashed lines) presented by Gelhar and Collins (1971), as modified by Voss and Provost (2008). B) Idealized representation of the domain (Bea et al., 2011)	2-63
Figure 2.14 2D mesh for the aquifer thermal energy storage problem.....	2-64

Validation report-page# 1-26

- Figure 2.15: Verification of density-dependent radial flow and energy transport (aquifer thermal storage) during hot water injection. MIN3P-THCm results using upstream and centered weighting are compared with SUTRA (Bea et al., 2011)..... 2-66
- Figure 2.16: Verification of density-dependent radial flow and energy transport (aquifer thermal storage) during groundwater withdrawal. MIN3P-THCm results using upstream weighting and centered weighting are compared with SUTRA (Bea et al., 2011) 2-67
- Figure 2.17: Verification of density-dependent flow, heat transport and solute transport (Henry-Hilleke problem). A) Domain and energy transport boundary conditions. B) Flow and solute transport boundary conditions. C) and D) Percent seawater isochlors, flow vectors, and normalized isotherms results obtained by MIN3P-THCm (left), SUTRA-MS and HST3D (right), respectively. SUTRA-MS results are represented as continuous lines. The continuous red line corresponds to the Henry and Hilleke numerical solution (0.5 percent seawater concentration and isotherm only), the HST3D code solution is presented by the dashed black line (Bea et al., 2011). 2-70
- Figure 2.18: Domain and boundary conditions for the transient thermohaline convection problems as given in Oldenburg and Pruess (1999), X relates to the mass fraction of brine to groundwater in relation to the source region ($X = 1$ in source) (Bea et al., 2011) 2-71
- Figure 2.19: Verification of thermo-hydraulic coupling for negative initial buoyancy. MIN3P-THCm results of density (left) and temperature (right) at 2 and 20 years are compared with the results from Geiger et al. (2006) (Bea et al., 2011)..... 2-72
- Figure 2.20: Verification of thermo-hydraulic coupling for positive initial buoyancy. MIN3P-THCm results of density (left) and temperature (right) at 2 and 20 years are compared with the results from Geiger et al. (2006) (Bea et al., 2011)..... 2-73
- Figure 2.21: Salt dome verification example. A) Domain geometry and boundary conditions for flow, energy and solute transport. B) Results obtained with MIN3P-THCm (left) are compared with FEFLOW (right) at different buoyancy ratios (Bea et al., 2011) 2-76
- Figure 2.22: Conceptual model of the 1D steady state diffusion problem for a radial coordinate system, a and b define the inner and outer reservoirs..... 2-78
- Figure 2.23: Comparison of analytical solution and concentration profiles obtained with MIN3P-THCm for the 1D steady-state diffusion problem in radial coordinates .. 2-80
- Figure 2.24: Conceptual model of the 1D transient diffusion problem for a radial coordinate system, a defines the outer radius..... 2-81
- Figure 2.25: Comparison of analytical solution and concentration profiles obtained with MIN3P-THCm for the 1D transient diffusion problem in radial coordinate..... 2-83
- Figure 2.26: Comparison of analytical solution (lines) and concentration profiles obtained with MIN3P-THCm for the 1D transient advective-dispersive problem in radial coordinate 2-86

Validation report-page# 1-27

- Figure 2.27: Comparison of vertical partial pressure profiles of $O_2(g)$ calculated with MIN3P-THCm in comparison to the Ogata-Banks solution at 0.02 days and 0.1 days (diffdry)..... 2-88
- Figure 2.28: Comparison of vertical partial pressure profiles of $O_2(g)$ calculated by MIN3P-THCm vs PYROX (left), and MIN3P-THCm vs Ogata-Banks equation (right) at 0.1 days, 1 day and 5 days..... 2-90
- Figure 2.29 Comparison of vertical partial pressure profiles of $O_2(g)$ calculated by MIN3P-THCm (solid lines), PYROX (dashed lines) and the Ogata-Banks analytical solution (symbols) at 1 day and 10 days..... 2-91
- Figure 2.30: Breakthrough curves of aqueous component concentrations affected by ion exchange reactions (line – MIN3P-THCm, symbol – PHREEQC V2)..... 2-93
- Figure 2.31: Cation-exchange problem. A) Physical and chemical properties of the domain. B) Spatial distribution of total concentrations of the major cations at 3000 days. C) Concentration of exchanged species at 3000 days. The MIN3P-THCm results (solid lines) agree well with PHAST (dashed lines)..... 2-95
- Figure 2.32: Simulated profiles of pH (top), concentrations of sorbed species (middle) and components (bottom) of the outflow solution for benchmark surfx 2-98
- Figure 2.33: Dedolomitization problem. A) Physical and chemical properties of the domain. B) Spatial distribution of total concentrations at 30000 days. C) Volumetric fractions of calcite ($CaCO_3$) and dolomite ($CaMg(SO_4)_2$) at 30000 days. MIN3P-THCm results (solids lines) match well with results from PHAST (dashed lines) (Bea et al., 2011)..... 2-100
- Figure 2.34: Comparison of simulated profiles by MIN3P-THCm and PYROX of O_2 partial pressure (top left) and volume fraction of pyrite (top right) at 10 and 20 years, respectively; and of time curves of pyrite oxidation rate (middle) and oxidized amount (bottom) at the observation point (elevation 0.25 m) 2-102
- Figure 2.35: Spatial profiles of porosity, volume fraction of calcite, hydraulic head at 10, 100 and 120 years, and flux time curve at the outflow boundary simulated by MIN3P-THCm, TOUGHREACT, HP1, PFlotran and CrunchFlow (Xie et al. 2014) 2-105
- Figure 2.36: Spatial profiles of porosity, volume fraction of gypsum and calcite, hydraulic head, and hydraulic conductivity at 10, 100 and 120 years, and flux time curve at the outflow boundary simulated by MIN3P-THCm, TOUGHREACT, PFlotran and CrunchFlow (Xie et al. 2014). 2-108
- Figure 2.37: Spatial profiles of porosity, hydraulic head, hydraulic conductivity at 10, 100 and 120 years, and flux time curve at the outflow boundary simulated by MIN3P-THCm, TOUGHREACT, PFlotran, HP1 and CrunchFlow (Xie et al. 2014).. 2-111
- Figure 2.38: Comparison of spatial volume fraction profiles (B3) of calcite, gypsum, ferrihydrite, gibbsite, siderite and jarosite at 10, 100 and 300 years simulated by MIN3P-THCm, TOUGHREACT, PFlotran, HP1 and CrunchFlow (Xie et al. 2014) 2-112

Validation report-page# 1-28

- Figure 2.39: Simulated profiles of aqueous concentrations (upper panel) and absorbed concentrations (lower panel) after one year..... 2-115
- Figure 2.40: Comparison of results obtained using MIN3P-THCm (symbols) with the analytical solution (lines) for breakthrough curves of Cl^- , C_2Cl_4 and C_6H_6 at $x=10\text{ m}$ 2-116
- Figure 2.41: Toluene verification problem. (A) Physical and chemical properties of the domain. (B) Spatial distribution of total concentrations at 5 days. (C) Spatial distribution of aerobic degradation rate of toluene ($C_6H_5CH_3$) at 5 days. The results for MIN3P-THCm (solid lines) are compared with PHAST (dashed lines) (Bea et al., 2011)..... 2-117
- Figure 2.42: Replacement of gypsum by polyhalite. (A) Physical and chemical properties of the domain. (B) and (C) Spatial distribution of total concentrations at 10 and 30 years, respectively. (D) and (E) Volumetric fractions of halite ($NaCl$), gypsum ($CaSO_4 \cdot 2H_2O$), and polyhalite ($Ca_2MgK_2(SO_4)_4 \cdot 2H_2O$), at 10 and 30 years, respectively. The MIN3P-THCm results (solid lines) are compared with PHAST (dashed lines) (Bea et al., 2011)..... 2-120
- Figure 2.43: Initial sorbed species concentration profiles simulated by MIN3P-THCm (lines) and CrunchFlow (symbols), left panel – sorbed species on site –X, right panel- sorbed species on site –Y..... 2-122
- Figure 2.44: Comparison of sorbed species concentration profiles at 10 hours simulated by MIN3P-THCm (lines) and CrunchFlow (symbols) left – sorbed species on site – X, right - sorbed species on site –Y..... 2-124
- Figure 2.45: Comparison of sorbed species concentration profiles at 50 hours simulated by MIN3P-THCm (lines) and CrunchFlow (symbols) left – sorbed species on site – X, right - sorbed species on site –Y..... 2-124
- Figure 2.46: Comparison of breakthrough curves at the outflow boundary calculated by MIN3P-THCm (lines) and CrunchFlow (symbols): (a) Total concentrations of components in the aqueous phase, (b) pH, (c) sorbed species' concentrations on site –X, (d) sorbed species' concentrations on site –Y..... 2-125
- Figure 2.47: Comparison of simulated concentration profiles obtained from MIN3P-THCm (lines), CrunchFlow (open symbols) and PHREEQC (filled symbols) at 100 days 2-127
- Figure 2.48: Comparison of simulated concentration profiles obtained from MIN3P-THCm (lines), CrunchFlow (symbols) at 100 days 2-129
- Figure 2.49: Evolution of Major Component in the Simulation of Cr(IV) Reduction under Denitrifying Conditions in a Flow-Through Column with Biomass Growth and Decay 2-133
- Figure 2.50: Concentration Profiles of Major Component in the Simulation of Cr(IV) Reduction under Denitrifying Conditions in a Flow-Through Column with Biomass Growth and Decay at day 100 2-133
- Figure 2.51: Salinity Inhibition Factor as a Function of Salinity (Points – Experimental

Validation report-page# 1-29

- Data from Brandt et al. 2001; Line – the Regression Equation)..... 2-136*
- Figure 2.52: Comparison of Concentration Profiles of HS⁻ (Solid Lines/Filled Symbols) and SO₄²⁻ (Dashed Lines/Open Symbols) (Left) and Profiles of Salinity (Right) at 1 (Blue), 5 (Red) and 10 (Black) Hours Simulated Using MIN3P-THCm (lines) to Those Simulated Using PHREEQC (Symbols) 2-137*
- Figure 2.53: Comparison of Breakthrough Curves of pH and Total Concentrations of Na⁺ and Cl⁻ (Top Left), Ca²⁺, K⁺, Mg²⁺ (Top Right), SO₄²⁻, CO₃²⁻ and HS⁻ (Bottom Right), and SI (saturation indexes) of Calcite, Anhydrite and Halite (Bottom Left) Simulated by MIN3P-THCm (Lines) to Those Calculated by PHREEQC (Symbols) Considered the SDSR Model..... 2-138*
- Figure 2.54: Comparison of Breakthrough Curves of pH and Total Concentrations of Na⁺ and Cl⁻ (Top Left), Ca²⁺, K⁺, Mg²⁺ (Top Right), SO₄²⁻, CO₃²⁻ and HS⁻ (Bottom Right), and SI (saturation indexes) of Calcite, Anhydrite and Halite (Bottom Left) Simulated by MIN3P-THCm (Lines) to Those Calculated by PHREEQC (Symbols) Without Considering the SDSR Model..... 2-139*
- Figure 2.55: Comparison of Concentration Profiles of HS⁻ (Solid Lines/Filled Symbols) and SO₄²⁻ (Dashed Lines/Open Symbols) (Left) and Profiles of Cl⁻ (Right) at 1 (Blue), 5 (Red) and 10 (Black) Hours Simulated Using MIN3P-THCm (lines) to Those Simulated Using PHREEQC (Symbols) 2-142*
- Figure 2.56: Comparison of Breakthrough Curves of pH and Total Concentrations of Na⁺ and Cl⁻ (Top Left), Ca²⁺, K⁺, Mg²⁺ (Top Right), SO₄²⁻, CO₃²⁻ and HS⁻ (Bottom Right), and SI (saturation indexes) of Calcite, Anhydrite and Halite (Bottom Left) Simulated by MIN3P-THCm (Lines) to Those Calculated by PHREEQC (Symbols) – With Inhibition of Sulfate Reduction by Cl⁻ 2-144*
- Figure 2.57: Comparison of Breakthrough Curves of pH and Total Concentrations of Na⁺ and Cl⁻ (Top Left), Ca²⁺, K⁺, Mg²⁺ (Top Right), SO₄²⁻, CO₃²⁻ and HS⁻ (Bottom Right), and SI (saturation indexes) of Calcite, Anhydrite and Halite (Bottom Left) Simulated by MIN3P-THCm (Lines) to Those Calculated by PHREEQC (Symbols) – Without Inhibition of Sulfate Reduction by Cl⁻ 2-145*
- Figure 2.58: Verification of the one-dimensional vertical stress implementation in MIN3P-THCm. A) Conceptual model depicting vertical loading on an aquifer with free drainage on surface. B) MIN3P-THCm results (symbols) match the analytical solution (solid lines) presented by Lemieux et al. (2008) (Bea et al., 2011) ... 2-147*
- Figure 3.1: Simulated time curves of saturation indices for albite and calcite (upper panel), and concentrations of selected components (lower panel) 3-150*
- Figure 3.2: Simulated time curves of SI of calcite (upper panel), and concentrations of selected species (lower panel) 3-152*
- Figure 3.3: Simulated results for pH dependent speciation of Cr(III) (left) and saturation indexes of excluded minerals (right) (benchmark Cr(III)) 3-153*
- Figure 3.4: Simulated results for pH dependent speciation of Fe(III) (left) and saturation indexes of excluded minerals (right) (benchmark Fe(III)) 3-155*

Validation report-page# 1-30

- Figure 3.5: Simulated profiles of NAPL volume fraction (upper panel), concentration of dissolved PCE (middle panel) and sorbed PCE (lower panel) (linsorb) 3-157
- Figure 3.6: Ligand binding by a hydrous oxide from a 10^{-7} M solution (demonstration example surfa2)..... 3-158
- Figure 3.7: Simulated results for the binding of a metal (Me^+) by a hydrous oxide from a 10^{-7} M solution (benchmark surfme2)..... 3-159
- Figure 3.8: Simulated hydraulic head contours at steady state. 3-162
- Figure 3.9: Simulated saturation contours and pressure head contours at steady state. . 3-164
- Figure 3.10: Simulated hydraulic head contours after 0.02 days. 3-165
- Figure 3.11: Simulated saturation contours and pressure head contours after 1 day.3-167
- Figure 3.12: Simulated hydraulic head contours at steady state. 3-169
- Figure 3.13: Simulated hydraulic head contours after 4 days. 3-171
- Figure 3.14: Simulated hydraulic head contours after 8 hours..... 3-172
- Figure 3.15: Concentration distributions at 1000 days for decoupled ($\partial p/\partial c = 0$; dashed lines) and coupled ($\partial p/\partial c = 0.7$; solid lines) hydrostatic simulations. Concentration contours have the unit g l⁻¹ (Bea et al., 2011)..... 3-174
- Figure 3.16: Concentration distributions for the hydrodynamic box simulations. Concentration contours (g L⁻¹) at 0 days (solid lines) and 4000 days (dashed lines) are coincident (Bea et al., 2011)..... 3-177
- Figure 3.17: Profiles of concentrations of aqueous species at 3 days for benchmark complex 3-180
- Figure 3.18: Boundary conditions: A carbonic acid solution enters from the bottom left, constant hydraulic head on the top ($h=0.0\text{ m}$) and bottom boundaries ($h=0.0014\text{ m}$). 3-181
- Figure 3.19: Simulated contours of the total CO_3^{2-} concentration (left) and the HCO_3^- concentration (right) at 4.0 days 3-182
- Figure 3.20: Comparison of simulated tracer concentration profiles by harmonic, arithmetic, and arithmetic De averaging methods 3-184
- Figure 3.21: Transient boundary concentrations (upper panel), simulated concentration profiles of components H^+ and CO_3^{2-} at 0.75 days (middle panel) and 4.5 days (bottom panel) for benchmark transrc..... 3-186
- Figure 3.22: Profiles of aqueous species' concentrations (up) and mineral fraction of calcite at 6 days (down)..... 3-189
- Figure 3.23: Simulated contours of pH (left) and calcite volume fraction (right) at 10 days 3-191
- Figure 3.24: Simulated profiles of pH (top left), concentrations of selected components (top right), mineral volume fractions (bottom left) and dissolution rates (bottom

Validation report-page# 1-31

right) for the demonstration example weather at 5.0 years.....	3-194
Figure 3.25: Simulated spatial profiles of total aqueous component concentrations (upper panel) and ion exchanged species (lower panel) at 25 hours (solid lines) and at 55 hours (dashed lines).....	3-196
Figure 3.26: Spatial profiles of $O_2(aq)$, NO_3^- , $Fe(II)$, $Mn(II)$ (left), and pH, alkalinity (right) at 0.0 years, 1.0 year, 3.0 years for demonstration example <i>comptran</i>	3-199
Figure 3.27: Spatial profiles of $O_2(aq)$, NO_3^- , $Fe(II)$, $Mn(II)$ (left), and pH, alkalinity (right) at 3.5 years, 5.0 years, and 6.0 years for demonstration example <i>comptran</i> ..	3-200
Figure 3.28: Profiles of simulated aqueous component concentration (a), gas partial pressure (b), degassing rate (c), degradation rates of organic contaminant (d) and pH (e) at 3 years	3-203
Figure 3.29: Simulated spatial profiles of partial pressures of the six organic contaminants and total gas pressures (p_{tot}) at 50 days (left), and saturation profiles of gas (S_g) and aqueous (S_a) phases at steady state (right).....	3-206
Figure 3.30: Simulated system mass evolution of the six organic components in the NAPL mixture	3-206
Figure 3.31: Simulated spatal profiles of pH (upper panel), concentrations of sorbed species (middle panel) and total aqueous component concentrations (lower panel) at 5 hours for demonstration example <i>surfa2</i>	3-208
Figure 3.32: Simulated profiles of pH (upper panel), concentrations of sorbed species (middle panel) and total aqueous component concentrations (lower panel) at 20 hours for benchmark <i>surfme2</i>	3-210
Figure 3.33: Simulated spatial profiles of pH (a), concentrations of contaminants (b) and selected components (c) and (d), volume fraction of minerals (e) and iron consumption rates (f) at 240 days. The gray background indicates the position of the reactive barrier (Zone 2).....	3-214
Figure 3.34: Simulated speatil profiles for the acid mine drainage generation problem at $T = 10$ years: a) pH and p_e , b) mineral volume fractions, c) selected total aqueous component concentrations, d) partial gas pressures	3-218
Figure 3.35: Simulated profiles of mineral volume fractions.....	3-222
Figure 3.36: Comparison of concentration time curves of simulated (s) to measured $\delta^{34}S$, SO_4^{2-} and $Fe(II)$ in the influent (in) and effluent (eff) (Gibson et al. 2011)....	3-223
Figure 3.37: Profiles of total concentrations of SO_4^{2-} , CO_3^{2-} HS^- and $H_2S(aq)$ (Top left), and of other main ions (top right), and of the volume fractions of minerals (bottom left) and of the mineral saturation indexes (bottom right) at 70 years	3-225
Figure 4.1: Schematic Diagram of the Simulation Domain Representing the Experimental Set-up Including the Inner Borehole (Radius= 3.1 cm) that Contains the Tracers in Solution, Filter (4 mm in Thickness), Gap (3 mm in Thickness), and OPA up to a Radius of 61.5 cm. The Thickness of the Test Chamber is $h = 1.04$ m. A Radial Coordinate System was Used for the Simulations.	4-228

Validation report-page# 1-32

- Figure 4.2: Comparison of Simulated (Lines) and Experimental (Symbols) Concentration Time Curves for HTO, Br⁻, I⁻, ⁶⁰Co²⁺ and ⁸⁵Sr²⁺ in the Borehole Solution during the DR-A Field Diffusion Experiment Phase I (Xie et al. 2014)..... 4-232
- Figure 4.3: Concentration profiles of sorbed Cs on three sites at 10 days (left) and 189 days (right) (solid red line – Cs-FES, dashed black line – Cs-II, dash dot blue line – Cs-PS) (Xie et al. 2014) 4-234
- Figure 4.4: Comparison of Simulated (Lines) and Experimental (Symbols) Concentration Time Curve for Cs⁺ in the Borehole Solution during the DR-A Field Diffusion Experiment Phase I (Xie et al. 2014) 4-235
- Figure 4.5: Comparison of Simulated (Lines) and Experimental (Symbols) Concentration Time Curves for HTO, Br⁻, I⁻, ⁶⁰Co²⁺ and ⁸⁵Sr²⁺ in the Borehole Solution during the DR-A Field Diffusion Experiment Phase II (Xie et al. 2014) 4-240
- Figure 4.6: Comparison of Simulated (Lines) and Experimental (Symbols) Cs⁺ Concentration Time Curves for Phase I and Phase II of the DR-A In-situ Diffusion Experiment after Diffusion Parameter Calibration (Xie et al. 2014) 4-242
- Figure 4.7: Comparison of Simulated (Lines) and Experimental (Symbols) Concentration Time Curves of Major Ions during the DR-A In-situ Diffusion Experiment Phase II after Diffusion Parameter Calibration (Xie et al. 2014) 4-243
- Figure 4.8: Simulated Total Concentration Profiles for HTO, Br⁻, Cl⁻ and I⁻ and Comparison to the Experimental Results in the Porewater of the Overcored Samples at 728 Days (Xie et al. 2014) 4-244
- Figure 4.9: Simulated Total Concentration Profiles for Na⁺, Ca²⁺, Mg²⁺ and K⁺ and Comparison to the Experimental Results in the Porewater of the Overcored Samples at 728 Days 4-245
- Figure 4.10: Simulated Profiles of Sorbed Species on Three Ion Exchange Sites (-PS, -FES and -II) at 728 Days (Xie et al. 2014) 4-245
- Figure 4.11: Comparison of the Simulated Total Concentration Profiles for HTO, ⁶⁰Co²⁺, Br⁻ and I⁻ in the Opalinus Clay at 735 days and in the Porewater of the Overcored Opalinus Clay Samples (Xie et al. 2014) 4-247
- Figure 4.12: Comparison of the Simulated Total Concentration Profiles for HTO, ⁶⁰Co²⁺, Br⁻ and I⁻ in the Opalinus Clay at 735 days and in the Porewater of the Overcored Opalinus Clay Samples (Xie et al. 2014) 4-249
- Figure 4.13: Schematic Diagram of the Simulation Domain Representing the Experimental Set-up Including the Source Reservoir (Bottom), Compacted Ca-montmorillonite (5 mm in Thickness) and Target Reservoir (Top) 4-251
- Figure 4.14: Comparison of simulated results and experimental data for accumulated CaSO₄ mass in the target reservoir for case B2.1 4-252
- Figure 4.15: Concept of Benchmark II: Gypsum Dissolution and CaSO₄ Diffusion Including the Reservoirs (Top and Bottom), Compacted Ca-montmorillonite (B2.2a) or Na-montmorillonite (B2.2b) and Thin Gypsum Powder Layer (Middle) 4-254

Validation report-page# 1-33

- Figure 4.16: Comparison of simulated results and experimental data for accumulated CaSO₄ mass in the target reservoir for case B2.2a 4-255*
- Figure 4.17: Comparison of simulated results and experimental data for accumulated Na₂SO₄ (left) and CaSO₄ (right) mass in the Top and Bottom reservoirs for case B2.2b 4-257*
- Figure 4.18: Model setup for multicomponent reactive transport experiment in bentonite 4-259*
- Figure 4.19: Time series of the simulated effluent composition and measured concentrations (min3p – results simulated by MIN3P-THCm; CF – results simulated by CrunchFlow). 4-261*

Validation report-page# 1-34

1 INTRODUCTION

The reactive transport code MIN3P-THCm has been under development on the basis of the MIN3P standard version since 1999 (Mayer 1999; Mayer et al. 2002). To verify the development, 125 examples are accumulated as the standard benchmarks up to the current version 1.0.433. Till now, most of these examples exist when the first MIN3P-THCm visual SVN repository was set up and are placed under the subfolders .\benchmarks_standard and .\benchmarking_nwmo_report. Newly added examples are located under the folder .\benchmarks_new_add and can be only executed with any version newer than the one when the examples were first added or updated (e.g. due to bug fix or modifications of keywords). The oldest version number required to run such examples can be easily recognized by the folder tag. For example, the multisite ion exchange model can be found under the subfolder .\benchmarks_new_add\multisite-ionx-V1.0.129, in which V1.0.129 indicates that the example was established at the version MIN3P-THCm v.1.0.129 and can be executed with this the following versions. If verification is through code intercomparison (e.g. CrunchFlow), the input files and databases for MIN3P-THCm and CrunchFlow (i.e. for verification) are placed in separate subfolders under this folder. Detailed descriptions of the corresponding theory, usage of the corresponding function are included in the MIN3P-THCm theory and the user manuals, respectively. It is important to note that only a selection of the examples are described in this validation report. The main reason is because some examples are very similar and test the same main functions with only minor differences in the input files or the documentation has been published as either technical reports or journal papers (Bea et al. 2011; Xie et al. 2014a and 2014b; Molins et al. 2015).

The report is organized as the following: 1. The validated examples (Section 2); 2. The demonstration examples (Section 3); 3. Validation examples against laboratory and in situ experiments (i.e Mont Terri in situ diffusion experiment) (Section 4).

2 VALIDATION EXAMPLES

In order to verify and validate the numerical implementations and demonstrate the functions of MIN3P-THCm through simulation examples, three types of validation approaches are used:

1. Validation is performed through comparison of simulated results with analytical solutions;
2. Validation is undertaken through code intercomparisons, i.e. the comparison of simulated results obtained by MIN3P-THCm and by published code(s) with equivalent functions;
3. Validation by comparison of MIN3P-THCm results to experimental data.

The procedure for code validation/verification for each new version consists of the following: When a new version or revision of MIN3P-THCm is completed, an automated script will be started that executes the new code on all existing validation and verification examples and new validation and verification cases that are designed to test the new functionalities. Results for existing verification examples will be compared to established results from the previous version of MIN3P-THCm. New validation or verification

Validation report-page# 2-36

examples will be benchmarked against existing established solutions obtained with an analytical model, experimental data or other numerical codes. This approach will identify any discrepancies that may arise due to code development, so that the developer can address them, or determine if they are insignificant. The new code will be accepted if all existing and new test examples are solved with either no differences, or insignificant differences.

2.1 BATCH REACTIONS

MIN3P-THCm provides many functions for geochemical batch reaction simulations including speciation calculations, ion exchange, sorption, surface complexation, kinetic reactions, mineral dissolution/precipitation and biogeochemical reactions. A collection of benchmarks is presented in the following subsections to test these functions. More functions for geochemical reaction simulations are embedded in the reactive transport verification benchmarks. A list of the geochemical batch reaction verification problems is provided in Table 2.1.

Table 2.1: List of batch reaction benchmarks

Name	Description of Main Features	Verification Type	Section
As(V)_surfx	Surface complexation	2	2.1.1
surfa	pH-dependent anion surface complexation	2	2.1.2
surfme	pH-dependent cation surface complexation	2	2.1.3
pitzer	Pitzer equations for reactions in highly saline solution	2	2.1.4

2.1.1 SURFACE COMPLEXATION OF ARSENATE

2.1.1.1 Problem definition

This hypothetical benchmark is an equilibrium batch reaction considering pH-dependent surface complexation of arsenate. A code intercomparison was undertaken with PHREEQC (Parkhurst and Appelo 1999).

2.1.1.2 Model setup

The geochemical system includes two aqueous components (H^+ and H_3AsO_4), one non-aqueous component ‘=FeOH(w)’ as the sorption surface, four secondary aqueous species (OH^- , H_2AsO_4^- , HAsO_4^{2-} and AsO_4^{3-}) and five sorbed species (=FeOH $_2^+$ (w), =FeO $^-$ (w), =FeH $_2$ AsO $_4$ (w), =FeHAsO $_4^-$ (w) and =FeOHAsO $_4^{3-}$ (w)). The initial geochemical conditions are listed in Table 2.2. The simulation was conducted for a pH range from 2 to 14 in 50 steps. The total concentration of H_3AsO_4 is 0.01 mol L^{-1} .

Validation report-page# 2-37

Table 2.2: Initial geochemical conditions for benchmark As(V)_surfx

Parameter	Initial condition	Unit
<i>Aqueous phase</i>		
H ⁺	2.0 [#]	pH
H ₃ AsO ₄	1.0×10 ⁻²	[mol l ⁻¹]

- a pH-sweep calculation is carried out using the keyword ‘ph_sweep’ (see the user manual section “INITIAL CONDITION – BATCH REACTIONS”)

2.1.1.3 Parameters

The parameters for the surface complexation reactions used for the simulations are summarized in Table 2.3. The reaction stoichiometries of the surface complexation reactions are summarized in Table 2.4.

Table 2.3: Physical parameters of surface site for verification problem As(V)_surfx

Parameter	Symbol	Value	Unit
Mass of surface site ‘=FeOH(w)’	M	100.0	[g solid L ⁻¹ H ₂ O]
Surface area of ‘=FeOH(w)’	S	10.0	[m ² g ⁻¹ solid]
Site density	D	6.02228	[sites nm ⁻²]

2.1.1.4 Results

The simulated results for the pH dependent surface complexation of arsenate are depicted in Figure 2.1. It is seen that when the pH is higher than 8.0, the dominant surface complex of arsenate is =FeH₂AsO₄(w). When the pH is lower than 4.0, the dominant surface complex of arsenate is =FeHAsO₄⁻(w). When the pH is in the range of 4.0 to 8.0, a mixture of =FeH₂AsO₄(w), =FeHAsO₄⁻(w) and =FeOHAsO₄³⁻(w) is present. These results compare well with those calculated by PHREEQC.

Table 2.4: Reaction stoichiometries of surface complextion reactions for benchmark As(V)_surfx

Surface complex	Surface	Reaction	logK
=FeOH ₂ ⁺ (w)	=FeOH(w)	=FeOH(w) + H ⁺ ↔ =FeOH ₂ ⁺ (w)	7.290
=FeO ⁻ (w)	=FeOH(w)	=FeOH(w) ↔ =FeO ⁻ (w) + H ⁺	-8.930
=FeH ₂ AsO ₄ (w)	=FeOH(w)	=FeOH(w) + H ₃ AsO ₄ ↔ ==FeH ₂ AsO ₄ (w) + H ₂ O	8.713
=FeHAsO ₄ ⁻ (w)	=FeOH(w)	=FeOH(w) + H ₃ AsO ₄ ↔ =FeHAsO ₄ ⁻ (w) + H ⁺ + H ₂ O	2.913
=FeOHAsO ₄ ³⁻ (w)	=FeOH(w)	=FeOH(w) + H ₃ AsO ₄ ↔ ==FeOHAsO ₄ ³⁻ (w) + 3H ⁺	-10.017

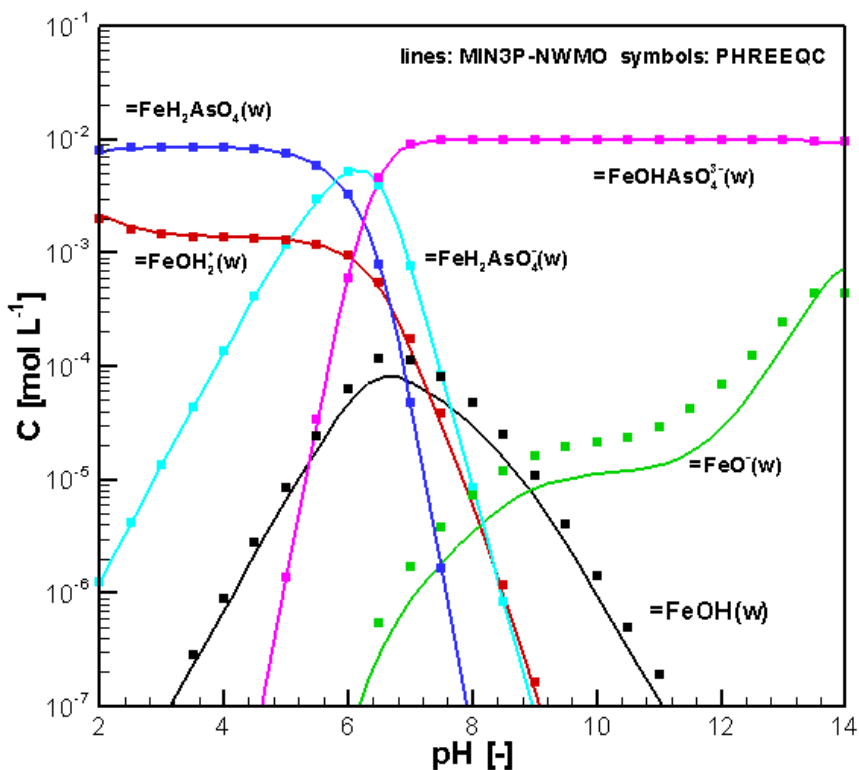


Figure 2.1 Comparison of concentrations of surface complexes vs pH simulated by MIN3P-THCm and PHREEQC (benchmark As(V)_surfx)

2.1.1.5 File locations

The input file is: *as(v)-surfx.dat* under folder
`.\benchmarks\benchmarks_standard\batch\as(V)_surfx`

Database can be found under: `.\benchmarks\database\default`

2.1.2 PH-DEPENDENT ANION SURFACE COMPLEXATION

2.1.2.1 Problem definition

This example demonstrates the pH-dependence of the binding of a ligand (A^-) to a hydrous oxide using a non-electrostatic surface complexation model. The reaction parameters are based on Example 9.3b (page 545) in Stumm and Morgan (1996).

2.1.2.2 Model setup

The geochemical system includes two aqueous components (H^+ and HA), one non-aqueous component ' $=SOH$ ' as 'surface', two secondary aqueous species (OH^- , A^-) and three sorbed species ($=SOH_2^+$, $=SO^-$ and $=SA$). The initial geochemical conditions are listed in Table

Validation report-page# 2-39

2.5. The simulation was conducted for a pH range from 0 to 14 in 50 steps. The total concentration of HA is 1.0×10^{-7} mol L⁻¹.

Table 2.5: Initial geochemical conditions for benchmark surfa

Parameter	Initial conditions	Unit
<i>Aqueous phase</i>		
H ⁺	0.0 [#]	pH
HA	1.0×10^{-7}	[mol L ⁻¹]

- a pH-sweep calculation is carried out using the keyword ‘ph_sweep’ (see the user manual section “INITIAL CONDITION – BATCH REACTIONS”)

The parameters for the surface complexation reactions are summarized in Table 2.6.

Table 2.6: Physical parameters for the surface for verification problem surfa (Stumm and Morgan 1996)

Parameter	Symbol	Value	Unit
Mass of surface site ‘=SOH’	M	1.0	[g solid L ⁻¹ H ₂ O]
Surface area of ‘=SOH’	S	10.0	[m ² g ⁻¹ solid]
Site density	D	6.02228	[sites nm ⁻²]

2.1.2.3 Results

The simulated results for geochemical speciation of an anion ligand (A⁻), as a function of pH, considering surface complexation are depicted in Figure 2.2. The results show that the speciation is highly pH dependent. Surface complex =SA is the main component for the anion A⁻ if the pH is between 3 and 6; however, when the pH is higher than 6 or lower than 2, the main species is A⁻ or HA, respectively. These results agree very well with those reported by Stumm and Morgan (1996) calculated using code Mac μ QL, which was adapted by Müller (1993) from the program MICROQL-II developed by Westall (1979).

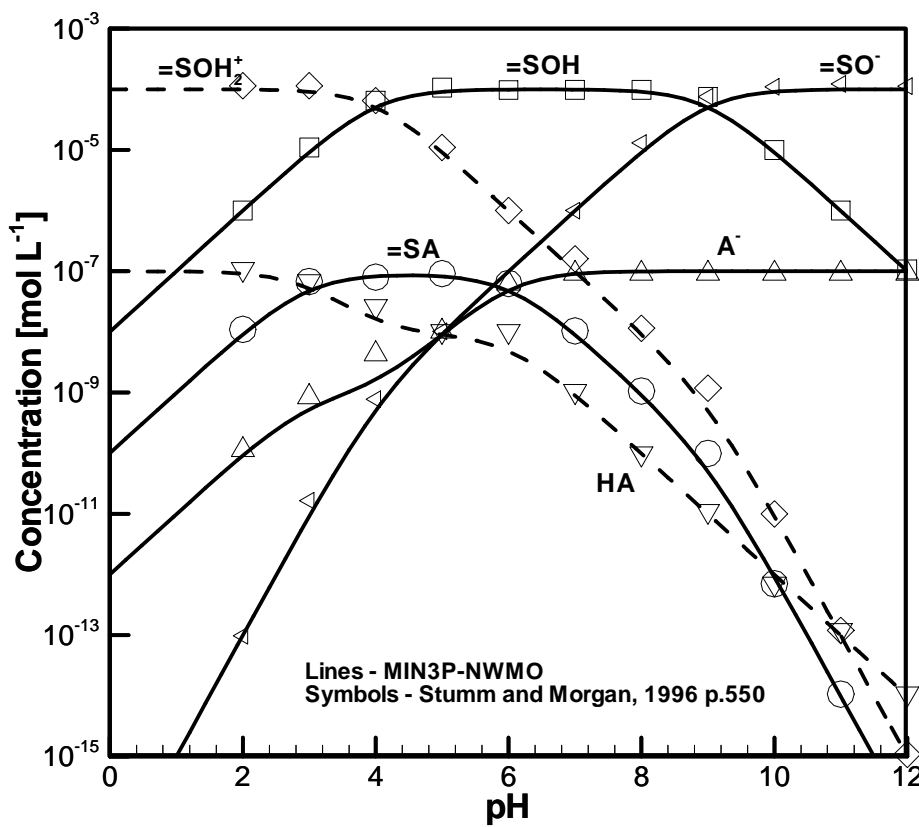


Figure 2.2 Comparison of simulated results for the ligand binding by a hydrous oxide from a 10⁻⁷ M solution by MIN3P-THCm and reported by Stumm and Morgan (1996) (benchmark surfa)

2.1.2.4 File locations

The input file is: *surfa.dat* under folder .\benchmarks\benchmarks_standard\batch\surfa
Database can be found under: .\benchmarks\database\surftest

2.1.3 PH-DEPENDENT CATION SURFACE COMPLEXATION

2.1.3.1 Problem definition

This example demonstrates the pH-dependence of the binding of a metal (Me²⁺) to a hydrous oxide using a non-electrostatic surface complexation model. The reaction parameters are based on Example 9.3a (page 545) in Stumm and Morgan (1996). This function is verified by the comparison of the simulated results to the data reported by Stumm and Morgan (1996).

Validation report-page# 2-41

2.1.3.2 Model setup

The geochemical system includes two aqueous components (H^+ and Me^{2+}), one non-aqueous component ‘=SOH’ as ‘surface’, one secondary aqueous species (OH^-) and three sorbed species ($=\text{SOH}_2^+$, $=\text{SO}^-$ and $=\text{SOMe}^+$). The initial geochemical conditions are listed in Table 2.7. The simulation was conducted for a pH range from 0 to 14 in 50 steps. The total concentration of Me^{2+} is 1.0×10^{-7} mol L⁻¹. The parameters for the surface complexation reactions are summarized in Table 2.8.

Table 2.7: Initial geochemical conditions for benchmark surfme

Parameter	Initial conditions	Unit
<i>Aqueous phase</i>		
H^+	0.0 [#]	pH
Me^{2+}	1.0×10^{-7}	[mol L ⁻¹]

- a pH-sweep calculation is carried out using the keyword ‘ph_sweep’ (see the user manual section “INITIAL CONDITION – BATCH REACTIONS”)

Table 2.8: Physical parameters for the surface for verification problem surfme (Stumm and Morgan 1996)

Parameter	Value	Unit
Mass of surface site ‘=SOH’	M	[g solid L ⁻¹ H ₂ O]
Surface area of ‘=SOH’	S	[m ² g ⁻¹ solid]
Site density	D	[sites nm ⁻²]

2.1.3.3 Results

The simulated geochemical speciation of a metal (Me^+) as a function of pH considering surface complexation is depicted in Figure 2.3. The surface complex $=\text{SOMe}^+$ is the main component for the metal for pH values greater than 5.0. Otherwise, the main species is Me^+ . These results closely agree with those provided by Stumm and Morgan (1996).

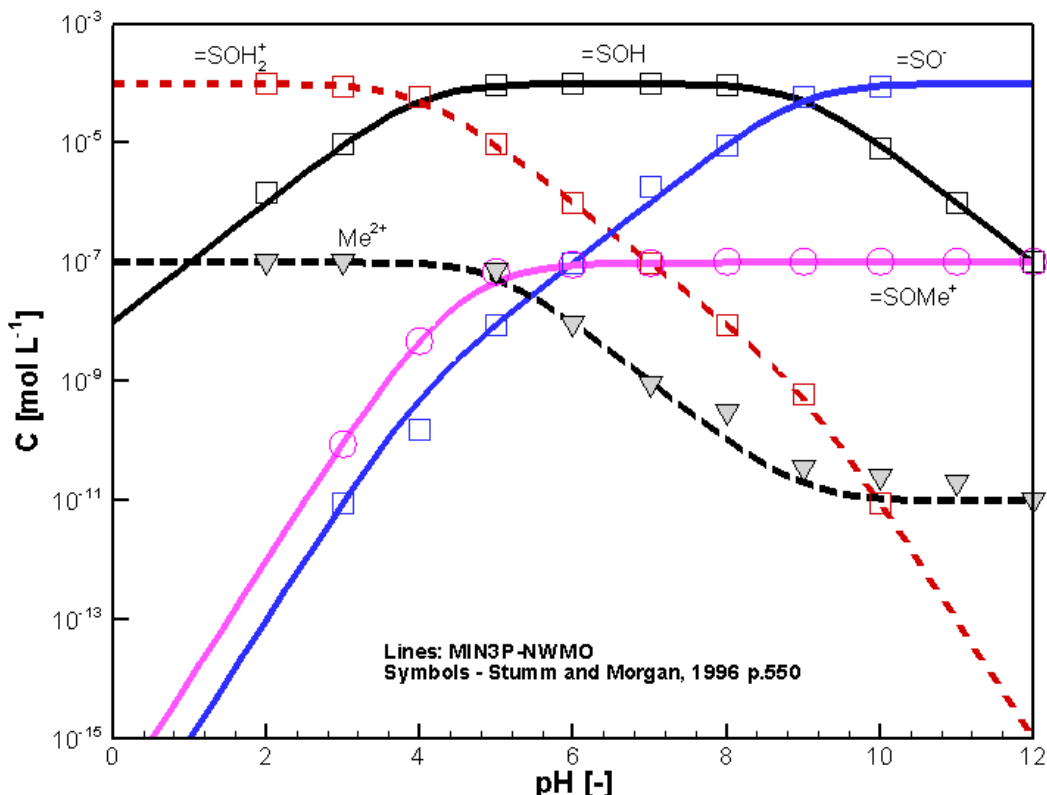


Figure 2.3 Comparison of simulated results for the binding of a metal (Me^+) by a hydrous oxide from a 10^{-7} M solution by MIN3P-THCm (lines) and calculated data by Stumm and Morgan (1996) (symbols) (benchmark surfme)

2.1.3.4 File locations

The input file is: *surfme.dat* under folder:

.\benchmarks\benchmarks_standard\batch\surfme

Database can be found under: *.\benchmarks\database\surftest*

2.1.4 PITZER EQUATION – CHEMICAL SPECIATION OF DEAD SEA WATER

2.1.4.1 Problem definition

The benchmark is defined to calculate the chemical speciation of Dead Sea Water, in order to verify the implementation of the Pitzer equations in MIN3P-THCm (Bea et al., 2011). The simulated results were compared to those calculated with PHREEQC (Parkhurst and Appelo 1999) and EQ3/6 (Worley 1992).

2.1.4.2 Model setup

The geochemical system includes eight aqueous components (H^+ , Cl^- , Na^+ , K^+ , Mg^{2+} , Ca^{2+} , CO_3^{2-} and SO_4^{2-}), 12 secondary species (MgHCO_3^{+} , $\text{CaSO}_4^{(\text{aq})}$, CaCl^+ , MgOH^+ , $\text{MgCO}_3^{(\text{aq})}$, HCO_3^- , $\text{CaCO}_3^{(\text{aq})}$, CaOH^+ , $\text{CO}_2^{(\text{aq})}$, HSO_4^- , and $\text{CaCl}_2^{(\text{aq})}$), one gas ($\text{CO}_2(\text{g})$) and 31 minerals as listed in Table 2.11. Initially, the total concentrations of all components in the Dead Sea Water were provided under standard conditions (25°C, 1bar) as listed in Table 2.9. The solution doesn't include any solids. The ionic strength of the solution is 2.0 M. Ion interactions were taken into consideration by applying the HMW model (Harvie et al., 1984) (see section 2.1.4.6 in the theory manual).

Table 2.9: Speciation of Dead Sea water – Model input (Bea et al., 2011)

Chemical parameters	Value
T [°C]	25
pH [-]	7
P [bar]	1
Component	Concentration [molality]
Na^+	1.7520
K^+	0.1739
Mg^{2+}	1.5550
Ca^{2+}	0.4274
Cl^-	5.8100
CO_3^{2-}	3.92×10^{-3}
SO_4^{2-}	6.30×10^{-3}

2.1.4.3 Parameters

The geochemical parameters used for the simulation were provided through a database created based on the thermodynamic database “data0.ypf.R2” (USDOE, 2007). The main parameters are: The Debye-Hückel limiting slope (A^ϕ) is 0.3915. All other parameters are listed in Appendix III.

2.1.4.4 Results

The results of chemical speciation calculations are in good agreement for all three codes (Table 2.10 - Table 2.11), (Bea et al., 2011).

2.1.4.5 File locations

The input file can be found under

`..\benchmarking_nwmo_report\ nwmo_verification_examples\d2__verification_pitzer_equations\min3p\verif-pitzer.dat`

Database can be found under: `.\benchmarks\database\default` (An additional file pitzer.xml derived from database data0.ypf.R2 from EQ3/6 database is needed)

Validation report-page# 2-44

Table 2.10: Speciation of Dead Sea Water – Aqueous Speciation (Bea et al., 2011)

Speciation	EQ3	PHREEQC	MIN3P-THCm
	[molality]	[molality]	[molality]
Cl ⁻	5.809	5.809	5.809
Na ⁺	1.752	1.752	1.752
Mg ²⁺	1.551	1.551	1.551
Ca ²⁺	0.4239	0.4235	0.4239
K ⁺	0.1739	0.1739	0.1739
SO ₄ ²⁻	4.038×10 ⁻³	3.782×10 ⁻³	4.106×10 ⁻³
MgHCO ₃ ⁺	3.6×10 ⁻³	3.648×10 ⁻³	3.474×10 ⁻³
CaSO _{4(aq)}	2.262×10 ⁻³	2.518×10 ⁻³	2.193×10 ⁻³
CaCl ⁺	1.198×10 ⁻³	1.366×10 ⁻³	1.227×10 ⁻³
MgOH ⁺	3.235×10 ⁻⁴	2.692×10 ⁻⁴	2.559×10 ⁻⁴
MgCO _{3(aq)}	1.256×10 ⁻⁴	1.042×10 ⁻⁴	1.046×10 ⁻⁴
HCO ₃ ⁻	9.756×10 ⁻⁵	9.251×10 ⁻⁵	1.445×10 ⁻⁴
CO ₃ ²⁻	5.526×10 ⁻⁵	3.918×10 ⁻⁵	4.335×10 ⁻⁵
CaCO _{3(aq)}	4.1×10 ⁻⁵	3.494×10 ⁻⁵	3.272×10 ⁻⁵
CaOH ⁺	4.571×10 ⁻⁶	3.804×10 ⁻⁶	3.394×10 ⁻⁶
CO _{2(aq)}	9.584×10 ⁻⁷	1.195×10 ⁻⁶	1.212×10 ⁻⁶
HSO ₄ ⁻	2.048×10 ⁻¹⁰	2.607×10 ⁻¹⁰	2.794×10 ⁻¹⁰
CaCl _{2(aq)}	1.142×10 ⁻¹⁵	1.195×10 ⁻¹⁵	1.072×10 ⁻¹⁵

Validation report-page# 2-45

Table 2.11: Speciation of Dead Sea Water – Mineral Saturation Indices (Bea et al., 2011)

Minerals	Saturation Indices		
	EQ3	PHREEQC	MIN3P-THCm
Anhydrite	0.02	0.02	0.01
Antarcticite	-3.31	-3.29	-3.33
Aragonite	0.62	0.56	0.548
Arcanite	-4.31	-4.33	-4.3
Bischofite	-2.75	-2.69	-2.75
Bloedite	-5.00	-5.02	-4.97
Calcite	0.80	0.67	0.70
Carnallite	-2.76	-2.69	-2.76
Dolomite	3.55	3.41	3.37
Epsomite	-2.37	-2.32	-2.35
Glauberite	-2.49	-2.46	-2.49
Gypsum	-0.03	-0.05	-0.04
Halite	-0.37	-0.35	-0.37
Hexahydrite	-2.54	-2.50	-2.52
Hydromagnesite	-2.43	-2.90	-2.93
Kainite	-3.79	-3.80	-3.78
Kieserite	-3.56	-3.53	-3.56
Lansfordite	-2.02	-2.11	-2.09
Leonhardtite	-2.93	-2.89	-2.91
Magnesite	1.16	1.08	1.09
Mirabilite	-3.41	-3.58	-3.38
Natron	-7.24	-7.33	-7.29
Nesquehonite	-1.92	-2.36	-1.86
Oxychloride-Mg	-2.65	-2.91	-2.93
Pentahydrite	-2.66	-2.62	-2.67
Pentasalt	-3.16	-2.55	-3.21
Polyhalite	-4.66	-4.69	-4.67
Sylvite	-1.06	-1.05	-1.06
Syngenite	-3.26	-3.19	-3.14
Thenardite	-3.13	-3.15	-3.11
Brucite	-1.97	-2.14	-2.16

2.2 GROUNDWATER FLOW AND WATER VAPOR TRANSPORT

MIN3P-THCm provides formulations for saturated and unsaturated flow simulations for 1D, 2D and 3D problems under isothermal conditions, as well as water vapor transport under non-isothermal conditions. A list of the validation examples for flow problems and a water vapor transport problem are given in Table 2.12.

Table 2.12: List of flow and evaporation benchmarks

Name	Description of Main Features	Validation Type	Section
drain1	1D gravity drainage in soil column	3	2.2.1
infil1	1D infiltration in soil column	3	2.2.2
haverk	1D drainage problem in sand column	2, 3	2.2.3
clement	2D transient water table mounding	3	2.2.4
verif-evap	1D water vapor movement	3	2.2.5

2.2.1 1D GRAVITY DRAINAGE IN SOIL COLUMN

2.2.1.1 Problem definition

This benchmark is a one dimensional drainage problem based on the experiments by Forsyth et al (1995). It involves simulations of drainage by gravity, following complete saturation.

2.2.1.2 Model setup

A 1D model with 6.0 m in depth is discretized into 121 control volumes yielding a discretization interval of 0.05 m for the interior control volumes and 0.025 m for the control volumes on the boundary. Initial condition for the flow problem is zero pressure head for the entire domain. Boundary conditions for the flow problem consist of a zero flux on the top boundary and zero pressure head on the bottom boundary.

2.2.1.3 Parameters

The physical parameters (material properties) used for the simulations are summarized in Table 2.13.

Table 2.13: Physical parameters for benchmark drain1

Parameter	Symbol	Value	unit
Length of domain	L	6.0	[m]
Porosity	ϕ	0.33	[$-$]
Hydraulic conductivity	K_{zz}	2.896×10^{-6}	[$m s^{-1}$]
Residual saturation	S_{ra}	0.0	[$-$]
Van Genuchten parameter α	α	1.43	[m^{-1}]
Van Genuchten parameter n	n	1.506	[$-$]

2.2.1.4 Results

Drainage was simulated for a period of 100 days, and the simulated water content at 1, 4, 2 and 100 days is given in Figure 2.4. The experimentally observed values of water content versus time are also shown. The numerical predictions are in good agreement with the experiment.

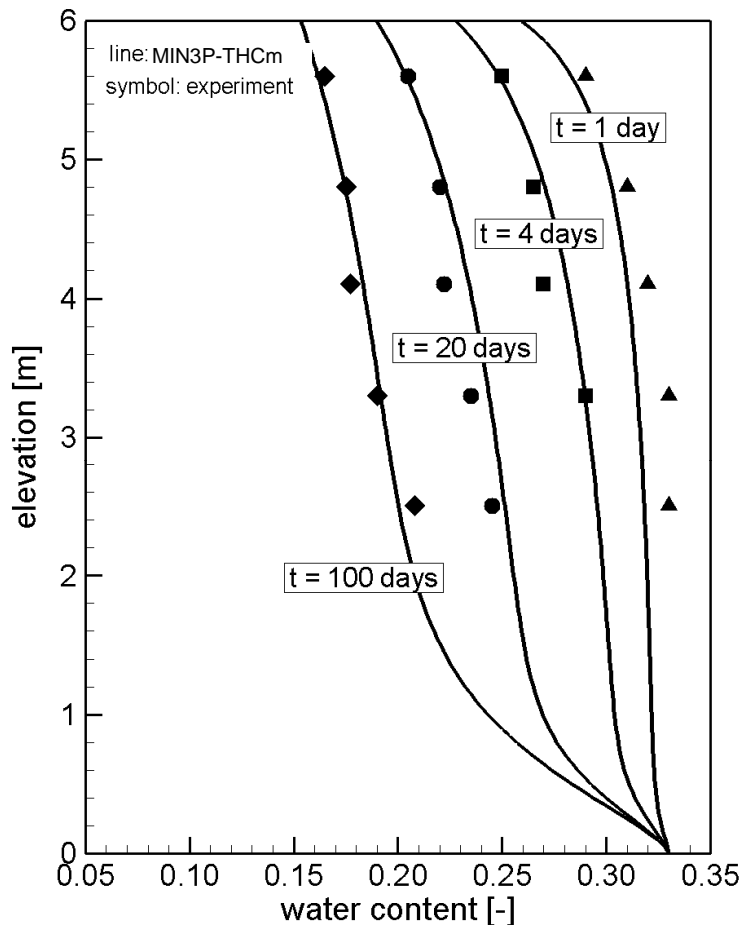


Figure 2.4 Comparison of Water Content Calculated by MIN3P-THCm vs Experimental Observation (drain1)

2.2.1.5 File locations

The input file is: *drain1.dat* under folder *.\benchmarks\benchmarks_standard\flow\drain1*

Validation report-page# 2-48

2.2.2 1D INFILTRATION IN SOIL COLUMN

2.2.2.1 Problem definition

This benchmark is a one dimensional drainage and infiltration problem reported by Forsyth et al (1995). It involves simulations of infiltration under constant inflow rate, following complete saturation.

2.2.2.2 Model setup

A 1D model with 6.0 m in depth is discretized into 121 control volumes yielding a discretization interval of 0.05 m for the interior control volumes and 0.025 m for the control volumes on the boundary. Initial condition for the flow problem is pressure head -7.25 m for the whole domain. Boundary conditions for the flow problem consist of an infiltration 2.31×10^{-6} m/s on the top boundary and pressure head -7.25 m on the bottom boundary.

2.2.2.3 Parameters

The physical parameters (material properties) used for the simulations are summarized in Table 2.14.

Table 2.14: Physical parameters for benchmark infill

Parameter	Symbol	Value	unit
Length of domain	L	6.0	[m]
Porosity	ϕ	0.33	[$-$]
Hydraulic conductivity	K_{zz}	2.896×10^{-6}	[$m s^{-1}$]
Residual saturation	S_{ra}	0.0	[$-$]
Van Genuchten parameter α	α	1.43	[m^{-1}]
Van Genuchten parameter n	n	1.506	[$-$]

2.2.2.4 Results

Infiltration was simulated for a period of 7.16 days, and the simulated saturation at 1.16 days, 4.16 days and 7.16 days is given in Figure 2.5. The numerical predictions are in good agreement with the results of HYDRUS reported by Forsyth et al (1995).

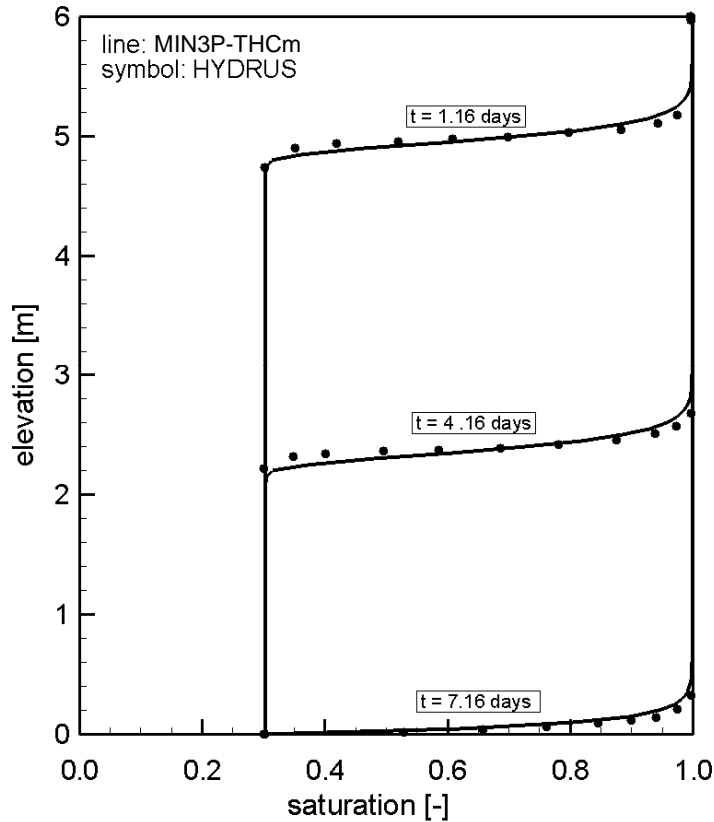


Figure 2.5: Comparison of Saturation Calculated by MIN3P-THCm vs HYDRUS (infil1)

2.2.2.5 File locations

The input file is: *infil1.dat* under folder *.\benchmarks\benchmarks_standard\flow\infil1*

2.2.3 1D DRAINAGE PROBLEM IN SAND COLUMN

2.2.3.1 Problem definition

This benchmark is a one dimensional drainage problem reported by Haverkamp et al (1977). It involves a simulation of water movement in a sand column with both saturated and unsaturated regions.

2.2.3.2 Model setup

A 1D model with 0.7 m in depth is discretized into 71 control volumes yielding a

Validation report-page# 2-50

discretization interval of 0.01 m for the interior control volumes and 0.005 m for the control volumes on the boundary. Initial condition for the flow problem is -0.615 m pressure head for the whole domain. Boundary conditions for the flow problem consist of a flux of 3.8×10^{-5} m s⁻¹ on the top boundary and a pressure head of -0.615 m at the bottom boundary.

2.2.3.3 Parameters

The physical parameters (material properties) used for the simulations are summarized in Table 2.15.

Table 2.15: Physical parameters for benchmark haverk

Parameter	Symbol	Value	unit
Length of domain	L	0.70	[m]
Porosity	ϕ	0.287	[\cdot]
Hydraulic conductivity	K_{zz}	9.44×10^{-5}	[m s ⁻¹]
Specific storage coefficient	S_s	1.0×10^{-3}	[m ⁻¹]
Residual saturation	S_{ra}	0.261	[\cdot]
Van Genuchten parameter α	α	3	[m ⁻¹]
Van Genuchten parameter n	n	4.4	[\cdot]

2.2.3.4 Results

Drainage was simulated for a period of 0.8 hours, and the simulated saturation at 0.1 to 0.8 hours is depicted in Figure 2.6. The experimentally observed values of saturation versus time are also shown. The numerical predictions are in good agreement with the results of HYDRUS.

2.2.3.5 File locations

The input file is: *haverk.dat* under folder *.\benchmarks\benchmarks_standard\flow\haverk-correct-upstream*

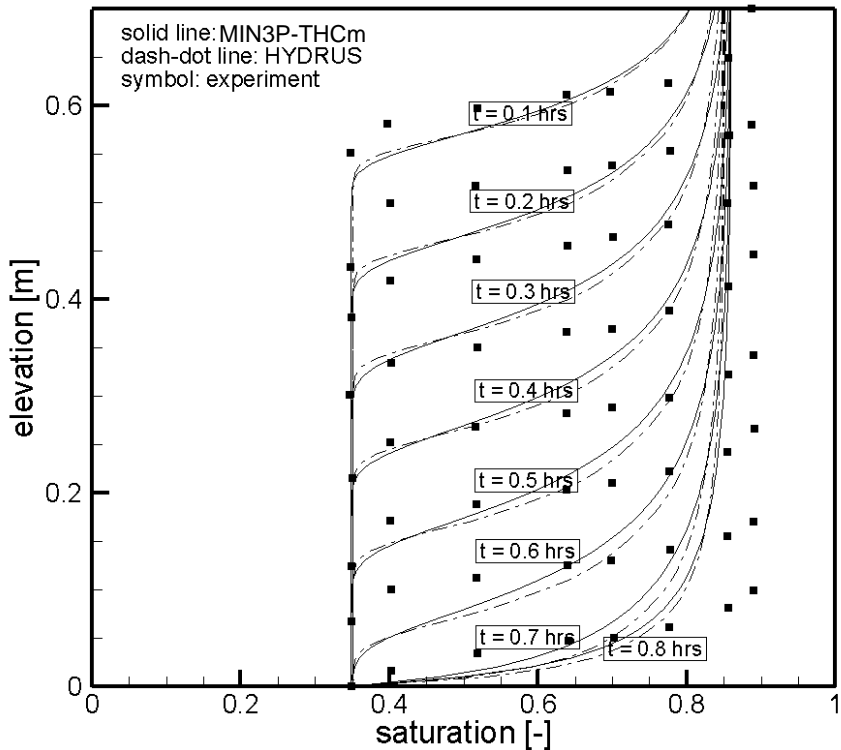


Figure 2.6 Comparison of Saturation Calculated by MIN3P-THCm vs HYDRUS and Experimental Observation (*haverk*)

2.2.4 2D TRANSIENT WATER TABLE MOUNDING

2.2.4.1 Problem definition

This benchmark is a two dimensional water flow problem reported by Vauclin et al (1979) in relation to the recharge of a water table aquifer. The approach is based on the physics of water transfer in the complete domain defined by both the saturated and unsaturated zones of soil. The schematic diagram of the flow domain and experimental details are given in Figure 2.7.

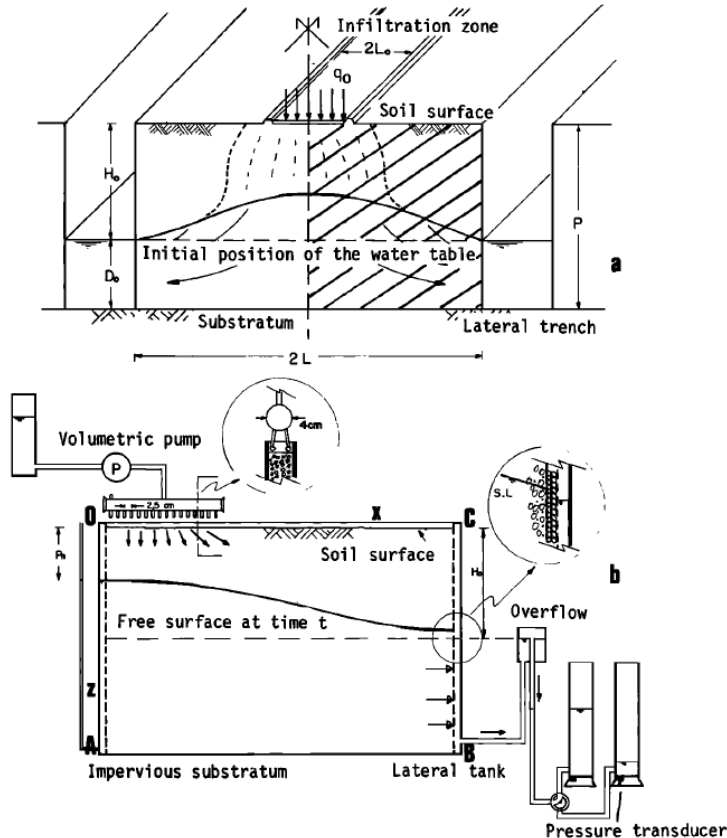


Figure 2.7 (a) Schematic diagram of the flow domain. (b) Experimental details and numerical simulation domain (Vauclin et al., 1979)

2.2.4.2 Model setup

A 2D model with 3.0 m in width and 2.0 m in height is discretized into 1271 control volumes yielding a discretization interval of horizontal 0.1 m and vertical 0.05 m for the interior control volumes and horizontal 0.05 m and vertical 0.025 m for the control volumes on the boundary. Initial condition for the flow problem is 0.65 m hydraulic head for the whole domain. Boundary conditions for the flow problem consist of a flux 4.11×10^{-5} m/s on the left-top boundary (0.5 m) and hydraulic head 0.65 m on the right side boundary.

2.2.4.3 Parameters

The physical parameters (material properties) used for the simulations are summarized in Table 2.16.

Table 2.16: Physical parameters for benchmark clement

Parameter	Symbol	Value	unit
Width of domain	L	3.0	[m]
Height of domain	L	2.0	[m]
Porosity	ϕ	0.3	[-]
Hydraulic conductivity	K_{zz}, K_{xx}	9.72×10^{-5}	[m s ⁻¹]
Specific storage coefficient	S_s	0.0	[m ⁻¹]
Residual saturation	S_{ra}	0.01	[-]
Van Genuchten parameter α	α	3.3	[m ⁻¹]
Van Genuchten parameter n	n	4.1	[-]

2.2.4.4 Results

Water flow was simulated for a period of 8 hours, and the simulated hydraulic head contours after 8 hours is given in Figure 2.8. The numerical predictions are in excellent agreement with the experiment results provided by Vauclin et al (1979).

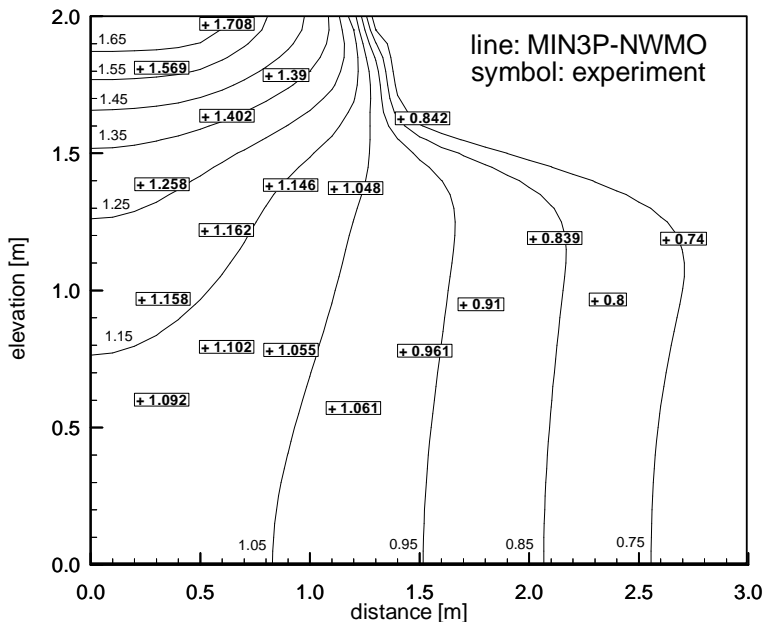


Figure 2.8 Comparison of hydraulic head contours after 8 hours calculated by MIN3P-THCm vs experimental observation

2.2.4.5 File locations

The input file is: *clement.dat* under folder
.\benchmarks\benchmarks_standard\flow\clement

2.2.5 1D WATER VAPOR MOVEMENT

2.2.5.1 Problem definition

This benchmark is a 1D water vapor flow reported by Mizayaki (1976), demonstrating condensation and movement of water vapor in sand under a temperature gradient.

2.2.5.2 Model setup

A 1D model with 0.1 m in depth is discretized into 150 control volumes yielding a discretization interval of 6.67×10^{-4} m for the interior control volumes and 3.33×10^{-4} m for the control volumes on the boundary. Initial condition of pressure head is -7000 m and initial condition of temperature is 23.5 °C for the whole domain. Boundary conditions for the verification problem consist of an atmospheric conditions at the top boundary and -0.27 m pressure head on the bottom boundary. Boundary conditions for temperature are 36.3 °C at the top boundary and 23.5 °C at the bottom boundary.

2.2.5.3 Parameters

The physical parameters (material properties) used for the simulations are summarized in Table 2.17.

Table 2.17: Physical parameters for benchmark verif-evap

Parameter	Symbol	Value	Unit
Length of domain	L	0.10	[m]
Porosity	ϕ	0.325	[\cdot]
Hydraulic conductivity	K_{zz}	4.0×10^{-4}	[$m s^{-1}$]
Specific storage coefficient	S_s	0.0	[m^{-1}]
Residual saturation	S_{ra}	0.083	[\cdot]
Van Genuchten parameter α	α	6.56	[m^{-1}]
Van Genuchten parameter n	n	4.71	[\cdot]
Specific heat of water	c_w	4180	[$J Kg^{-1} ^\circ C^{-1}$]
Specific heat of vapour	c_v	630	[$J Kg^{-1} ^\circ C^{-1}$]
Specific heat of solid	c_s	1920	[$J Kg^{-1} ^\circ C^{-1}$]
Water thermal conductivity in z-direction	λ_w	0.60	[$W m^{-1} ^\circ C^{-1}$]
Solid thermal conductivity in z-direction	λ_s	1.40	[$W m^{-1} ^\circ C^{-1}$]

2.2.5.4 Results

Water vapor flow was simulated for a period of 30 days, and the simulated water content at 5, 10, 16 and 30 days is given in Figure 2.9. The experimentally observed values of water content versus time are also shown. The numerical predictions are in good agreement with the experiment.

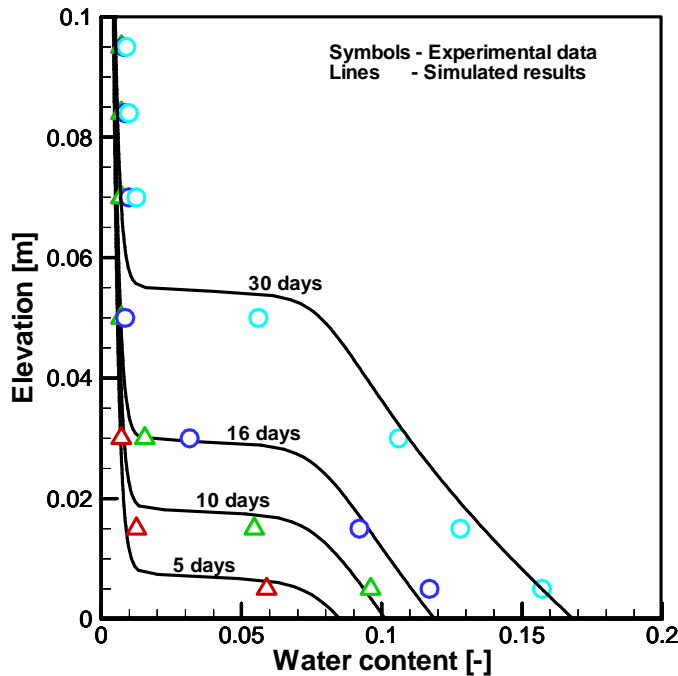


Figure 2.9 Comparison of Water Content Calculated by MIN3P-THCm vs Experimental Observation

2.2.5.5 File locations

The input file is: *verif-evap.dat* under folder
`.\benchmarking_nwmo_report\verification_examples\miyazaki1976`

2.3 DENSITY DEPENDENT FLOW AND CONSERVATIVE SOLUTE TRANSPORT

This section describes the verification of the equations implemented in MIN3P-THCm for simulating coupled density-driven flow and solute transport. Two verified benchmarking problems are presented to document the accuracy of MIN3P-THCm. The emphasis is placed on benchmarking problems with solutions constrained by established mathematical results.

The Elder fluid convection benchmarking problem (Elder, 1967), for which an exact solution does not exist (Diersch and Kolditz, 2002), was included in the current evaluation due to its extensive use in model benchmarking (Oldenburg and Pruess, 1995; Ackerer et

Validation report-page# 2-56

al., 1999; Oltean and Buès, 2001; Frolkovic and Schepper, 2001; Diersch and Kolditz, 2002; Simpson and Clement, 2003). MIN3P-THCm results for the modified Henry seawater intrusion problem (Henry, 1964; Simpson and Clement, 2004) were benchmarked against a published semi-analytic solution.

The verification examples for density dependent flow problems are listed in Table 2.18.

Table 2.18: List of density dependent flow benchmarks

Name	Description of Main Features	Verification Type	Section
elder	Elder problem (2D fluid convection driven by a thermal gradient)	2	2.3.1
henry	Modified Henry problem (2D lateral saltwater intrusion into aquifer)	1	2.3.2

2.3.1 ELDER PROBLEM

2.3.1.1 Problem definition

This benchmark is a 2D density dependent flow problem reported by Voss and Souza (1987) based on laboratory investigations of fluid convection driven by a thermal gradient (Elder, 1967). It tests 2D fluid convection resulting from solute concentration gradients. Simulated results were compared to the simulations by software d³f (Frolkovic and Schepper, 2001).

2.3.1.2 Model setup

The Elder problem domain consists of a two-dimensional vertical cross-section depicting a zone of freshwater underlying a source of brines. The domain is in 300 m horizontal by 150 m vertical, and discretized using a 8192-node grid with $\Delta x = \Delta z = 2.4$ m. A constant concentration of 0 g l^{-1} was assigned to the entire bottom boundary and C_s on the half upper right boundary. No flow boundaries were assigned to all four sides of the domain. A constant fluid pressure of 0 Pa was assigned to the upper left corner of the domain (Voss and Souza, 1987). The model domain and boundary conditions for the Elder problem are illustrated in Figure 2.10.

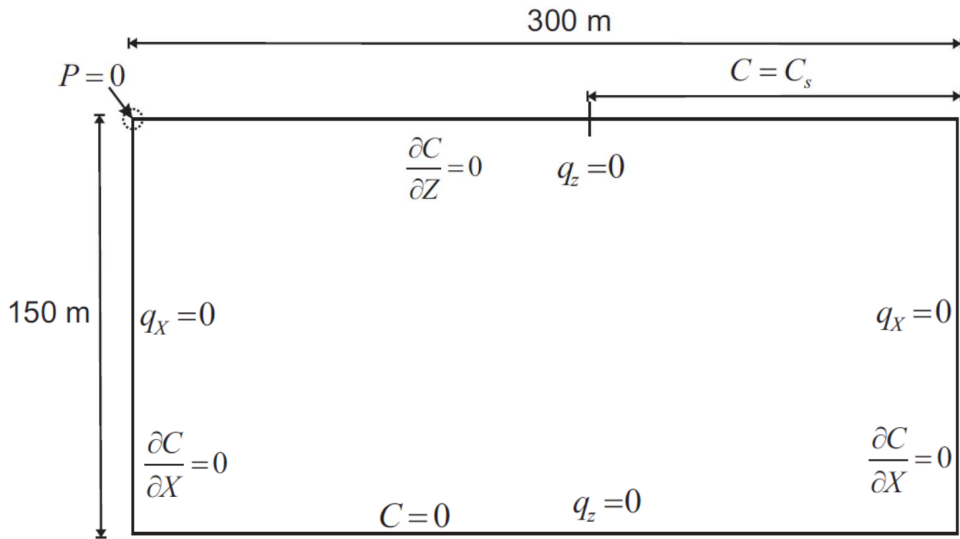


Figure 2.10 Elder problem domain and boundary conditions (Bea et al., 2011)

2.3.1.3 Parameters

The Elder problem was simulated for a period of 20 years using the parameter values presented by Voss and Souza (1987). The Van Leer (1974) flux limiting scheme was used in MIN3P-THCm to simulate advective solute transport. The flow and transport parameters are summarized in Table 2.19.

Table 2.19: Parameters for Elder Convection Problem (Bea et al., 2011)

Parameter	Symbol	Value	Units
Hydraulic conductivity	K	4.75×10^{-6}	[m s ⁻¹]
Porosity	ϕ	0.1	[⁻]
Specific storage	S _s	0.0	[m ⁻¹]
Longitudinal dispersivity	α_l	0.0	[m]
Transverse dispersivity	α_t	0.0	[m]
Molecular diffusion coefficient	D ₀	0.0	[m ² s ⁻¹]
Saltwater density	ρ_s	1200	[kg m ⁻³]
Freshwater density	ρ_0	1000	[kg m ⁻³]
Maximum density ratio	ρ_{max}	1.2	[⁻]
Coefficient of density variation	$\partial \rho / \partial c$	0.7	[⁻]
Saltwater concentration	C _s	285.7	[g L ⁻¹]

2.3.1.4 Results

Figure 2.11 compares MIN3P-THCm solute concentration results with published results of the d³f simulator for the same level of grid discretization (Frolkovic and Schepper, 2001). The d³f model was selected for the current comparison because it has provided the best

Validation report-page# 2-58

agreement with published saltpool upconing experiments (Diersch and Kolditz, 2002; Oswald and Kinzelbach, 2004). Figure 2.11 shows the results for simulation times of 4, 7, and 20 years, during which density-driven flow causes the development and downward movement of dense brine fingers. The two sets of results are in close agreement, and the stationary solute distribution at 20 years is consistent with other published results for a comparable level of grid discretization (Oldenburg and Pruess, 1995; Ackerer et al., 1999; Oltean and Buès, 2001).

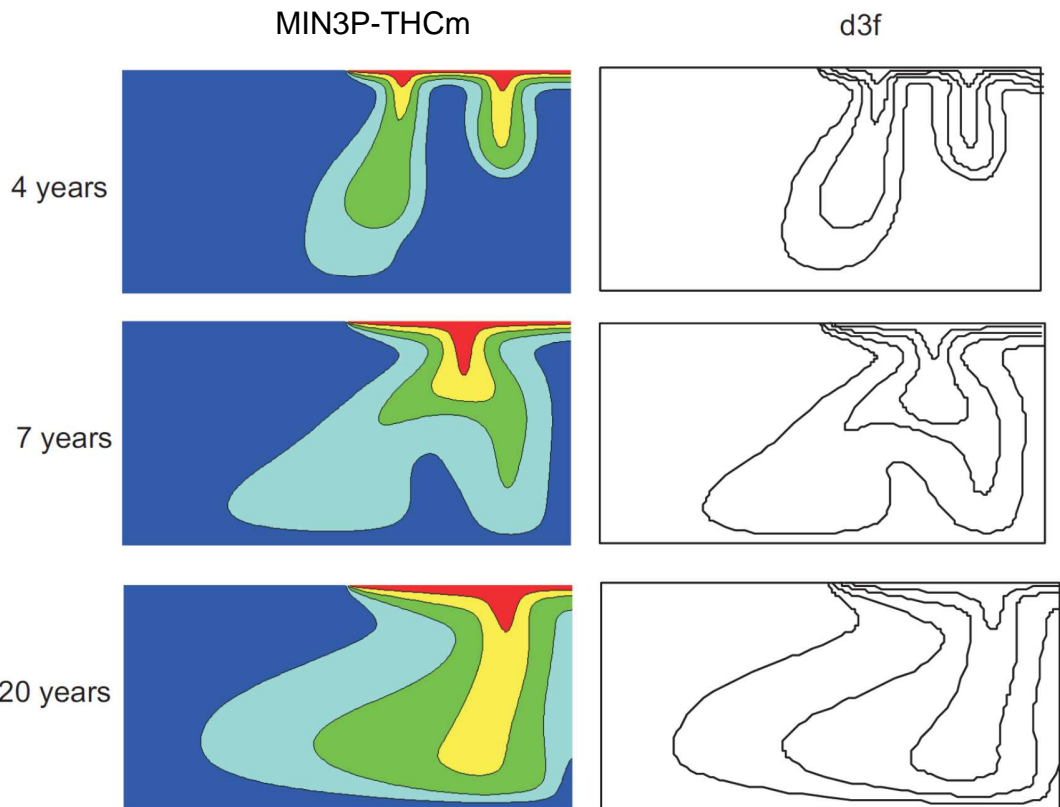


Figure 2.11 Solute concentration results for the Elder problem simulated by MIN3P-THCm (left) and d³f (right). The relative concentration contours are, from top to bottom, 0.8, 0.6, 0.4 and 0.2 of the saltwater source concentration (Bea et al., 2011)

2.3.1.5 File locations

The input file can be found under

`\benchmarking_nwmo_report\ nwmo_verification_examples\d32_elder_problem\elder.dat`

Database directory is a subfolder under the folder of the input file: `\database\kmno4_unix`

2.3.2 MODIFIED HENRY PROBLEM

2.3.2.1 Problem definition

The Henry problem (Henry, 1964) depicts lateral saltwater intrusion into a homogeneous confined aquifer and the development of a mixing zone between freshwater and saltwater. The Henry problem has been widely used as a test case of density-dependent groundwater flow models (e.g. Kipp, 1986; Voss and Souza, 1987; Ackerer et al., 1999; Guo and Langevin, 2002). However, the merits of this problem for code benchmarking have been scrutinized due to the weak coupling between flow and solute transport (Simpson and Clement, 2003). Simpson and Clement (2004) proposed a modification to the Henry problem, reducing the constant freshwater flux by 50%, to increase the coupling between fluid flow and solute transport and thus the numerical difficulty. This modified problem definition was used to benchmark MIN3P-THCm (Bea et al., 2011).

2.3.2.2 Model setup

The domain consists of a two-dimensional vertical cross-section, bounded on the top and bottom by no flow boundaries (Figure 2.12A). A constant freshwater flux is applied to the left boundary, representing aquifer flow. The right model boundary represents a hydrostatic column of seawater, with a fixed concentration. The model domain is 2 m horizontal by 1 m vertical, and was discretized using a uniform grid with 861 control volumes with $\Delta x = \Delta z = 0.05$ m.

2.3.2.3 Parameters

The MIN3P-THCm simulation of the modified Henry problem was performed using the parameter values provided by Simpson and Clement (2004). The flow and transport parameters are summarized in Table 2.20. The Henry problem was simulated for a period of 0.833 days, representing the point at which a stationary solute distribution was achieved.

Table 2.20: Parameters for Modified Henry Saltwater Intrusion Problem (Bea et al., 2011)

Parameter	Symbol	Value	Units
Hydraulic conductivity	K	10^{-2}	[m s ⁻¹]
Porosity	ϕ	0.35	[⁻]
Specific storage	S_s	0.0	[m ⁻¹]
Longitudinal dispersivity	α_l	0.0	[m]
Transverse dispersivity	α_t	0.0	[m]
Molecular diffusion coefficient	D_0	1.89×10^{-5}	[m ² s ⁻¹]
Freshwater flux per unit width	q_x	3.3×10^{-5}	[m s ⁻¹]
Saltwater density	ρ_s	1025	[kg m ⁻³]
Freshwater density	ρ_0	1000	[kg m ⁻³]
Maximum density ratio	ρ_{\max}	1.025	[⁻]
Coefficient of density variation	$\partial \rho / \partial c$	0.7125	[⁻]
Saltwater concentration	C_s	35.0	[g L ⁻¹]

2.3.2.4 Results

Figure 2.12B compares the MIN3P-THCm simulation results with results from the semi-analytical solution presented by Simpson and Clement (2004). The results show the encroachment of a wedge of saltwater into the freshwater aquifer, in the opposite direction of groundwater flow. The MIN3P-THCm results are in excellent agreement with the semi-analytical solution given by Simpson and Clement (2004).

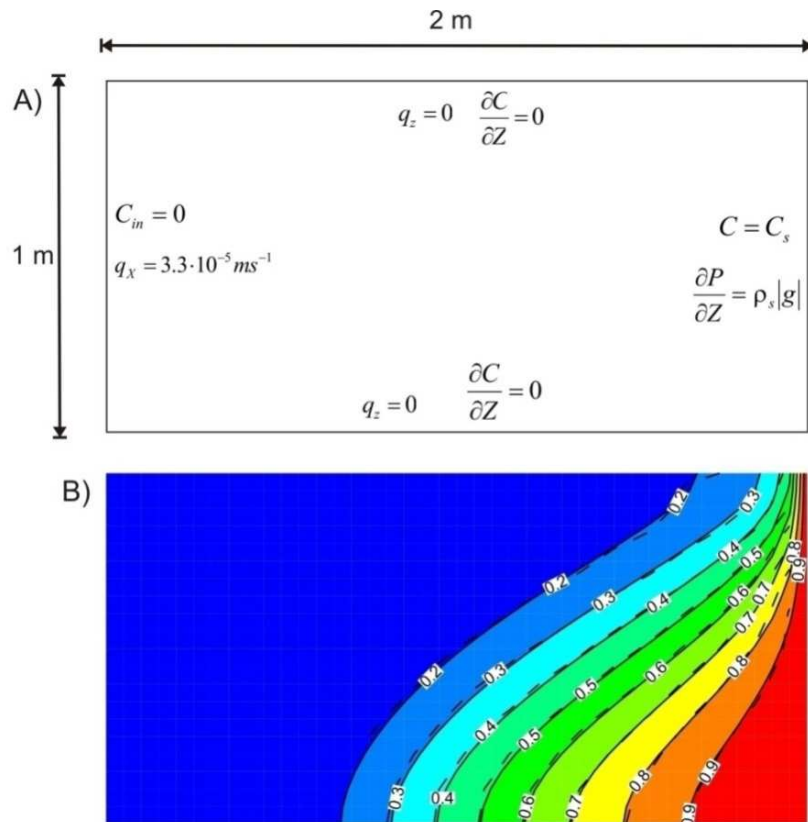


Figure 2.12 The modified Henry problem for lateral saltwater intrusion. (A) Simulation domain with flow and transport boundary conditions. (B) Relative solute concentration results at 0.833 d for MIN3P-THCm (solid lines) and the semi-analytical solution of Simpson and Clement (2004) (dashed lines) (Bea et al., 2011)

2.3.2.5 File locations

The input file can be found under

`..\benchmarking_nwmo_report\nwmo_verification_examples_D33\d33_modified_henry_problem\henry.dat`

Database directory is a subfolder under the folder of the input file: `\database\kmno4_unix`

2.4 ENERGY BALANCE

The validation and verification of the energy transport equations (and their coupling with the fluid and solute transport equations) implemented in MIN3P-THCm was carried out by the comparisons of the simulated results by MIN3P-THCm to results by analytical or calculated by other codes published in the literature (e.g. salt-dome thermo-haline convection) (Bea et al., 2011). The validation and verification examples of energy balance problems are listed in Table 2.21.

Table 2.21: List of energy balance benchmarks

Name	Description of Main Features	Verification Type	Section
radial-flow	flow with energy transport (1D radial)	1	2.4.1
verif-sutra	aquifer thermal energy storage (2D radial)	2	2.4.2
henry-hilleke	Henry-Hilleke problem (2D)	1 and 2	2.4.3
thermohaline	Thermal-haline convection (2D)	2	2.4.4
salt-dome	Salt dome problems	2	2.4.5

2.4.1 RADIAL FLOW WITH ENERGY TRANSPORT (ANALYTICAL SOLUTION)

2.4.1.1 Problem definition

The first problem involves radial groundwater flow with energy transport as presented by Voss and Provost (2008). The problem domain consists of a confined aquifer of thickness b [m], with a fully penetrating injection well (see Figure 2.13B). Fluid is injected at a rate Q , with a temperature of T^* , into the aquifer which is initially at a uniform temperature of T_0 . For this problem, the fluid density and viscosity are approximately constant because the injected fluid temperature differs only slightly from the ambient fluid temperature; i.e., (T^*-T_0) is small.

2.4.1.2 Model setup

The mesh consists of one row of elements with element width expanding from $\Delta r_{\min}=2.5$ [m] by a factor 1.06, to $r=395.0$ [m], and then maintaining constant element width of $\Delta r=24.2$ [m] to $r_{\max}=1000.0$ [m]. Element height, b , is 10.0 [m]. Mesh thickness is set for radial coordinates, $B_i=2\pi r_i$ (Voss and Provost, 2008). For comparison of the results, the output time levels were set the same as those in Voss and Provost (2008), which used a constant time step at $\Delta t=4021.0$ [s] and outputs are obtained for times steps numbered 225, 450, 900, 1800, corresponding to 10.5, 21, 42 and 84 days.

2.4.1.3 Parameters

The parameters used for the simulation were listed in Table 2.22.

Validation report-page# 2-62

Table 2.22: Parameters for Radial Flow Problem with Energy Transport (Bea et al., 2011)

Parameter	Value	Unit
Solid density	2650	[kg m ⁻³]
Fresh-water density	1000	[kg m ⁻³]
Injection rate Q	312.15	[kg s ⁻¹]
Porosity	0.2	[-]
Permeability	1.02×10^{-11}	[m ²]
Water specific thermal capacity	4182	[J kg ⁻¹ °C ⁻¹]
Solid specific thermal capacity	840	[J kg ⁻¹ °C ⁻¹]
Water thermal conductivity	0.6	[J s ⁻¹ m ⁻¹ °C ⁻¹]
Solid thermal conductivity	3.5	[J s ⁻¹ m ⁻¹ °C ⁻¹]
Heat capacity of water	4182	[J kg ⁻¹ °C ⁻¹]
T ₀ (initial condition in aquifer)	0	[°C]
T* (injected water)	1	[°C]
$\frac{\partial \rho}{\partial TDS}$	0	[-]
$\frac{\partial \rho}{\partial T}$	0	[kg m ⁻³ °C ⁻¹]
α_L	4	[m]
α_T	1	[m]

2.4.1.4 Results

MIN3P-THCm results are compared with an approximate analytical solution from Gelhar and Collins (1971), as modified by Voss and Provost (2008):

$$\left(\frac{T - T_0}{T^* - T_0} \right) = \frac{1}{2} erfc \left[\frac{r^2 - (r^*)^2}{2 \sqrt{\left(\frac{4}{3} \alpha_L \right) (r^*)^3 + \left(\frac{\lambda_{aq}}{A_T} \right) (r^*)^4}} \right] \quad \text{Equation 1-1}$$

where the parameter A_T is defined by:

$$A_T = \frac{\phi \alpha_w}{c_{aq}} A \quad \text{Equation 1-2}$$

with A given by:

$$A = \frac{Q}{2\pi \phi b \rho} \quad \text{Equation 1-3}$$

and c_{aq} defined as:

Validation report-page# 2-63

$$c_{aq} = \phi \rho c_w + (1 - \phi) \rho_s c_s \quad \text{Equation 1-4}$$

The parameters λ_{aq} and r^* in Equation 1-1 are given by:

$$\lambda_{aq} = \phi \lambda_w + (1 - \phi) \lambda_s \quad \text{Equation 1-5}$$

$$r^* = \sqrt{2A_T t} \quad \text{Equation 1-6}$$

where ρ is the fluid density [$M\ L^{-3}$], α_L is the longitudinal dispersivity [L], c_{aq} , c_w and c_s are the heat capacities for the aquifer, fluid and solid, respectively [$L^2\ T^{-2}\ \Theta^{-1}$], and λ_{aq} , λ_w and λ_s are thermal conductivities for the aquifer, fluid and solid, respectively [$L\ M\ T^{-3}\ \Theta^{-1}$].

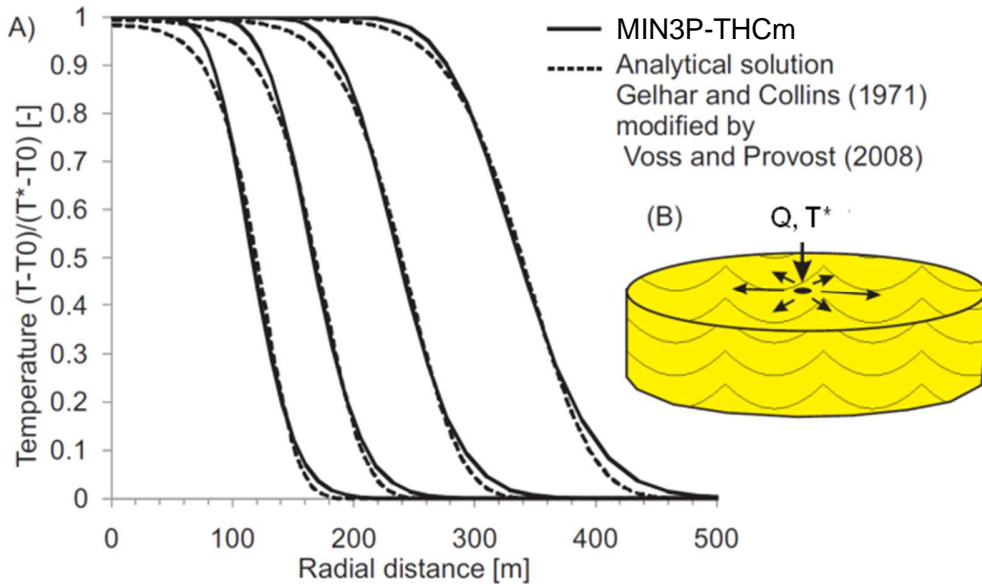


Figure 2.13 Temperature profiles at 10.5, 21, 42 and 84 days (from left to right) for the radial flow with energy transport benchmark. A) MIN3P-THCm results (solid lines) are compared with the analytical solution (dashed lines) presented by Gelhar and Collins (1971), as modified by Voss and Provost (2008). B) Idealized representation of the domain (Bea et al., 2011)

2.4.1.5 File locations

The input file can be found under

Validation report-page# 2-64

..\benchmarking_nwmo_report\ nwmo_verification_examples_D4\d41_radial_flow_energy\ \radial-flow.dat

Database directory is a subfolder under the folder of the input file: \database\default

2.4.2 AQUIFER THERMAL ENERGY STORAGE (2D RADIAL)

2.4.2.1 Problem definition

This verification example includes density-dependent flow and energy transport (aquifer thermal energy storage) in radial coordinate. Hot water was injected into an aquifer for storage (injection stage for 90 days) and later withdrawn as an energy source (pumping for 90 days). A code intercomparison was conducted with SUTRA (Voss and Provost, 2008).

2.4.2.2 Model setup

The mesh is 30.0 [m] in height discretized into 10 control volumes and 246.0 [m] in radial coordinate axial discretized into 35 control volumes (Figure 2.14).

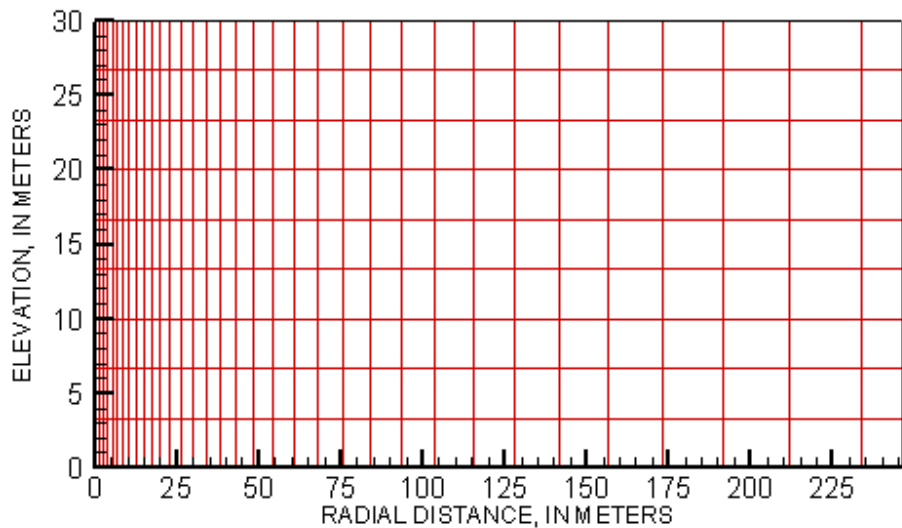


Figure 2.14 2D mesh for the aquifer thermal energy storage problem

2.4.2.3 Parameters

Model parameters are provided in Table 2.23.

Validation report-page# 2-65

Table 2.23: Parameters for aquifer thermal energy storage problem (density-dependent Flow and energy transport) (Bea et al., 2011)

Parameter	Value	Unit
Solid density	2650	[kg m ⁻³]
Fresh-water density	1000	[kg m ⁻³]
Injection rate Q_{in}	200	[kg s ⁻¹]
Porosity	0.35	[-]
Permeability	1.02×10^{-10}	[m ²]
Water specific thermal capacity	4182	[J kg ⁻¹ °C ⁻¹]
Solid specific thermal capacity	840	[J kg ⁻¹ °C ⁻¹]
Water thermal conductivity	0.6	[J s ⁻¹ m ⁻¹ °C ⁻¹]
Solid thermal conductivity	3.5	[J s ⁻¹ m ⁻¹ °C ⁻¹]
Heat capacity of water	4182	[J kg ⁻¹ °C ⁻¹]
T_0	20	[°C]
T_{in}	60	[°C]
$\frac{\partial \rho}{\partial TDS}$	0	[-]
$\frac{\partial \rho}{\partial T}$	-0.375	[kg m ⁻³ °C ⁻¹]
α_L	4	[m]
α_T	1	[m]

2.4.2.4 Results

Simulation results at 30 and 90 days during the injection stage are shown in Figure 2.15. Results at 30 and 90 days into the pumping stage are shown in Figure 2.16. The MIN3P-THCm results are compared with results obtained with the numerical model SUTRA (Voss and Provost, 2008), with equivalent spatial discretization. To test the influence of the density weighting in the Darcy flux terms, the MIN3P-THCm simulations were conducted using both upstream and centered weighting.

Figure 2.15 and Figure 2.16 show that the centered weighting scheme produces less numerical dispersion in the thermal transition zone, and overall provides results which agree better with the SUTRA. The thermal transition zone widens throughout the injection-production cycle, due to both dispersion and heat conduction. The top of the transition zone tips away from the well during the entire cycle, due to the buoyancy of the hotter water. The combination of these two effects causes cooler water to reach the bottom of the withdrawal well much earlier than if density differences had been ignored.

Validation report-page# 2-66

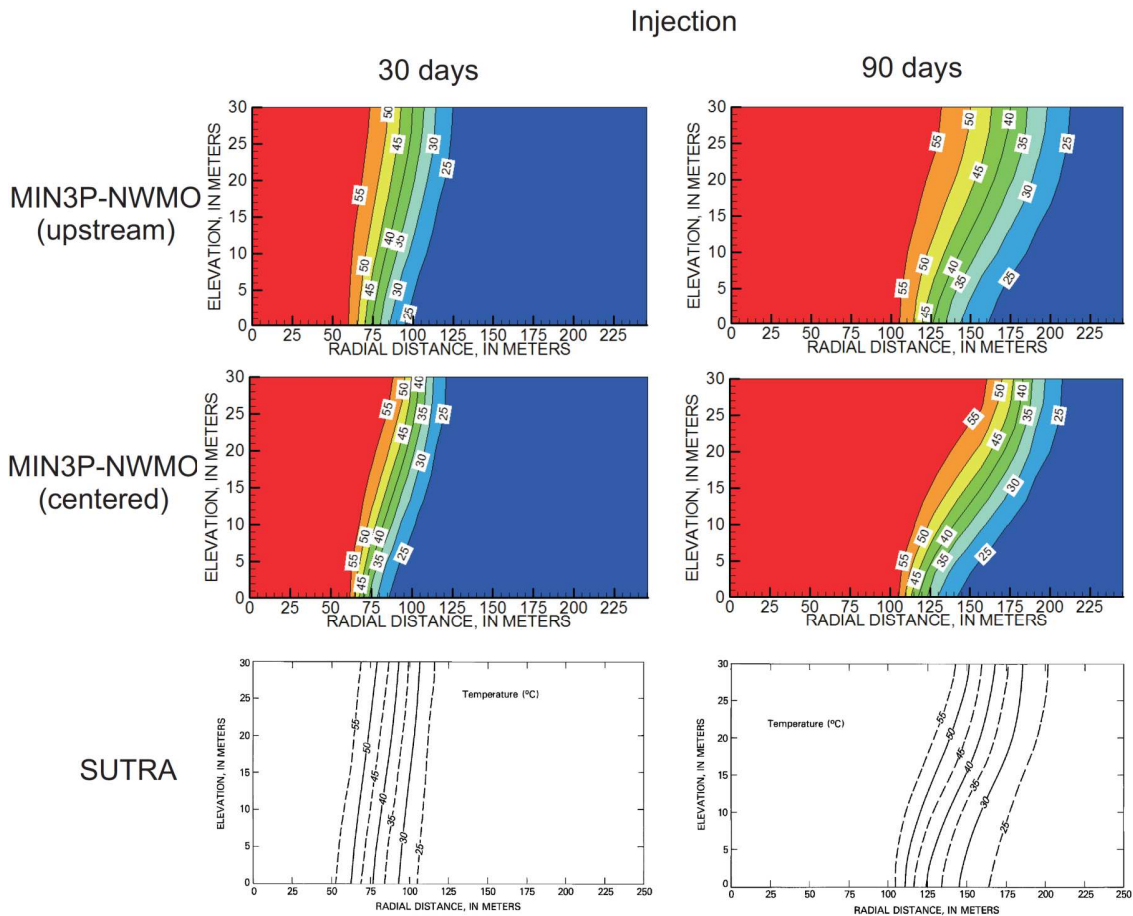


Figure 2.15: Verification of density-dependent radial flow and energy transport (aquifer thermal storage) during hot water injection. MIN3P-THCm results using upstream and centered weighting are compared with SUTRA (Bea et al., 2011)

Validation report-page# 2-67

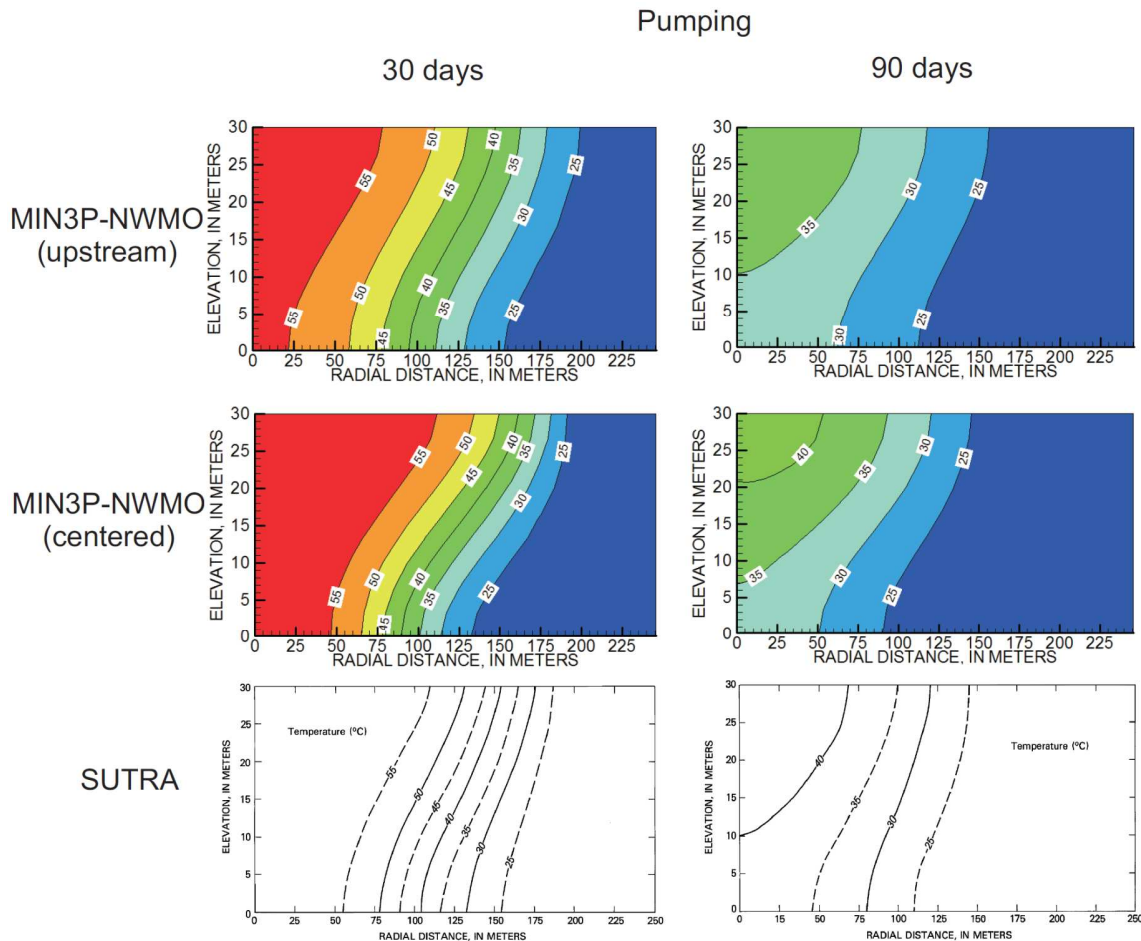


Figure 2.16: Verification of density-dependent radial flow and energy transport (aquifer thermal storage) during groundwater withdrawal. MIN3P-THCm results using upstream weighting and centered weighting are compared with SUTRA (Bea et al., 2011)

2.4.2.5 File locations

The input files (upstream) can be found under

```
..\benchmarking_nwmo_report\nwmo_verification_examples_D4\d42_density_dep_energ
y\upstream\injection (or pumpin)\verif-sutra
```

Database directory is a subfolder under the folder of the input file: \database\default

The input files (centered) can be found under

```
..\benchmarking_nwmo_report\nwmo_verification_examples_D4\d42_density_dep_energ
y\centered\injection (or pumpin)\verif-sutra
```

Database directory is a subfolder under the folder of the input file: \database\default

2.4.3 DENSITY DEPENDENT FLOW WITH HEAT AND SOLUTE TRANSPORT (HENRY-HILLEKE PROBLEM)

2.4.3.1 Problem definition

This benchmark considers seawater intrusion into a non-isothermal confined aquifer under transient conditions (Henry and Hilleke, 1972). Freshwater flows from an inland boundary over dense saline water, which enters from a seaward boundary, and discharges in the upper portions of the vertical seaward boundary.

2.4.3.2 Model setup

The benchmark simulated in a two-dimensional cross section (in 1.0 m in length and 1.0 m in height). An aspect ratio equal to unity and a spatial discretization about 0.025 m for horizontal and vertical direction are used. Initially, hydrostatic pressure conditions are present throughout the aquifer with linear variations of seawater concentrations and temperatures (see Figure 2.17A and Figure 2.17B).

2.4.3.3 Problem definition

Model parameters are tabulated in Table 2.24.

Table 2.24: Parameters for Henry-Hilleke problem (density-dependent flow, heat and solute transport) (Bea et al., 2011)

Parameter	Value	Unit
Solid density	2600	[kg m ⁻³]
Fresh-water density	1000	[kg m ⁻³]
Sea-water density	1024.99	[kg m ⁻³]
Dynamic fluid viscosity	10 ⁻³	[kg m ⁻¹ s ⁻¹]
Concentration C _s	35.7	[kg m ⁻³]
Concentration C _{in}	0	[kg m ⁻³]
Injection rate Q _{in}	8.33×10 ⁻⁶	[kg s ⁻¹]
Porosity	0.35	[−]
Permeability	1.2×10 ⁻⁹	[m ²]
Diffusion- dispersion (solute transport)	2.38×10 ⁻⁵	[m ² s ⁻¹]
Diffusion- dispersion (energy transport)	2.38×10 ⁻⁴	[m ² s ⁻¹]
Water thermal conductivity	995.73	[J s ⁻¹ m ⁻¹ °C ⁻¹]
Solid thermal conductivity	0	[J s ⁻¹ m ⁻¹ °C ⁻¹]
Specific heat capacity of water	4182	[J kg ⁻¹ °C ⁻¹]
Rock Density	2650	[kg m ⁻³]
Tmin	5	[°C]
Tmax	50	[°C]
$\frac{\partial \rho}{\partial TDS}$	0.7	[−]
$\frac{\partial \rho}{\partial T}$	-0.375	[kg m ⁻³ °C ⁻¹]

Validation report-page# 2-69

2.4.3.4 Results

Results obtained with MIN3P-THCm are compared with SUTRA-MS (Hughes and Sanford, 2004) and HST3D (Kipp, 1986) and are shown in Figure 2.17. The original results by Henry and Hilleke (1972) are also shown for 50% of seawater density and temperature increase (continuous red line). The results show that at time zero, heat begins to be transported inward from the top, bottom, and left boundaries, and seawater begins to intrude the freshwater system by moving in laterally under the freshwater from the seawater boundary. Seawater intrusion in the aquifer is primarily the result of the greater density of the seawater. Lateral temperature variations at the top and bottom of the aquifer and vertical temperature variations at the freshwater boundary increase vertical freshwater fluid movement and intrusion of seawater at the base of the aquifer when compared to a similar isothermal case (not shown). As shown in Figure 2.17, simulated temperatures for MIN3P-THCm, SUTRA-MS and HST3D compare favorably with each other. The MIN3P-THCm results show more solute dispersion in comparison with the other models, which is likely due to the use of upstream weighting in the transport equations.

2.4.3.5 File locations

The input file can be found under

`..\benchmarking_nwmo_report\ nwmo_verification_examples_D4\d43_density_dep_heat_solute\henry-hilleke.dat`

Database directory is a subfolder under the folder of the input file: `\database\default`

Validation report-page# 2-70

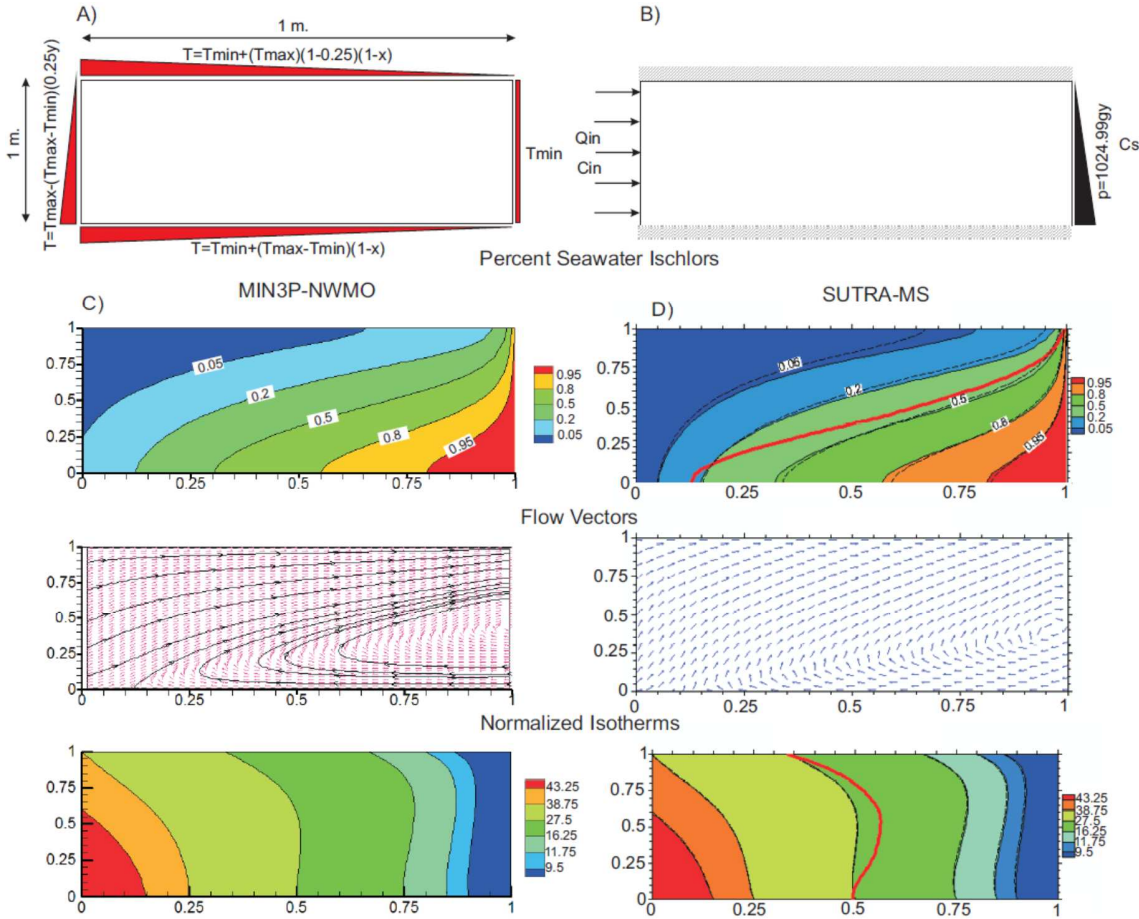


Figure 2.17: Verification of density-dependent flow, heat transport and solute transport (Henry-Hilleke problem). A) Domain and energy transport boundary conditions. B) Flow and solute transport boundary conditions. C) and D) Percent seawater isochlors, flow vectors, and normalized isotherms results obtained by MIN3P-THCm (left), SUTRA-MS and HST3D (right), respectively. SUTRA-MS results are represented as continuous lines. The continuous red line corresponds to the Henry and Hilleke numerical solution (0.5 percent seawater concentration and isotherm only), the HST3D code solution is presented by the dashed black line (Bea et al., 2011).

2.4.4 THERMO-HALINE CONVECTION

2.4.4.1 Problem definition

Thermo-haline examples are commonly used in the validation of coupled thermal-hydraulic and transport models (e.g. Oldenburg and Pruess, 1998; 1999; Geiger et al., 2006). In these types of problems the flow and transport equations are strongly coupled through the temperature and salinity control on fluid density (ρ) and viscosity (μ). Here, a thermal convection example involving the separation of a thermal plume and a salt plume by transient thermo-haline double-advection convection, for a NaCl–CaCl₂-H₂O system,

Validation report-page# 2-71

was simulated. Although this problem was initially studied numerically by Oldenburg and Pruess (1999), results are compared with more recent work (Geiger et al., 2006).

2.4.4.2 Model setup

In the present work, different equations of state for the NaCl-CaCl₂-H₂O system are used (i.e. HMW (Harvie et al., 1984) model based on Pitzer equations (Pitzer, 1973, 1991; Pitzer and Kim 1974), but the differences with respect to the equations of state presented by Oldenburg and Pruess (1999) and Geiger et al. (2006) are small. The domain and boundary conditions for this example are shown in Figure 2.18. In this case, the domain was uniformly discretized using 64 cells resulting with a grid spacing of about 39 m, which is similar to the discretization used by Geiger et al. (2006).

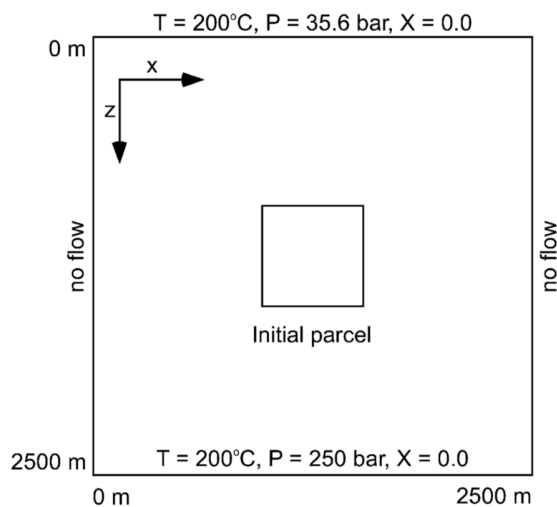


Figure 2.18: Domain and boundary conditions for the transient thermohaline convection problems as given in Oldenburg and Pruess (1999), X relates to the mass fraction of brine to groundwater in relation to the source region (X = 1 in source) (Bea et al., 2011)

2.4.4.3 Parameters

Key parameter values are provided in Table 2.25.

2.4.4.4 Results

Results for two different initial conditions (i.e. either positive or negative initial buoyancy in the central region of the domain) are shown in Figure 2.19 and Figure 2.20. Overall there is good agreement between the two sets of numerical simulations for both fluid density and temperature. For the initially negatively buoyant case (see Figure 2.19), thermal and brine plumes separate, and the high-density zone that evolves below the initial parcel location moves downward while the warm water plume rises after plume separation. For the initially positive buoyancy brine parcel (see Figure 2.20), the overall motion of

Validation report-page# 2-72

fluid is upward. In this case, because the temperature front is thermally retarded, a high fluid density zone is predicted to develop above a low-density region.

Table 2.25: Parameters for thermo-haline convection problems (Bea et al., 2011)

Parameter	Value	Unit
<i>Positive initial buoyancy</i>		
Initial parcel temperature	300	°C
Initial parcel brine mass fraction	0.14	[\cdot]
Initial parcel density	831	[kg m $^{-3}$]
<i>Negative initial buoyancy</i>		
Initial parcel temperature	250	°C
Initial parcel brine mass fraction	0.47	[\cdot]
Initial parcel density	919	[kg m $^{-3}$]
Reservoir temperature	200	°C
Reservoir initial mass fraction	0	[\cdot]
Reservoir liquid density	875	[kg m $^{-3}$]
Porosity	0.1	[\cdot]
Permeability	5×10^{-14}	[m 2]
Molecular diffusion	10^{-8}	[m 2 s $^{-1}$]
Formation conductivity	1.8	[J s $^{-1}$ m $^{-1}$ °C $^{-1}$]
Specific heat capacity of rock	1000	[J kg $^{-1}$ °C $^{-1}$]
Specific heat capacity of water	4184	[J kg $^{-1}$ °C $^{-1}$]
Bulk density of rock	2650	[kg m $^{-3}$]

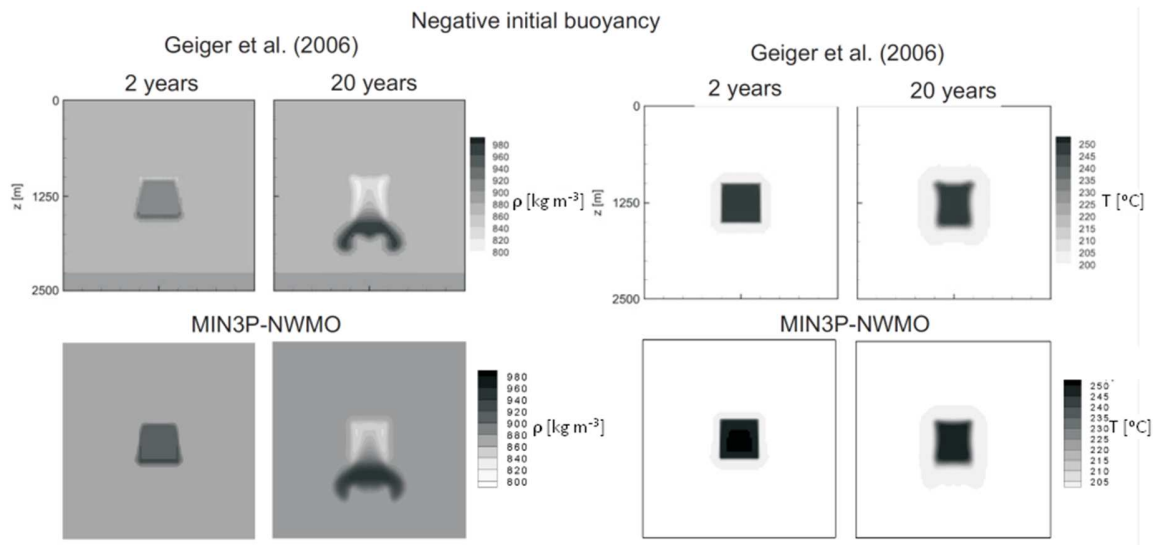


Figure 2.19: Verification of thermo-hydraulic coupling for negative initial buoyancy. MIN3P-THCm results of density (left) and temperature (right) at 2 and 20 years are compared with the results from Geiger et al. (2006) (Bea et al., 2011)

Validation report-page# 2-73

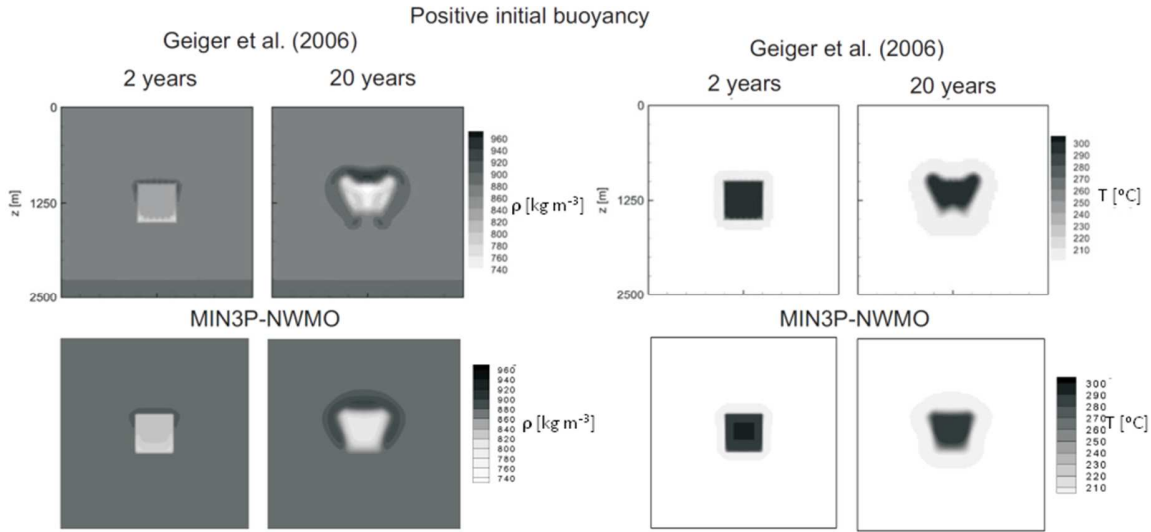


Figure 2.20: Verification of thermo-hydraulic coupling for positive initial buoyancy. MIN3P-THCm results of density (left) and temperature (right) at 2 and 20 years are compared with the results from Geiger et al. (2006) (Bea et al., 2011)

2.4.4.5 File locations

The input file (negative buoyancy) can be found under

`..\benchmarking_nwmo_report\ nwmo_verification_examples_D4\ D44_thermo_haline_convective\negative_buoyancy\ free-thermohaline-convection.dat`

Database directory is a subfolder under the folder of the input file: `\database\default`

The input file (negative buoyancy) can be found under

`..\benchmarking_nwmo_report\ nwmo_verification_examples_D4\ D44_thermo_haline_convective\positive_buoyancy\ free-thermohaline-convection.dat`

Database directory is a subfolder under the folder of the input file: `\database\default`

2.4.5 SALT DOME PROBLEM

2.4.5.1 Problem definition

The salt dome problem is an idealization of flow over a salt dome. In this case, fluid flow, energy, and solute transport are coupled through density because density is treated as a function of temperature as well as solute concentrations. This relationship can be expressed in form of the buoyancy ratio B as:

$$B = \frac{\frac{\partial \rho}{\partial TDS} \Delta TDS}{\frac{\partial \rho}{\partial T} \Delta T}$$
Equation 1-7

2.4.5.2 Model setup

The geometry and boundary conditions for the problem are shown in Figure 2.21A. The domain extends 900 m horizontally and 300 m vertically (i.e. the aspect ratio about 3). The aquifer is considered homogeneous and isotropic and the hydraulic head varies linearly along the top boundary. All remaining boundaries are impervious to flow. Thermohaline extension of the salt dome problem involves the superposition of an upward thermal gradient, which tends to destabilize the brine plume due to the resulting buoyant forces. Accordingly, the bottom of the aquifer is assigned a constant normalized temperature (i.e. $T=1$), while the top boundary is assigned a normalized temperature of zero (i.e. $T=0$). The upper boundary is additionally constrained by a heat flux of zero. The side walls of the domain are assumed impervious for solute mass and adiabatic (insulated) for heat.

2.4.5.3 Parameters

Key parameter values for flow and transport are provided in Table 2.26.

2.4.5.4 Results

Results obtained with MIN3P-THCm and FEFLOW at a simulation time of 100 years for three different buoyancy ratios are shown in Figure 2.21B. Although these two codes use different numerical approaches (finite volumes and finite elements, respectively), the results are comparable. The differences that are noticed, particularly for the lowest buoyancy ratio of 2, may be attributable to different spatial interpolation of temperature-dependent variables (i.e. density and viscosity). In the finite volume method (MIN3P-THCm), density is only interpolated between the center of adjacent cells, whereas it is interpolated at Gauss points, for instance, in the finite element method.

2.4.5.5 File locations

The input files *salt-dome.dat* can be found under

`..\benchmarking_nwmo_report\nwmo_verification_examples_D45\d45_salt_dome_problem\d80_b5`

`..\benchmarking_nwmo_report\nwmo_verification_examples_D452\d200_b2`

`..\benchmarking_nwmo_report\nwmo_verification_examples_D453\d133_b3`

Databases are a subfolder under the folder of the input files: `\database\default`

Validation report-page# 2-75

Table 2.26: Parameters for Salt-Dome Problem (Bea et al., 2011)

Parameter	Value	Unit
Aspect ratio	3	-
Bouyancy ratio	2,3,5	-
Solid bulk density	1000	[kg m ⁻³]
Fresh-water density	1000	[kg m ⁻³]
C _{in} (initial concentration)	0	[mol l ⁻³]
Porosity	0.20	[-]
Hydraulic conductivity	1.09852×10^{-5}	[m s ⁻¹]
Molecular difussion coefficient (solute transport)	1.39×10^{-8}	[m ² s ⁻¹]
Longitudinal dispersivity of solute	20.0	[m]
Transverse dispersivity of solute	2.0	[m]
Longitudinal thermal dispersivity	20.0	[m]
Transverse thermal dispersivity	2.0	[m]
Transverse horizontal thermal dispersivity	2.0	[m]
Water thermal conductivity	0.65	[J s ⁻¹ m ⁻¹ °C ⁻¹]
Solid thermal conductivity	3.0	[J s ⁻¹ m ⁻¹ °C ⁻¹]
Specific heat capacity of water	4200	[J kg ⁻¹ °C ⁻¹]
Specific heat capacity of solid	2520	[J kg ⁻¹ °C ⁻¹]

Validation report-page# 2-76

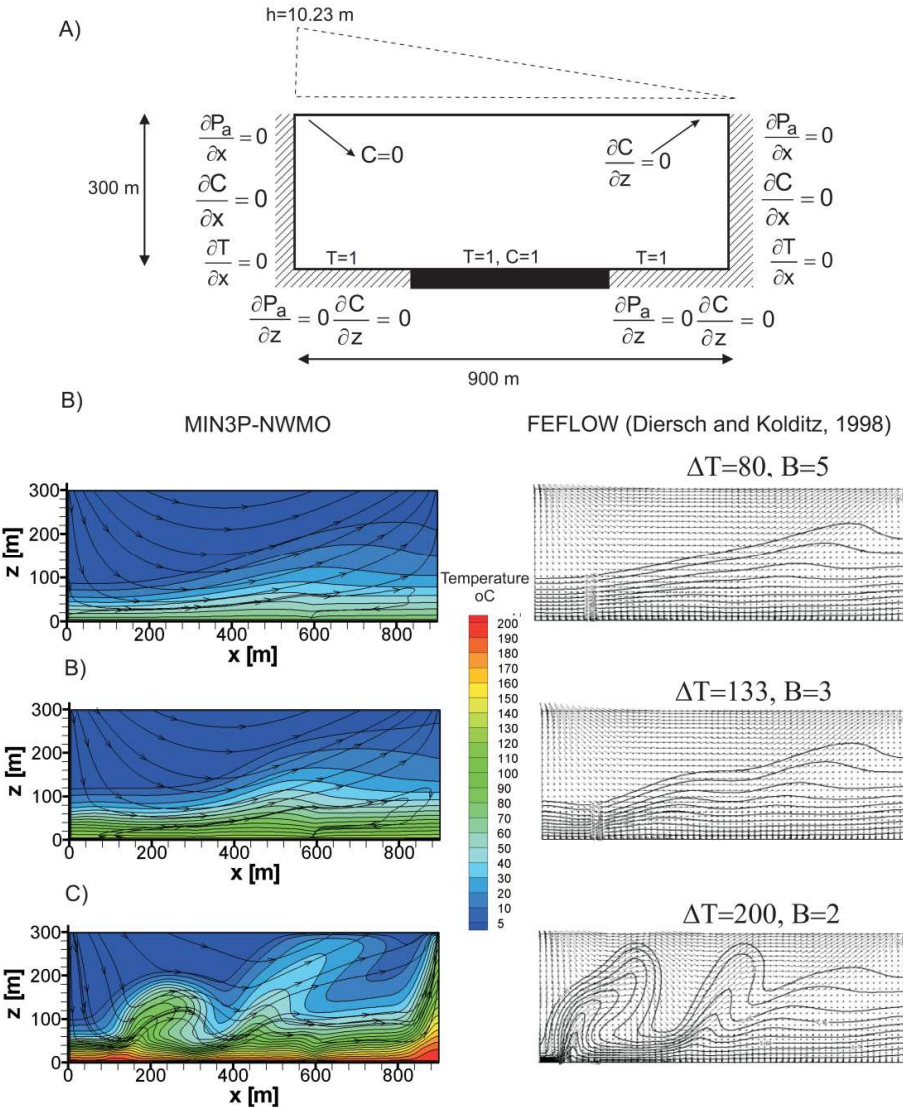


Figure 2.21: Salt dome verification example. A) Domain geometry and boundary conditions for flow, energy and solute transport. B) Results obtained with MIN3P-THCm (left) are compared with FEFLOW (right) at different buoyancy ratios (Bea et al., 2011)

2.5 MULTICOMPONENT REACTIVE TRANSPORT

MIN3P-THCm provides formulations to simulate multicomponent reactive transport for saturated and unsaturated conditions in 1D, 2D and 3D Cartesian and radial-coordinates. The validation and verification examples for multicomponent reactive transport problems are listed in Table 2.27.

Table 2.27: List of reactive transport benchmarks

Name	Description of Main Features	Verification Type	Section
diff_rc_s	Diffusion, steady-state, radial coordinates	1	2.5.1
diff_rc_t	Diffusion, transient, radial coordinates	1	2.5.2
disper_rc	Diffusion and dispersion, radial coordinates	1	2.5.3
diffdry	Gas diffusion, constant moisture content, dry conditions	1	2.5.4
diffvar	Gas diffusion, variable moisture content	1, 2	2.5.5
diffwet	Gas diffusion, constant moisture content, wet conditions	2	2.5.6
ex11	Cation exchange – comparison with PHREEQC	2	2.5.7
caex	Cation exchange – comparison with PHAST	2	2.5.8
surfx	Trace metal mobility - surface complexation	2	2.5.9
dedo	Dedolomization – mineral dissolution precipitation	2	2.5.10
pyrox	Pyrite oxidation and gas diffusion in vadose zone	2	2.5.11
perm1_new	Porosity-permeability changes – permeability enhancement	2	2.5.12
perm2_new	Porosity-permeability changes - clogging with simple chemistry	2	2.5.13
perm3_new	Porosity-permeability changes – clogging with complex chemistry	2	2.5.14
retardation	Linear retardation of PCE and benzene	1	2.5.15
degradation	Aerobic degradation of toluene – intra-aqueous kinetics	2	2.5.16
saline	Reactive transport under highly saline conditions – Pitzer equations	2	2.5.17
ionx-2m	Multisite ion exchange	2	2.5.18
MCD-2	Multicomponent diffusion (MCD)	2	2.5.19
MCD-rc	MCD in radial coordinate	2	2.5.20
Column2	Microbially mediated chromium reduction	2	2.5.21
sul2pqc	Salinity dependent sulfate reduction –option 1	2	2.5.22
sulpqc	Salinity dependent sulfate reduction –option 2	2	2.5.23

2.5.1 STEADY-STATE DIFFUSION - RADIAL COORDINATES

2.5.1.1 Problem definition

This benchmark is a 1D steady-state diffusion problem for a radial coordinate system without advection. It is verified against analytical solution (Crank 1975).

2.5.1.2 Model setup

A 1D model with a radius of 1.0 m is discretized into 500 control volumes. The origin is defined by a borehole with a radius of $3.9493d-2$ m (a) (Figure 2.22). A tracer (HTO) is the only component considered in this problem. The initial tracer concentration (IC) in the entire domain and concentrations in the borehole and at the right boundary (BC) are listed in Table 2.28.

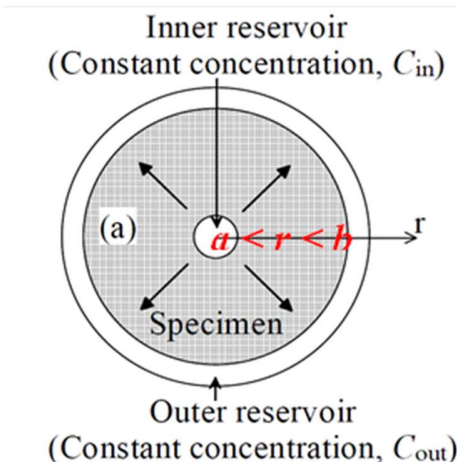


Figure 2.22: Conceptual model of the 1D steady state diffusion problem for a radial coordinate system, a and b define the inner and outer reservoirs

Table 2.28: Initial and boundary conditions for reactive transport

Parameter	Initial Condition	Boundary Condition	Unit
<i>Aqueous phase</i>		borehole right	
HTO	1.0×10^{-100}	1.0	1.0×10^{-100} [mol l ⁻¹]

2.5.1.3 Parameters

The parameters of the porous medium are: porosity and tortuosity are set to 0.5 and 0.2, respectively for the entire domain. The free aqueous phase diffusion coefficient (D_0) is 3.75×10^{-8} m² s⁻¹. The effective diffusion coefficient (D_e) is calculated:

Validation report-page# 2-79

$$D_e = \phi\tau D_0 \quad \text{Equation 1-8}$$

In which ϕ is the porosity, and τ is the tortuosity.

2.5.1.4 Analytical solution

The analytic solution is derived from the following equation (Crank 1975):

$$\frac{d}{dr} \left(r D \frac{dC}{dr} \right) = 0, \quad a < r < b, \quad \text{Equation 1-9}$$

With constant boundary conditions:

$$C(a, t \rightarrow \infty) = C_1 \quad \text{Equation 1-10}$$

$$C(b, t \rightarrow \infty) = C_2 \quad \text{Equation 1-11}$$

The solution becomes:

$$C = \frac{C_1 \ln \left(\frac{b}{r} \right) + C_2 \ln \left(\frac{r}{a} \right)}{\ln \left(\frac{b}{a} \right)} \quad \text{Equation 1-12}$$

In which a and b are the inner and outer radii, C_1 and C_2 are the constant concentrations in the inner reservoir (i.e. borehole surface) and the outer reservoir (i.e. outer cylinder surface), respectively.

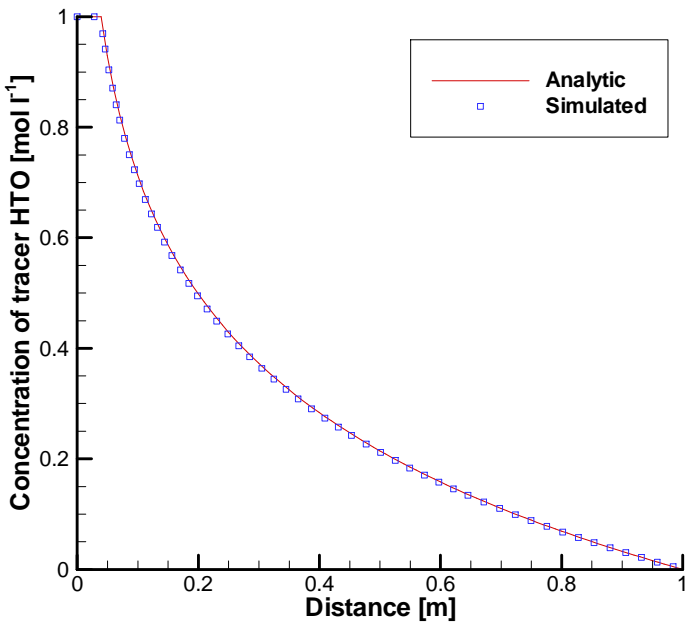


Figure 2.23: Comparison of analytical solution and concentration profiles obtained with MIN3P-THCm for the 1D steady-state diffusion problem in radial coordinates

2.5.1.5 Results

The simulated concentration profile at steady-state is verified against the analytical solution (Figure 2.23). MIN3P-THCm results compare favorably to the results of the analytical solution.

2.5.1.6 File locations

The input file for the 1D steady-state diffusion problem in radial coordinates can be found at:

`.\benchmarks\benchmarks_standard\reactran\diff_rc_s\diff-rc-s.dat`

Database can be found under: `.\benchmarks\database\default`

2.5.2 TRANSIENT DIFFUSION - RADIAL COORDINATES

2.5.2.1 Problem definition

This benchmark is a 1D transient diffusion problem for a radial coordinate system without advection. It is verified against the analytical solution (Crank 1975).

2.5.2.2 Model setup

A 1D model with a radius of 1.0 m is discretized into 500 control volumes. This model represents a 2D solid cylinder with $r_{out} = a$ (Figure 2.24). The tracer HTO is the only component considered in the problem. The initial tracer concentration (IC) in the entire domain and concentrations at the center and outer boundaries (BC) are listed in Table 2.29. The tracer diffuses from the outer boundary into the cylinder.

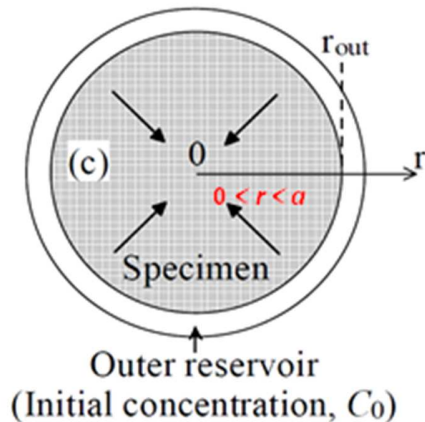


Figure 2.24: Conceptual model of the 1D transient diffusion problem for a radial coordinate system, a defines the outer radius

Table 2.29: Initial and boundary conditions for reactive transport

Parameter	Initial Condition	Boundary Condition	Unit
<i>Aqueous phase</i>		center outer	
HTO	1.0×10^{-100}	1.0×10^{-100} 1.0	[mol l ⁻¹]

2.5.2.3 Parameters

The parameters of the porous medium are: porosity and tortuosity are set to 1 and 0.1, respectively for the entire domain. The free aqueous phase diffusion coefficient (D_0) is $3.75 \times 10^{-8} \text{ m}^2 \text{ s}^{-1}$. The effective diffusion coefficient (D_e) is calculated as:

$$D_e = \phi \tau D_0 \quad \text{Equation 1-13}$$

In which ϕ is the porosity, and τ is the tortuosity.

2.5.2.4 Analytical solution

The analytical solution is derived from the equation (Crank 1975):

Validation report-page# 2-82

$$\frac{\partial C}{\partial t} = \frac{1}{r} \frac{\partial}{\partial r} \left(r D \frac{\partial C}{\partial r} \right), \quad 0 < r < a, \quad \text{Equation 1-14}$$

With constant boundary conditions:

$$C = C_0, \quad r = a, t \geq 0,$$

$$C = f(r), \quad 0 < r < a, t = 0,$$

When $f(r) = C_1$, for small times and large r/a , the solution is:

$$\begin{aligned} \frac{C - C_1}{C_0 - C_1} &= \sqrt{\frac{a}{r}} \operatorname{erfc} \frac{a-r}{2\sqrt{Dt}} + \frac{(a-r)\sqrt{Dt}a}{4ar\sqrt{r}} i \operatorname{erfc} \frac{a-r}{2\sqrt{Dt}} \\ &\quad + \frac{(9a^2 - 7r^2 - 2ar)Dt}{32ar^2\sqrt{ar}} i^2 \operatorname{erfc} \frac{a-r}{2\sqrt{Dt}} + \dots \end{aligned} \quad \text{Equation 1-15}$$

in which

$$\begin{aligned} 2n i^n \operatorname{erfc}(x) &= 2n \int_x^\infty i^{n-1} \operatorname{erfc}(\xi) d\xi \\ &= i^{n-2} \operatorname{erfc}(x) - 2xi^{n-1} \operatorname{erfc}(x), \end{aligned} \quad \text{Equation 1-16}$$

where a is the outer radius, C_0 is the constant concentration at the outer boundary, C_1 is the initial tracer concentration in the domain. In the current calculation, only the first two terms are considered, which provides sufficient accuracy for the early time period (Crank 1975).

2.5.2.5 Results

Simulated concentration profiles for four selected output times are verified against the analytical solution (Figure 2.25). Results obtained with MIN3P-THCm are in perfect agreement with the analytical solution.

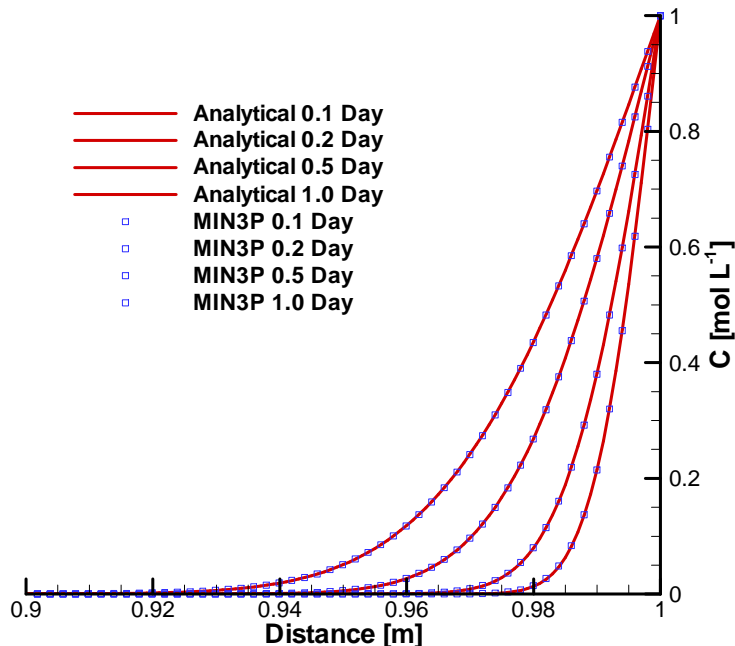


Figure 2.25: Comparison of analytical solution and concentration profiles obtained with MIN3P-THCm for the 1D transient diffusion problem in radial coordinate

2.5.2.6 File locations

The input file for the 1D transient diffusion problem for a radial coordinate system can be found under:

`.\benchmarks\benchmarks_standard\reactran\diff_rc_t\diff-rc-t.dat`

Database can be found under: `.\benchmarks\database\default`

2.5.3 TRANSIENT ADVECTIVE-DISPERSIVE TRANSPORT – RADIAL COORDINATES

2.5.3.1 Problem definition

This benchmark is a 1D transient dispersive transport problem for a radial coordinate system, which simulates the dispersive transport of a tracer under radial flow conditions from an injection well. It is verified against the analytical solution derived by Hsieh (1986).

2.5.3.2 Model setup

A 1D model with a radius of 1000 m is discretized into 1000 control volumes. The tracer Cl^- is the only component considered in the problem. The initial tracer concentration (IC)

Validation report-page# 2-84

in the entire domain and concentrations at the center and at the outer boundary (BC) are listed in Table 2.30. The tracer is injected from the center with a flow rate of $6.25 \times 10^{-3} \text{ m s}^{-1}$ and migrates outwards, subject to advective-dispersive transport.

Table 2.30: Initial and boundary conditions for flow and reactive transport

Parameter	Initial Condition	Boundary Condition	Unit
Aqueous phase		center outer	
Cl ⁻	$1.0 \times 10^{-1} 00$	1.0 1.0×10^{-100}	[mol l ⁻¹]
Hydraulic head	0.0	- 0.0	[m]
Specified flux	-	6.25×10^{-3} -	[m s ⁻¹]

2.5.3.3 Parameters

The parameters of the porous medium are: porosity is set to 0.2, specific storage is $1.0 \times 10^{-10} \text{ m}^{-1}$, longitudinal dispersivity is 10 m, transverse radial dispersivity is 0 m. The free aqueous phase diffusion coefficient (D_0) is $1.0 \times 10^{-10} \text{ m}^2 \text{ s}^{-1}$, which is relatively small and its effect on the mass transport can be neglected.

2.5.3.4 Analytical solution

The governing equation for radial advective-dispersive transport of a conservative tracer in a steady radial flow field from an injection well can be written as (Hoopes and Harleman 1967):

$$\frac{\partial C}{\partial t} + \frac{A}{r} \frac{\partial C}{\partial r} = \alpha \frac{A}{r} \frac{\partial^2 C}{\partial r^2}, \quad r > r_w, \quad t > 0, \quad \text{Equation 1-17}$$

where

$$A = Q / (2\pi b\phi) \quad \text{Equation 1-18}$$

in which c is the tracer concentration in the radial flow field, r is the radial distance from the center line of the injection well, t is the time from the start of the injection, α is the longitudinal dispersivity in radial direction, Q is the volumetric rate of tracer injection, b is the thickness of the aquifer and ϕ is the porosity. The initial and boundary conditions are:

$$\begin{aligned} C(r, 0) &= 0, \quad r > r_w, t = 0, \\ C(r_w, t) &= C_0, \quad t > 0, \\ C(r \rightarrow \infty, t) &\rightarrow 0, \quad t > 0 \end{aligned}$$

For the following dimensionless form

$$G = \frac{C}{C_0}, \quad \rho = \frac{r}{\alpha}, \quad \rho_w = \frac{r_w}{\alpha}, \quad \tau = \frac{At}{\alpha^2}$$

Validation report-page# 2-85

the analytical solution can be derived (Hsieh 1986) as:

$$G(\rho, \tau) = 1 - \int_0^{\infty} F(v) dv \quad \text{Equation 1-19}$$

where

$$F(v) = \frac{2\exp[-v^2\tau + \frac{\rho - \rho_w}{2}]}{\pi v} \frac{Ai(y)Bi(y_w) - Ai(y_w)Bi(y)}{[Ai(y_w)]^2 + [Bi(y_w)]^2} \quad \text{Equation 1-20}$$

in which y and y_w are defined as:

$$y = \frac{1 - 4\rho v^2}{ev^{\frac{4}{3}}} \quad \text{Equation 1-21}$$

$$y_w = \frac{1 - 4\rho_w v^2}{ev^{\frac{4}{3}}} \quad \text{Equation 1-22}$$

$Ai(z)$ and $Bi(z)$ are the Airy functions and can be found in Hsieh (1986).

2.5.3.5 Results

The simulated concentration profiles at selected times is verified against the analytical solution (Figure 2.26). Results obtained with MIN3P-THCm are in perfect agreement with the analytical solution.

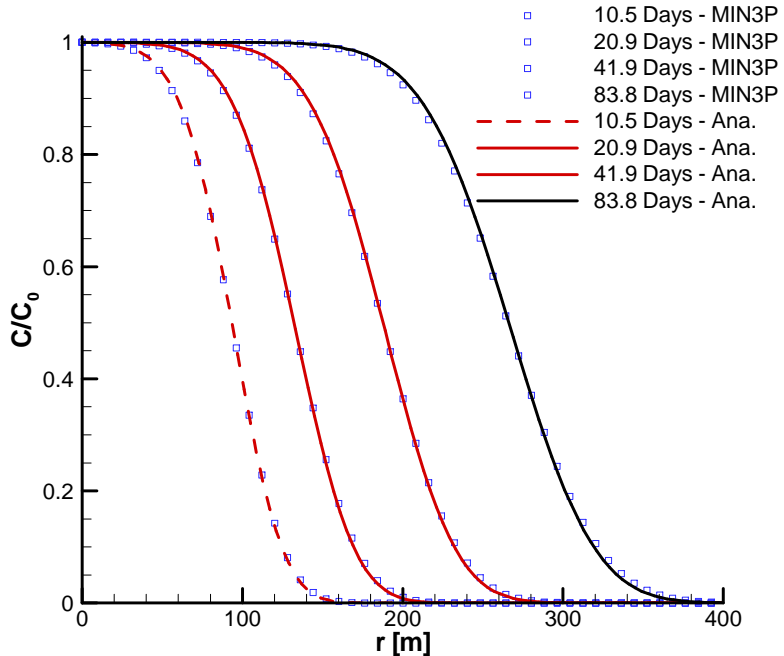


Figure 2.26: Comparison of analytical solution (lines) and concentration profiles obtained with MIN3P-THCm for the 1D transient advective-dipsersive problem in radial coordinate

2.5.3.6 File locations

The input file for the benchmark can be found under

.\benchmarks\benchmarks_standard\reactran\disper-rc\disp-rc.dat

Database can be found under: .\benchmarks\database\default

2.5.4 GAS DIFFUSION WITH CONSTANT MOSTURE CONTENT - DRY CONDITIONS

2.5.4.1 Problem definition

This benchmark is designed to test vadose zone gas transport subject to dry conditions. Numerical results are compared to the Ogata-Banks analytical solution (Ogata and Banks 1961).

2.5.4.2 Model setup

A 1D vertical model, 1.5 m in depth is discretized into 26 control volumes. Oxygen diffuses into the domain from the top boundary. Oxygen in the gas phase O₂(g) and the

Validation report-page# 2-87

aqueous phase O₂(aq) phase is considered in this problem. However, only the diffusive transport of O₂(g) is calculated to allow direct comparison with the Ogata-Banks solution.

The initial concentration (IC) and boundary conditions (BC) are listed in Table 2.31. It should be noted that in this example MIN3P-THCm uses O₂(aq) to define the initial and boundary concentrations. The boundary conditions for the flow problem are set to ensure a “0”-gradient and no flow conditions.

Table 2.31: Initial and boundary conditions for flow and reactive transport

Parameter	Initial Condition	Boundary Condition	Unit
<i>Aqueous phase</i>		top bottom	
O ₂ (aq)	1.0×10 ⁻¹⁰	2.63×10 ⁻⁴ second	[mol l ⁻¹]
Hydraulic head	-1000.0	-1000.0 -1001.5	[m]

2.5.4.3 Parameters

The parameters for the porous medium are listed in Table 2.32. The tortuosity correction is calculated with the model of Millington and Quirk (1961).

For the unsaturated soil properties: the van Genuchten equation (see Equation 2-6 in the theory manual is used for the calculation of water and gas saturations (van Genuchten, 1980).

Table 2.32: Physical parameters for benchmark *diffdry*

Parameter	Symbol	Value	unit
Length of domain	L	1.5	[m]
Porosity	ϕ	0.5	[−]
Hydraulic conductivity	K _{zz}	1.0×10 ⁻⁶	[m s ⁻¹]
Diffusion coefficient for aqueous phase	D ₀ ^a	0.0	[m ² s ⁻¹]
Diffusion coefficient for gaseous phase	D ₀ ^g	1.5×10 ⁻⁵	[m ² s ⁻¹]
Residual saturation	S _{ra}	0.01	[−]
Van Genuchten parameter α	α	3.5	[m ⁻¹]
Van Genuchten parameter n	n	1.4	[−]

2.5.4.4 Results

The simulated concentration profile at for two selected output times are verified against the Ogata-Banks analytical solution (Figure 2.27). Results obtained with MIN3P-THCm are in very good agreement with the analytical solution.

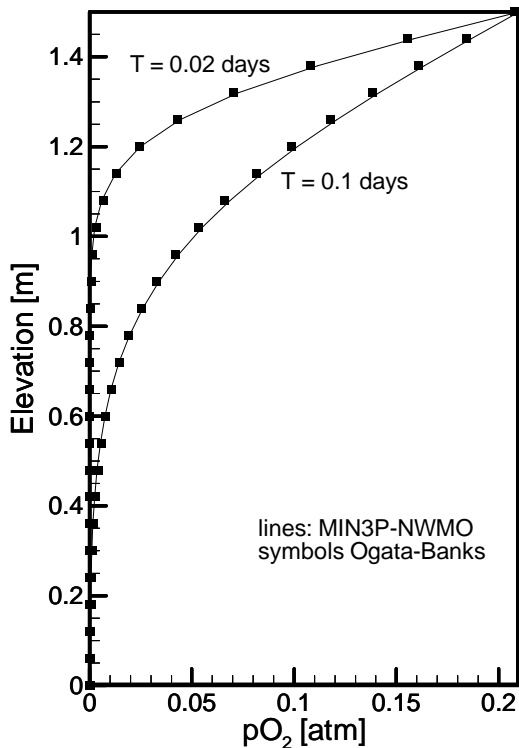


Figure 2.27: Comparison of vertical partial pressure profiles of $O_2(g)$ calculated with MIN3P-THCm in comparison to the Ogata-Banks solution at 0.02 days and 0.1 days (diffdry)

2.5.4.5 File locations

The input file for the benchmark can be found under

`.\benchmarks\benchmarks_standard\reactran\diffdry\diffdry.dat`

Database can be found under: `.\benchmarks\database\default`

2.5.5 GAS DIFFUSION WITH VARIABLE MOISTURE CONTENT

2.5.5.1 Problem definition

This benchmark is a 1D vertical gas transport problem for a domain with variable moisture content. This benchmark is verified by code intercomparison of MIN3P-THCm with PYROX - a numerical model that simulates one-dimensional, kinetically controlled diffusion of oxygen into the vadose zone of mine tailings and the subsequent oxidation of sulfide minerals, such as pyrite (Wunderly et al., 1996) and a modified version of the Ogata

Validation report-page# 2-89

bank solution with variable diffusion coefficients.

2.5.5.2 Model setup

A 1D model, 1.5 m in depth, is discretized into 26 control volumes. Oxygen in the gas phase - O₂(g) and the aqueous phase - O₂(aq) are considered. However, only the diffusive transport of gas O₂(g) is calculated.

The initial concentration (IC) and boundary conditions (BC) for this verification problem are listed in Table 2.33. It should be noted that in this example MIN3P-THCm uses O₂(aq) to define the initial and boundary concentrations. The boundary conditions for the flow problem are set to ensure a “0”-gradient and no flow conditions.

Table 2.33: Initial and boundary conditions for flow and reactive transport

Parameter	Initial Condition	Boundary Condition	Unit
Aqueous phase		top bottom	
O ₂ (aq)	1.0×10 ⁻¹⁰	2.63×10 ⁻⁴ second	[mol l ⁻¹]
Hydraulic head	0.0	- -0.2	[m]
Specified flux	-	0 -	[m s ⁻¹]

2.5.5.3 Parameters

Parameters for the porous medium are the same as those for benchmark *diffdry* (see section 2.5.4, Table 2.32).

2.5.5.4 Results

The simulated profiles of O₂(g) partial pressure are depicted in Figure 2.28. O₂(g) ingress occurs from the top into the column. The simulated results by MIN3P-THCm are very close to the results calculated by PYROX (Wunderly et al. 1996) and the modified Ogata-Banks analytical solution (Ogata and Banks 1961). Discrepancies at late time (5 days) are due to boundary effects, as the modified Ogata Banks solution assumes a semi-infinite domain, while the numerical solutions assume a second-type (zero-flux) boundary at the lower boundary.

2.5.5.5 File locations

The input file for the benchmark can be found under

.\benchmarks\benchmarks_standard\reactran\diffvar\diffvar.dat

Database can be found under: .\benchmarks\database\default

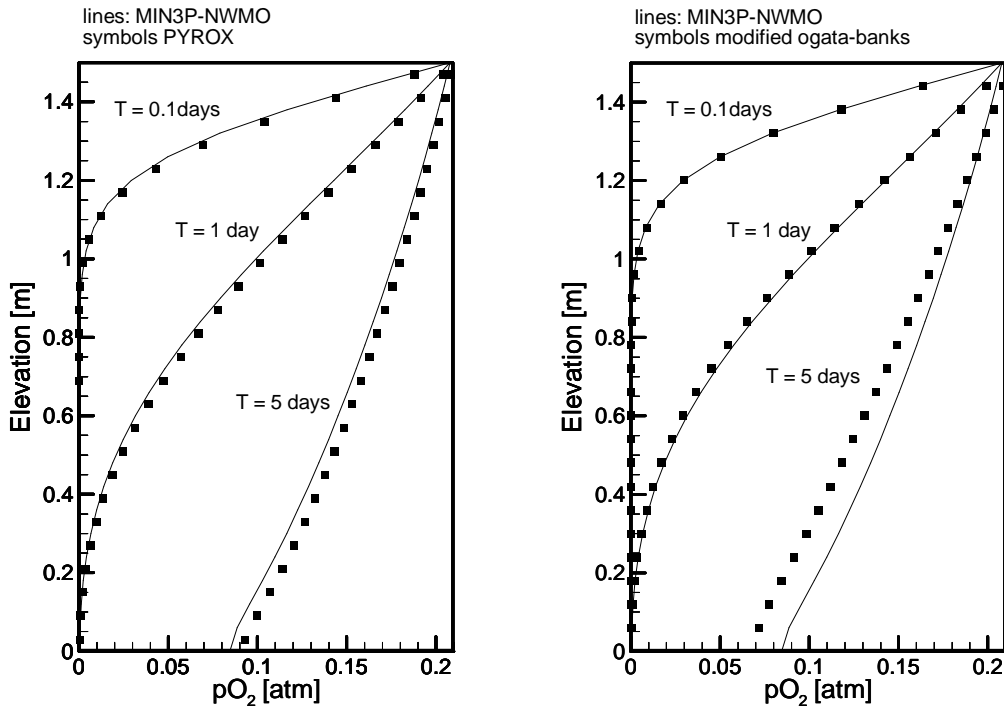


Figure 2.28: Comparison of vertical partial pressure profiles of $O_2(g)$ calculated by MIN3P-THCm vs PYROX (left), and MIN3P-THCm vs Ogata-Banks equation (right) at 0.1 days, 1 day and 5 days.

2.5.6 GAS DIFFUSION WITH CONSTANT MOISTURE CONTENT – WET CONDITIONS

2.5.6.1 Problem definition

This benchmark is for the verification of gas diffusion in the unsaturated zone for wet conditions by comparison with the Ogata-Banks analytical solution (Ogata and Banks 1961) and results calculated by PYROX (Wunderly et al., 1996).

2.5.6.2 Model setup

A 1D model, 1.5 m in depth, is discretized into 26 control volumes. Oxygen in the gas phase $O_2(g)$ and aqueous phase $O_2(aq)$ are considered in this problem.

The initial concentration (IC) and boundary conditions (BC) for this verification example are listed in Table 2.34. It should be noted that in this example MIN3P-THCm uses $O_2(aq)$ to define the initial and boundary concentrations. The boundary conditions for the flow problem are set to ensure a “0”-gradient and no flow conditions.

Table 2.34: Initial and boundary conditions for flow and reactive transport

Parameter	Initial Condition	Boundary Condition	Unit
Aqueous phase		top bottom	
O ₂ (aq)	1.0×10 ⁻¹⁰	2.63×10 ⁻⁴ second	[mol l ⁻¹]
Hydraulic head	-0.1	1.3 -0.2	[m]

2.5.6.3 Parameters

Parameters for the porous medium are the same as those for benchmark *diffdry* (see section 2.5.4, Table 2.32).

2.5.6.4 Results

The simulated profiles of O₂(g) partial pressures at one and ten days were depicted in Figure 2.29. O₂(g) ingresses into the column from the top of the domain. The simulated results by MIN3P-THCm match the results calculated by PYROX (Wunderly et al. 1996) and the Ogata-Banks solution (Ogata and Banks 1961).

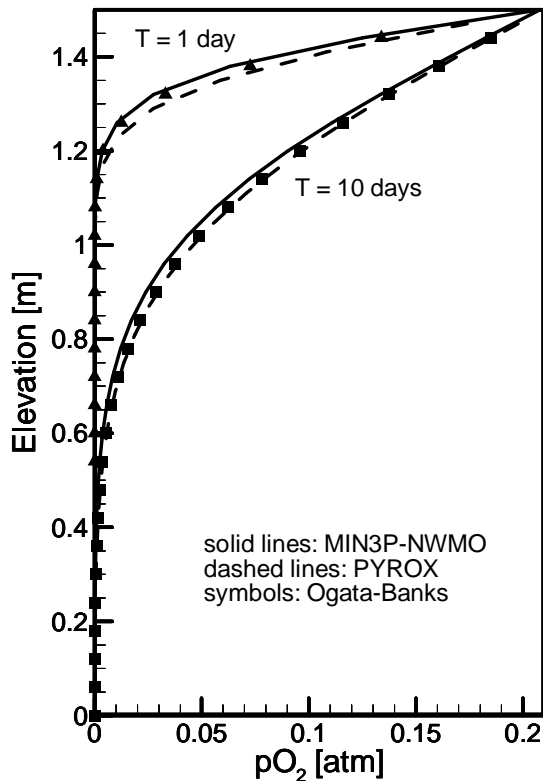


Figure 2.29 Comparison of vertical partial pressure profiles of O₂(g) calculated by MIN3P-THCm (solid lines), PYROX (dashed lines) and the Ogata-Banks analytical solution (symbols) at 1 day and 10 days.

2.5.6.5 File locations

The input file for the benchmark can be found under

.\benchmarks\benchmarks_standard\reactran\diffwet\diffwet.dat

Database can be found under: .\benchmarks\database\default

2.5.7 CATION EXCHANGE – EXAMPLE 1

2.5.7.1 Problem definition

This benchmark is a cation exchange example based on PHREEQC V2 example 11 from Appelo and Postma (Appelo and Postma 2005). It simulates advective mass transport in saturated porous media affected by ion exchange processes under steady-state flow conditions.

2.5.7.2 Model setup

A 1D model, 0.80 m in length, is discretized into 41 control volumes. The domain is homogeneous. The hydraulic head at the left boundary is constant (0.8 m), while the hydraulic head on the right border is 0.0 m. With the infiltration of a CaCl₂-solution from the left boundary into the porous medium containing exchangeable K-X and Na-X cations, ion exchange processes are depicted at the end of the column. The initial condition (IC) of the pore water and boundary condition at the inflow boundary (BC) are listed in Table 2.35.

Table 2.35: Initial and boundary conditions (IC & BC)

Parameter	Initial condition	Boundary Condition	Unit
Na ⁺	1.0×10 ⁻³	1.0×10 ⁻⁸	[mol l ⁻¹]
K ⁺	2.0×10 ⁻⁴	1.0×10 ⁻⁸	[mol l ⁻¹]
Ca ²⁺	1.0×10 ⁻⁸	6.0×10 ⁻⁴	[mol l ⁻¹]
Cl ⁻	1.0×10 ⁻⁸	1.2×10 ⁻³	[mol l ⁻¹]
H ⁺	7.0	7.0	pH
O ₂ (aq)	12.5	12.5	pe
NO ₃ ⁻	1.2×10 ⁻³	1.0×10 ⁻⁸	[mol l ⁻¹]

2.5.7.3 Parameters

The parameters of the porous medium are: porosity is 0.50, hydraulic conductivity is 1.39×10⁻⁵ [m/s], dry bulk density is 1.875 [g cm⁻³] and the cation exchange capacity (CEC) is 2.93×10⁻² [meq/100 g solid].

2.5.7.4 Results

Simulated results are verified against results obtained with PHREEQC V2. Breakthrough curves for the concentrations of the main aqueous components at the outflow are depicted in Figure 2.30. Chloride, a conservative solute which was not initially present in the pore water, reaches the outflow boundary after about five hours. The sodium initially present in the column exchanged with the incoming calcium and displaced potassium and is eluted as long as there remains sodium adsorbed on the exchanger. The midpoint of the breakthrough curve for sodium occurs at about 12 hours. Because potassium has a higher affinity for the exchanger than sodium, potassium is released after sodium, resulting in a peak of aqueous K concentrations at about 15 hours. After all potassium has been released, the concentration of calcium increases to a steady-state value equal to the concentration at the inflow boundary. Results obtained with MIN3P-THCm compare favorably to those of PHREEQC V2.

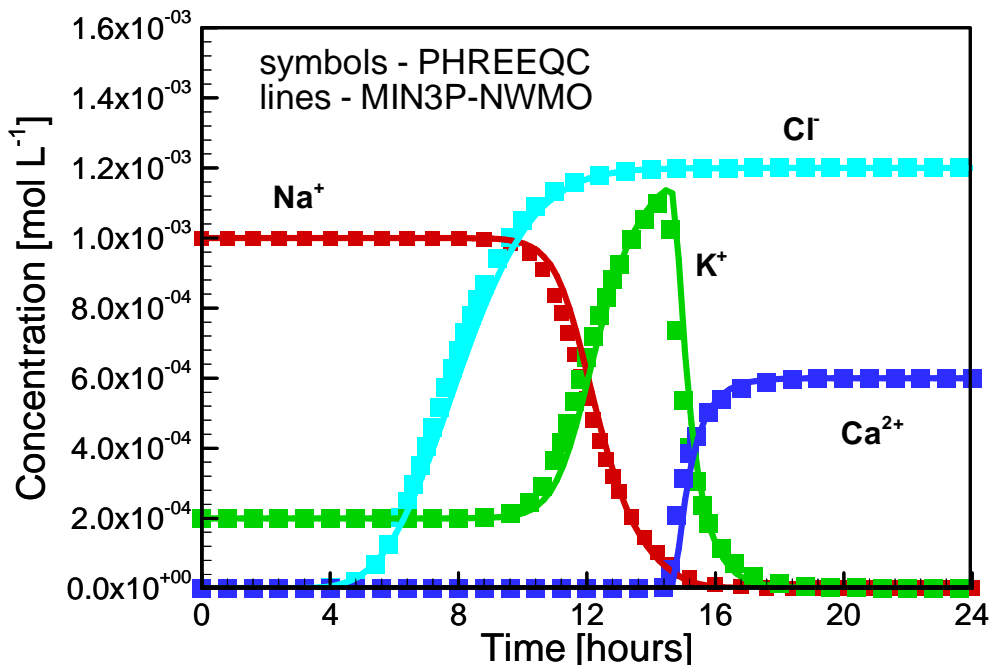


Figure 2.30: Breakthrough curves of aqueous component concentrations affected by ion exchange reactions (line – MIN3P-THCm, symbol – PHREEQC V2)

2.5.7.5 File locations

The input file is: *ex11.dat* under folder
 .\benchmarks\benchmarks_standard\reactran\ex11

Database can be found under: .\benchmarks\database\default

Validation report-page# 2-94

2.5.8 CATION EXCHANGE – EXAMPLE 2

2.5.8.1 Problem definition

The following example provides a second test case to evaluate cation exchange processes under advective-dispersive transport conditions. The simulated results of MIN3P-THCm are compared to results calculated with PHAST (Parkhurst et al. 2005).

2.5.8.2 Model setup

A 1D model, 10.0 m in length, is discretized into 41 control volumes (including two half cells at both ends). Constant hydraulic heads were set at the inflow (3.0 m) and outflow (0.0 m) boundaries. The domain is initially dominated by a sodium-potassium-nitrate (Na-K-NO₃) solution in equilibrium with a cation exchanger, and is then flushed by a solution rich in calcium and chloride (Ca-Cl) (Table 2.36 and Figure 2.31A).

Table 2.36: Composition of Initial and Boundary Waters and Chemical Parameters of the Domain (Cation Exchange Problem)

Parameter	Boundary water	Initial Water	Unit
H ⁺	7.0	7.0	pH
Ca ²⁺	6×10 ⁻⁴	10 ⁻⁹	[mol l ⁻¹]
Cl ⁻	1.2×10 ⁻³	6×10 ⁻⁹	[mol l ⁻¹]
K ⁺	10 ⁻⁹	2×10 ⁻⁴	[mol l ⁻¹]
Na ⁺	10 ⁻⁹	10 ⁻³	[mol l ⁻¹]
NO ₃ ⁻	10 ⁻⁹	1.2×10 ⁻³	[mol l ⁻¹]
Ionic strength	1.8×10 ⁻³	1.2×10 ⁻³	[M]

2.5.8.3 Parameters

The main parameters of the porous medium are listed in Table 2.37.

Table 2.37: Parameters of the porous media (Cation Exchange Problem)

Parameter	Symbol	Value	unit
Length of domain	L	10.0	[m]
Porosity	ϕ	0.3	[-]
Dry density	ρ _d	1875.0	[kg m ⁻³]
Hydraulic conductivity	K _{xx}	1.16×10 ⁻⁵	[m s ⁻¹]
Longitudinal dispersivity	α _L	0.1	[m]
Transverse dispersivity	α _τ	0.01	[m]
Cation exchange capacity	CEC	17.5	[meq (100g) ⁻¹]

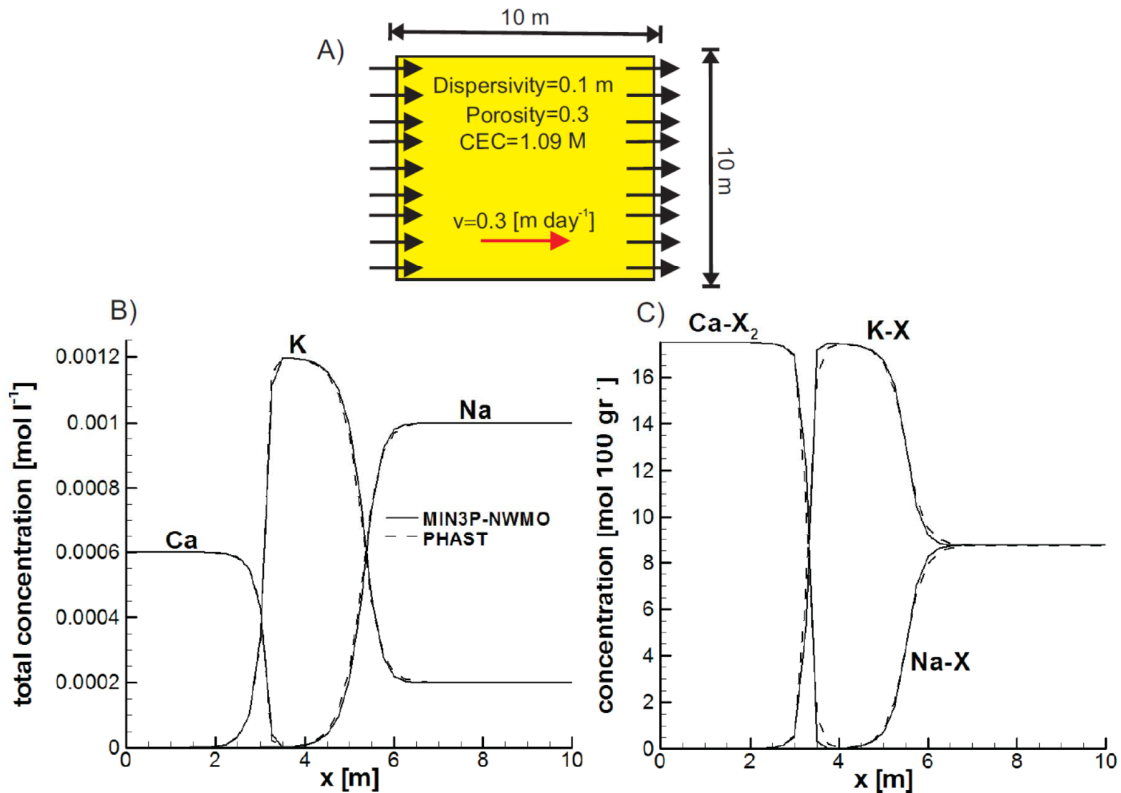


Figure 2.31: Cation-exchange problem. A) Physical and chemical properties of the domain. B) Spatial distribution of total concentrations of the major cations at 3000 days. C) Concentration of exchanged species at 3000 days. The MIN3P-THCm results (solid lines) agree well with PHAST (dashed lines)

2.5.8.4 Results

The spatial distributions of total concentrations of the major cations at 3000 days are presented in Figure 2.31B. The spatial distributions of exchanged species are presented in Figure 2.31C. Simulation results demonstrate the replacement of Na^+ and K^+ by Ca^{2+} . The results obtained with MIN3P-THCm agree very well with the solution obtained using PHAST (Figure 2.31B and C). Because the spatial and temporal discretization was the same for both numerical solutions, it is believed that the slightly more dispersed concentration profiles for the PHAST model are due to operator-splitting errors introduced by the solution algorithm.

2.5.8.5 File locations

The input file *ionexch.dat* can be found under

`..\benchmarking_nwmo_report\ nwmo_verification_examples_D5\d52_cation_exchange\ min3p`

Validation report-page# 2-96

Database can be found under: .\benchmarks\database\default

2.5.9 TRACE METAL MOBILITY AND SURFACE COMPLEXATION

2.5.9.1 Problem definition

This benchmark is a one-dimensional reactive transport problem considering surface complexation during advective-dispersive transport in saturated porous media. This example demonstrates the effect of surface complexation of trace metals (Zn^{2+} , Cu^{2+}) to a ferrous hydrous oxide using a non-electrostatic surface complexation model. A code intercomparison was undertaken with PHREEQC V2.

2.5.9.2 Model setup

A 1D model, 16.0 m in length, is discretized into 101 control volumes yielding a discretization interval of 0.16 m for the interior control volumes and 0.08 m for the control volumes on the boundary. A steady-state saturated flow condition is examined. Boundary conditions are constant hydraulic heads at the inflow boundary (1.4m) and the outflow boundary (0.0m). The geochemical system includes six aqueous components (H^+ , Fe^{3+} , SO_4^{2-} , Zn^{2+} , Fe^{2+} and Cu^{2+}), one non-aqueous component ‘=FeOH(s)’ defining the sorption sites, 30 secondary aqueous species (OH^- , $H_2SO_4(aq)$, $FeOH^+$, $FeOH_3^-$, $FeSO_4(aq)$, $FeHSO_4^+$, $FeOH_2(aq)$, $FeOH^{2+}$, $FeSO_4^+$, $FeHSO_4^{2+}$, $FeOH_2^{+}$, $FeOH_3(aq)$, $FeOH_4^-$, $Fe(SO_4)_2^-$, $Fe_2(OH)_2^{4+}$, $Fe_3(OH)_4^{5+}$, $ZnOH^+$, $Zn(OH)_2(aq)$, $Zn(OH)_3^-$, $Zn(OH)_4^{2-}$, $ZnSO_4(aq)$, $Zn(SO_4)_2^{2-}$, CuO_2^{2-} , $CuOH^+$, $Cu(OH)_2(aq)$, $Cu(OH)_3^-$, $Cu(OH)_4^{2-}$, $Cu_2(OH)_2^{2+}$, $CuSO_4(aq)$, HSO_4^-) and five surface-complexed species (= $FeOH_2^+(s)$, = $FeO^-(s)$, = $FeOZn^+(s)$, = $FeOCu^+(s)$ and = $FeOFe^+(s)$) are considered. The initial and boundary hydraulic and geochemical conditions are listed in Table 2.38. The boundary conditions (BCs) for flow are first type – constant hydraulic heads. The BCs for reactive transport are: third type at the inflow boundary, and second type (free outflow) at the outflow boundary.

Table 2.38: Initial and boundary conditions for flow and reactive transport

Parameter	Initial condition	Boundary Conditions		Unit
<i>Aqueous phase</i>		Inflow	outflow	
H^+	8.1	3.0		pH
Fe^{3+}	1.0×10^{-10}	1.0×10^{-10}		[mol L ⁻¹]
SO_4^{2-}	1.0×10^{-5}	2.5×10^{-3}		[mol L ⁻¹]
Zn^{2+}	1.0×10^{-7}	1.0×10^{-3}	Free exit	[mol L ⁻¹]
Fe^{2+}	1.0×10^{-5}	1.0×10^{-5}		[mol L ⁻¹]
Cu^{2+}	1.0×10^{-7}	1.0×10^{-3}		[mol L ⁻¹]
<i>Hydraulic condition</i>				
Hydraulic head	0.0	1.4	0.0	[m]

Validation report-page# 2-97

2.5.9.3 Parameters

The physical parameters (material properties) and the parameters for the surface complexation reactions used for the simulations are summarized in Table 2.39. The reaction stoichiometries of the surface complexation reactions are summarized in Table 2.40.

Table 2.39: Physical parameters for benchmark *surf*x

Parameter	Symbol	Value	Unit
Length of domain	L	16.0	[m]
Porosity	ϕ	0.25	[-]
Hydraulic conductivity	K_{zz}	1.0×10^{-3}	[m s ⁻¹]
Diffusion coefficient	D_0^a	1.0×10^{-9}	[m ² s ⁻¹]
Longitudinal dispersivity	α_l	0.01	[m]
Mass of surface site ‘=FeOH(s)’	M	100.0	[g solid L ⁻¹ H ₂ O]
Surface area of ‘=FeOH(s)’	S	10.0	[m ² g ⁻¹ solid]
Site density	D	6.02228	[sites nm ⁻²]

Table 2.40: Reaction stoichiometries of surface complexation reactions

Surface complex	Surface	Reaction	logK
=FeOH ₂ ⁺ (s)	=FeOH(s)	=FeOH(s) + H ⁺ ↔ =FeOH ₂ ⁺ (s)	7.29
=FeO ⁻ (s)	=FeOH(s)	=FeOH(s) ↔ =FeO ⁻ (s) + H ⁺	-8.93
=FeOZn ⁺ (s)	=FeOH(s)	=FeOH(s) + Zn ²⁺ ↔ =FeOZn ⁺ (s) + H ⁺	0.99
=FeOCu ⁺ (s)	=FeOH(s)	=FeOH(s) + Cu ²⁺ ↔ =FeOCu ⁺ (s) + H ⁺	2.89
=FeOFe ⁺ (s)	=FeOH(s)	=FeOH(s) + Fe ²⁺ ↔ =FeOFe ⁺ (s) + H ⁺	0.70

2.5.9.4 Results

Comparisons of breakthrough curves of pH, sorbed species concentration and component concentrations at the outflow simulated by MIN3P-THCm and by PHREEQC V2 show excellent agreement as depicted in Figure 2.32. With the infiltration of the low pH solution with much higher concentrations of Zn²⁺ and Cu²⁺, surface complexes =FeOZn⁺(s) and =FeOCu⁺(s) tend to form, occupying free surface sites =FeO⁻(s) initially present in the domain. As =FeOH₂⁺(s) increases with the decrease of the pH (Figure 2.32 up and middle), Zn and Cu are released (Figure 2.32 bottom), leading to the breakthrough of trace metal peaks exceeding the inflow concentrations.

Validation report-page# 2-98

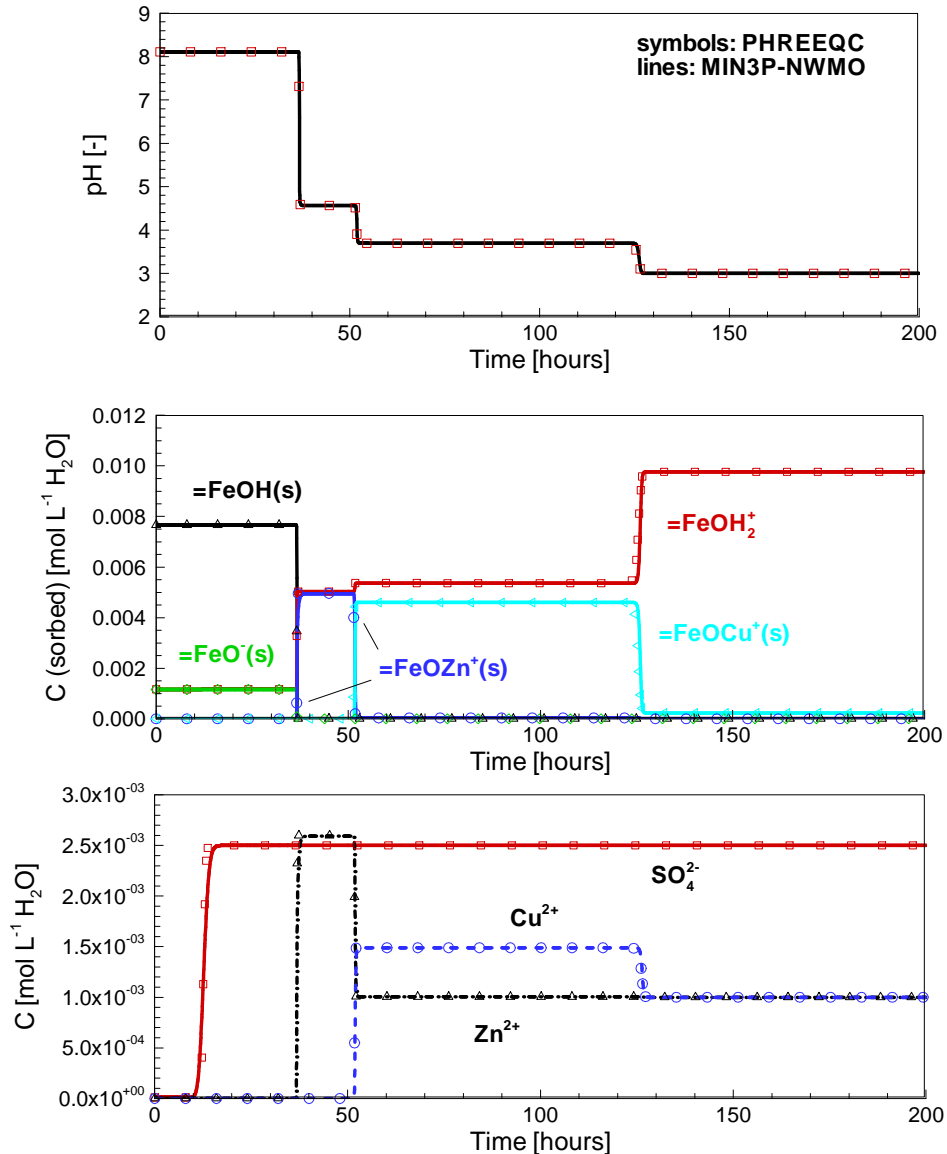


Figure 2.32: Simulated profiles of pH (top), concentrations of sorbed species (middle) and components (bottom) of the outflow solution for benchmark surfx

2.5.9.5 File locations

The input file is: *surfx.dat* under folder *.\benchmarks\benchmarks_standard\reactran\surfx*
 Database can be found under: *\benchmarks\database\default*

Validation report-page# 2-99

2.5.10 DEDOLOMIZATION – DISSOLUTION-PRECIPITATION REACTIONS

2.5.10.1 Problem definition

The benchmark is designed to simulate dedolomitization as an example for the dissolution/precipitation of mineral phases and MIN3P-THCm results are compared with the results obtained using the reactive transport code PHAST (Parkhurst et al., 2005). The replacement of dolomite by calcite is simulated by the infiltration of Ca-rich acidic water, undersaturated with respect to calcite and dolomite, into an aquifer that initially only contains dolomite.

2.5.10.2 Parameters

The initial volumetric content of dolomite in the aquifer is 0.2. The chemical compositions of the initial and boundary waters are presented in Table 2.41. Physical and chemical parameters for the simulation domain are depicted in Figure 2.33A.

Table 2.41: Composition of initial and boundary waters (dedolomization) (Bea et al., 2011)

Parameter	Boundary water	Initial water	Unit
H ⁺	3.0	7.0	pH
Ca ²⁺	4.15×10 ⁻³	1.19×10 ⁻³	[mol l ⁻¹]
Mg ²⁺	7.12×10 ⁻⁵	8.85×10 ⁻⁴	[mol l ⁻¹]
Cl ⁻	2.40×10 ⁻⁴	1.44×10 ⁻³	[mol l ⁻¹]
Na ⁺	9.90×10 ⁻⁵	1.00×10 ⁻⁴	[mol l ⁻¹]
CO ₃ ²⁻	5.50×10 ⁻⁵	1.11×10 ⁻⁴	[mol l ⁻¹]
SO ₄ ²⁻	4.82×10 ⁻³	8.50×10 ⁻⁴	[mol l ⁻¹]
Ionic strength	1.50×10 ⁻²	6.00×10 ⁻³	[mol l ⁻¹]

2.5.10.3 Results

The simulation results show the replacement of dolomite by calcite, and subsequent dissolution of calcite (see Figure 2.33B and Figure 2.33C). The results obtained with MIN3P-THCm are virtually identical to the results obtained using PHAST (Parkhurst et al., 2005). Small differences may be attributed to the different solution algorithms used by the codes, for example, MIN3P-THCm uses a global implicit method, while PHAST uses an operator splitting method, which is known to introduce an operator splitting error (Calderhead and Mayer, 2004).

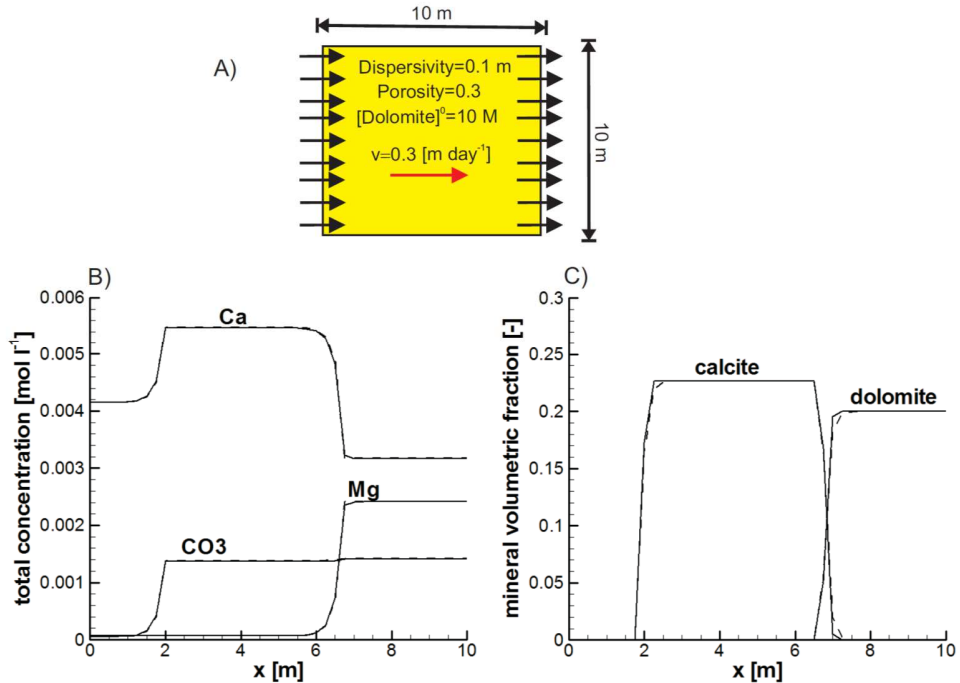


Figure 2.33: Dedolomitization problem. A) Physical and chemical properties of the domain. B) Spatial distribution of total concentrations at 30000 days. C) Volumetric fractions of calcite (CaCO_3) and dolomite ($\text{CaMg}(\text{SO}_4)_2$) at 30000 days. MIN3P-THCm results (solids lines) match well with results from PHAST (dashed lines) (Bea et al., 2011)

2.5.10.4 File locations

The input file *dedo.dat* can be found under

```
..\benchmarking_nwmo_report\ nwmo_verification_examples_D5\d51_dedolomitization\min3p-nwmo
```

Database can be found under: .\benchmarks\database\default

2.5.11 PYRITE OXIDATION AND GAS DIFFUSION IN THE VADOSE ZONE

2.5.11.1 Problem definition

This benchmark is a one-dimensional problem involving O₂ gas diffusion and pyrite oxidation, which is used to evaluate the shrinking core reaction model and gas diffusion provided by Wunderly et al (1996). A code intercomparison of MIN3P-THCm and PYROX was undertaken.

2.5.11.2 Model setup

A 1D model, 1.5 m in depth, is discretized into 121 control volumes yielding a discretization interval of 0.05 m for the interior control volumes and 0.025 m for the control volumes on the boundary. All reactions considered can be expressed by 4 components (SO_4^{2-} , H^+ , Fe^{2+} and $\text{O}_2(\text{aq})$). One gas ($\text{O}_2(\text{g})$) and one mineral (pyrite) are considered in the simulation. The initial and boundary conditions are listed in Table 2.42. Boundary conditions are a specified flux of 0 m s^{-1} at the top boundary and a hydraulic head of -0.2 m at the bottom boundary. For reactive transport, the BCs consist of a mixed type boundary condition at the top boundary and a free outflow boundary condition at the bottom. The concentration of $\text{O}_2(\text{g})$ is determined internally based on Henry's law.

Table 2.42: Initial and boundary conditions for flow and reactive transport

Parameter	Initial Condition	Boundary Conditions		Unit
<i>Aqueous phase</i>		top	bottom	
SO_4^{2-}	1.0×10^{-10}	1.0×10^{-10}		[mol l^{-1}]
Fe^{2+}	1.0×10^{-10}	1.0×10^{-10}	(free exit)	[mol l^{-1}]
$\text{O}_2(\text{aq})$	1.0×10^{-10}	2.63×10^{-4}		[mol l^{-1}]
pH	6.29	3.0		pH
<i>Mineral</i>				
Pyrite	0.5	-	-	[$\text{m}^3 \text{ m}^{-3}$]
<i>Hydraulic condition</i>				
Hydraulic head	1.5	-	-0.2 (first)	[m]
Specified flux	-	0.0 (second)	-	[m s^{-1}]

2.5.11.3 Parameters

The physical parameters (material properties) used for the simulations are summarized in Table 2.43. The shrinking core reaction parameters for the pyrite oxidation by O_2 are given in Table 2.44. A detailed description of all parameters can be found in section 4.6.2 in the user manual.

Table 2.43: Physical parameters for benchmark pyrox

Parameter	Symbol	Value	Unit
Length of domain	L	1.50	[m]
Porosity	ϕ	0.50	[\cdot]
Hydraulic conductivity	K_{zz}	1.0×10^{-6}	[m s^{-1}]
Residual saturation	S_{ra}	0.05	[\cdot]
Van Genuchten parameter α	α	3.50	[m^{-1}]
Van Genuchten parameter n	n	1.40	[\cdot]
Diffusion coefficient, aqueous	D_0^a	0.0	[$\text{m}^2 \text{ s}^{-1}$]
Diffusion coefficient, gas	D_0^g	1.89×10^{-5}	[$\text{m}^2 \text{ s}^{-1}$]
Longitudinal dispersivity	α_l	0.1	[m]

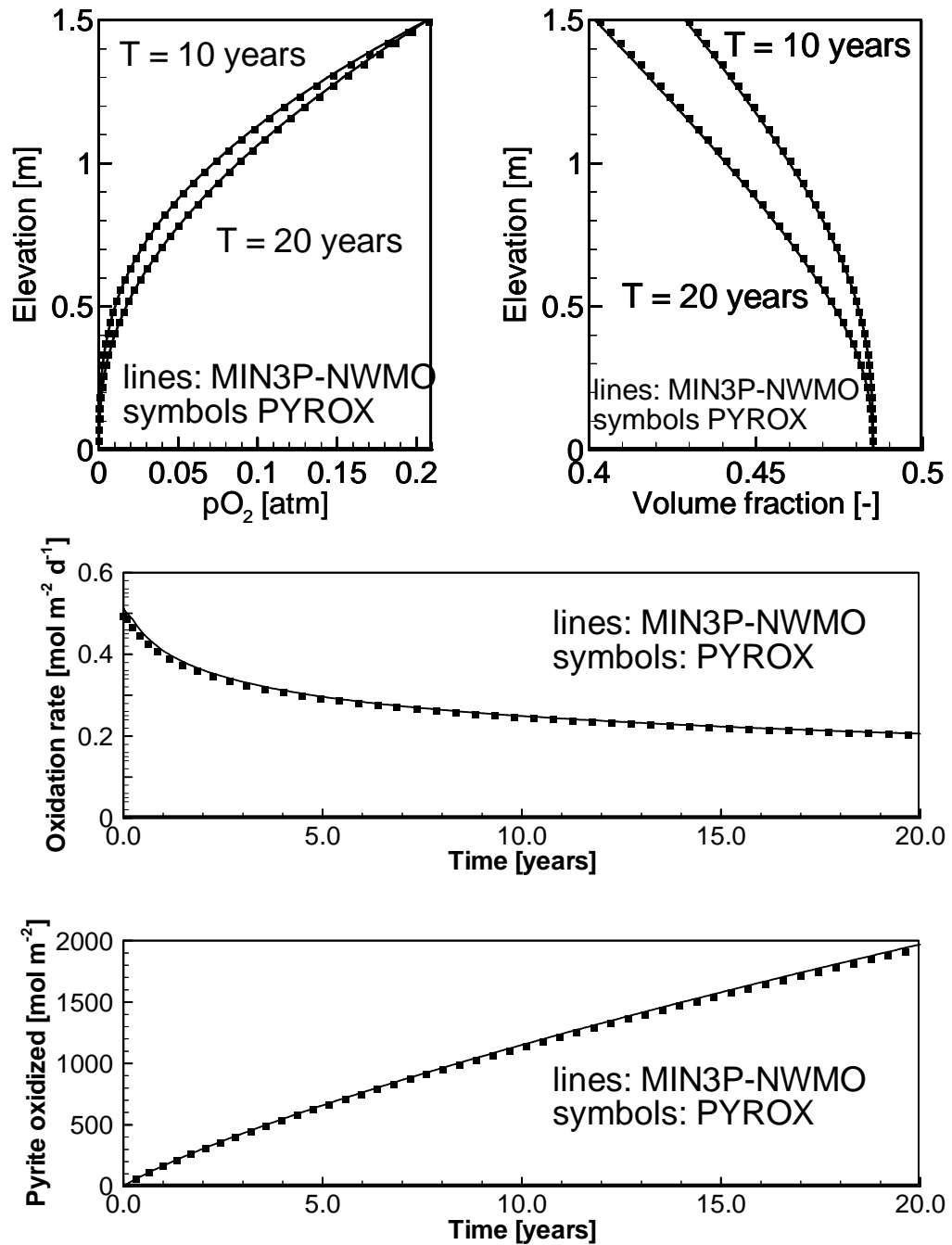


Figure 2.34: Comparison of simulated profiles by MIN3P-THCm and PYROX of O_2 partial pressure (top left) and volume fraction of pyrite (top right) at 10 and 20 years, respectively; and of time curves of pyrite oxidation rate (middle) and oxidized amount (bottom) at the observation point (elevation 0.25 m)

Table 2.44: The shrinking core reaction parameters for pyrite oxidation

Parameter	Symbol	Value	Unit
Scaling factor	S_i	4.15×10^{-6}	[\cdot]
Initial radius of the particle	r_i^P	7.00×10^{-5}	[m]
Initial radius of the unreacted portion of the particle	r_i^R	6.93×10^{-5}	[m]
Free phase diffusion coefficient of O ₂ (aq) in water	D_{iI}^m	2.41×10^{-9}	[m ² s ⁻¹]
Stoichiometric coefficient of oxygen in the reaction equation	v_{iI}^m	3.5	[\cdot]

2.5.11.4 Results

Comparisons of simulated results by MIN3P-THCm and PYROX (Wunderly et al., 1996) are depicted in Figure 2.34 and show very good agreement. O₂(g) ingresses from the top of the column into the soil (Figure 2.34 top left), causing pyrite oxidation owing to the reaction with oxygen (Figure 2.34 top right). The pyrite oxidation rate decreases with time at an observation point at the elevation of 0.25 m (Figure 2.34 middle) due to the formation of a leached layer. The cumulative mass of pyrite oxidized increases with time at the same observation point (Figure 2.34 bottom).

2.5.11.5 File locations

The input file is: *pyrox.dat* under folder

.\benchmarks\benchmarks_standard\reactran\pyrox

Database can be found under: .\benchmarks\database\default

2.5.12 POROSITY-PERMEABILITY ENHANCEMENT DUE TO MINERAL DISSOLUTION

2.5.12.1 Problem definition

This benchmark has been designed to evaluate formulations for permeability-porosity relationships affected by dissolution reactions. The porosity change in each grid cell is calculated by summation over the volume fraction changes of the minerals that occurred between the new time step ($t + \Delta t$) and that at the previous time step (t). Assuming that porosity changes are occurring slowly, porosity in each cell is explicitly updated after completion of each time step:

$$\phi^{t+\Delta t} = \phi^t - \sum_{i=1}^{N_m} (\varphi_i^{t+\Delta t} - \varphi_i^t) \quad \text{Equation 1-23}$$

The hydraulic conductivity K is also updated at the end of each time step according to the Carman-Kozeny relationship:

Validation report-page# 2-104

$$K^{t+\Delta t} = \left[\frac{(\phi^{t+\Delta t})^3}{(1 - \phi^{t+\Delta t})^2} \right] \left[\frac{(1 - \phi^t)^2}{(\phi^t)^3} \right] K^t \quad \text{Equation 1-24}$$

2.5.12.2 Model setup

A 1D model, 2 m in length, is discretized into 81 control volumes. The initial conditions (IC) and boundary conditions (BC) for flow and mass transport are listed in Table 2.45.

A solution with low pH (pH=3.0) enters from the left hand side with the inflowing groundwater. This solution causes the dissolution of calcite in the domain.

Table 2.45: Initial and boundary conditions for flow and reactive transport

Parameter	Initial Condition	Boundary Condition		Unit
<i>Aqueous phase</i>		left	right	
Ca ²⁺	1.566×10 ⁻⁴	1.0×10 ⁻⁴		[mol l ⁻¹]
CO ₃ ²⁻	2.566×10 ⁻⁴	1.0×10 ⁻²	(free exit)	[mol l ⁻¹]
SO ₄ ²⁻	1.0×10 ⁻¹⁰	6.457×10 ⁻⁴		[mol l ⁻¹]
H ⁺	9.375	3.0		pH
<i>Mineral</i>				
Calcite	0.30	-	-	[m ³ m ⁻³]
<i>Hydraulic condition</i>				
Hydraulic head	0.0	0.007 (first)	0.0 (first)	[m]

2.5.12.3 Parameters

The parameters of the porous medium are: porosity is 0.35, hydraulic conductivity is 1.16×10⁻⁴ m s⁻¹, longitudinal dispersivity is 0.0 m, and the diffusion coefficient is set to 0 m₂ s⁻¹. Calcite is the only mineral considered in the benchmark. Calcite dissolution is surface controlled. The chemical reaction equation and kinetic parameters are provided in Table 2.46 and Table 2.47 (see section 4.6.1 in the user manual).

Table 2.46: Thermodynamic mineral reaction parameters

Mineral	Reaction	logK ₂₅
Calcite	Ca ²⁺ + CO ₃ ²⁻ ↔ CaCO ₃	8.4750

Table 2.47: Kinetic parameters for minerals

Mineral	k _i ^{m,0} [mol mineral L ⁻¹ bulk s ⁻¹]	Density [g cm ⁻³]	Mol. weight [g mol ⁻¹]	Molar volume [cm ³ mol ⁻¹]	Update type
Calcite	5.0×10 ⁻⁸	2.7100	100.0894	36.93336	twothird

k_i^{m,0} is the initial rate constant for the dissolution of the minerals

2.5.12.4 Results

The simulated profiles of porosity, calcite volume fraction and hydraulic head at 10, 100 and 1200 years are depicted in Figure 2.35. With the intrusion of the low pH solution from the left boundary, calcite dissolves and results in an increase of porosity. Consequently, the hydraulic conductivity increases as well and the hydraulic head distribution is also reestablished accordingly. The flux increases gradually with the calcite dissolution and abruptly when calcite becomes depleted in the entire domain.

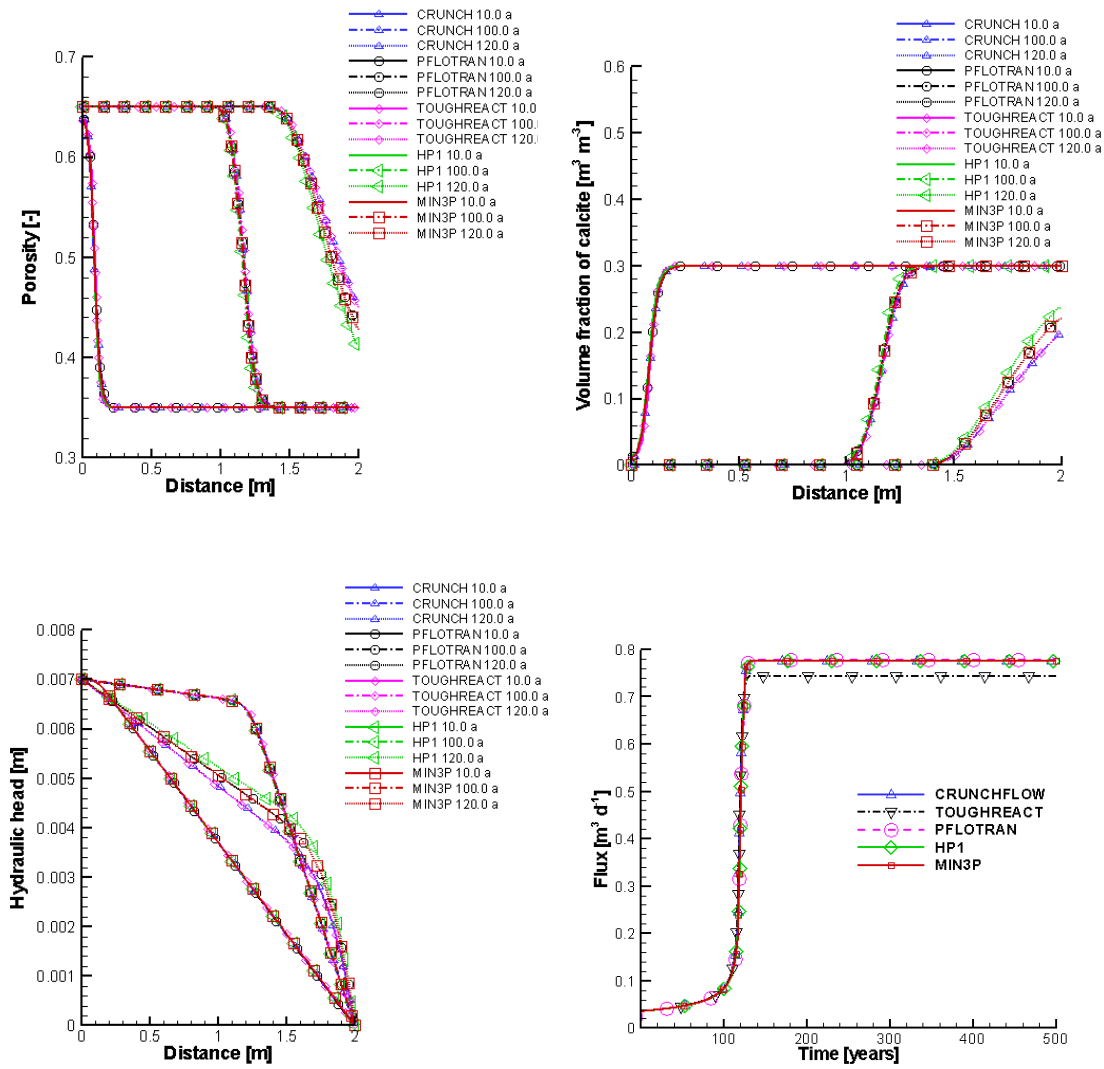


Figure 2.35: Spatial profiles of porosity, volume fraction of calcite, hydraulic head at 10, 100 and 120 years, and flux time curve at the outflow boundary simulated by MIN3P-THCm, TOUGHREACT, HP1, PFlotran and CrunchFlow (Xie et al. 2014)

Validation report-page# 2-106

The comparison of simulated results by MIN3P-THCm with those calculated by TOUGHREACT, HP1, PFlotran and CrunchFlow show very good agreement (Xie et al. 2014).

2.5.12.5 File locations

The input file for the benchmark can be found under

`.\benchmarks\benchmarks_standard\reactran\perm1_new`

Database can be found under: `.\benchmarks\database\default`

2.5.13 CLOGGING DUE TO MINERAL DISSOLUTION/PRECIPITATION – SIMPLE CHEMISTRY

2.5.13.1 Problem definition

This benchmark is designed to evaluate permeability-porosity relationships affected by dissolution-precipitation reactions involving calcite and gypsum. Similar to verification case 2.5.12, this benchmark also considers the infiltration of a sulfuric acid solution into a rock matrix containing calcite in an otherwise non-reactive rock matrix, but with much higher SO_4^{2-} concentrations. Consequently, gypsum precipitates resulting in a ‘clogging’ effect that decreases the porosity and permeability of the porous medium.

2.5.13.2 Model setup

A 1D model, 2 m in length, is discretized into 81 control volumes. The initial concentration (IC) and boundary conditions (BC) for flow and mass transport are listed in Table 2.48. A solution with low pH ($\text{pH}=3.0$) enters from the left hand side with inflowing groundwater, causing the dissolution of calcite in the domain.

Table 2.48: Initial and boundary conditions for flow and reactive transport

Parameter	Initial Condition	Boundary Conditions		Unit
<i>Aqueous phase</i>		left	right	
Ca^{2+}	1.69512×10^{-4}	1.0×10^{-4}		$[\text{mol l}^{-1}]$
CO_3^{2-}	2.69500×10^{-4}	1.0×10^{-2}	(free exit)	$[\text{mol l}^{-1}]$
SO_4^{2-}	1.69512×10^{-4}	0.2		$[\text{mol l}^{-1}]$
Na^+	3.2×10^{-4}	0.3956		$[\text{mol l}^{-1}]$
H^+	9.33	3.0		pH
<i>Mineral</i>				
Calcite	0.30	-	-	$[\text{m}^3 \text{ m}^{-3}]$
Gypsum	0.00	-	-	$[\text{m}^3 \text{ m}^{-3}]$
<i>Hydraulic condition</i>				
Hydraulic head	0.0	0.007 (first)	0.0 (first)	[m]

2.5.13.3 Parameters

The parameters of the porous medium are: porosity is 0.35, hydraulic conductivity is $1.16 \times 10^{-5} \text{ m s}^{-1}$, longitudinal dispersivity is 0.0 m, and the diffusion coefficient is $0.0 \text{ m}^2 \text{ s}^{-1}$. Calcite and gypsum are considered in the benchmark as surface-controlled kinetic reactions (see section “Dissolution-precipitation reactions” in the theory manual). Their chemical reaction equations and kinetic parameters are provided in Table 2.49 and Table 2.50.

Table 2.49: Mineral reaction parameters

Mineral	Reaction	$\log K_{25}$
Calcite	$\text{Ca}^{2+} + \text{CO}_3^{2-} \leftrightarrow \text{CaCO}_3$	8.4750
Gypsum	$\text{Ca}^{2+} + \text{SO}_4^{2-} + 2\text{H}_2\text{O} \leftrightarrow \text{CaSO}_4 \cdot 2\text{H}_2\text{O}$	4.5800

Table 2.50: Kinetic parameters of minerals

Mineral	$k_i^{m,0}$ [mol mineral L ⁻¹ bulk s ⁻¹]	Density [g cm ⁻³]	Mol. weight [g mol ⁻¹]	Molar volume [cm ³ mol ⁻¹]	Update type
Calcite	5.0×10^{-8}	2.7100	100.0894	36.93336	twothird
Gypsum	5.0×10^{-8}	2.3200	172.1722	74.21216	constant

$k_i^{m,0}$ is the initial rate constant for the dissolution of the minerals

2.5.13.4 Results

The simulated profiles of porosity, calcite volume fraction and hydraulic head at 10, 100 and 1000 years and flux time curve at outflow boundary are depicted in Figure 2.36. With the intrusion of the low pH solution from the left boundary, calcite dissolves and gypsum precipitates. Porosity changes along the domain depending on the net volume change at each control volume. At 100 years, the maximal volume fraction (VF) of gypsum amounts to 56.3 % and of calcite 8.01 % at x=0.425 m, which results in the decrease of porosity to 0.0069. At 1000 years, the minimum porosity decreases to 0.0018 at the same position (x=0.425 m) owing to the higher VF of gypsum of 57.4 % and a VF of calcite of 7.47 %. Consequently, the hydraulic conductivity decreases as well and the hydraulic head distribution is being reestablished accordingly with a sharp gradient at x=0.425 m. The flux decreases gradually over time. The comparison of simulated results by MIN3P-THCm with those calculated by TOUGHREACT, PFlotran and CrunchFlow showed very good agreement (Xie et al. 2014).

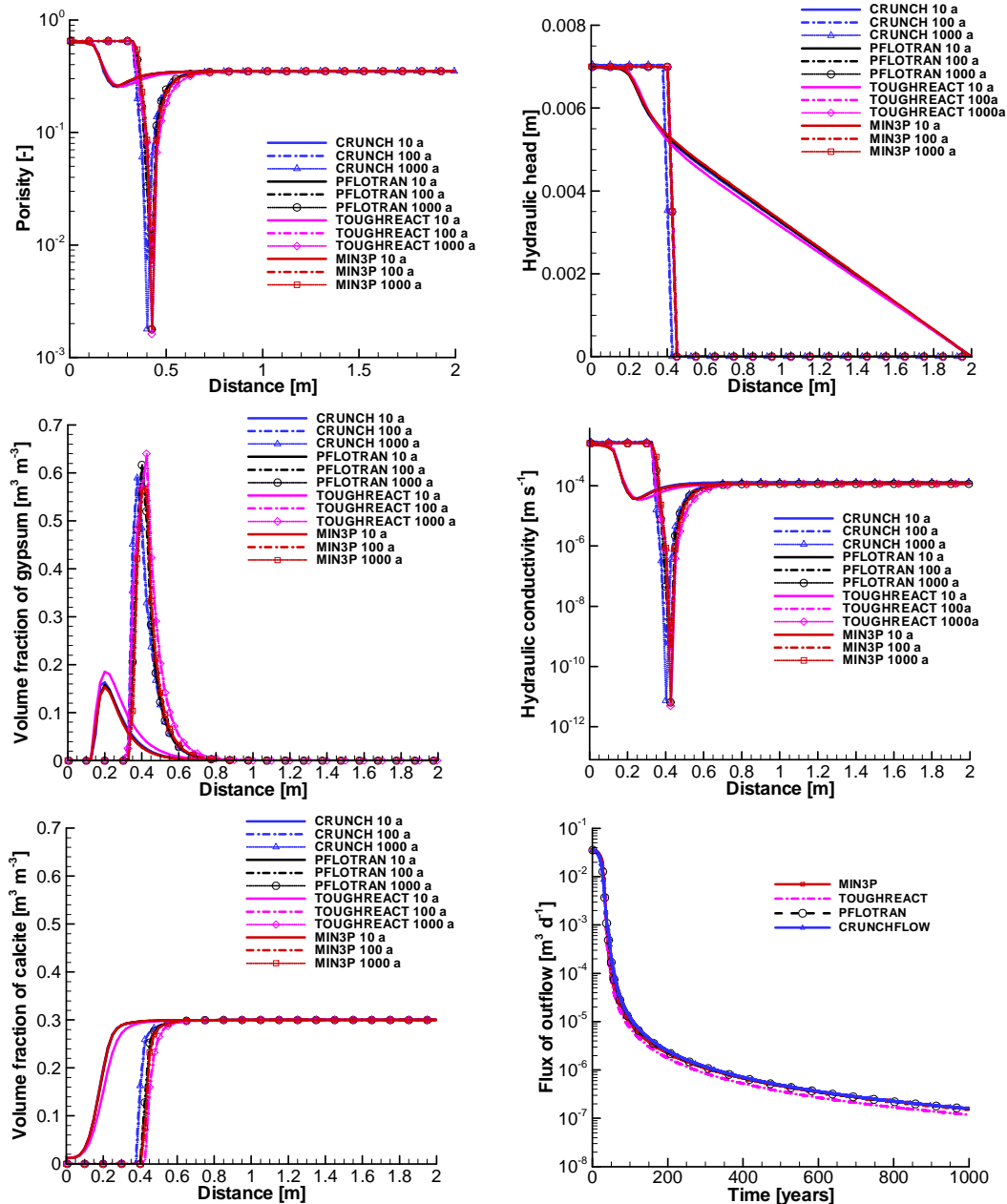


Figure 2.36: Spatial profiles of porosity, volume fraction of gypsum and calcite, hydraulic head, and hydraulic conductivity at 10, 100 and 120 years, and flux time curve at the outflow boundary simulated by MIN3P-THCm, TOUGHREACT, PFlotran and CrunchFlow (Xie et al. 2014).

2.5.13.5 File locations

The input file for the benchmark can be found under

`.\benchmarks\benchmarks_standard\reactran\perm2_new`

Database can be found under: `.\benchmarks\database\default`

Validation report-page# 2-109

2.5.14 CLOGGING DUE TO MINERAL DISSOLUTION/PRECIPITATION – COMPLEX CHEMISTRY

2.5.14.1 Problem definition

This benchmark is designed to evaluate permeability-porosity relationships affected by the dissolution and precipitation of multiple mineral phases, namely calcite, gypsum, ferrihydrite, siderite, gibbsite and jarosite. Redox equilibrium for $\text{Fe}^{2+}/\text{Fe}^{3+}$ is also considered. The geochemical system includes eight primary components H^+ , CO_3^{2-} , Ca^{2+} , SO_4^{2-} , Fe^{3+} , Fe^{2+} , Al^{3+} , K^+ , $\text{O}_2(\text{aq})$ and Na^+ , 40 secondary species and six minerals.

2.5.14.2 Model setup

A 1D model, 2 m in length, is discretized into 81 control volumes. The initial concentration (IC) and boundary conditions (BC) for flow and mass transport are listed in Table 2.51. A solution with low pH (pH=3.0) enters from the left hand side with inflowing groundwater, causing the dissolution of calcite, siderite and gibbsite in the domain, and leading to the formation and redissolution of a number of secondary minerals.

Table 2.51: Initial and boundary conditions for flow and reactive transport

Parameter	Initial Condition	Boundary Conditions		Unit
<i>Aqueous phase</i>		left	right	
Ca^{2+}	1.69512×10^{-4}	1.0×10^{-4}		[mol l ⁻¹]
CO_3^{2-}	1.89480×10^{-4}	1.0×10^{-2}		[mol l ⁻¹]
SO_4^{2-}	1.69512×10^{-4}	0.1		[mol l ⁻¹]
Na^+	1.5430×10^{-3}	9.0920×10^{-2}		[mol l ⁻¹]
Al^{3+}	1.0×10^{-5}	1.4300×10^{-2}	(free exit)	[mol l ⁻¹]
K^+	1.0×10^{-5}	7.6700×10^{-5}		[mol l ⁻¹]
Fe^{2+}	9.9674×10^{-6}	1.1389×10^{-8}		[mol l ⁻¹]
Fe^{3+}	3.2679×10^{-8}	2.2300×10^{-2}		[mol l ⁻¹]
H^+	7.0	3.0		pH
$\text{O}_2(\text{aq})$	2.0	17.53		pe
<i>Mineral</i>				
Calcite	0.22	-	-	[m ³ m ⁻³]
Gypsum	0.00	-	-	[m ³ m ⁻³]
Ferrihydrite	0.00	-	-	[m ³ m ⁻³]
Jarosite	0.00	-	-	[m ³ m ⁻³]
Gibbsite	0.05	-	-	[m ³ m ⁻³]
Siderite	0.05	-	-	[m ³ m ⁻³]
<i>Hydraulic condition</i>				
Hydraulic head	0.0	0.007 (first)	0.0 (first)	[m]

Validation report-page# 2-110

2.5.14.3 Parameters

The parameters of the porous media are: porosity is 0.35, hydraulic conductivity is $1.16 \times 10^{-5} \text{ m s}^{-1}$, longitudinal dispersivity is 0.0 m, and diffusion coefficient is 0.0 $\text{m}^2 \text{s}^{-1}$. All minerals in the benchmark are considered as surface-controlled kinetic reactions (see section “Dissolution-precipitation reactions” in the theory manual. Their chemical reaction equations and kinetic parameters are provided in Table 2.52 and Table 2.53.

Table 2.52: Mineral reaction parameters

Mineral	Reaction	logK ₂₅
Calcite	$\text{Ca}^{2+} + \text{CO}_3^{2-} \leftrightarrow \text{CaCO}_3$	8.4750
Gypsum	$\text{Ca}^{2+} + \text{SO}_4^{2-} + 2\text{H}_2\text{O} \leftrightarrow \text{CaSO}_4 \cdot 2\text{H}_2\text{O}$	4.5800
Ferrihydrite	$\text{Fe}^{3+} + 3\text{H}_2\text{O} \leftrightarrow \text{Fe(OH)}_3 + 3\text{H}^+$	-4.8910
Jarosite	$\text{K}^+ + 3\text{Fe}^{3+} + 2\text{SO}_4^{2-} + 6\text{H}_2\text{O} \leftrightarrow \text{KFe}_3(\text{SO}_4)_2(\text{OH})_6 + 6\text{H}^+$	9.2100
Gibbsite	$\text{Al}^{3+} + 3\text{H}_2\text{O} \leftrightarrow \text{Al(OH)}_3 + 3\text{H}^+$	-8.1100
Siderite	$\text{Fe}^{2+} + \text{CO}_3^{2-} \leftrightarrow \text{FeCO}_3$	10.4500

Table 2.53: Kinetic parameters of minerals

Mineral	$k_i^{m,0}$ [mol mineral L ⁻¹ bulk s ⁻¹]	Density [g cm ⁻³]	Mol. weight [g mol ⁻¹]	Molar volume [cm ³ mol ⁻¹]	Update type
Calcite	5.0×10^{-8}	2.7100	100.0894	36.93336	twothird
Gypsum	5.0×10^{-8}	2.3200	172.1722	74.21216	constant
Ferrihydrite	5.0×10^{-9}	4.3713	104.8692	23.99039	constant
Jarosite	5.0×10^{-9}	3.2000	494.8100	154.6281	constant
Gibbsite	5.0×10^{-10}	2.3500	78.0037	33.19306	twothird
Siderite	5.0×10^{-9}	3.9600	115.8564	29.25667	twothird

$k_i^{m,0}$ is the initial rate constant for the dissolution of the minerals

2.5.14.4 Results

The simulated spatial profiles of porosity, hydraulic conductivity and hydraulic head at 10, 100 and 1000 years and flux time curve at the outflow boundary are depicted in Figure 2.37, and the profiles of volume fraction of all six minerals are depicted in Figure 2.38. With the intrusion of the low pH and high pe solution from the left boundary, calcite dissolves and other minerals like gypsum, siderite, gibbsite, ferrihydrite and jarosite dissolve/precipitate depending on the time and location and thus forming various porosity peaks along the profile at different time levels. Consequently, the porosity decreases near the infiltration boundary. At 10 years, the minimum porosity reduces from the initial value of 0.35 to 0.05 at 0.25 m, showing a tendency of clogging. The “clogging” point develops and moves further. After 100 years, however, the clogging point moves slowly (Figure 2.37 top left). The flux also decreases over time due to the associated permeability reduction (Figure 2.37 bottom right).

The comparison of simulated results by MIN3P-THCm with those calculated by

TOUGHREACT, PFlotran and CrunchFlow show very good agreement (Xie et al. 2014).

2.5.14.5 File locations

The input file for the benchmark can be found under

`.\benchmarks\benchmarks_standard\reactran\perm3_new`

Database can be found under: `.\benchmarks\database\default`

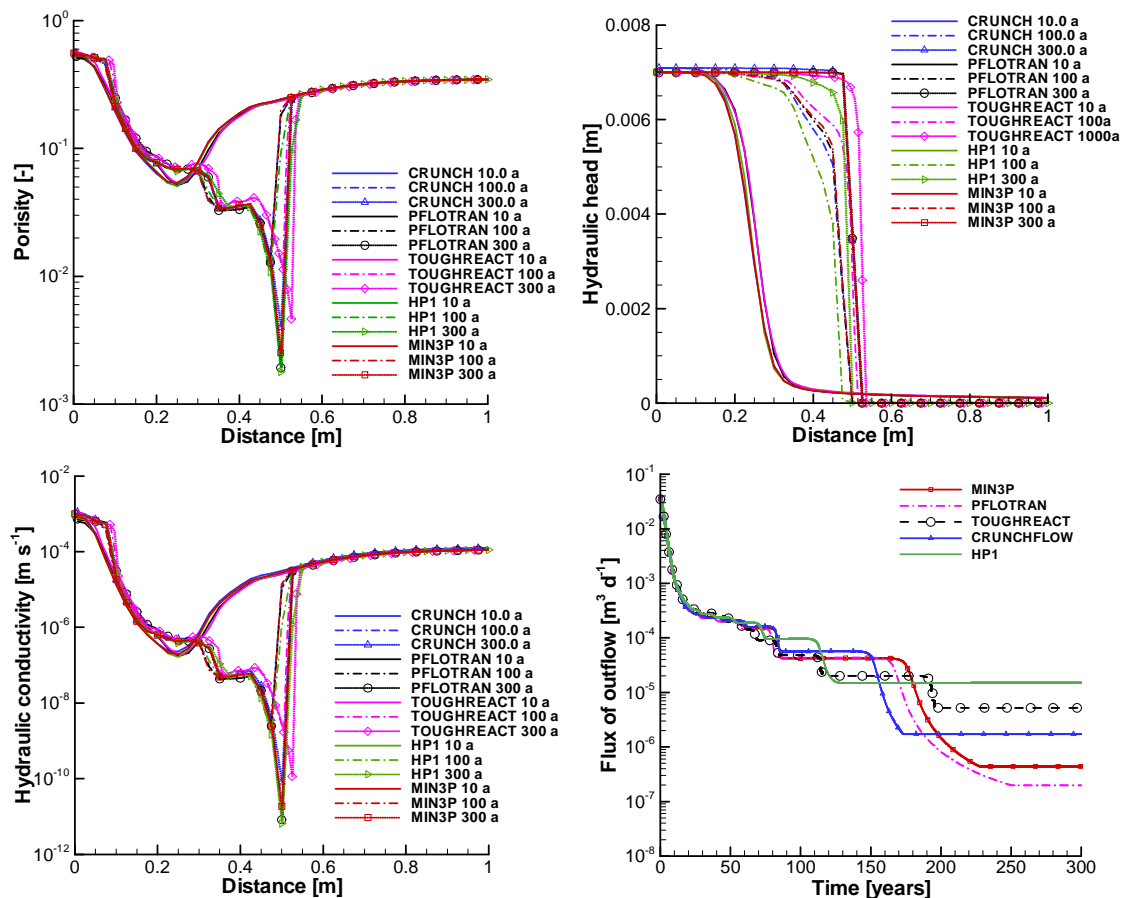


Figure 2.37: Spatial profiles of porosity, hydraulic head, hydraulic conductivity at 10, 100 and 120 years, and flux time curve at the outflow boundary simulated by MIN3P-THCm, TOUGHREACT, PFlotran, HP1 and CrunchFlow (Xie et al. 2014).

Validation report-page# 2-112

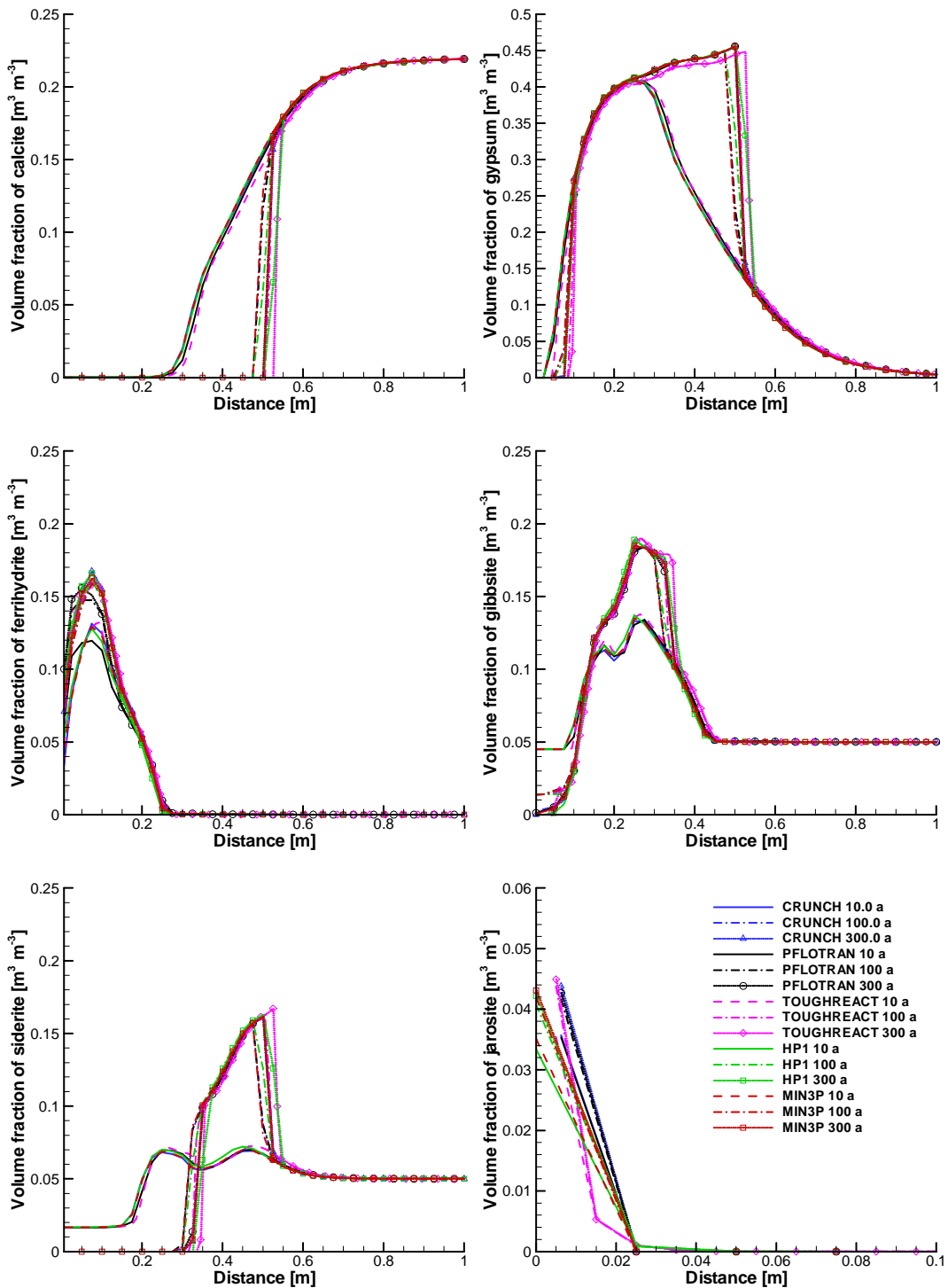


Figure 2.38: Comparison of spatial volume fraction profiles (B3) of calcite, gypsum, ferrihydrite, gibbsite, siderite and jarosite at 10, 100 and 300 years simulated by MIN3P-THCm, TOUGHREACT, PFlotran, HP1 and CrunchFlow (Xie et al. 2014)

2.5.15 LINEAR RETARDATION OF PCE AND BENZENE

2.5.15.1 Problem definition

This benchmark is a one dimensional problem involving linear adsorption of contaminants during advective-diffusive transport in saturated porous media under steady-state flow conditions. The NAPL (non-aqueous phase liquid) contaminants considered are PCE (C_2Cl_4) and benzene (C_6H_6). The MIN3P-THCm results are verified against an analytical solution.

2.5.15.2 Model set-up

A 1D model, 100.0 m in length, is discretized into 2001 control volumes yielding a discretization interval of 0.05 m for the interior control volumes and 0.025 m for the control volumes on the boundary. Transport simulations were carried out under steady-state saturated flow conditions. The flow boundary conditions are constant hydraulic heads of 1.0 m at the left boundary and 0.0 m at the right boundary, respectively. It is assumed that both PCE and benzene exist in the aqueous phase without any degradation and chemical reactions. The migration is driven by advection and diffusion with linear adsorption. The initial and boundary hydraulic and geochemical conditions are listed in Table 2.54.

Table 2.54: Initial and boundary conditions for flow and reactive transport

Parameter	Initial Condition	Boundary Conditions	Unit
<i>Aqueous phase</i>			
Cl^-	1.0×10^{-10}	left 0.10	right [mol l ⁻¹]
C_2Cl_4 (PCE)	1.0×10^{-10}	0.20 (free exit)	[mol l ⁻¹]
C_6H_6 (Benzene)	1.0×10^{-10}	0.15	[mol l ⁻¹]
<i>Hydraulic condition</i>			
Hydraulic head	1.0	1.0 (first) 0.0 (first)	[m]

2.5.15.3 Parameters

The physical parameters (material properties) used for the simulations are summarized in Table 2.55. The sorption coefficients (K_s) of C_2Cl_4 and C_6H_6 are 5.0 and 2.0, respectively. It is important to note that K_s in MIN3P-THCm is defined as:

$$K_s = \frac{\rho_b}{\phi} K_D \quad \text{Equation 1-25}$$

In which ρ_b is the bulk dry density in [kg L⁻¹], ϕ is the volumetric porosity [-], and K_D is the adsorption distribution coefficient [L kg⁻¹].

Table 2.55: Physical parameters for benchmark raoult

Parameter	Symbol	Value	Unit
Length of domain	L	100.0	[m]
Porosity	ϕ	0.50	[\cdot]
Hydraulic conductivity	K_{xx}	1.0×10^{-4}	[$m\ s^{-1}$]
Diffusion coefficient	D_0^a	1.0×10^{-7}	[$m^2\ s^{-1}$]
Longitudinal dispersivity	α_l	0.0	[m]
Sorption coefficient of C_2Cl_4	K_s	5.0	[\cdot]
Sorption coefficient of C_6H_6	K_s	2.0	[\cdot]

2.5.15.4 Analytical solution

For a steady state one-dimensional flow through a homogeneous isotropic porous media with constant material properties, the mass transport equation considering advection, diffusion and retardation (linear sorption) can be described as (Ogata and Banks 1961):

$$\frac{\partial C}{\partial t} + \frac{\rho_b}{R} \cdot \frac{\partial S}{\partial t} + \frac{q}{R} \cdot \frac{\partial C}{\partial x} = D_{xx} \cdot \frac{\partial^2 C}{\partial x^2} \quad \text{Equation 1-26}$$

In which C is the aqueous concentration [mol L^{-1}], S is the adsorbed concentration [mol kg^{-1}], t is time [s], ρ_b is bulk density [kg L^{-1}], q is flow rate [m s^{-1}], x is distance [m], D_{xx} is dispersion coefficient in x-direction [$\text{m}^2 \text{s}^{-1}$], R is the retardation factor [\cdot] described as:

$$R = 1 + \frac{\rho_b}{\phi} K_D = 1 + K_s \quad \text{Equation 1-27}$$

With the initial condition

$$C(x, t = 0) = C_0 \quad \forall x \quad \text{Equation 1-28}$$

And boundary conditions

$$C(x = 0, t) = C_1 \quad \forall t \quad C(x \rightarrow \infty, t) = C_0 \quad \forall t \quad \text{Equation 1-29}$$

The following analytical solution can be derived (according to Kolditz et al. 2012):

$$C = C_0 + \frac{C_1 - C_0}{2} \left[erfc \left(\frac{x - v \cdot t/R}{2 \cdot \sqrt{D_{xx} \cdot t/R}} \right) + exp \left(\frac{v \cdot x}{D_{xx}} \right) \cdot erfc \left(\frac{x + v \cdot t/R}{2 \cdot \sqrt{D_{xx} \cdot t/R}} \right) \right] \quad \text{Equation 1-30}$$

In which v is the fluid velocity [m s^{-1}].

2.5.15.5 Results

Simulated results show that both contaminants C_2Cl_4 and C_6H_6 are retarded in comparison to the conservative tracer Cl^- (Figure 2.39).

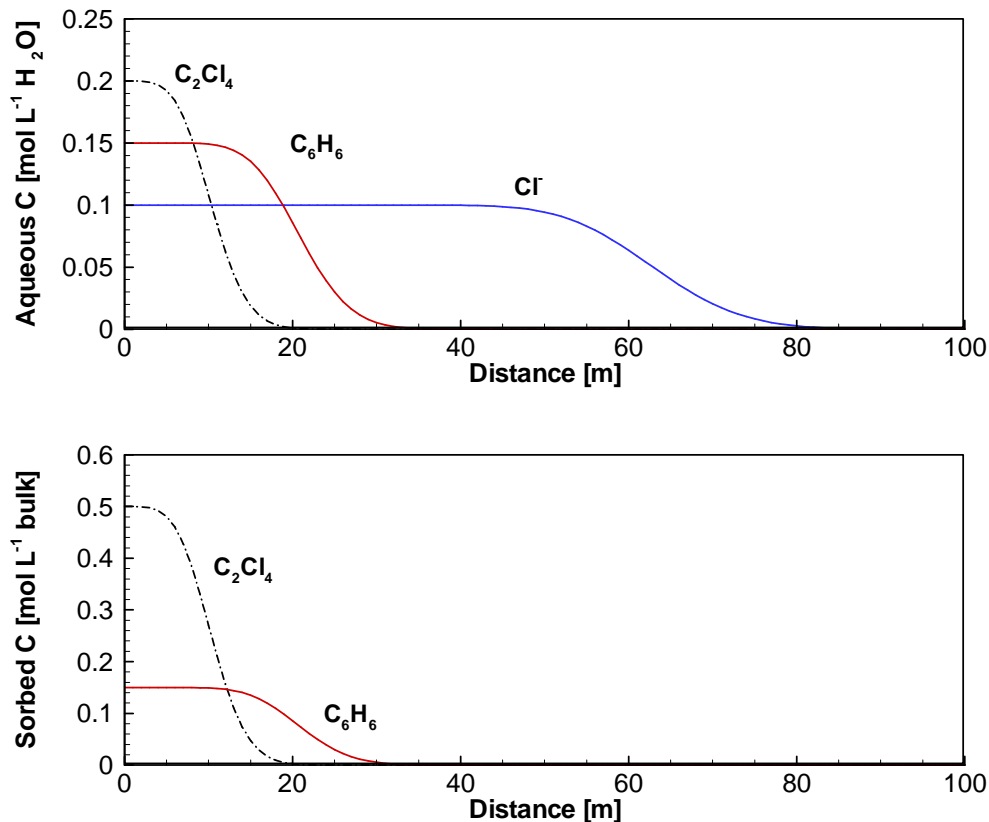


Figure 2.39: Simulated profiles of aqueous concentrations (upper panel) and absorbed concentrations (lower panel) after one year

The simulated breakthrough curves of Cl^- , C_2Cl_4 and C_6H_6 at 10 m from the left boundary agree well with the analytical solutions (Figure 2.40).

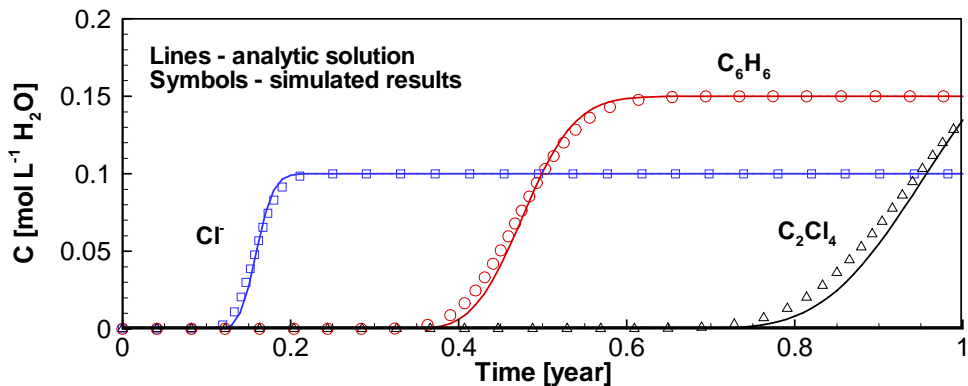


Figure 2.40: Comparison of results obtained using MIN3P-THCm (symbols) with the analytical solution (lines) for breakthrough curves of Cl^- , C_2Cl_4 and C_6H_6 at $x=10 \text{ m}$

2.5.15.6 File locations

The input file is: retardation.dat under folder
`.\benchmarks\benchmarks_standard\reactran\retardation`

Database can be found under: `.\benchmarks\database\default`

2.5.16 AEROBIC DEGRADATION OF TOLUENE

2.5.16.1 Problem definition

This example simulates an aquifer that initially contains groundwater with substantial dissolved oxygen, affected by the infiltration of a strongly reducing groundwater containing toluene ($\text{C}_6\text{H}_5\text{CH}_3$). Under these conditions, toluene is degraded using $\text{O}_2(\text{aq})$ as the electron acceptor according to the following reaction:



The degradation of toluene in the mixing zone of the two solutions leads to a decrease in dissolved oxygen and an increase of total dissolved inorganic carbon.

2.5.16.2 Model set-up

The chemical compositions of the initial and boundary waters are presented in Table 2.56. Physical properties of the domain are illustrated in Figure 2.41A.

Validation report-page# 2-117

Table 2.56: Toluene Degradation Problem: Composition of Initial and Boundary Waters
(Bea et al., 2011)

Parameter	Boundary water	Initial Water	Unit
H^+	7	7	pH
$\text{C}_6\text{H}_5\text{CH}_3$	10^{-3}	10^{-10}	[mol l ⁻¹]
$\text{O}_2(\text{aq})$	10^{-10}	10^{-3}	[mol l ⁻¹]
Cl^-	10^{-3}	10^{-10}	[mol l ⁻¹]
Na^+	10^{-3}	10^{-10}	[mol l ⁻¹]
CO_3^{2-}	10^{-10}	10^{-10}	[mol l ⁻¹]
Ionic strength	10^{-3}	10^{-7}	[mol l ⁻¹]

2.5.16.3 Results

Simulation results for total concentrations of carbonate, toluene and oxygen, and the rate of toluene oxidation in the dispersive mixing zone, are shown for MIN3P-THCm and PHAST in Figure 2.41B. The spatial distribution of the aerobic degradation rate for toluene at 5 days is shown in Figure 2.41C. The results of MIN3P-THCm are essentially identical with the PHAST results.

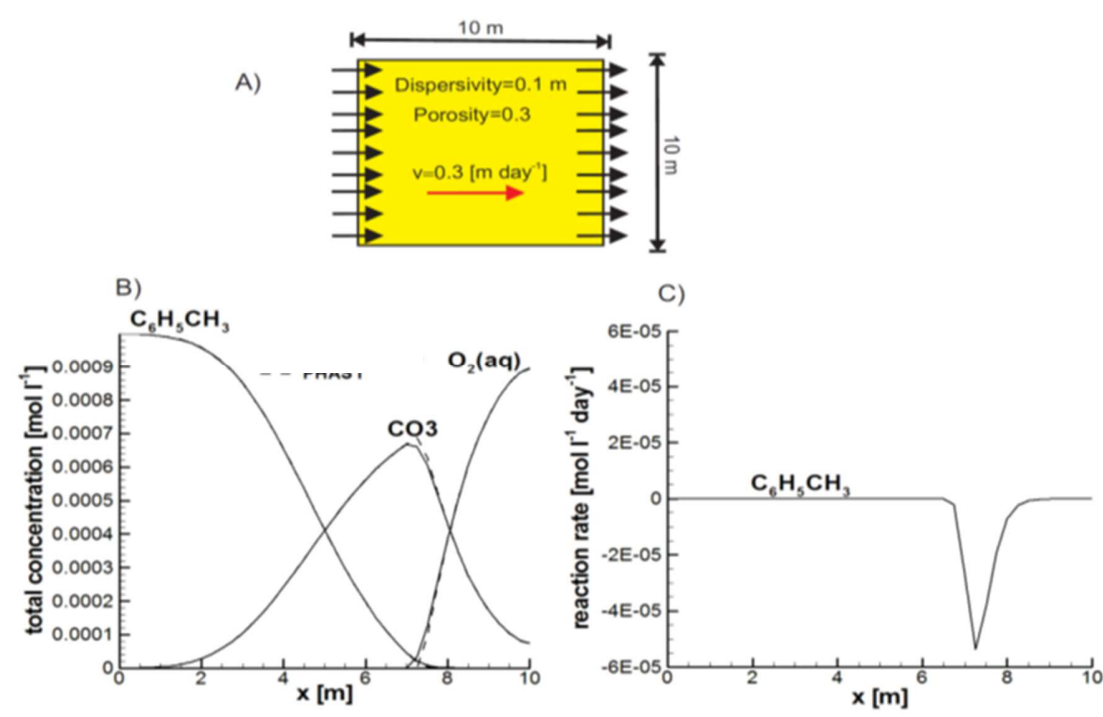


Figure 2.41: Toluene verification problem. (A) Physical and chemical properties of the domain. (B) Spatial distribution of total concentrations at 5 days. (C) Spatial distribution of aerobic degradation rate of toluene ($\text{C}_6\text{H}_5\text{CH}_3$) at 5 days. The results for MIN3P-

Validation report-page# 2-118

THCm (solid lines) are compared with PHAST (dashed lines) (Bea et al., 2011)

2.5.16.4 File locations

The input file *biod.dat* can be found under

..\benchmarking_nwmo_report\ nwmo_verification_examples_D5\d53_aerobic_degradation\min3p\

Database is a subfolder under the folder of the input file: \database\default

2.5.17 REACTIVE TRANSPORT IN HIGHLY SALINE SOLUTION

2.5.17.1 Problem definition

This verification example is a one dimensional problem to evaluate the capabilities of MIN3P-THCm in dealing with reactive transport at high solute concentrations. It is verified against PHAST. The test consists of a one-dimensional reactive transport simulation in which a K-enriched solution in equilibrium with halite (NaCl) and polyhalite ($\text{Ca}_2\text{MgK}_2(\text{SO}_4)_4 \cdot 2\text{H}_2\text{O}$) migrates through a column initially in equilibrium with halite and gypsum ($\text{CaSO}_4 \cdot 2\text{H}_2\text{O}$) (see Bea et al., 2011).

2.5.17.2 Model set-up

The domain in 1 m is discretized into 100 control volumes. The compositions of initial and boundary solutions are detailed in Table 2.57.

Table 2.57: Replacement of gypsum by polyhalite: composition of initial and boundary waters of the domain (Bea et al., 2011)

Parameter	Boundary water	Initial water	Unit
H^+ (pH)	7.3	8.1	[-]
Ca^{2+}	3.8×10^{-3}	1.1×10^{-2}	[mol l $^{-1}$]
Mg^{2+}	2.2	6.3×10^{-1}	[mol l $^{-1}$]
Cl^-	6.48	5.94	[mol l $^{-1}$]
K^+	7.43	1.2×10^{-1}	[mol l $^{-1}$]
Na^+	2.72	5.178	[mol l $^{-1}$]
Br^-	10^{-6}	1.0×10^{-9}	[mol l $^{-1}$]
CO_3^{2-}	5.1×10^{-5}	1.7×10^{-5}	[mol l $^{-1}$]
SO_4^{2-}	5.6×10^{-1}	2.3×10^{-1}	[mol l $^{-1}$]
Ionic strength	13.83	7.35	[mol l $^{-1}$]

2.5.17.3 Parameters

Physical and chemical parameters of the problem are presented in Figure 2.42A. The porosity and dispersivity are 0.4 and 0.01 m, respectively. The Pitzer equations are used

Validation report-page# 2-119

to calculate the activities of aqueous species. For major components, the virial coefficients are taken from Harvie et al. (1984) and Greenberg and Möller (1989), as tabulated in Appendix B.5 in Bea et al. (2011).

2.5.17.4 Results

The problem was also solved with PHAST (Parkhurst et al., 2005), allowing for a direct comparison between the results.

The spatial distributions of total concentration of Ca^{2+} , Na^+ , K^+ and SO_4^{2-} and the volumetric content of mineral phases at 10 and 30 years are shown in Figure 2.42. Gypsum was completely dissolved from the domain at the end of the simulation (total simulated time was approximately 100 years). The precipitation/dissolution of halite is controlled by the precipitation of polyhalite. When polyhalite starts to precipitate, halite is partially redissolved (results not shown). The results obtained with MIN3P-THCm and PHAST are in good agreement for both aqueous species and mineral phases.

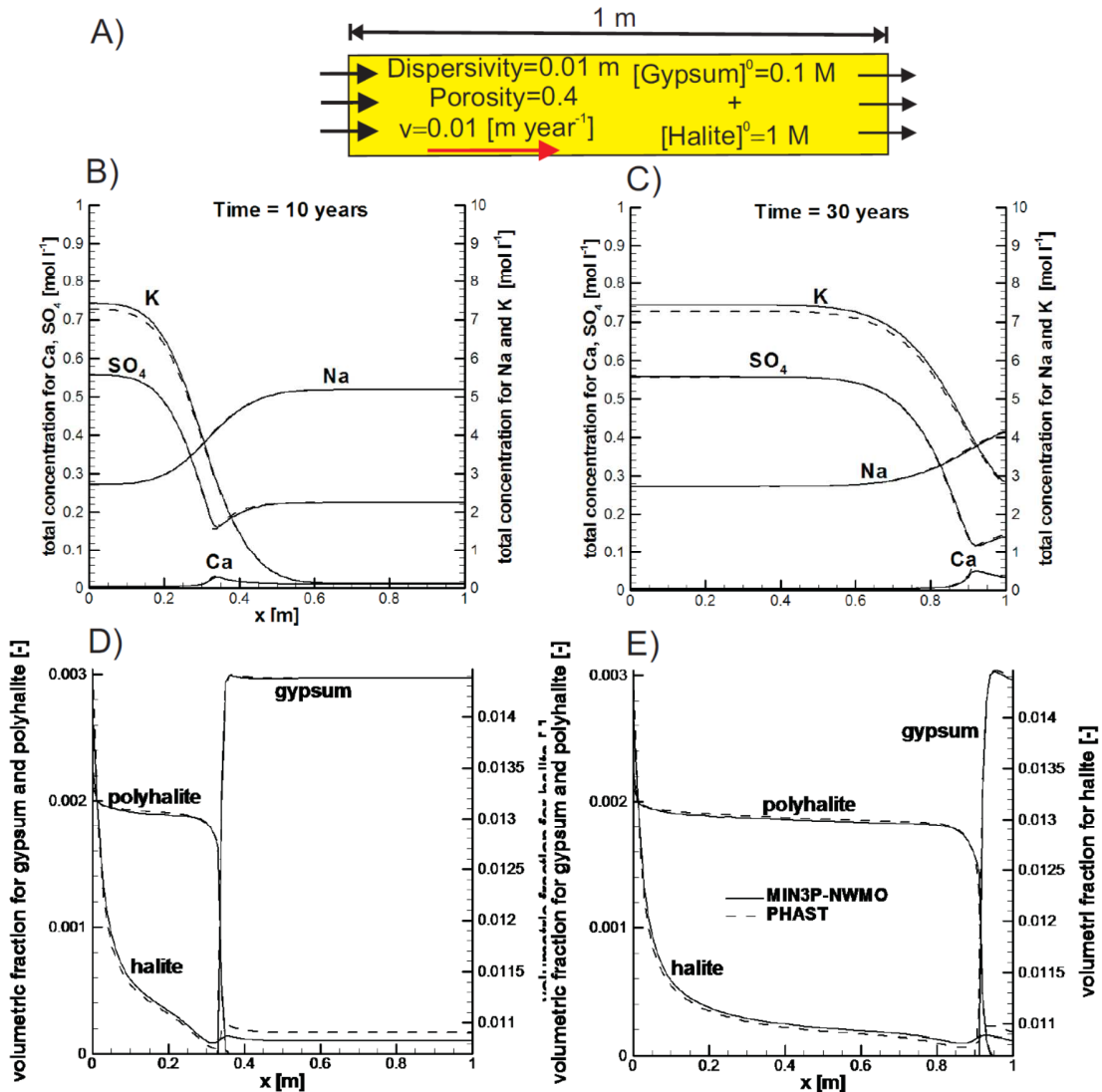


Figure 2.42: Replacement of gypsum by polyhalite. (A) Physical and chemical properties of the domain. (B) and (C) Spatial distribution of total concentrations at 10 and 30 years, respectively. (D) and (E) Volumetric fractions of halite (NaCl), gypsum ($\text{CaSO}_4 \cdot 2\text{H}_2\text{O}$), and polyhalite ($\text{Ca}_2\text{MgK}_2(\text{SO}_4)_4 \cdot 2\text{H}_2\text{O}$), at 10 and 30 years, respectively. The MIN3P-THCM results (solid lines) are compared with PHAST (dashed lines) (Bea et al., 2011)

2.5.17.5 File locations

The input file *polyhal-pitz.dat* can be found under

`..\benchmarking_nwmo_report\nwmo_verification_examples_D6\d6_rt_highly_saline\min3p\`

Database is a subfolder under the folder of the input file: `\database\default`

2.5.18 MULTISITE ION EXCHANGE (IONX-2M)

2.5.18.1 Problem definition

This hypothetical benchmark is a multisite ion exchange problem with two material groups under steady state flow conditions. It was verified through code intercomparison using CrunchFlow.

2.5.18.2 Model set up

A 1D model, 16.0 m in length, was discretized into 101 control volumes, yielding a discretization interval of 0.16 m for the interior control volumes and 0.08 m for the control volumes on the boundary. The domain contains two materials: material I is present from 0-8.0 m, while the rest is composed of material II. For simplicity, both materials have the same hydraulic and transport parameters, and pore water with the same initial chemical composition. The fractions of the two ion exchange sites -X and -Y in the materials are different (see Table 2.59 below). The flow boundary conditions consist of a specified hydraulic head of 1.4 m on the left boundary and 0.0 m on the right boundary. A plume with higher concentrations of Zn^{2+} , Pb^{2+} and Ca^{2+} enters the domain from the left boundary and then undergoes multi-site ion exchange in response to advective and diffusive transport. The initial condition is obtained by determining the exchanger composition on the two exchange sites in equilibrium with the pore water. Consequently, the dominant sorbed species within material group I are $Mg-X_2$ and $Na-X$, and $Mg-Y_2$ and $Na-Y$ within the material group II (Figure 2.43). The chemical compositions of the initial and boundary waters are listed in Table 2.58.

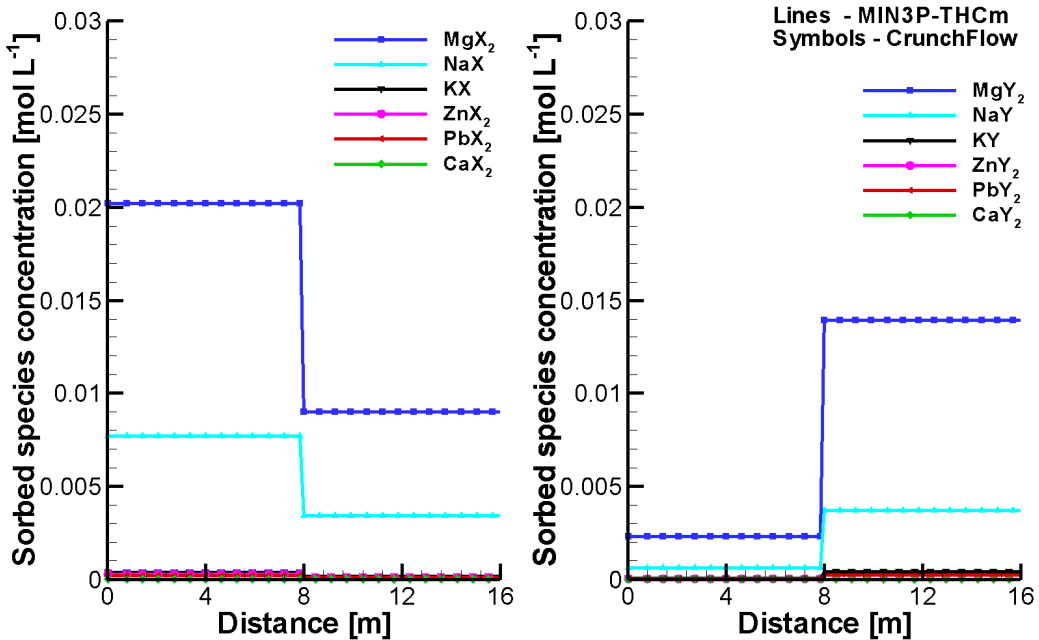


Figure 2.43: Initial sorbed species concentration profiles simulated by MIN3P-THCm (lines) and CrunchFlow (symbols), left panel – sorbed species on site –X, right panel– sorbed species on site –Y

Table 2.58: Composition of initial and boundary pore waters

Parameter	Boundary water	Initial Water	Unit	Remarks
H ⁺	3.0	8.0	-	pH
SO ₄ ²⁻	3.645×10 ⁻³	5.147×10 ⁻⁴	[mol l ⁻¹]	Charge balance
Zn ²⁺	10 ⁻³	10 ⁻⁷	[mol l ⁻¹]	free
Pb ²⁺	10 ⁻³	10 ⁻⁷	[mol l ⁻¹]	free
Ca ²⁺	10 ⁻³	10 ⁻¹⁰	[mol l ⁻¹]	free
Mg ²⁺	10 ⁻¹⁰	10 ⁻⁵	[mol l ⁻¹]	free
K ⁺	10 ⁻¹⁰	10 ⁻⁵	[mol l ⁻¹]	free
Na ⁺	10 ⁻¹⁰	10 ⁻³	[mol l ⁻¹]	free

2.5.18.3 Parameters

The physical parameters (material properties) and the parameters for the multisite ion exchange reactions used for the simulations are summarized in Table 2.59.

Validation report-page# 2-123

Table 2.59: Physical and chemical parameters for benchmark

Parameter	Symbol	Value	Unit
Length of domain	L	16.0	[m]
Porosity	ϕ	0.25	[-]
		1.0×10^{-3}	
Hydraulic conductivity	K_{zz}	1.0×10^{-9}	$[\text{m s}^{-1}]$
Free phase diffusion coefficient	D_0	9	$[\text{m}^2 \text{s}^{-1}]$
Longitudinal dispersivity	α_l	0.01	[m]
Soil bulk density	ρ_d	1.875	$[\text{g cm}^{-3}]$
Cation Exchange Capacity (CEC)	CEC	0.733	$[\text{meq (100g)}^{-1} \text{solid}]$
CEC fraction of site -X in material I	$F-X_I$	90%	[-]
CEC fraction of site -Y in material I	$F-Y_I$	10%	[-]
CEC fraction of site -X in material II	$F-X_2$	40%	[-]
CEC fraction of site -Y in material II	$F-Y_2$	60%	[-]

The ion exchange reactions for both sites ‘-X’ and ‘-Y’ are listed in Table 2.60. Exchange coefficients for the ‘-Y’ sites were assumed to be 50% larger than for the ‘-X’ sites, to provide a testing platform for the multi-site ion exchange model.

Table 2.60: Ion exchange reactions used in the simulation

Cation exchange reactions		Selectivity coefficients ($\log K_c$)
1	$2\text{Na-X} + \text{Mg}^{2+} \rightleftharpoons \text{Mg-X}_2 + 2\text{Na}^+$	0.6
2	$\text{Na-X} + \text{K}^+ \rightleftharpoons \text{K-X} + \text{Na}^+$	0.7
3	$2\text{Na-X} + \text{Zn}^{2+} \rightleftharpoons \text{Zn-X}_2 + 2\text{Na}^+$	0.8
4	$2\text{Na-X} + \text{Pb}^{2+} \rightleftharpoons \text{Pb-X}_2 + 2\text{Na}^+$	1.0458
5	$2\text{Na-X} + \text{Ca}^{2+} \rightleftharpoons \text{Ca-X}_2 + 2\text{Na}^+$	0.8
6	$\text{Na-X} + \text{Na}^+ \rightleftharpoons \text{Na-X} + \text{Na}^+$	0.0
7	$2\text{Na-Y} + \text{Mg}^{2+} \rightleftharpoons \text{Mg-Y}_2 + 2\text{Na}^+$	0.9
8	$\text{Na-Y} + \text{K}^+ \rightleftharpoons \text{K-Y} + \text{Na}^+$	1.05
9	$2\text{Na-Y} + \text{Zn}^{2+} \rightleftharpoons \text{Zn-Y}_2 + 2\text{Na}^+$	1.2
10	$2\text{Na-Y} + \text{Pb}^{2+} \rightleftharpoons \text{Pb-Y}_2 + 2\text{Na}^+$	1.5687
11	$2\text{Na-Y} + \text{Ca}^{2+} \rightleftharpoons \text{Ca-Y}_2 + 2\text{Na}^+$	1.2
12	$\text{Na-Y} + \text{Na}^+ \rightleftharpoons \text{Na-Y} + \text{Na}^+$	0.0

2.5.18.4 Results

Due to the ingress of water with higher concentrations of Zn^{2+} , Pb^{2+} and Ca^{2+} , Mg^{2+} and Na^+ become displaced from the exchange sites, resulting in a decrease of the exchanged

Validation report-page# 2-124

species concentrations $Mg-X_2$, $Mg-Y_2$, $Na-X$ and $Na-Y$, and an increase of $Zn-X_2$, $Zn-Y_2$, $Pb-X_2$, $Pb-Y_2$, $Ca-X_2$ and $Ca-Y_2$ (Figure 2.44, Figure 2.45). Displaced Mg^{2+} and Na^+ are transported downwards.

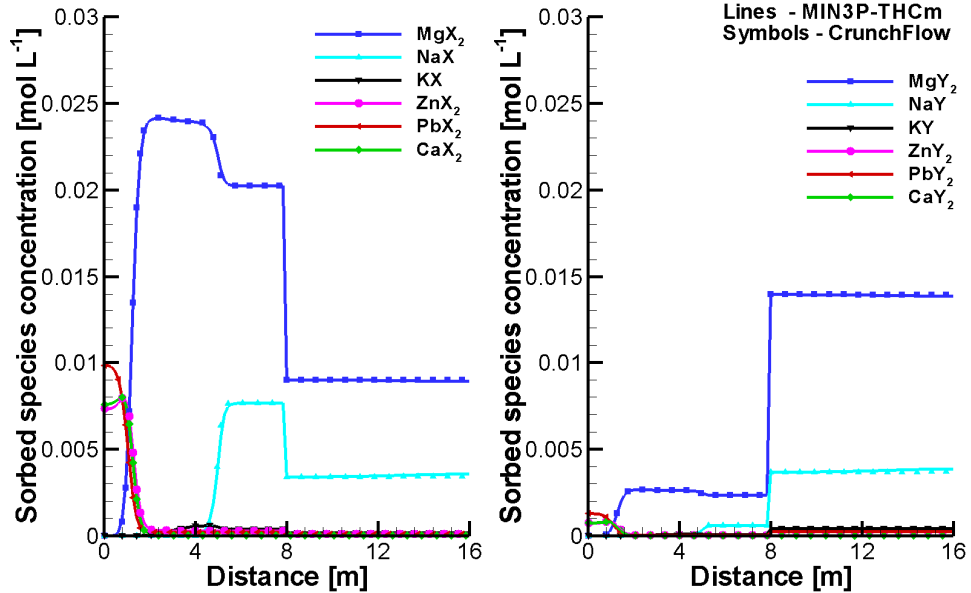


Figure 2.44: Comparison of sorbed species concentration profiles at 10 hours simulated by MIN3P-THCm (lines) and CrunchFlow (symbols) left – sorbed species on site -X, right - sorbed species on site -Y

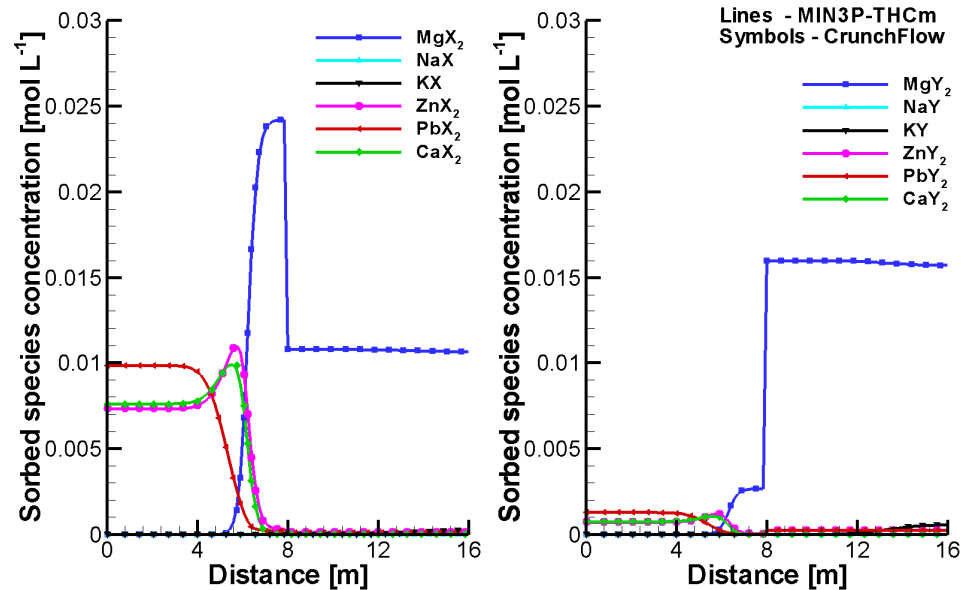


Figure 2.45: Comparison of sorbed species concentration profiles at 50 hours simulated by MIN3P-THCm (lines) and CrunchFlow (symbols) left – sorbed species on site -X, right - sorbed species on site -Y

Owing to the stronger selectivity of both ion exchange sites for Mg in comparison to Na, Mg is displacing Na from both ‘-X’ and ‘-Y’ sites. Breakthrough curves of total aqueous component concentrations, pH, and concentrations of the sorbed species at the outflow are depicted in Figure 2.46. In comparison to the results simulated by CrunchFlow, the simulated results by MIN3P-THCm are in very good agreement.

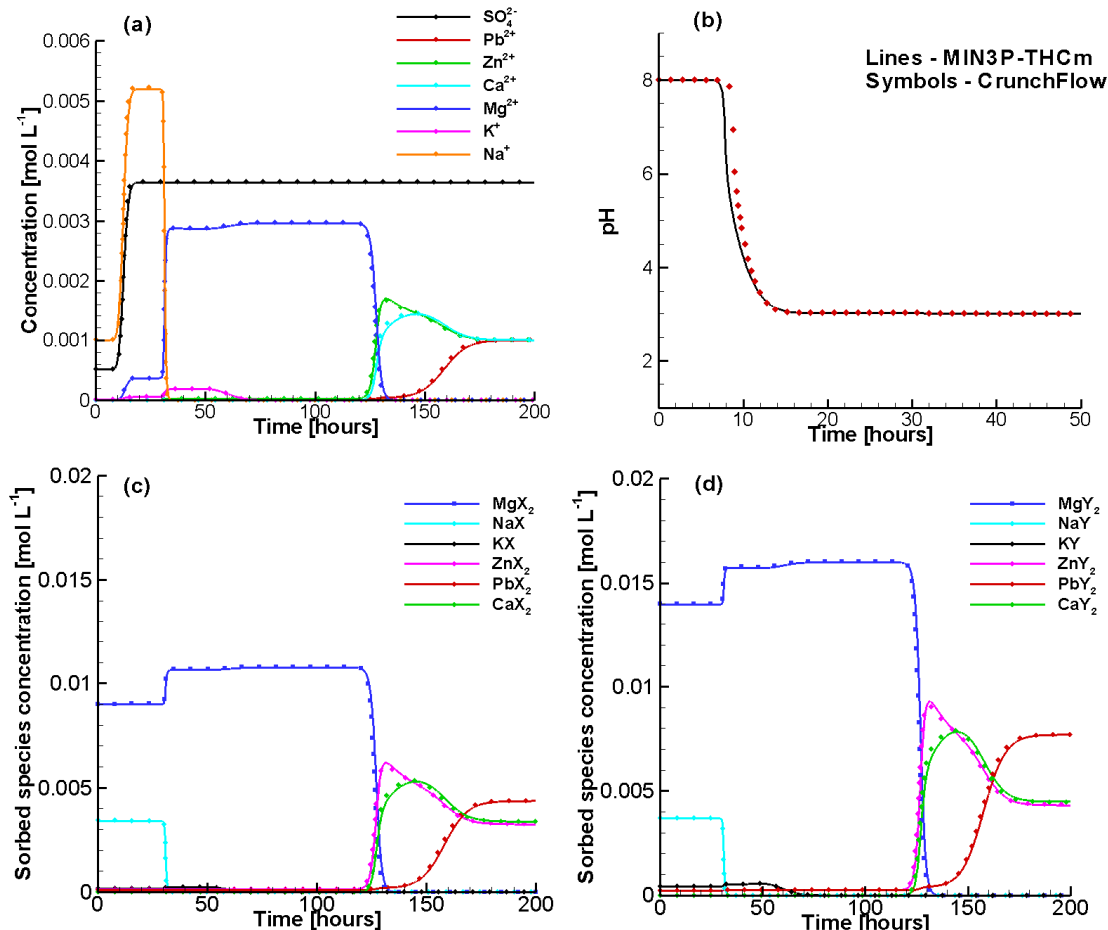


Figure 2.46: Comparison of breakthrough curves at the outflow boundary calculated by MIN3P-THCm (lines) and CrunchFlow (symbols): (a) Total concentrations of components in the aqueous phase, (b) pH, (c) sorbed species' concentrations on site -X, (d) sorbed species' concentrations on site -Y

2.5.18.5 Data location

Input file: .\Benchmark\benchmarks_new_add\multisite-ionx-V1.0.129\ionx-m-2domains\ionx-2m.dat

Database: .\Benchmark\benchmarks_new_add\multisite-ionx-V1.0.129\database\surfx-ionx-phreeqc1

2.5.19 MULTICOMPONENT DIFFUSION

The multicomponent diffusion formulation implemented in MIN3P-THCm version 1.0.203 was verified through several benchmarks (Rasouli 2016) by making comparisons to results by CrunchFlow (Steefel 2008) and PHREEQC (Appelo and Wersin 2007; Appelo et al. 2010).

2.5.19.1 Problem definition

The problem involves the diffusion of nitric acid into a NaCl solution. In this example the electrostatic forces between species in solution result in the electromigration of species present in the background solution (NaCl) in the absence of a concentration gradient. The electrochemical interactions also slow down the diffusion of the species with higher D_0 (H^+ and Cl^-) and speed up the diffusion of species with lower D_0 (NO_3^- and Na^+).

2.5.19.2 Model setup

The electromigration problem was simulated in a 1 m long, one-dimensional, horizontal domain, with a dilute NaCl background solution with pH = 6 (Figure 2.47). Nitric acid was allowed to diffuse into the domain from the left hand side boundary. The model was discretized into 100 cells with $\Delta x = 0.01$ m and the simulations were executed for a period of 100 days.

2.5.19.3 Parameters

The key model parameters are summarized in Table 2.61.

Table 2.61: Selected model parameters used for the simulation of nitric acid diffusion in saltwater

Transport Parameters	Symbol	Value	Units
Porosity	ϕ	0.25	-
Molecular diffusion coefficients (D_0)	$D_0(H^+)$ $D_0(Na^+)$ $D_0(Cl^-)$ $D_0(NO_3^-)$	9.311×10^{-9} 1.334×10^{-9} 2.032×10^{-9} 1.902×10^{-9}	$m^2 s^{-1}$

2.5.19.4 Results

Figure 2.47 compares the species concentration profiles at 100 days. The concentration profiles of Na^+ and Cl^- within the domain show differing concentration gradients, although both species were initially present at the same concentration throughout the column, and the concentrations of both ions are the same in the boundary solutions (Figure 2.47). This behavior is caused by the multicomponent diffusion effect. Because H^+ diffuses faster than the anion NO_3^- (e.g. Table 2.61.), a local charge imbalance is generated within the domain

that in turn provides the driving force for the diffusion of Na^+ and Cl^- to maintain charge balance in the solution. Na^+ is displaced from the domain, while Cl^- is drawn into the domain to maintain local charge balance. Consequently, the concentration of Cl^- is higher than Na^+ . The concentration difference of H^+ and NO_3^- reaches a maximum at a position of $x=0.3 \text{ m}$ after 100 days, coinciding with the location where the concentrations of Na^+ and Cl^- differ the most (Figure 2.47). Excellent agreement is obtained between MIN3P-THCm, CrunchFlow and PHREEQC.

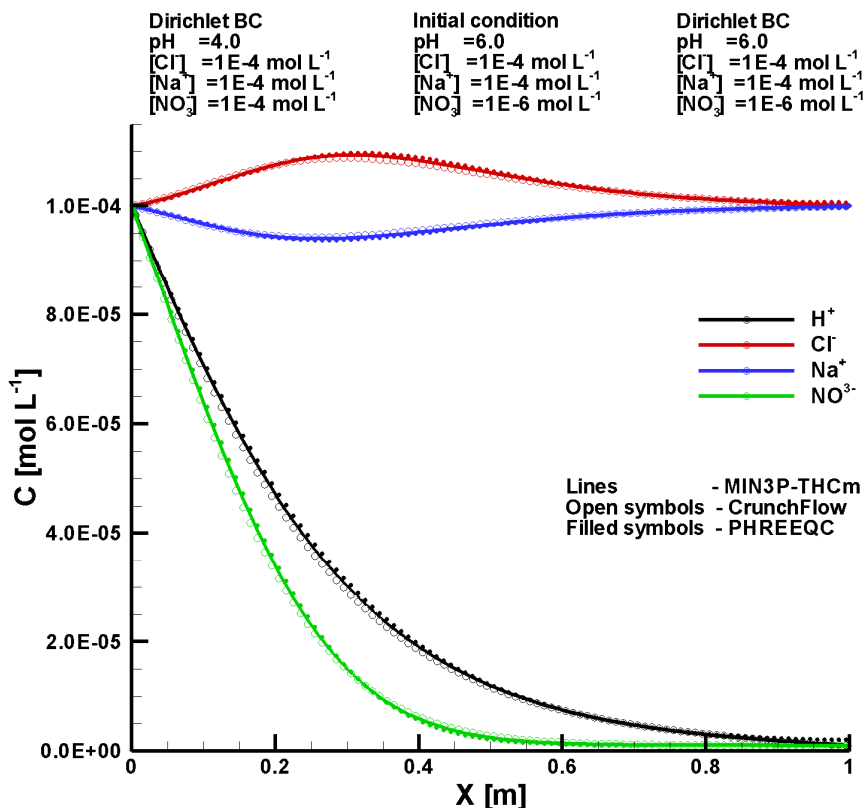


Figure 2.47: Comparison of simulated concentration profiles obtained from MIN3P-THCm (lines), CrunchFlow (open symbols) and PHREEQC (filled symbols) at 100 days

2.5.19.5 File location

Input file:

`.\Benchmark\benchmarks_standard\reactran\MCD-2\min3p\test.dat`

Databases:

`.\Benchmark\benchmarks_standard\reactran\MCD-2\min3p\database\`

Validation report-page# 2-128

2.5.20 MULTICOMPONENT DIFFUSION IN RADIAL COORDINATE

This benchmark is designed to verify the multicomponent diffusion (MCD) model in radial coordinate through code intercomparison using CrunchFlow.

2.5.20.1 Problem definition

The problem is based on the benchmark as described in section 2.5.19 concerning the geochemical system, material and diffusion parameters. The difference lies in the radial coordinate and boundary conditions.

2.5.20.2 Model setup

The electromigration problem was simulated in a 1 m long, one-dimensional in radial coordinate, horizontal domain, with a dilute NaCl background solution with pH = 6 (Figure 2.48). Nitric acid was allowed to diffuse into the domain from the right hand side (outer) boundary. The model was discretized into 100 cells with $\Delta r = 0.01$ m and the simulations were executed for a period of 100 days.

2.5.20.3 Parameters

The key model parameters are summarized in Table 2.61.

2.5.20.4 Results

Figure 2.48 compares the species concentration profiles at 100 days. The concentration profiles of Na^+ and Cl^- within the domain show differing concentration gradients, although both species were initially present at the same concentration throughout the column (Figure 2.48). This behavior is caused by the multicomponent diffusion effect. Because H^+ diffuses faster than the anion NO_3^- (Table 2.61), a charge imbalance is generated within the domain that in turn provides the driving force for the diffusion of Na^+ and Cl^- to maintain local charge balance in the solution. Na^+ is displaced from the domain, while Cl^- is drawn into the domain to maintain charge balance. Consequently, the concentration of Cl^- is higher than Na^+ . The concentration difference of H^+ and NO_3^- reaches a maximum at a position of $r=0.7$ m after 100 days, coinciding with the location where the concentrations of Na^+ and Cl^- differ the most (Figure 2.48). Excellent agreement is obtained between MIN3P-THCm and CrunchFlow.

2.5.20.5 File location

Input file:

`.\Benchmark\benchmarks_standard\reactran\MCD-2-r\min3p\mcd-rc.dat`

Databases:

`.\Benchmark\benchmarks_standard\reactran\MCD-2-r\min3p\database\`



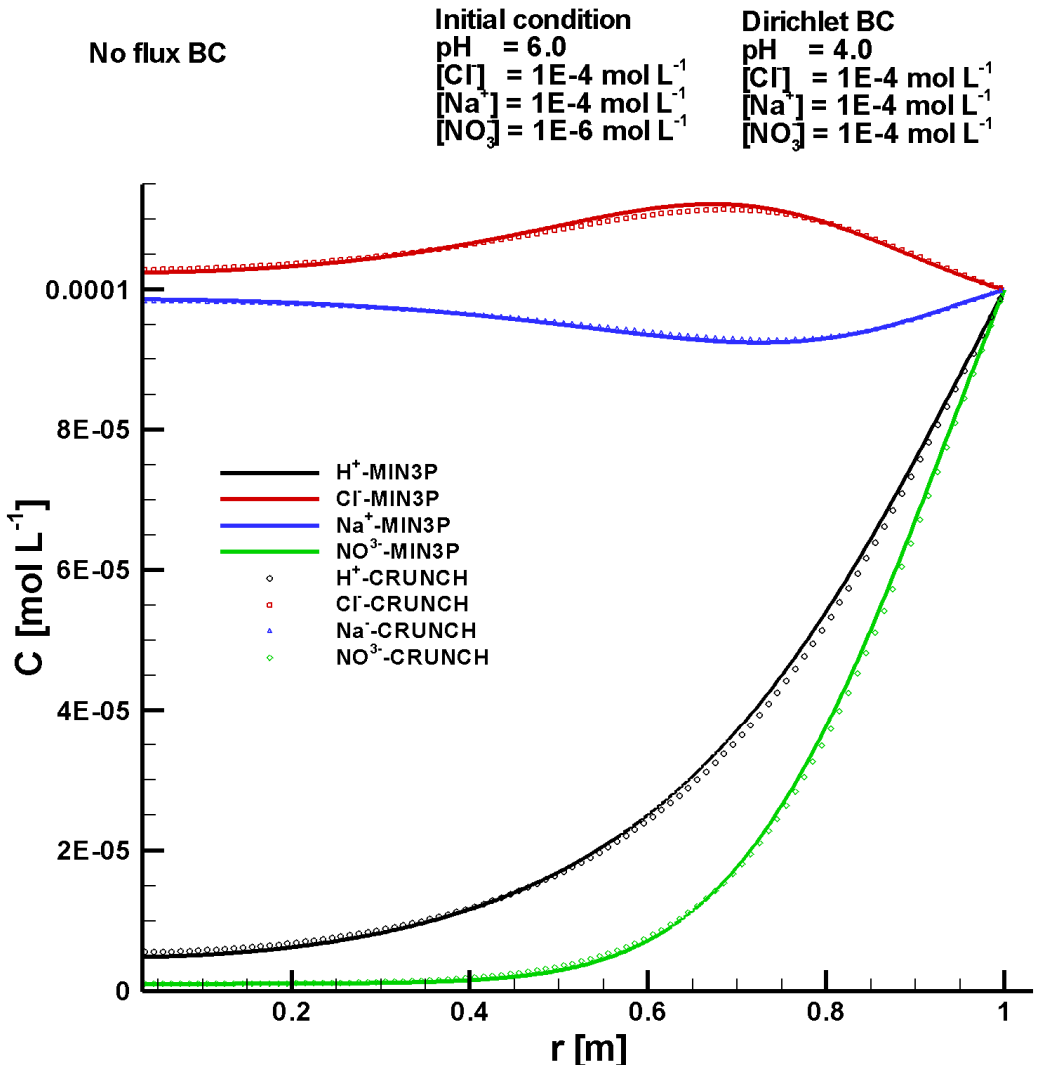


Figure 2.48: Comparison of simulated concentration profiles obtained from MIN3P–THCm (lines), CrunchFlow (symbols) at 100 days

2.5.21 MICROBIALLY MEDIATED CHROMIUM REDUCTION

This benchmark is designed to verify the function of biomass growth and decay through code intercomparison with CrunchFlow, PHT3D and ToughReact (Molins et al. 2014).

2.5.21.1 Problem definition

This benchmark involves the stimulation of microbially mediated chromium reduction under denitrifying conditions in biostimulated flow through column experiment permeated at a constant flow rate with a solution containing acetate as electron donor, nitrate as electron acceptor and chromate. The geochemical and biogeochemical system includes 12

Validation report-page# 2-130

primary components (i.e. H⁺, Na⁺, Ca²⁺, Cl⁻, CO₃²⁻, Acetate (CH₃COO⁻), NO₃⁻, N₂(aq), NH₄⁺, CrO₄²⁻ and Cr(OH)₂⁺), 20 secondary aqueous species, 2 biomass components (i.e. C₅H₇O₂N for active and C₅H₇O₂N(d) for dead biomass), 2 gases (i.e. CO₂(g) and N₂(g)) and two minerals (i.e. Calcite and Cr(OH)₃(a)). Additionally, 6 intra-aqueous kinetic reactions are also considered to simulate the biomass growth including two anabolic pathways (one that used NH₄⁺ and the other one that uses NO₂⁻ as nitrogen sources for biomass growth), two catabolic pathways of denitrification and two catabolic pathways for Cr(IV) reduction (Table 2.62).

Table 2.62: Stoichiometry of Microbially Mediated Reactions (Based on Molins et al. 2014)

No .	Reaction	Primary species									
		H ⁺	CO ₃ ²⁻	Acetat e	NO ₃ ⁻	NO ₂ ⁻	N ₂ (aq)	NH ₄ ⁺	CrO ₄ ²⁻	Cr(OH) ₂ ⁺	C ₅ H ₇ O ₂ N
R1	Overall fe=0.6 NO ₃ ⁻ > NO ₂ ⁻	0.045	0.15	-0.125	-0.3	0.3	0	-0.02	0	0	0.02
R2	Overall fe=0.6 NO ₂ ⁻ > N ₂ (aq)	-0.155	0.15	-0.125	0	-0.2	0.1	-0.02	0	0	0.02
R3	Overall fe=0.6 Assimilator y NO ₃ ⁻ > NO ₂ ⁻	.0326 9	.1731	-0.125	-0.3	.284 6	0	0	0	0	.015385
R4	Overall fe=0.6 Assimilator y NO ₂ ⁻ > N ₂ (aq)	-.1673 1	.1731	-0.125	0	-.215 4	0.1	0	0	0	.015385
R5	Cr reduction (NO ₃ ⁻)	-.1541 7	0.25	-0.125	0	0	0	0	-.3333	0.3333	0
R6	Cr reduction (NO ₂ ⁻)	-.1541 7	0.25	-0.125	0	0	0	0	-.3333	0.3333	0

* Stoichiometric coefficients for products > 0 and for reactants <0; H₂O might be needed for the balance of the reaction equations.

2.5.21.2 Model setup

The problem was simulated in a 0.1 m long, one-dimensional column treated with a constant flow rate (1.0x10⁻⁶ m s⁻¹) with a stock solution containing acetate as electron donor, nitrate as electron acceptor, biomass and chromite. Denitrifying bacteria initially uniformly distributed in the soil mediate nitrate reduction and co-metabolic chromium reduction by using acetate as electron donor. The initial concentration of biomass is 5.0x10⁻⁵ mol L⁻¹, and the inlet concentration of nitrate and acetate are 1.5 and 1.0 mmol L⁻¹, respectively. The simulation was executed for a period of 100 days.

Validation report-page# 2-131

Table 2.63: Replacement of gypsum by polyhalite: composition of initial and boundary waters of the domain (Molins et al., 2014)

Parameter	Boundary water	Initial water	Unit
H ⁺	7.0	7.0	pH
Na ⁺	5.25×10 ⁻³	5.25×10 ⁻³	[mol l ⁻¹]
Ca ²⁺	1.60×10 ⁻³	1.60×10 ⁻³	[mol l ⁻¹]
Cl ⁻	4.45×10 ⁻³	4.45×10 ⁻³	[mol l ⁻¹]
CO ₃ ²⁻	1.25×10 ⁻³	1.25×10 ⁻³	[mol l ⁻¹]
CH ₃ COO ⁻	1.50×10 ⁻³	1.50×10 ⁻³	[mol l ⁻¹]
NO ₃ ⁻	1.50×10 ⁻³	1.50×10 ⁻³	[mol l ⁻¹]
NO ₂ ⁻	1.00×10 ⁻³³	1.00×10 ⁻³³	[mol l ⁻¹]
N ₂ (aq)	1.00×10 ⁻³³	1.00×10 ⁻³³	[mol l ⁻¹]
NH ₄ ⁺	2.50×10 ⁻⁴	2.50×10 ⁻⁴	[mol l ⁻¹]
CrO ₄ ²⁻	5.00×10 ⁻⁶	5.00×10 ⁻⁶	[mol l ⁻¹]
Cr(OH) ₂ ⁺	1.00×10 ⁻³³	1.00×10 ⁻³³	[mol l ⁻¹]
C ₅ H ₇ O ₂ N	1.00×10 ⁻¹⁵	5.00×10 ⁻⁵	[mol l ⁻¹]
C ₅ H ₇ O ₂ N(d)	1.00×10 ⁻¹⁵	1.00×10 ⁻¹⁵	[mol l ⁻¹]
Ionic strength	0.01	0.01	[mol l ⁻¹]
Calcite		0.1	[m ⁻³ m ⁻³]
Cr(OH) ₃		0.0	

2.5.21.3 Parameters

The rate constant and kinetic parameters for microbially mediated reactions are summarized in Table 2.64. It is important to note that MIN3P-THCm uses [s⁻¹] for rate constant of the reactions, which is different than the unit [mol cell⁻¹ s⁻¹] described in the paper (Molins et al. 2014). The transformation factor is the mass of a biomass cell (C₅H₇O₂N) in 2x10⁻¹⁵ mol C₅H₇O₂N cell⁻¹.

The diffusion coefficient for all mobile species is assumed to be 10⁻⁹ m² s⁻¹.

The decay parameter of biomass (b) is 0.00432 day⁻¹. Biomass is treated as immobile aqueous component but only exist in the pore network. As the porosity is 0.4, the decay rate scaled into pore system in MIN3P-THCm is 1.25x10⁻⁷ s⁻¹. Biomass detachment is, however, not included in the simulation. Biomass decay is the only way of considering the biomass decrease such as death.

2.5.21.4 Results

Figure 2.49 depicted the breakthrough curves of the major components in the simulation of the Cr(IV) reduction under denitrifying conditions in a flow-through column with biomass growth and decay. Oxidation of acetate takes place by sequentially using NO₃⁻ and NO₂⁻ as electron acceptors. Reduction of Cr(IV) is linked to nitrate reduction by including Monod terms for NO₃⁻ and NO₂⁻ in different pathways associate each to NO₃⁻ and NO₂⁻, respectively (R5 and R6 in Table 2.62). Therefore, two periods of Cr(IV)

Validation report-page# 2-132

reduction are observed, each related to the main electron acceptor used for the acetate oxidation. Consequently, the concentrations of acetate and CrO_4^{2-} decrease and that of biomass increases.

Table 2.64: Rate Constant and Kinetic Parameters for Microbially Mediated Reactions
 (Based on Molins et al. 2014)

No .	Aqueous kinetics	Rate constant [s ⁻¹]	Monod term half saturations					Inhibition half saturation	
			Acetate	NO_3^-	NO_2^-	CrO_4^{2-}	NH_4^+	NO_3^-	NH_4^+
			[mol L ⁻¹]					[mol L ⁻¹]	
R1	Overall fe=0.6 $\text{NO}_3^- \rightarrow \text{NO}_2^-$	4E-5	2.03E-5	1.06E-5			1E-6		
R2	Overall fe=0.6 $\text{NO}_2^- \rightarrow \text{N}_2(\text{aq})$	2E-5	2.03E-5		1.06E-5		1E-6	1.06E-5	
R3	Overall fe=0.6 Assimilatory $\text{NO}_3^- \rightarrow \text{NO}_2^-$	4E-6	2.03E-5		1.06E-5				1.06E-5
R4	Overall fe=0.6 Assimilatory $\text{NO}_2^- \rightarrow \text{N}_2(\text{aq})$	2E-6	2.03E-5		1.06E-5		1E-6	1.06E-5	1.06E-5
R5	Cr reduction (NO_3^-)	4.755E-8	2.03E-5	1.06E-5		1E-7	1E-6		
R6	Cr reduction (NO_2^-)	1.586E-8	2.03E-5		1.06E-5	1E-7	1E-6	1.06E-5	

Figure 2.50 depicted the concentration profiles of the major components in the simulation of the Cr(IV) reduction in the column at day 100. The nutrient for the biomass growth flow into the column, biomass increases from the inflow boundary through the oxidation of the acetate by sequentially using NO_3^- and NO_2^- as electron acceptors. At day 100, NO_3^- exists only within about 0.025 m from the inflow boundary. In the rest of the domain, NO_2^- has to be used. The associated Cr(IV) reduction decreases the mobile CrO_4^{2-} into immobile solid $\text{Cr(OH)}_3(\text{s})$. Excellent agreement for this benchmark and several related benchmarks are obtained between MIN3P-THCm, PHT3D, TOUGHREACT and CrunchFlow (Molins et al. 2014).

Validation report-page# 2-133

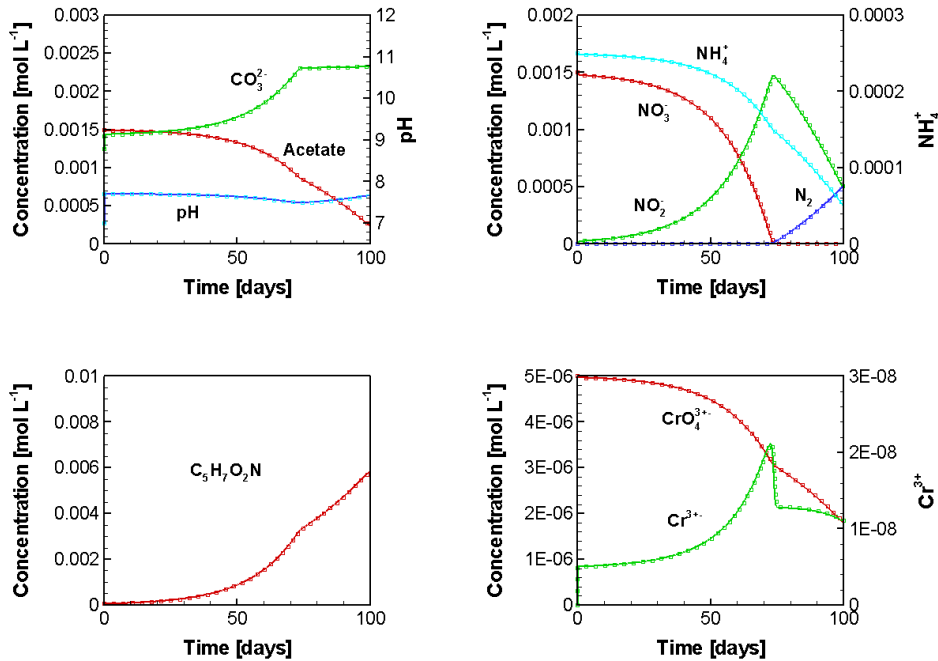


Figure 2.49: Evolution of Major Component in the Simulation of Cr(IV) Reduction under Denitrifying Conditions in a Flow-Through Column with Biomass Growth and Decay

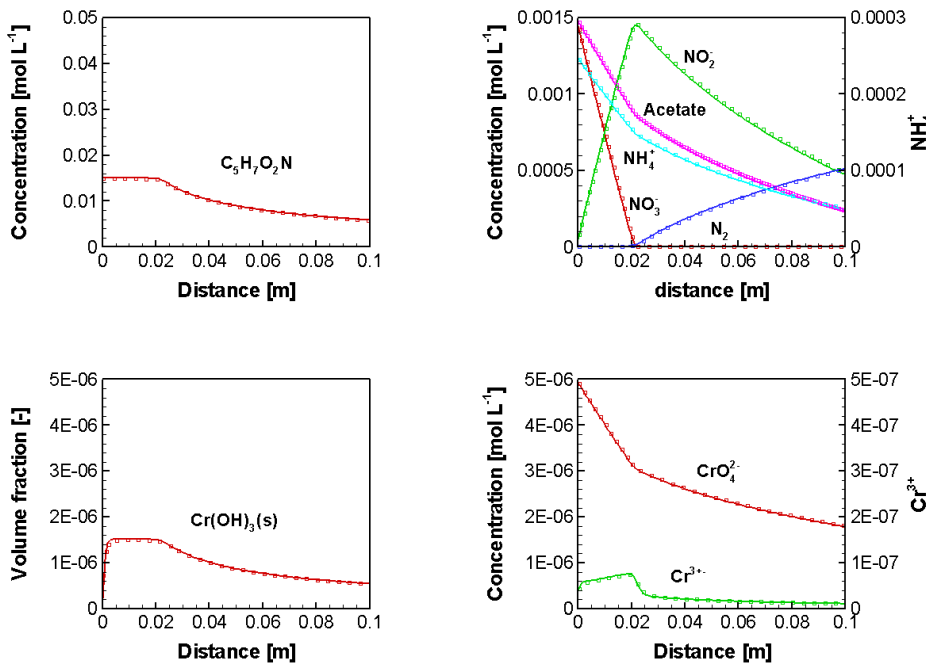


Figure 2.50: Concentration Profiles of Major Component in the Simulation of Cr(IV) Reduction under Denitrifying Conditions in a Flow-Through Column with Biomass Growth and Decay at day 100

Validation report-page# 2-134

2.5.21.5 File location

Input file:

.\Benchmark\benchmarks_new_add\biomass-V1.0.56\column2\

Databases:

.\Benchmark\benchmarks_new_add\biomass-V1.0.56\database\default

2.5.22 SALINITY DEPENDENT SULFATE REDUCTION – OPTION 1

2.5.22.1 Problem definition

This example verifies the salinity dependent sulfate reduction (SDSR) model through code comparison using MIN3P-THCm v1.0.441 against PHREEQC v3.0 (Parkhurst and Appelo 2013).

2.5.22.2 Model setup

A 1D model, 16.0 m in length, is discretized into 200 control volumes. The domain is homogeneous and fully saturated. The domain contains calcite, anhydrite, halite and organic substance (CH_2O). The initial hydraulic head is 0.0 m across the domain. The hydraulic head at the in- and outflow boundaries are 1.4 m and 0.0 m, respectively. Initially, the column was filled with highly saline solutions based on Hobbs et al. (2011) (Table 2.65). With the infiltration of fresh water (chemical composition according to Bea et al. 2011) from the left side, the composition of the aqueous species of the pore water in the column changes over time. The geochemical system includes 10 primary species (Ca^{2+} , Na^+ , Mg^{2+} , K^+ , Cl^- , SO_4^{2-} , H^+ , CO_3^{2-} , HS^- and $\text{O}_2(\text{aq})$), and 22 secondary species. The initial compositions (IC) of the aqueous species and minerals in the domain, and the compositions of the fresh water (BC) are listed in Table 2.65.

Table 2.65: Initial and boundary conditions (IC & BC) of the aqueous and mineral compositions for the example sulpqc

Parameter	IC \$	BC (inflow) ^c	Unit
Aqueous component concentration			
Ca^{2+}	9600.00	8.40	$[\text{mg l}^{-1}]$
Na^+	94000.00	189.00	$[\text{mg l}^{-1}]$
Mg^{2+}	3400.00	0.097	$[\text{mg l}^{-1}]$
K^+	2600.00	72.00	$[\text{mg l}^{-1}]$
Cl^-	193000.00	164.00	$[\text{mg l}^{-1}]$
SO_4^{2-}	600.00	1.0×10^{-10}	$[\text{mg l}^{-1}]$
pH	5.95	7.0	$[-]$
CO_3^{2-}	76.00	164.00	$[\text{mg l}^{-1}]$
HS^-	1.0×10^{-10}	1.0×10^{-10}	$[\text{mg l}^{-1}]$

Validation report-page# 2-135

Eh	-200.00	200.00	[mV]
Mineral volume fraction			
Parameter	IC	Unit	
CH ₂ O	0.10	[m ³ m ⁻³]	
Calcite	0.10	[m ³ m ⁻³]	
Anhydrite	0.32	[m ³ m ⁻³]	
Halite	0.30	[m ³ m ⁻³]	

[#] - From Hobbs et al. (2011), Table A-3, Sample ID: CFN-161; ^{\$} - From Hobbs et al. (2011), Table A-5, Sample ID: SF-3; ^C - Bea et al. (2011)

2.5.22.3 Parameters

The physical parameters of the porous medium are: porosity is 0.25; hydraulic conductivity is 1.0×10^{-3} m s⁻¹, dispersivity is 0.01 m. The diffusion coefficients of all components are set the same in 1.0×10^{-9} m² s⁻¹.

Experimental data showed that some sulfate reducing bacteria can survive under anaerobic and hypersaline conditions and tend to thrive within certain saline conditions depending on the background solution conditions that the bacteria live in (Forti et al. 2007; Brandt et al. 2001). We select a set of the experimental data by Brandt et al. (2001) to account for the salinity effect on the biogenic sulfate reducing activity (Figure 2.51). The inhibition coefficient k_{sal} for the salinity dependent sulfate reduction model is thus calculated according to the following regression equation based on the experimental data (Brandt et al. 2001, Figure 2.51).

$$k_{sal} = -0.2716 + 0.0211S - 9.455 \times 10^{-5}S^2 - 3.20 \times 10^{-8}S^3 \quad \text{Equation 2-32}$$

which S stands for salinity in [g L⁻¹]. To avoid negative values, k_{sal} is calculated using Equation 2-32 when the salinity S is between 13.8 and 228 g L⁻¹; if S is lower than 13.8 or higher than 228 g L, k_{sal} will be set the values calculated using the boundary salinity (S) values (i.e. 13.8 and 228 g L⁻¹) according to Equation 2-32.

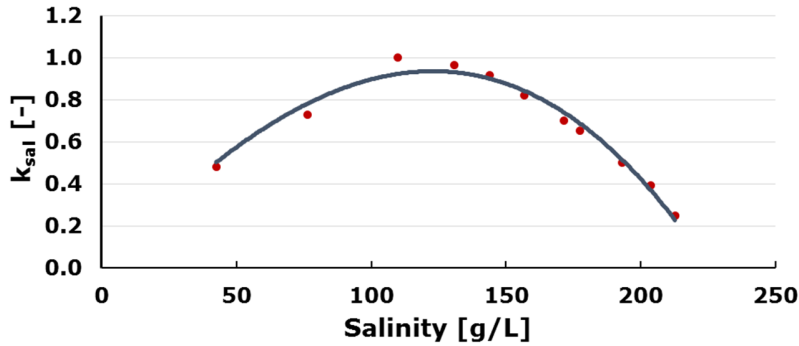


Figure 2.51: Salinity Inhibition Factor as a Function of Salinity (Points – Experimental Data from Brandt et al. 2001; Line – the Regression Equation).

Other parameters applied are: $k_s = 1.62 \times 10^{-3}$ mol L⁻¹ and $k_{sulf} = 6.9 \times 10^{-9}$ mol L⁻¹ bulk s⁻¹ (Gibson et al. 2011). $K_{H_2S}^{in}$ and $K_{O_2}^{in}$ are assumed to be 3.125×10^{-6} mol L⁻¹. The geochemical database is based on MINTEQ database (Allison et al. 1991) for MIN3P-THCm, and the database file pitzer.dat for PHREEQC. For both calculations, all individual-ion activity coefficients are scaled according to the MacInnes' convention (MacInnes 1919).

2.5.22.4 Results

Simulated results are depicted in Figure 2.52 and Figure 2.53. Figure 2.52 (left) showed the concentration profiles of HS⁻ (solid lines) and SO₄²⁻ (dashed lines) at 1, 5 and 10 hours. Figure 2.52(right, solid lines) depicted the corresponding profiles of salinity at 1, 5 and 10 hours, respectively. The salinity of the pore water in the column decreases substantially with the infiltration of fresh water from the left side. Due to the salinity dependence of the sulfate reduction reaction, HS⁻ concentration remains very low where salinity is high even though the concentration of SO₄²⁻ is high. Therefore, a peak of HS⁻ concentration appears around the transition zone with intermediate salinity and high concentration of SO₄²⁻. The peak concentration of HS⁻ accumulates with the time and moves forwards along the flow path.

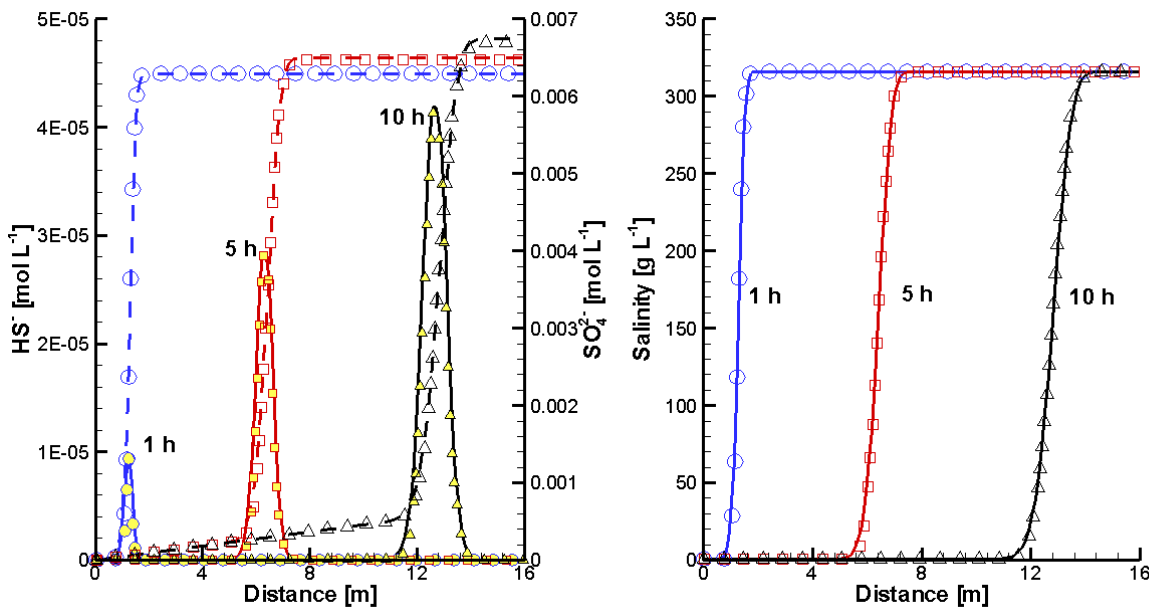


Figure 2.52: Comparison of Concentration Profiles of HS^- (Solid Lines/Filled Symbols) and SO_4^{2-} (Dashed Lines/Open Symbols) (Left) and Profiles of Salinity (Right) at 1 (Blue), 5 (Red) and 10 (Black) Hours Simulated Using MIN3P-THCm (lines) to Those Simulated Using PHREEQC (Symbols)

Figure 2.53 depicts the breakthrough curves of pH, component concentrations and the saturation indexes (SI) of minerals. Calcite is in equilibrium with the pore water while halite is slightly undersaturated. But SI of anhydrite is -0.8 - apparently undersaturated. Within about 12 hours, the concentrations of the components Na^+ , Cl^- , Ca^{2+} , K^+ and Mg^{2+} except SO_4^{2-} remains almost constant. The concentration of SO_4^{2-} increases gradually from 6.2×10^{-3} mol L $^{-1}$ to 6.8×10^{-3} mol L $^{-1}$ within 12 hours owing to the dissolution of anhydrite in the column. After about 12 hours, the fresh water reaches the end of the column and the concentrations of most main components (Na^+ , Cl^- , Ca^{2+} , K^+ , Mg^{2+} and SO_4^{2-}) except HS^- decreases significantly. The concentration of HS^- at the end of the column remains very low due to the high salinity, but substantially increases after 12 hours indicating the arrival of the migration front of the fresh water. A peak concentration of HS^- in 4.7×10^{-5} mol L $^{-1}$ occurs at about 13 hours and then decreases substantially indicating the total replacement of the hypersaline solution by fresh water.

Comparison of the simulated results by MIN3P-THCm (lines in Figure 2.52 and Figure 2.53) to those by PHREEQC (symbols in Figure 2.52 and Figure 2.53) showed very good agreement.

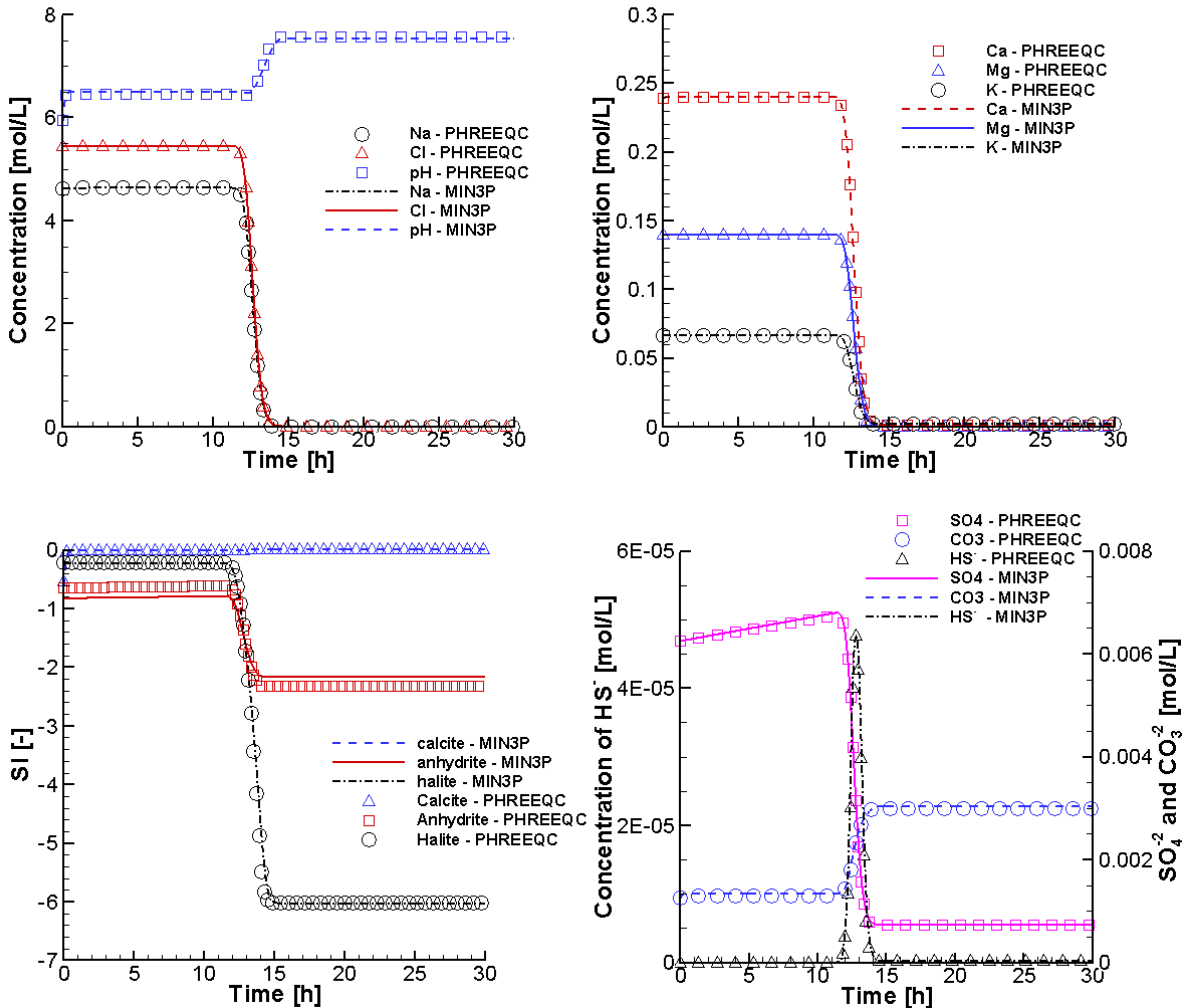


Figure 2.53: Comparison of Breakthrough Curves of pH and Total Concentrations of Na⁺ and Cl⁻ (Top Left), Ca²⁺, K⁺, Mg²⁺ (Top Right), SO₄²⁻, CO₃²⁻ and HS⁻ (Bottom Right), and SI (saturation indexes) of Calcite, Anhydrite and Halite (Bottom Left) Simulated by MIN3P-THCm (Lines) to Those Calculated by PHREEQC (Symbols) Considered the SDSR Model

To demonstrate the influence of the SDSR model on the simulation results, a comparison calculation is performed with the same example as mentioned above by switching off the SDSR model using MIN3P-THCm and PHREEQC. Figure 2.54 depicted the simulated breakthrough curves of pH and total component concentrations, together with the SI curves the minerals. In comparison to those breakthrough curves obtained by considering the SDSR model mentioned above, most of them except HS⁻ and CO₃²⁻ showed no visual difference (compare Figure 2.53 and Figure 2.54). However, substantial difference exists in the total concentration of HS⁻ as expected. If the salinity effect on the sulfate reduction

reaction is not taken into account, HS^- forms from the beginning of the simulation and increases rapidly within 12 hours and reaches the peak value of 8.1×10^{-5} mol L⁻¹ at about 12 hours. Within the first 12 hours, the pH is about 6.4, slightly lower than the previous case in 6.5. Consequently, the concentration of CO_3^{2-} increases slightly indicating the dissolution of more calcite. From 12 to 15 hours, the total concentration of HS^- drops rapidly to 3.9×10^{-5} mol L⁻¹ and remains constant thereafter, indicating the stable supply of SO_4^{2-} due to the dissolution of the anhydrite when fresh water flows through the column.

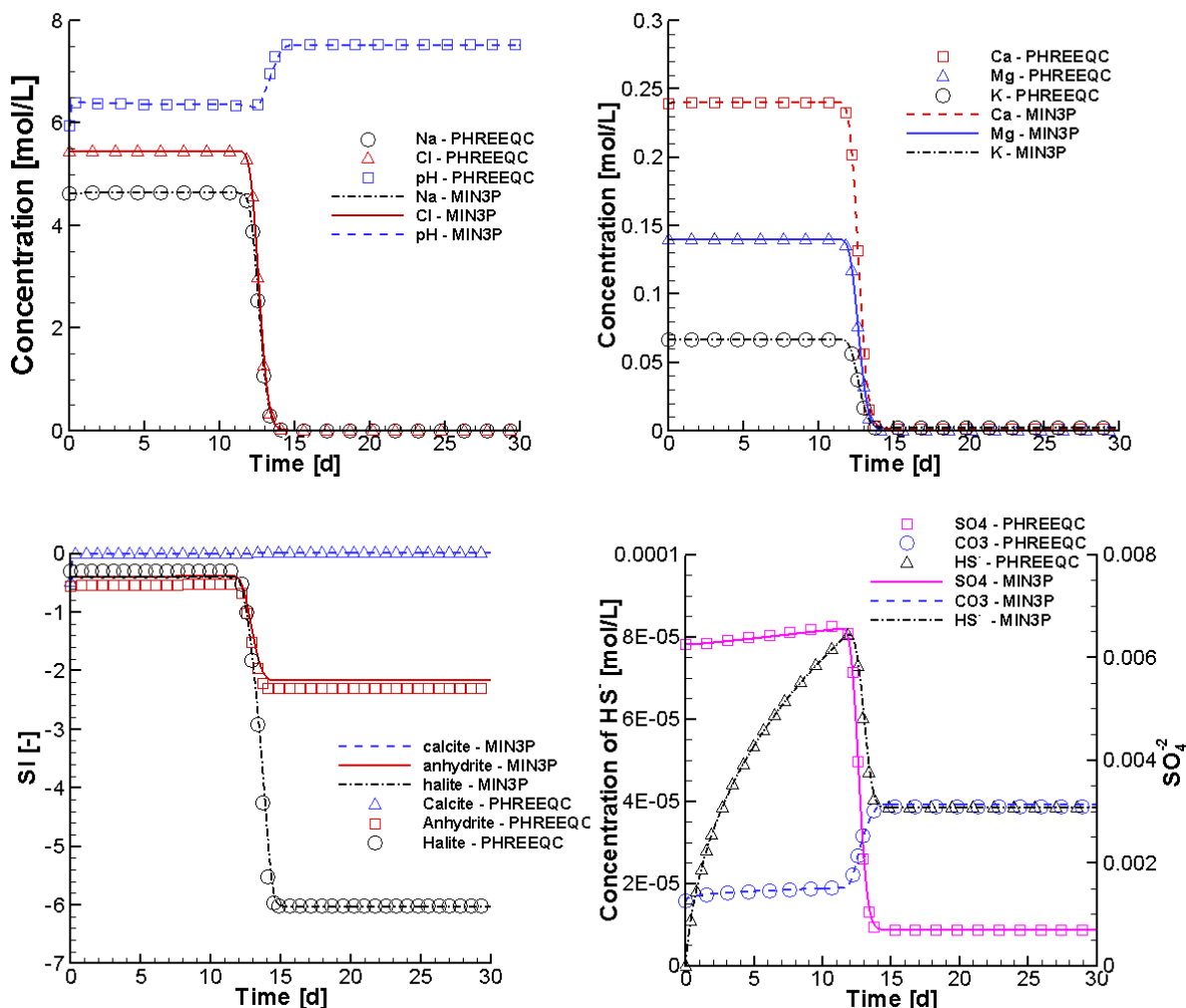


Figure 2.54: Comparison of Breakthrough Curves of pH and Total Concentrations of Na^+ and Cl^- (Top Left), Ca^{2+} , K^+ , Mg^{2+} (Top Right), SO_4^{2-} , CO_3^{2-} and HS^- (Bottom Right), and SI (saturation indexes) of Calcite, Anhydrite and Halite (Bottom Left) Simulated by MIN3P-THCm (Lines) to Those Calculated by PHREEQC (Symbols) Without Considering the SDSR Model

Validation report-page# 2-140

2.5.22.5 File location

Input file for the case considering SDSR Model:

.\Benchmark\benchmarks_new_add\sulfur-V1.0.431\verification\sul2pqc\sul2pqc.dat

Input file for the case not considering SDSR Model:

.\Benchmark\benchmarks_new_add\sulfur-V1.0.431\verification\sul2pqc-n\sul2pqc.dat

Databases:

.\Benchmark\benchmarks_new_add\sulfur-V1.0.431\verification\database\default

2.5.23 SALINITY DEPENDENT SULFATE REDUCTION – OPTION 2

2.5.23.1 Problem definition

This example verifies the salinity dependent sulfate reduction (SDSR) model through code comparison using MIN3P-THCm v1.0.512 against PHREEQC v3.0 (Parkhurst and Appelo 2013).

2.5.23.2 Model setup

A 1D model, 16.0 m in length, is discretized into 200 control volumes. The domain is homogeneous and fully saturated. The domain contains calcite, anhydrite, halite and organic substance (CH_2O). The initial hydraulic head is 0.0 m across the domain. The hydraulic head at the in- and outflow boundaries are 1.4 m and 0.0 m, respectively. Initially, the column was filled with highly saline solutions based on Hobbs et al. (2011) (Table 2.65). With the infiltration of fresh water (chemical composition according to Bea et al. 2011) from the left side, the composition of the aqueous species of the pore water in the column changes over time. The geochemical system includes 10 primary species (Ca^{2+} , Na^+ , Mg^{2+} , K^+ , Cl^- , SO_4^{2-} , H^+ , CO_3^{2-} , HS^- and $\text{O}_2(\text{aq})$), and 22 secondary species. The initial compositions (IC) of the aqueous species and minerals in the domain, and the compositions of the fresh water (BC) are listed in Table 2.65.

2.5.23.3 Parameters

The physical parameters for the homogeneous porous medium are: a porosity of 0.25; a hydraulic conductivity of $1.0 \times 10^{-3} \text{ m s}^{-1}$, and a dispersivity of 0.01 m. The diffusion coefficients of all components are set at $1.0 \times 10^{-9} \text{ m}^2 \text{ s}^{-1}$.

Based on the observational data from the southern Ontario region of the Michigan basin, sulfidic waters exist at shallow to intermediate depths (up to around 200 m), while at greater depths the concentration of total sulfide is commonly low (Carter et al. 2015). It is therefore assumed that biogenic sulfate reduction is almost completely suppressed due to the extremely high salinity ($>200 \text{ g L}^{-1}$) that is known to exist at greater depths (Hobbs et al. 2011). In order to simulate this effect, the formulation must be able to simulate the transition from a high level of activity of sulfate reducing bacteria to no activity due to high

Validation report-page# 2-141

salinity, while being continually differentiable. Standard hyperbolic inhibition formulations (e.g. Mayer et al., 2001, see also terms for sulfide and oxygen inhibition in equation 2.2 of this report) were evaluated, but were found inadequate to capture the transition from active sulfate reduction to completely inhibited conditions. Alternative formulations can be derived to meet these requirements based on cosine or Gaussian functions, or tabulated values. A cosine function was selected because of its simplicity and ease of implementation. Similar formulations were previously used in medical science to simulate the inhibition effect of medicine on organ functions (Pfister et al. 2004). The inhibition term as a function of chloride concentration is here expressed as:

$$k_{sal} = \begin{cases} 1 & , if S < C_L \\ [\cos(a * S + b) + 1]/2 & , if C_L \leq S \leq C_H \\ 0 & , if S > C_H \end{cases} \quad \text{Equation 2-33}$$

where S is the concentration of Cl^- [mol L^{-1}]. The coefficients a and b can be determined based on Cl^- concentration levels C_H and C_L . Below concentration C_L , there is no inhibition of sulfate reduction, while above concentration C_H , sulfate reduction is completely inhibited. The rate of biogenic sulfate reduction between these two concentration values is assumed to follow a cosine function, with the parameters a and b defined according to Equation 2-34 and Equation 2-35:

$$a = \frac{180}{C_H - C_L} \quad \text{Equation 2-34}$$

$$b = -aC_L \quad \text{Equation 2-35}$$

The values for C_H and C_L are 1.41 mol L^{-1} and 0.076 mol L^{-1} , respectively, which are calibrated based on the observational data (Carter et al. 2015). Other reaction rate parameters are: $k_s = 1.62 \times 10^{-3} \text{ mol L}^{-1}$ and $k_{sulf} = 6.9 \times 10^{-9} \text{ mol (L bulk)}^{-1}\text{s}^{-1}$ (Gibson et al. 2011). $K_{H_2S}^{in}$ and $K_{O_2}^{in}$ are calibrated in this work to be $3.125 \times 10^{-5} \text{ mol L}^{-1}$ and $3.125 \times 10^{-9} \text{ mol L}^{-1}$, respectively. The geochemical thermodynamic database is based on the MINTEQ database for MIN3P-THCm with the extension of Pitzer parameters based on the EQ3/6 Yucca Mountain database (Bea et al. 2011). The pitzer.dat database coming with PHREEQC is used in this study for PHREEQC (Parkhurst and Appelo 2013) simulations. For the simulations using both codes, all individual-ion activity coefficients are scaled according to the MacInnes' convention (MacInnes 1919).

2.5.23.4 Results

Simulated results for total concentrations are depicted in Figure 2.55 and Figure 2.56.

Validation report-page# 2-142

Figure 2.55 (left) shows the concentration profiles for HS^- (solid lines) and SO_4^{2-} (dashed lines) at 1, 5 and 10 hours. Figure 2.55 (right, solid lines) depicts the corresponding concentration profiles of Cl^- at 1, 5 and 10 hours, respectively. The Cl^- concentration in the column decreases substantially with the infiltration of fresh water from the left side Figure (right). Due to the dependence of sulfate reduction on Cl^- , HS^- concentrations remain very low where Cl^- concentrations are high, even though the concentration of SO_4^{2-} is high as well. Therefore, a peak of elevated HS^- concentrations appears in the transition zone with intermediate salinity (Cl^- -concentrations) and high SO_4^{2-} . Peak concentrations of HS^- increase with time and move along the flow path.

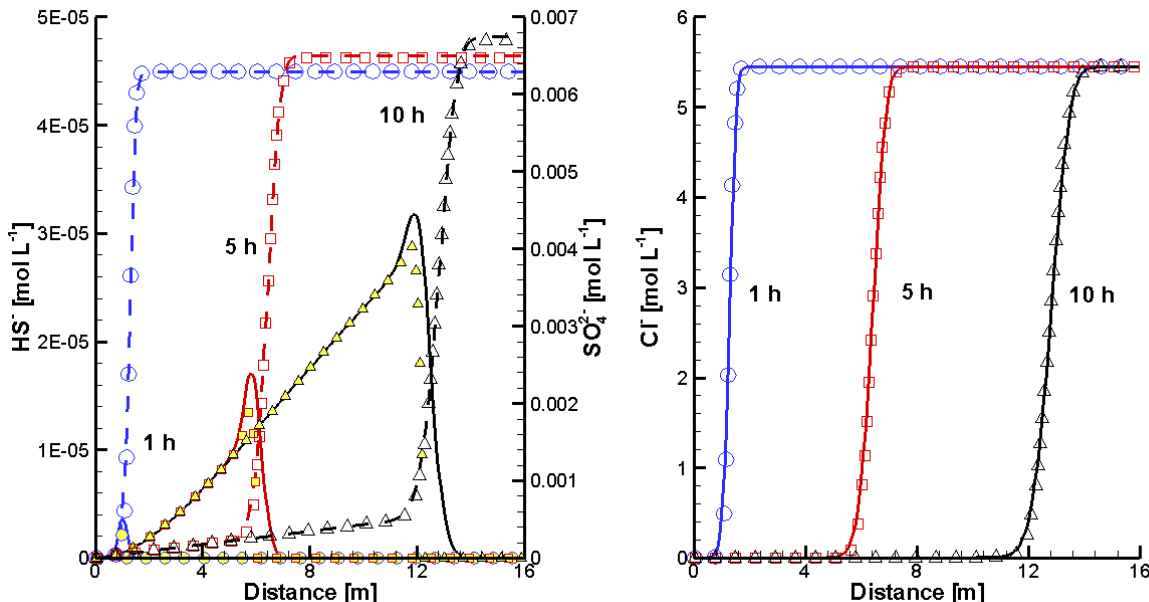


Figure 2.55: Comparison of Concentration Profiles of HS^- (Solid Lines/Filled Symbols) and SO_4^{2-} (Dashed Lines/Open Symbols) (Left) and Profiles of Cl^- (Right) at 1 (Blue), 5 (Red) and 10 (Black) Hours Simulated Using MIN3P-THCm (lines) to Those Simulated Using PHREEQC (Symbols)

Figure 2.56 depicts the breakthrough curves of pH, component concentrations and the saturation indices (SI) of minerals. Calcite is in equilibrium with the pore water ($\text{SI} = 0.0$), while halite is slightly undersaturated ($\text{SI} < 0.0$). The initial saturation index of anhydrite is -0.8. Therefore, anhydrite dissolves and the concentration of SO_4^{2-} increases with time. Within about 12 hours, the concentrations of the components Na^+ , Cl^- , Ca^{2+} , K^+ and Mg^{2+} remain almost constant. The concentration of SO_4^{2-} increases gradually from $6.2 \times 10^{-3} \text{ mol L}^{-1}$ to $6.8 \times 10^{-3} \text{ mol L}^{-1}$ within 12 hours. After 12 hours, the fresh water reaches the end of the column and the concentrations of the main components (Na^+ , Cl^- , Ca^{2+} , K^+ , Mg^{2+} and

Validation report-page# 2-143

SO_4^{2-}) approach constant levels. The concentration of HS^- at the end of the column remains initially low due to elevated Cl^- concentrations, but substantially increases after 12 hours indicating the arrival of the migration front of the fresh water. The concentration of HS^- increases thereafter and reaches a plateau at 5.0×10^{-5} mol L⁻¹ at about 13 hours.

Comparison of the simulated results obtained by MIN3P-THCm (lines in Figure 2.55 and Figure 2.56 with those obtained by PHREEQC (symbols in Figure 2.55 and Figure 2.56) show very good agreement. Figure 2.55(left) shows a small difference in the concentration profiles for HS^- , which may be due to the different spatial and temporal weighting schemes employed by the two codes or differences in the thermodynamic database used by the two codes. The good agreement builds confidence in the correct implementation of the SDSR model in MIN3P-THCm and PHREEQC.

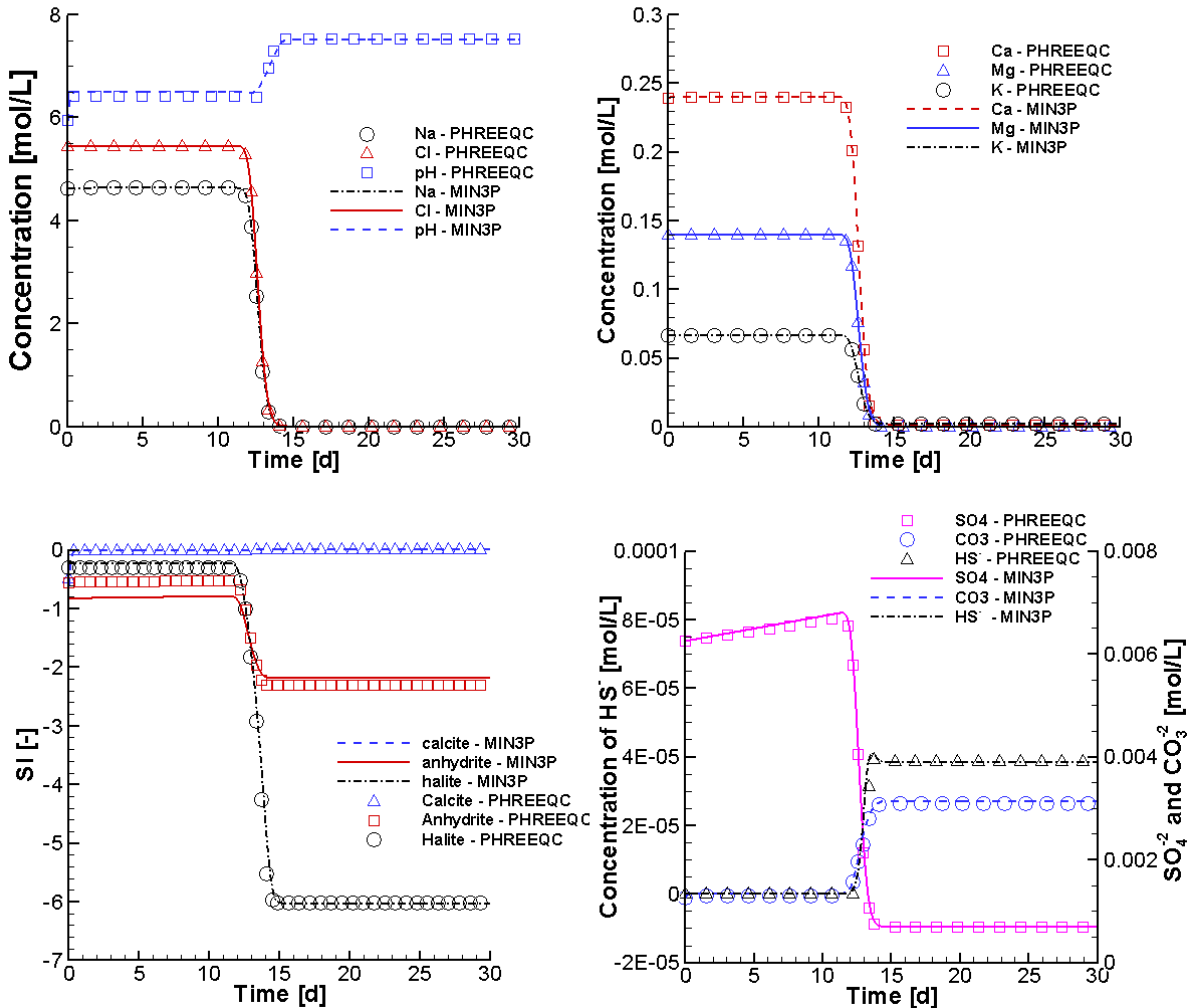


Figure 2.56: Comparison of Breakthrough Curves of pH and Total Concentrations of Na⁺ and Cl⁻ (Top Left), Ca²⁺, K⁺, Mg²⁺ (Top Right), SO₄²⁻, CO₃²⁻ and HS⁻ (Bottom Right), and SI (saturation indexes) of Calcite, Anhydrite and Halite (Bottom Left) Simulated by MIN3P-THCm (Lines) to Those Calculated by PHREEQC (Symbols) – With Inhibition of Sulfate Reduction by Cl⁻

To demonstrate the influence of the SDSR inhibition term on the results, comparison simulations were performed for the same example, but without the SDSR inhibition term. Figure 2.56 depicts the simulated breakthrough curves for pH and total component concentrations, together with the SI curves of the minerals. In comparison to the breakthrough curves obtained with the SDSR inhibition term, most components with the exception of HS⁻ and CO₃²⁻ show no significant differences (compare Figure 2.55 and Figure 2.56). However, as expected, substantial differences exist for the total

concentrations of HS^- . If the influence of salinity on sulfate reduction is not taken into account, HS^- forms from the beginning of the simulation and increases rapidly within 12 hours, reaching peak concentrations of 8.1×10^{-5} mol L⁻¹ at about 12 hours. From 12 to 15 hours, the total concentration of HS^- drops rapidly to 3.9×10^{-5} mol L⁻¹ and remains constant thereafter, due to the stable supply of SO_4^{2-} from the dissolution of the anhydrite.

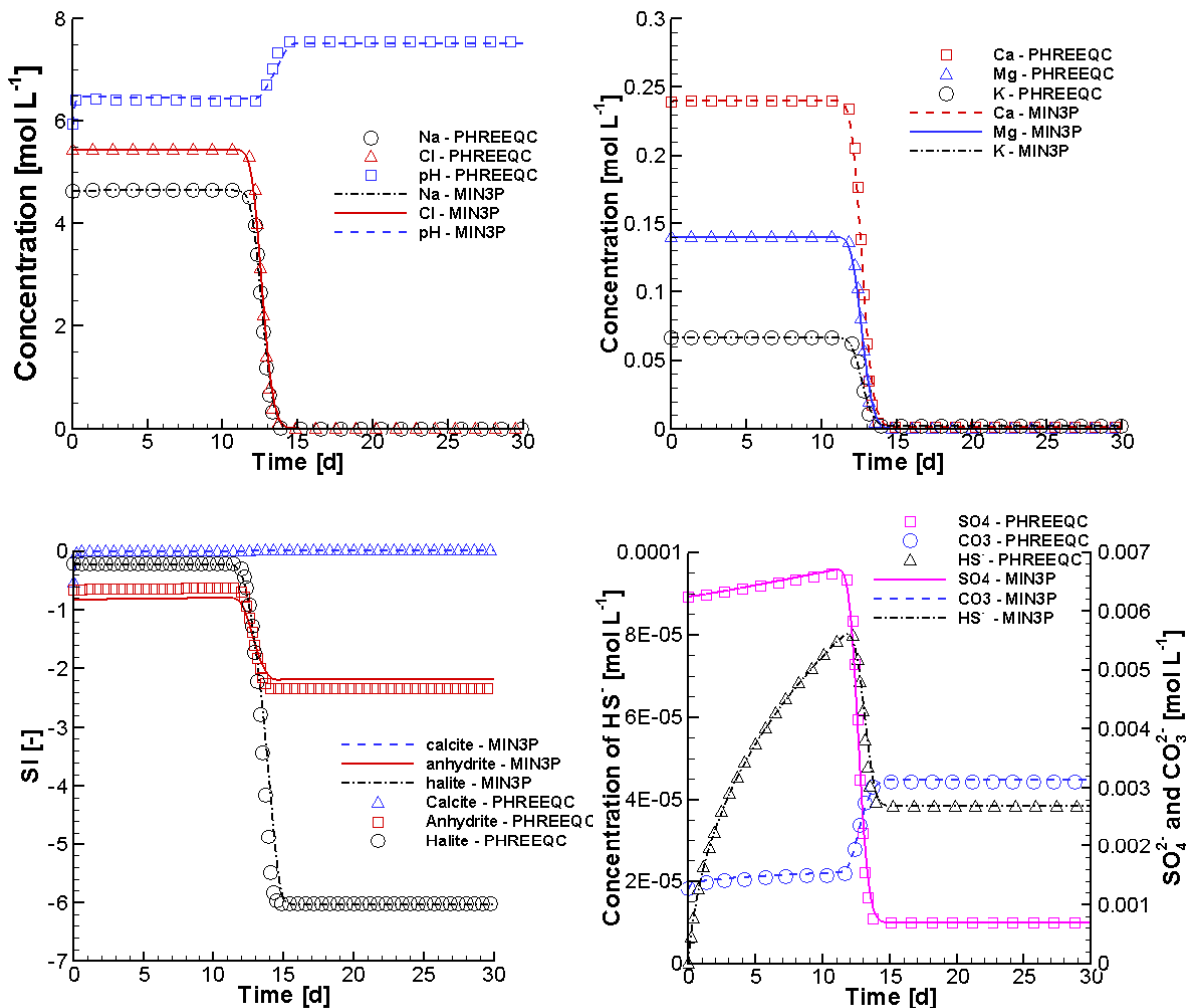


Figure 2.57: Comparison of Breakthrough Curves of pH and Total Concentrations of Na^+ and Cl^- (Top Left), Ca^{2+} , K^+ , Mg^{2+} (Top Right), SO_4^{2-} , CO_3^{2-} and HS^- (Bottom Right), and SI (saturation indexes) of Calcite, Anhydrite and Halite (Bottom Left) Simulated by MIN3P-THCm (Lines) to Those Calculated by PHREEQC (Symbols) – Without Inhibition of Sulfate Reduction by Cl^-

2.5.23.5 File location

Input file for the case considering SDSR Model:

.\Benchmark\benchmarks_new_add\sulfur-V1.0.431\verification\sul2pqc-cos\sul2pqc.dat

Input file for the case not considering SDSR Model:

.\Benchmark\benchmarks_new_add\sulfur-V1.0.431\verification\sul2pqc-n\sul2pqc.dat

Databases:

.\Benchmark\benchmarks_new_add\sulfur-V1.0.431\verification\database\default

2.6 HYDROMECHANICAL COUPLING

2.6.1 VERIFICATION OF VERTICAL STRESS

2.6.1.1 Problem definition

This benchmark is 1D hydromechanical coupling problem for the verification of the one-dimensional vertical stress implementation. It is verified against the analytical solution presented by Lemieux et al. (2008) and Bea et al. (2011).

2.6.1.2 Model set-up

A 1D model with 10000.0 m in depth is discretized into 1000 control volumes yielding a discretization interval of 10.0 m for the interior control volumes and 5.0 m for the control volumes on the boundary.

2.6.1.3 Results

The analytical solution was applied to a one-dimensional semi-infinite vertical column of fully saturated sand (Figure 2.58A). In this case, a load is applied to the top boundary at a constant rate ($\sim 0.32 \text{ m year}^{-1}$, e.g. it could represent the ice sheet loading in a glaciation scenario). The top of the column is drained and the bottom is a no-flow boundary condition. Model parameters are described in Lemieux et al. (2008). The analytical solution in space (z) and time (t) for the hydraulic head ($h(z, t)$) is (Lemieux et al. 2008, Bea et al. 2011)

$$h(z, t) = \frac{\zeta}{\rho_f g} \frac{\partial \sigma_{zz}}{\partial t} \left[t - \left(t + \frac{z^2}{2D} \right) erfc \left(\frac{z}{2\sqrt{Dt}} \right) + z \sqrt{\frac{t}{\pi D}} \exp \left(-\frac{z^2}{4Dt} \right) \right] \quad \text{Equation 1-36}$$

where D is the hydraulic diffusivity defined as $D = k / S_s$ [$L^2 T^{-1}$].

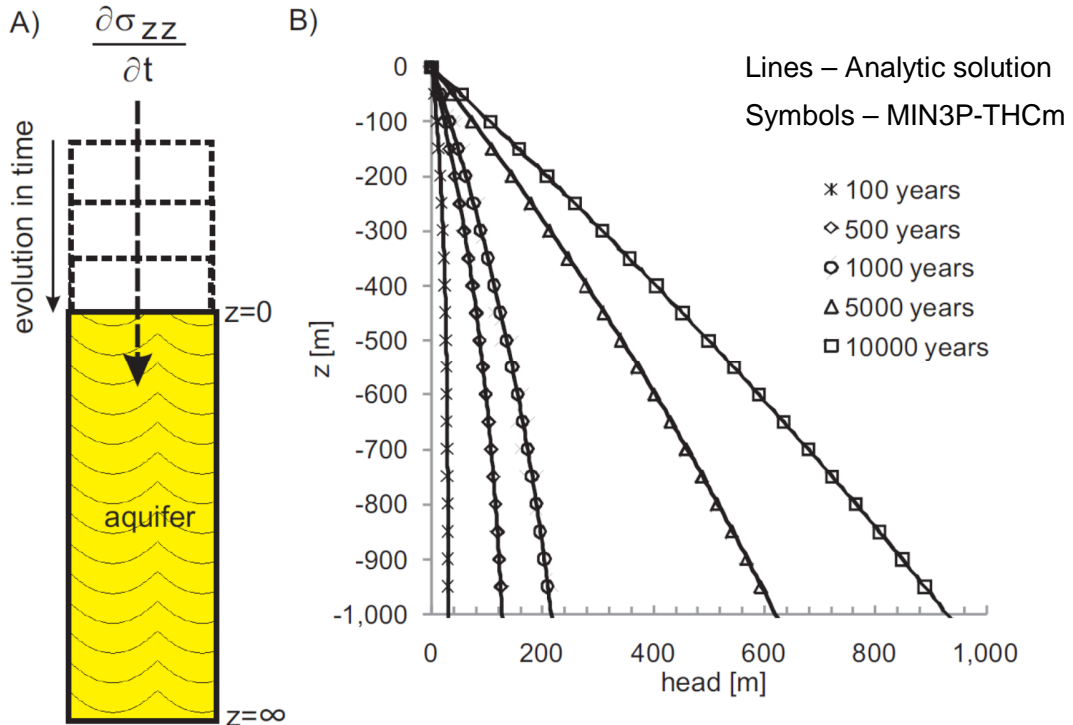


Figure 2.58: Verification of the one-dimensional vertical stress implementation in MIN3P-THCm. A) Conceptual model depicting vertical loading on an aquifer with free drainage on surface. B) MIN3P-THCm results (symbols) match the analytical solution (solid lines) presented by Lemieux et al. (2008) (Bea et al., 2011)

The vertical distributions of pressure head at different times are shown in Figure 2.58B. The pressure heads increase with time as a consequence of the temporally constant loading. Note that the MIN3P-THCm results agree well with the analytical results obtained using the Equation 1-36.

2.6.1.4 File locations

The input file can be found under

`..\benchmarking_nwmo_report\ nwmo_verification_examples\d1_verification_vertical_stress\basin.dat`

Database is a subfolder under the folder of the input file: `\database\default`

3 DEMONSTRATION EXAMPLES

3.1 BATCH REACTIONS

MIN3P-THCm provides many functions for geochemical batch reaction simulations including solution mixing, ion exchange, sorption, surface complexation, kinetic reactions, mineral dissolution/precipitation and biogeochemical reactions. A collection of geochemical batch reaction examples are listed in Table 3.1. These examples are also used in during code testing after each code revision.

Table 3.1: List of geochemical batch reaction test examples

Example Name	Description of Main Features	Section
albite	Kinetic dissolution of calcite and albite in a batch reactor	3.1.1
appelo	Kinetic dissolution of calcite in a batch reactor	3.1.2
Cr(III)	pH-dependent speciation of chromium	3.1.3
Fe(III)	pH-dependent speciation of iron	3.1.4
linsorb	Dissolution and sorption of PCE - linear isotherm	3.1.5
surfa2	pH-dependent anion surface complexation with implicit model	3.1.6
surfme2	pH-dependent cation surface complexation with implicit model	3.1.7

3.1.1 KINETIC DISSOLUTION OF CALCITE AND ALBITE IN A BATCH REACTOR

3.1.1.1 Problem definition

This demonstration example is a geochemical batch reaction with kinetically controlled mineral dissolution of calcite and albite with parallel reaction pathways.

3.1.1.2 Model setup

The geochemical system includes six aqueous components (H^+ , Ca^{2+} , Na^+ , H_4SiO_4 , Al^{3+} , CO_3^{2-}), 14 secondary aqueous species (OH^- , HCO_3^- , $\text{H}_2\text{CO}_3(\text{aq})$, CaOH^+ , CaHCO_3^+ , $\text{CaCO}_3(\text{aq})$, H_3SiO_4^- , $\text{H}_2\text{SiO}_4^{2-}$, NaCO_3^- , $\text{NaHCO}_3(\text{aq})$, Al(OH)^{2+} , Al(OH)_2^+ , $\text{Al(OH)}_3(\text{aq})$ and Al(OH)_4^-), two minerals (calcite and albite). The initial geochemical conditions are listed in Table 3.2.

Validation report-page# 3-149

Table 3.2: Initial geochemical conditions for demonstration example *albite*

Parameter	Initial Condition	Unit
<i>Aqueous phase</i>		
Ca^{2+}	1.69512×10^{-5}	[mol l ⁻¹]
Na^+	1.00×10^{-6}	[mol l ⁻¹]
CO_3^{2-}	2.69512×10^{-5}	[mol l ⁻¹]
H_4SiO_4	1.00×10^{-6}	[mol l ⁻¹]
Al^{3+}	1.00×10^{-6}	[mol l ⁻¹]
H^+	2.154×10^{-4}	[mol l ⁻¹]
<i>Mineral</i>		
Calcite	5.00×10^{-4}	[m ³ m ⁻³]
Albite	5.00×10^{-1}	[m ³ m ⁻³]

3.1.1.3 Parameters

The model for updates of surface area used for the simulation is the geometric model. Related parameters are given in Table 3.3. The pH-dependent kinetic reaction of albite is described by a model with two parallel reaction pathways (Wollast and Chou 1985) as described in section “Surface-controlled rate expressions” in the user manual.

Table 3.3: Geometric update model parameters for calcite and albite for demonstration example *albite*

Parameter	Symbol	Calcite	Albite	Unit
Surface area	S	0.10	0.10	[m ² l ⁻¹ bulk]
Initial particle radius	r_i	1.5×10^{-4}	1.5×10^{-4}	[m]
Particle radius	r_s	1.5×10^{-4}	1.5×10^{-4}	[m]
Minimum particle radius	r_{min}	3.0×10^{-7}	3.0×10^{-7}	[m]

3.1.1.4 Results

Simulated results show that the initial solution is not in equilibrium with calcite and albite (Figure 3.1 – upper panel). The time needed for calcite to reach equilibrium with the solution (saturation index (SI) =0) was about 3 days, while that for albite is about 400 days. The concentrations of selected components Ca^{2+} , Na^+ , H_4SiO_4 , Al^{3+} , CO_3^{2-} increase (Figure 3.1 - lower panel).

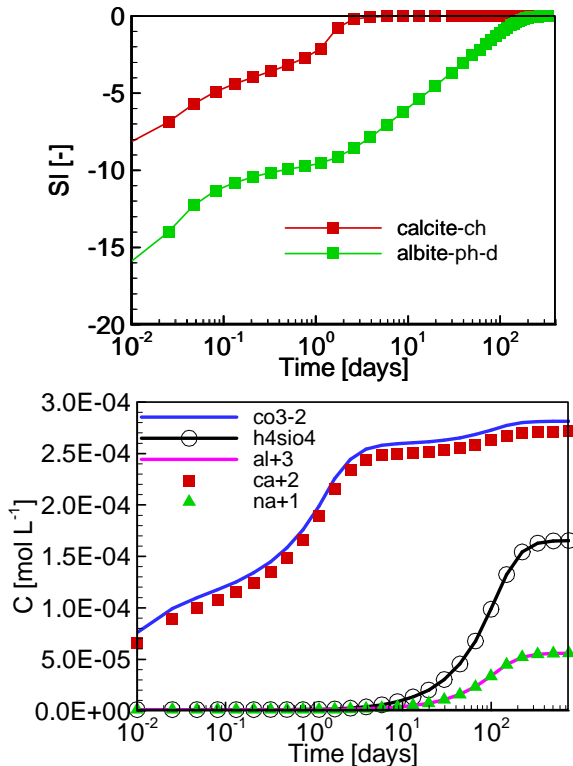


Figure 3.1: Simulated time curves of saturation indices for albite and calcite (upper panel), and concentrations of selected components (lower panel)

3.1.1.5 File locations

The input file is: *albite.dat* under folder *.\benchmarks\benchmarks_standard\batch\albite*
 Database can be found under: *..\benchmarks\database\default*

3.1.2 KINETIC DISSOLUTION OF CALCITE IN A BATCH REACTOR

3.1.2.1 Problem definition

This demonstration example is a geochemical batch problem involving the kinetically controlled mineral dissolution of calcite with three parallel reaction pathways.

3.1.2.2 Model setup

The geochemical system includes three aqueous components (H^+ , Ca^{2+} , and CO_3^{2-}), three secondary aqueous species (OH^- , HCO_3^- , $\text{H}_2\text{CO}_3(\text{aq})$), one mineral (calcite). The initial geochemical conditions are listed in Table 3.4.

Table 3.4: Initial geochemical conditions for demonstration example *appelo*

Parameter	Initial Condition	Unit
<i>Aqueous phase</i>		
H ⁺	2.0×10^{-3}	[mol l ⁻¹]
CO ₃ ²⁻	1.0×10^{-3}	[mol l ⁻¹]
Ca ²⁺	1.0×10^{-11}	[mol l ⁻¹]
<i>Mineral</i>		
Calcite	1.0×10^{-2}	[m ³ m ⁻³]

3.1.2.3 Parameters

The kinetic model used for the simulation was geometric model. Related parameters are listed in Table 3.5. The pH dependent kinetic reaction of albite was described by a model with three parallel reaction pathways as described in section “Surface-controlled rate expressions” in the user manual (Wollast and Chou 1985).

Table 3.5: Geometric update model parameters for calcite

Parameter	Symbol	Calcite	Unit
Surface area	S	0.10	[m ² l ⁻¹ bulk]
Initial particle radius	r _i	3.0×10^{-5}	[m]
Particle radius	r _s	3.0×10^{-5}	[m]
Minimum particle radius	r _{min}	3.0×10^{-7}	[m]

3.1.2.4 Results

Simulated results show that the initial solution is not in equilibrium with calcite (Figure 2.5 - upper panel). The time needed for calcite to reach equilibrium with the solution (saturation index (SI) =0) is about 0.25 days. The concentrations of selected species Ca²⁺, HCO₃⁻, H₂CO₃(aq), OH⁻, CO₃²⁻ increase (Figure 2.5 – lower panel).

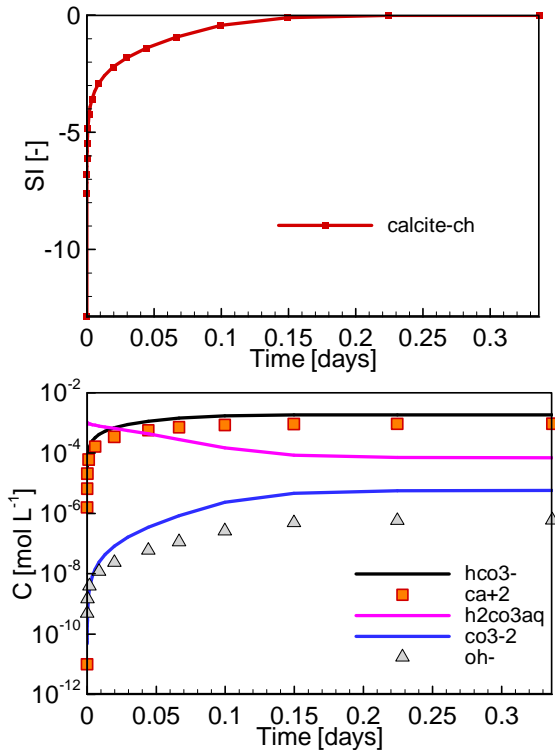


Figure 3.2: Simulated time curves of SI of calcite (upper panel), and concentrations of selected species (lower panel)

3.1.2.5 File locations

The input file is: *appelo.dat* under folder:
 .\benchmarks\benchmarks_standard\batch\appelo

Database can be found under: ..\benchmarks\database\default

3.1.3 PH-DEPENDENT SPECIATION OF CHROMIUM

3.1.3.1 Problem definition

This demonstration example is a geochemical batch reaction considering pH dependent complexation of Cr(III).

3.1.3.2 Model setup

The geochemical system includes two aqueous components (H^+ and Cr(OH)_2^+), six secondary aqueous species (OH^- , Cr^{3+} , Cr(OH)_2^{2+} , $\text{Cr(OH)}_3(\text{aq})$, Cr(OH)_4^- and CrO_2^-) and three excluded minerals (Cr_2O_3 , $\text{Cr(OH)}_3(\text{am})$ and $\text{Cr(OH)}_3(\text{c})$). The initial geochemical conditions are listed in Table 3.6. The simulation was conducted for a pH range from 0 to

Validation report-page# 3-153

14 in 50 steps. The total concentration of $\text{Cr}(\text{OH})_2^+$ is 1.0×10^{-4} [mol l⁻¹]. The excluded minerals were included to monitor their saturation indices as a function of pH.

Table 3.6: Initial geochemical condition for demonstration example Cr(III)

Parameter	Initial Condition	Unit
<i>Aqueous phase</i>		
H^+	0.0 [#]	pH
$\text{Cr}(\text{OH})_2^+$	1.0×10^{-4}	[mol l ⁻¹]

- a pH-sweep calculation is carried out using the keyword ‘ph_sweep’ (see section “INITIAL CONDITION – BATCH REACTIONS” in the user manual)

3.1.3.3 Results

The simulated results for the pH-dependent species concentration of Cr(III) and saturation indexes (SI) of excluded minerals are depicted in Figure 3.3. Cr^{3+} is the main species when pH is lower than 4.0. Increasing the pH results in concentration peaks of $\text{Cr}(\text{OH})^{2+}$, $\text{Cr}(\text{OH})_2^+$ and $\text{Cr}(\text{OH})_3(\text{aq})$. When pH is higher than 12.0, the main species are $\text{Cr}(\text{OH})_4^-$ and CrO_2^- (Figure 3.3 left). As for potential minerals, none of the selected minerals tend to precipitate if pH is lower than 4.0. For higher pH values, the SIs of Cr_2O_3 , $\text{Cr}(\text{OH})_3(\text{am})$ and $\text{Cr}(\text{OH})_3(\text{c})$ indicate supersaturated conditions (Figure 3.3 right).

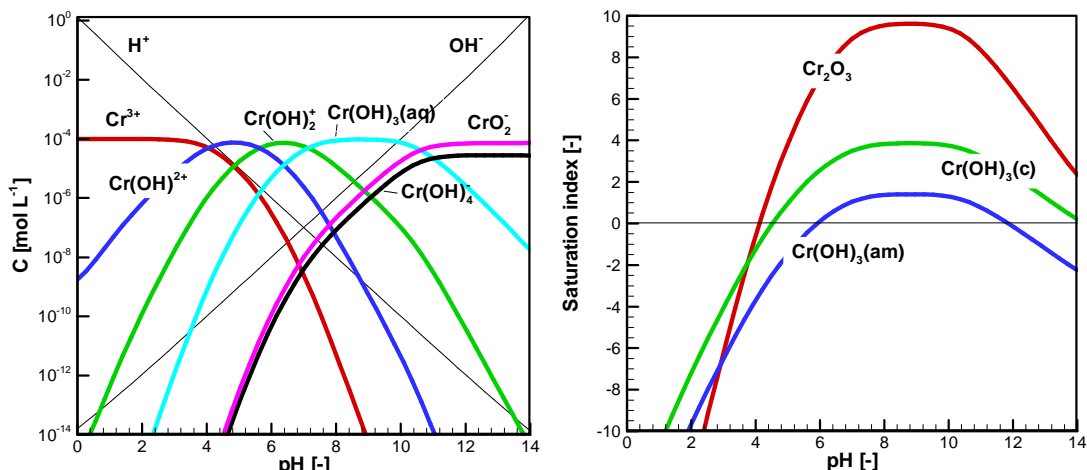


Figure 3.3: Simulated results for pH dependent speciation of Cr(III) (left) and saturation indexes of excluded minerals (right) (benchmark Cr(III))

3.1.3.4 File locations

The input file is: *phsweep.dat* under folder:

.\benchmarks\benchmarks_standard\batch\Cr(III)

Database can be found under: *.\benchmarks\database\default*

Validation report-page# 3-154

3.1.4 PH-DEPENDENT SPECIATION OF IRON

3.1.4.1 Problem definition

This demonstration example is a geochemical batch reaction considering pH dependent complexation of Fe(III).

3.1.4.2 Model setup

The geochemical system includes two aqueous components (H^+ and Fe^{3+}), seven secondary aqueous species (OH^- , Fe(OH)^{2+} , Fe(OH)_2^{2+} , $\text{Fe(OH)}_3(\text{aq})$, Fe(OH)_4^- , $\text{Fe}_2(\text{OH})_2^{4+}$ and $\text{Fe}_3(\text{OH})_4^{5+}$), and five excluded minerals (ferrihydrite, goethite, hematite, maghemite and lepidocrocite). The initial geochemical conditions are listed in Table 3.7. The simulation was conducted for a pH range from 0.0 to 14.0 in 50 steps. The total concentration of Fe^{3+} is 1.0×10^{-4} [mol L⁻¹]. The excluded minerals were included to monitor their saturation indices as a function of pH.

Table 3.7: Initial geochemical condition for demonstration example *Fe(III)*

Parameter	Initial Condition	Unit
<i>Aqueous phase</i>		
H^+	0.0 [#]	pH
Fe^{3+}	1.0×10^{-4}	[mol L ⁻¹]

- a pH-sweep calculation is carried out using the keyword ‘ph_sweep’ (see section “INITIAL CONDITION – BATCH REACTIONS” in the user manual)

3.1.4.3 Results

The simulation results for the pH dependent Fe(III) speciation and saturation indexes (SI) of excluded minerals are depicted in Figure 3.4. Fe^{3+} is the main species when pH is lower than 2.0. Increasing the pH results in concentration peaks of Fe(OH)^{2+} , Fe(OH)_2^{2+} , $\text{Fe(OH)}_3(\text{aq})$, $\text{Fe}_2(\text{OH})_2^{4+}$ and $\text{Fe}_3(\text{OH})_4^{5+}$. When pH is higher than 12.0, the main species is Fe(OH)_4^- (Figure 3.4 left). As for potential minerals, no minerals tend to precipitate if pH is lower than 0.9 (Figure 3.4 right).

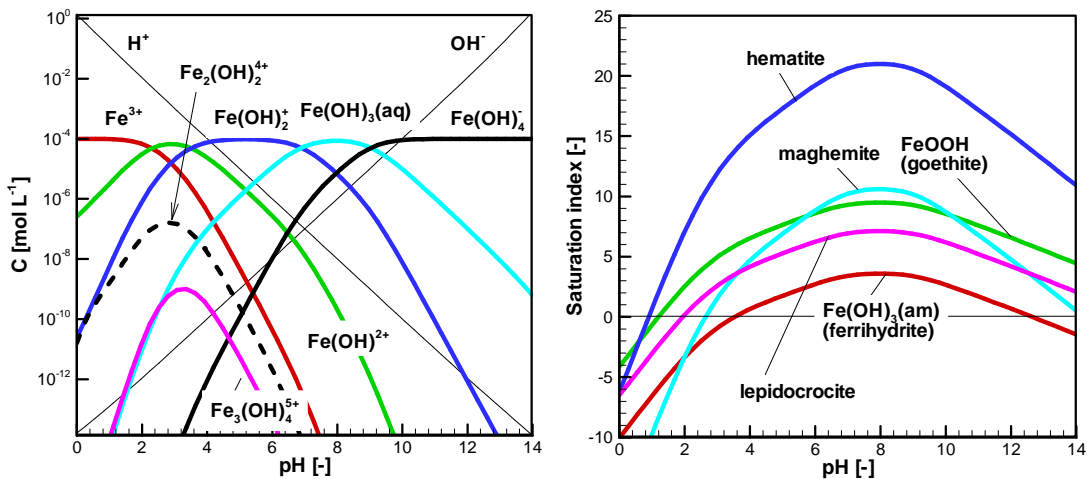


Figure 3.4: Simulated results for pH dependent speciation of Fe(III) (left) and saturation indexes of excluded minerals (right) (benchmark Fe(III))

3.1.4.4 File locations

The input file is: *phsweep.dat* under folder:
 .\benchmarks\benchmarks_standard\batch\Fe(III)

Database can be found under: .\benchmarks\database\default

3.1.5 DISSOLUTION AND SORPTION OF PCE - LINEAR ISOTHERM

3.1.5.1 Problem definition

This demonstration example is a geochemical batch reaction considering linear isotherm sorption and dissolution of the NAPL contaminant PCE (C_2Cl_4).

3.1.5.2 Model setup

The geochemical system includes three aqueous components (Cl^- and C_2Cl_4 and H^+), one sorbing species and a NAPL phase ($C_2Cl_4(n)$). Dissolution of $C_2Cl_4(n)$ is kinetically controlled and simulated according to the ‘twothird’ model (see the theory manual section “LINEAR RETARDATION OF PCE AND BENZENE”). The parameters for the dissolution and kinetic reactions are listed in Table 3.8 and Table 3.9, respectively. The initial geochemical conditions are listed in Table 3.10. The sorption coefficient (K_s) of C_2Cl_4 is 5.0 (see section 2.5.15).

Table 3.8: NAPL reaction parameter – demonstration example linsorb

NAPL phase	Reaction	logK ₂₅
$C_2Cl_4(n)$	$C_2Cl_4 \leftrightarrow C_2Cl_4(r)$	3.04

Table 3.9: Kinetic parameters of C₂Cl₄(n)

Mineral	$k_i^{m,0}$ [m ² mineral L ⁻¹ bulk]	Density [g cm ⁻³]	Mol. weight [g mol ⁻¹]	Molar volume [cm ³ mol ⁻¹]	Update type
C ₂ Cl ₄ (n)	1.0×10 ⁻⁹	1.62	165.83	102.37	twothird

Table 3.10: Initial geochemical conditions - demonstration example linsorb

Parameter	Initial Condition	Unit
<i>Aqueous phase</i>		
Cl ⁻	1.0×10 ⁻⁷	[mol l ⁻¹]
C ₂ Cl ₄	1.0×10 ⁻¹⁰	[mol l ⁻¹]
H ⁺	1.0×10 ⁻⁷	[mol l ⁻¹]
<i>NAPL phase</i>		
C ₂ Cl ₄ (n)	1.0×10 ⁻²	[-]

3.1.5.3 Results

The simulated results for the linear sorption and dissolution of PCE are depicted in Figure 3.5. Initially, there was little PCE in the aqueous phase (Figure 3.5 - middle panel). With the dissolution of the C₂Cl₄(n) (Figure 3.5 – upper panel), the concentrations of PCE in the aqueous phase and in the sorbed phase increase. After about 80 days, an equilibrium state is achieved.

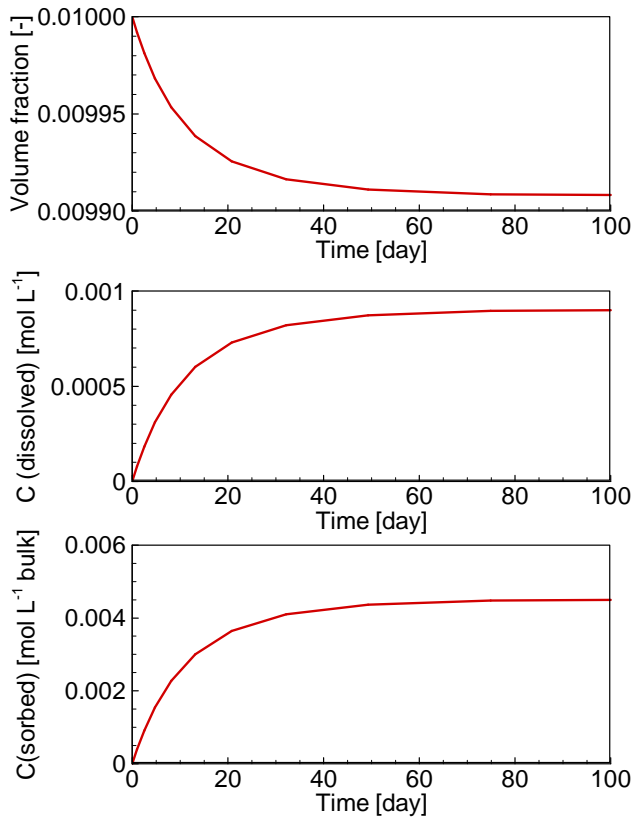


Figure 3.5: Simulated profiles of NAPL volume fraction (upper panel), concentration of dissolved PCE (middle panel) and sorbed PCE (lower panel) (linsorb)

3.1.5.4 File locations

The input file is: *linsorb.dat* under folder:

.\benchmarks\benchmarks_standard\batch\linsorb

Database can be found under: *.\benchmarks\database\default*

3.1.6 PH-DEPENDENT ANION SURFACE COMPLEXATION WITH IMPLICIT METHOD

3.1.6.1 Problem definition

This demonstration example is the same as the example *surfa* (see section 2.1.2) in the model setup and complex surface properties but differs in the treatment of surface site initialization. The example *surfa* assumes that surface sites are explicitly included, specified total concentrations contain sorbed and aqueous species, which implies that mass will be distributed between the aqueous phase and surface sites during speciation calculations. In the current example, the implicit surface complexation model assumes that

Validation report-page# 3-158

the solution composition is fixed and determines the concentrations of the surface complexes based on a fixed solution composition and the specified surface site parameters.

The model set up and parameters for the surface complexation model are the same as the example surfa (see section 2.1.2, Table 2.6).

3.1.6.2 Results

The simulated results using the implicit method for the calculation of the surface sites in the current example ensures that the total concentration of aqueous components HA is maintained at the specified concentration 1.0×10^{-7} M, while the concentration of the surface complex =SA is calculated based on the specified total aqueous concentration. The total mass of A in the system is higher than the specified total aqueous composition. At pH value of 4.5, the concentration of surface complex =SA shows a peak value of 5.7×10^{-7} M.

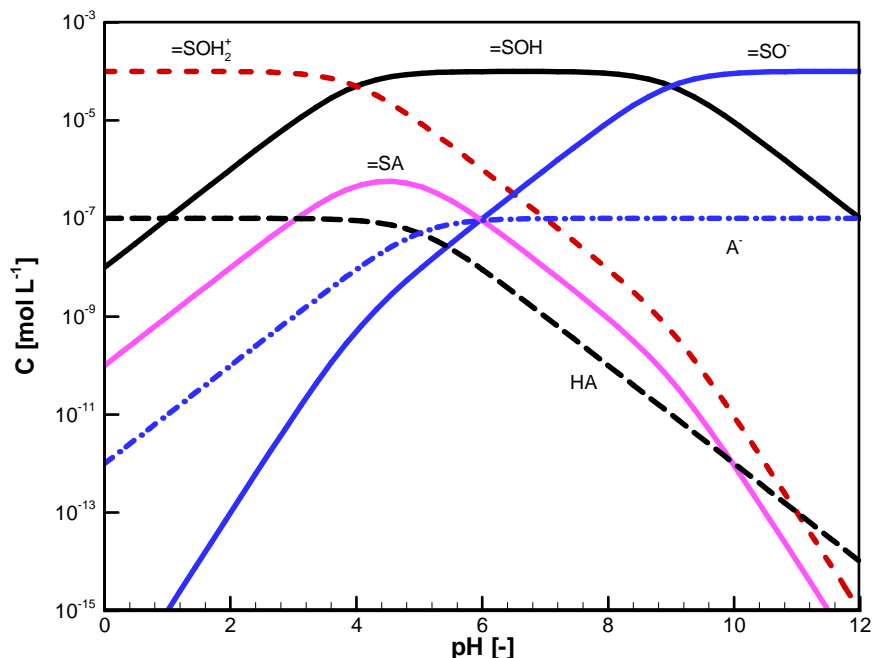


Figure 3.6: Ligand binding by a hydrous oxide from a 10^{-7} M solution (demonstration example surfa2)

3.1.6.3 File locations

The input file is: *surfa2.dat* under folder:
.\benchmarks\benchmarks_standard\batch\surfa2

Database can be found under: *.\benchmarks\database\surftest*

3.1.7 PH DEPENDENT CATION SURFACE COMPLEXATION WITH IMPLICIT METHOD

3.1.7.1 Problem definition

This test example is the same as the example surfme (section 2.1.3) in the model setup and complex surface properties but differs in the treatment of surface site initialization. The example surfme assumes that surface sites are explicitly included, specified total concentrations contain sorbed and aqueous species, which implies that mass will be distributed between the aqueous phase and surface sites during speciation calculations. The total mass of Me in the system amounts to 1.0×10^{-7} M. In the current example, the implicit surface complexation model assumes that the solution composition is fixed and determines the concentrations of the surface complexes based on a fixed solution composition and the specified surface site parameters. The total mass of Me in the system is thus higher than 1.0×10^{-7} M.

The model set up and parameters for the surface complextion model are the same as the example surfa (see section 2.1.3, Table 2.8).

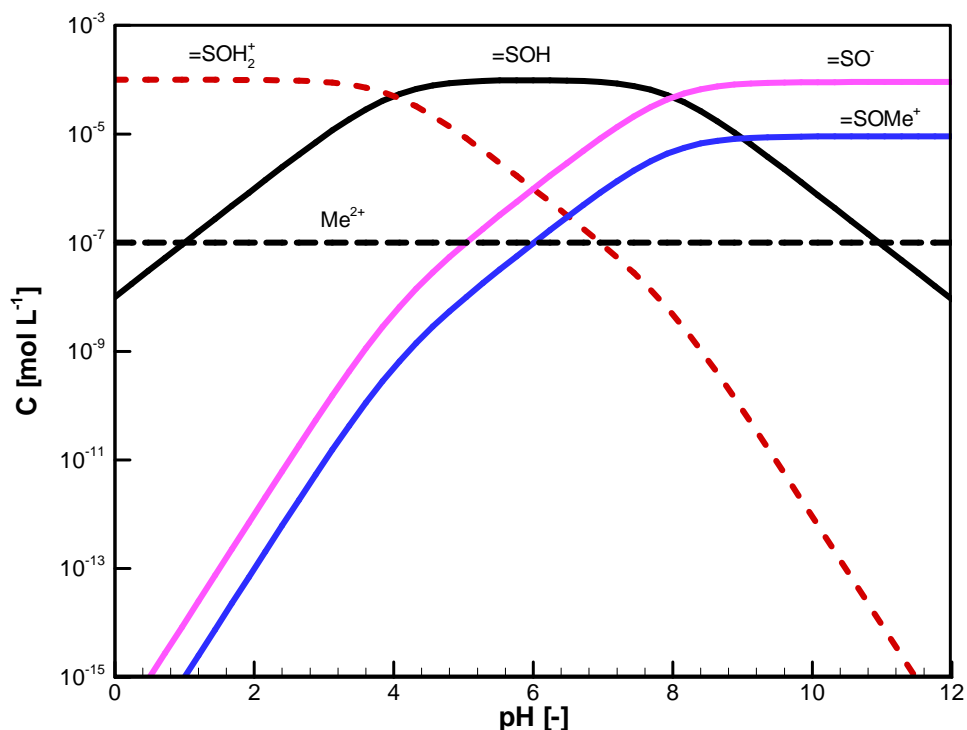


Figure 3.7: Simulated results for the binding of a metal (Me^+) by a hydrous oxide from a 10^{-7} M solution (benchmark surfme2)

Validation report-page# 3-160

3.1.7.2 Results

The simulated geochemical speciation of the metal (Me^+) as a function of pH considering surface complexation is depicted in Figure 3.7. Simulated results show that the concentration of the aqueous component Me^{2+} remains constant ($1.0 \times 10^{-7} \text{ M}$) although pH changed from 0.0 to 12.0. Surface complex $=\text{SOMe}^+$ is the main component for the metal Me^+ if pH exceeds 6.0.

3.1.7.3 File locations

The input file is: *surfme2.dat* under folder:

.\\benchmarks\\benchmarks_standard\\batch\\surfme2

Database can be found under: *.\\benchmarks\\database\\surftest*

3.2 GROUNDWATER FLOW

MIN3P-THCm provides formulations for saturated and unsaturated flow for 1D, 2D and 3D problems. Several examples as listed in Table 3.11 are provided to demonstrate the usage of MIN3P-THCm:

Table 3.11: List of flow test examples

Name	Description of Main Features	Section
stedfs	2D steady state fully-saturated flow	3.2.1
stedvs	2D steady state variably-saturated flow	3.2.2
tranfs	2D transient fully-saturated flow	3.2.3
tranvs	2D transient variably-saturated flow	3.2.4
shlomo	2D variably-saturated steady state flow with seepage face	3.2.5
shlomot	2D variably-saturated transient flow with seepage face	3.2.6
clem3d	3D variably-saturated flow	3.2.7

3.2.1 2D STEADY STATE FULLY-SATURATED FLOW

3.2.1.1 Problem definition

This demonstration example simulates two-dimensional steady state fully-saturated flow.

3.2.1.2 Model setup

A 2D model, 1.0 m in width, and 1.0 m in height, is discretized into 121 control volumes yielding a discretization interval of 0.1 m for the interior control volumes and 0.05 m for the control volumes on the boundary. Boundary conditions for the flow problem consist of a flux $5.79 \times 10^{-5} \text{ m s}^{-1}$ across a central region (0.1 m in length) of the top boundary, and an outflow boundary at the lower left corner of the domain with a hydraulic head 2.0 m.

3.2.1.3 Parameters

The physical parameters (material properties) used for the simulations are summarized in Table 3.12.

Table 3.12: Physical parameters for demonstration example stedfs

Parameter	Symbol	Value	Unit
Width of domain	L	1.0	[m]
Height of domain	L	1.0	[m]

3.2.1.4 Results

Water flow was simulated at steady state, and the simulated hydraulic head contours are

shown in Figure 3.8.

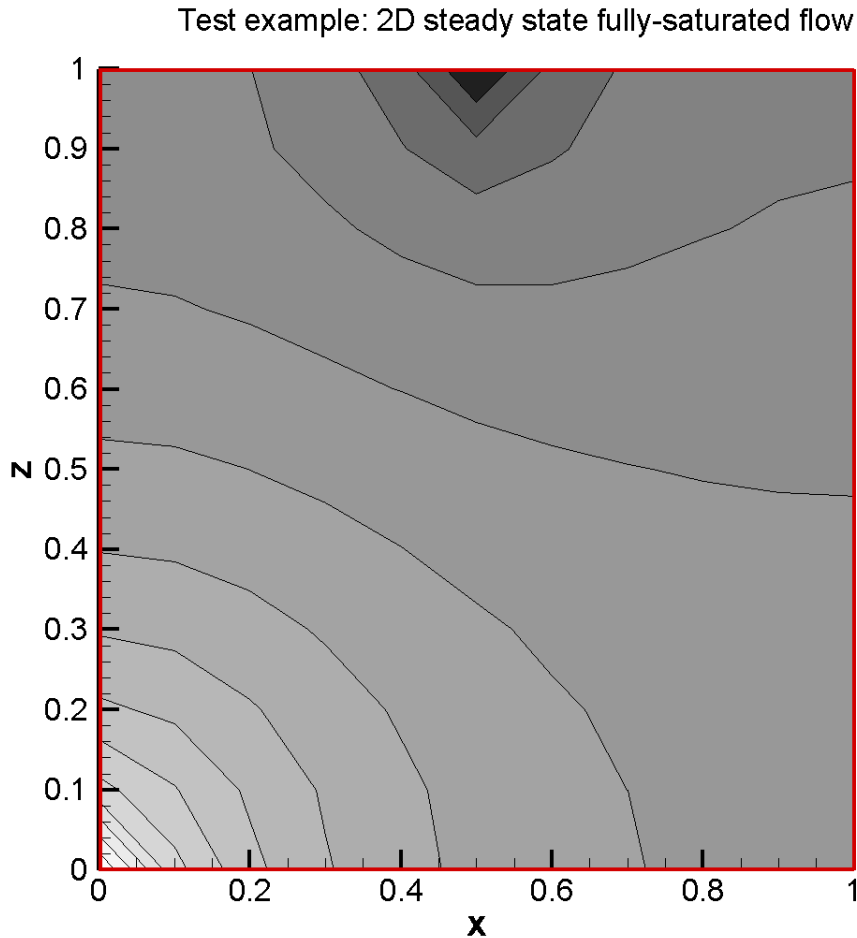


Figure 3.8: Simulated hydraulic head contours at steady state.

3.2.1.5 File locations

The input file is: *stedfs.dat* under folder *.\benchmarks\benchmarks_standard\flow\stedfs*

3.2.2 2D STEADY STATE VARIABLY-SATURATED FLOW

3.2.2.1 Problem definition

This demonstration example is a two dimensional steady state variably-saturated flow problem. The domain contains two parts: the left-middle part of the domain is of low hydraulic conductivity and the other part is of high hydraulic conductivity.

3.2.2.2 Model setup

A 2D model with 1.0 m in width and 2.0 m in height is discretized into 441 control volumes yielding a discretization interval of 0.05 m in width and 0.1 m in height for the interior control volumes and 0.025 m in width and 0.05 m in height for the control volumes on the boundary. Initial condition for the flow problem is pressure head 1.0 m for the whole domain. Boundary conditions for the flow problem consist of a flux $1.74 \times 10^{-6} \text{ m s}^{-1}$ on the left-top boundary (0.2 m), and outflow boundary for the right-bottom boundary (0.5 m) with zero pressure head.

3.2.2.3 Parameters

The physical parameters (material properties) used for the simulations are summarized in Table 3.13.

Table 3.13: Physical parameters for demonstration example stedvs

Parameter	Symbol	Value	Unit
Width of domain	L	1.0	[m]
Height of domain	L	2.0	[m]
Porosity	ϕ	1.0	[-]
Hydraulic conductivity zone 1	K_{zz}	1.16×10^{-5}	[m s ⁻¹]
Hydraulic conductivity zone 2	K_{zz}	1.16×10^{-13}	[m s ⁻¹]

3.2.2.4 Results

Water flow is simulated at steady state, the simulated saturation contours and pressure head contours are given in Figure 3.9.

old - lines / new - flood

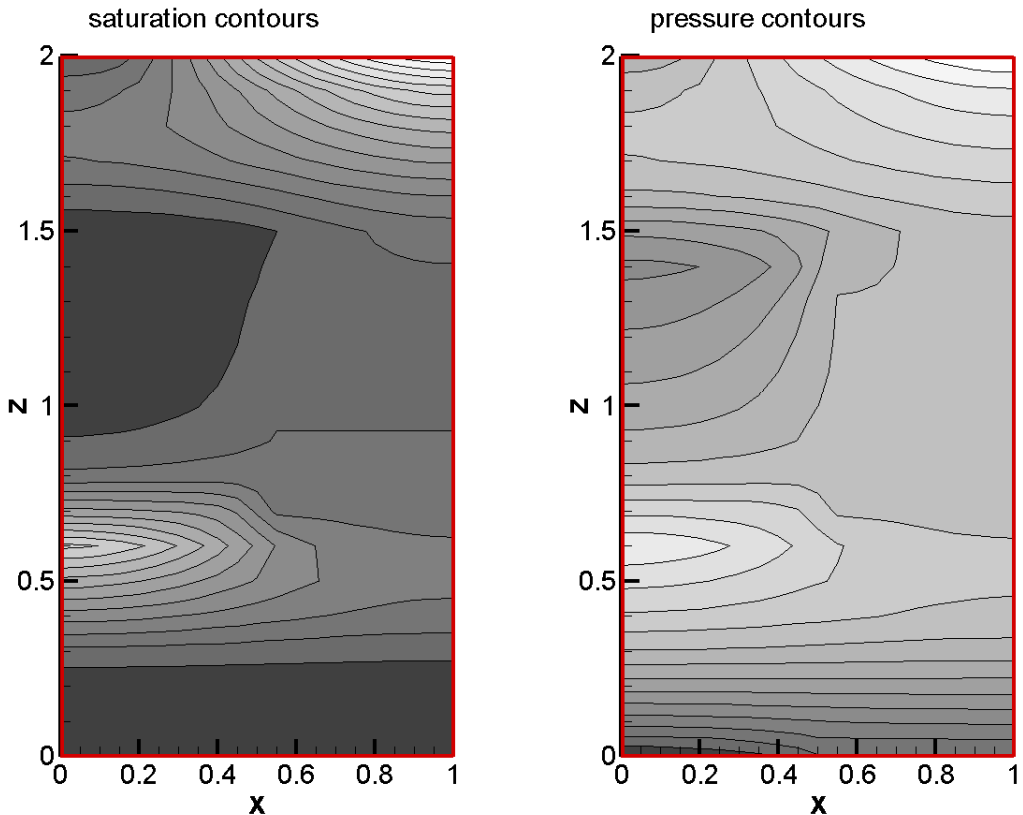


Figure 3.9: Simulated saturation contours and pressure head contours at steady state.

3.2.2.5 File locations

The input file is: *stedvs.dat* under folder *.\benchmarks\benchmarks_standard\flow\stedvs*

3.2.3 2D TRANSIENT FULLY-SATURATED FLOW

3.2.3.1 Problem definition

This demonstration example is a two dimensional transient fully-saturated flow problem.

3.2.3.2 Model setup

A 2D model with 1.0 m in width and 1.0 m in height is discretized into 121 control volumes yielding a discretization interval of 0.1 m for the interior control volumes and 0.05 m for the control volumes on the boundary. Initial condition for the flow problem is hydraulic head 2.0 m for the entire domain. Boundary conditions for the flow problem consist of a flux 5.79×10^{-5} m/s in the center (0.02 m) of top boundary, and outflow boundary for the

left bottom boundary with hydraulic head 2.0 m.

3.2.3.3 Parameters

The physical parameters (material properties) used for the simulations are summarized in.

Table 3.14: Physical parameters for demonstration example transfs

Parameter	Symbol	Value	Unit
Width of domain	L	1.0	[m]
Height of domain	L	1.0	[m]
Porosity	ϕ	1.0	[-]
Hydraulic conductivity zone 1	K_{xx}, K_{zz}	1.16×10^{-5}	[m s ⁻¹]
Specific storage coefficient	S_s	1.0×10^{-3}	[-]

3.2.3.4 Results

Water flow was simulated for a period of 0.02 days, and the simulated hydraulic head contours is given in Figure 3.10.Figure 3.8

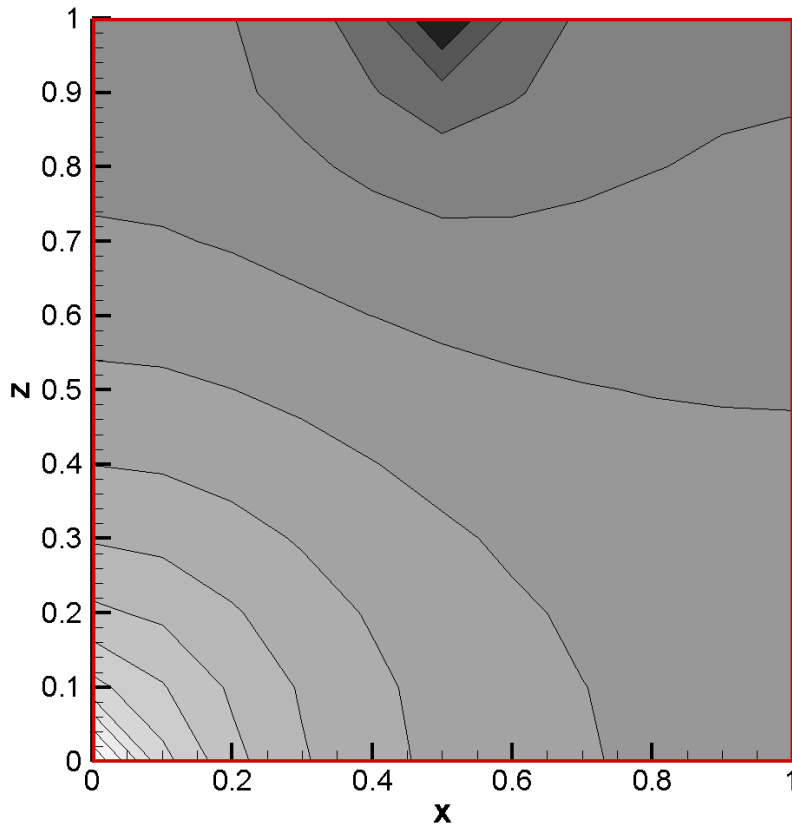


Figure 3.10: Simulated hydraulic head contours after 0.02 days.

Validation report-page# 3-166

3.2.3.5 File locations

The input file is: *transf.dat* under folder *.\benchmarks\benchmarks_standard\flow\transf*

3.2.4 2D TRANSIENT VARIABLY-SATURATED FLOW

3.2.4.1 Problem definition

This demonstration example is a two-dimensional transient variably-saturated flow problem. The domain contains two parts: the left-middle part of the domain is of low hydraulic conductivity and the other part is of high hydraulic conductivity.

3.2.4.2 Model setup

A 2D model, 1.0 m in width and 2.0 m in height, is discretized into 441 control volumes yielding a discretization interval of 0.05 m in width and 0.1 m in height for the interior control volumes and 0.025 m in width and 0.05 m in height for the control volumes on the boundary. Initial condition for the flow problem is hydraulic head 2.0 m for the whole domain. Boundary conditions for the flow problem consist of a flux $5.79 \times 10^{-5} \text{ m s}^{-1}$ across a central region (0.1 m in length) of the top boundary, and an outflow boundary at the lower left corner of the domain with a hydraulic head 2.0 m.

3.2.4.3 Parameters

The physical parameters (material properties) used for the simulations are summarized in Table 3.15.

Table 3.15: Physical parameters for demonstration example transv

Parameter	Symbol	Value	Unit
Width of domain	L	1.0	[m]
Height of domain	L	2.0	[m]
Porosity	ϕ	0.3	[-]
Hydraulic conductivity zone 1	K_{zz}	1.16×10^{-5}	[m s ⁻¹]
Hydraulic conductivity zone 2	K_{zz}	1.16×10^{-13}	[m s ⁻¹]

3.2.4.4 Results

Water flow was simulated at steady state, the simulated saturation contours and pressure head contours are provided in Figure 3.11.

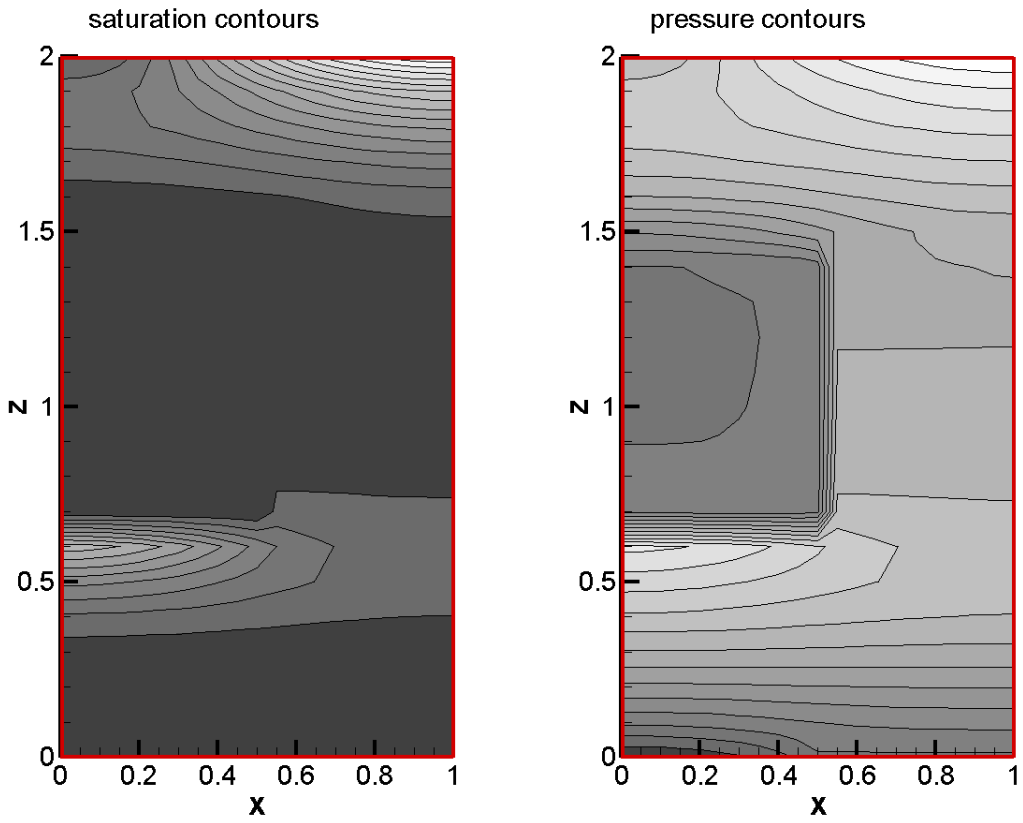


Figure 3.11: Simulated saturation contours and pressure head contours after 1 day.

3.2.4.5 File locations

The input file is: *tranvs.dat* under folder *.\benchmarks\benchmarks_standard\flow\tranvs*

3.2.5 2D VARIABLY-SATURATED STEADY STATE FLOW WITH SEEPAGE

3.2.5.1 Problem definition

This demonstration example is a two-dimensional variably-saturated steady state flow problem reported by Davis and Neuman (1983). The approach is based on the physics of water transfer in the complete domain defined by both the saturated and unsaturated zones of soil.

3.2.5.2 Model setup

A 2D model, 6.0 m in width and 1.2 m in height is discretized into 3146 control volumes yielding a discretization interval of 0.05 m in width and 0.048 m in height for the interior control volumes and 0.025 m in width and 0.024 m in height for the control volumes on

Validation report-page# 3-168

the boundary. The initial condition for the flow problem is a hydraulic head of 0 m for the entire domain. Boundary conditions for the flow problem consist of a flux $1.20 \times 10^{-6} \text{ m s}^{-1}$ on the top boundary, a hydraulic head of 0 m on the left bottom boundary, and a seepage face conditions for the left boundary.

3.2.5.3 Parameters

The physical parameters (material properties) used for the simulations are summarized in Table 3.16.

Table 3.16: Physical parameters for demonstration example shlomo

Parameter	Symbol	Value	Unit
Width of domain	L	6.0	[m]
Height of domain	L	1.2	[m]
Porosity	ϕ	0.348	[-]
Hydraulic conductivity	K_{zz}, K_{xx}	6.43×10^{-5}	[m s ⁻¹]
Specific storage coefficient	S_s	0.0	[-]
Residual saturation	S_{ra}	0.04954	[-]
Van Genuchten parameter α	α	3.43	[m ⁻¹]
Van Genuchten parameter n	n	4.7068	[-]

3.2.5.4 Results

Water flow was simulated at steady state, and the simulated hydraulic head contours are provided in Figure 3.12.

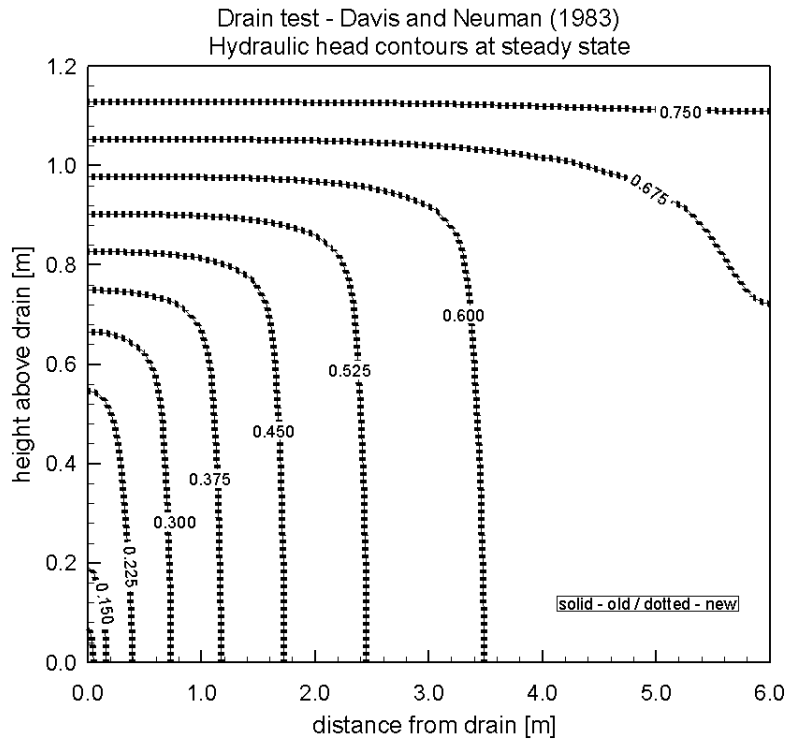


Figure 3.12: Simulated hydraulic head contours at steady state.

3.2.5.5 File locations

The input file is: *shlomo.dat* under folder:

.\benchmarks\benchmarks_standard\flow\shlomo

3.2.6 2D VARIABLY-SATURATED TRANSIENT FLOW WITH SEEPAGE

3.2.6.1 Problem definition

This demonstration example is a two-dimensional variably-saturated transient flow problem reported by Davis and Neuman (1983). The approach is based on the physics of water transfer in the complete domain defined by both the saturated and unsaturated zones of soil.

3.2.6.2 Model setup

A 2D model with 6.0 m in width and 1.2 m in height is discretized into 3025 control volumes yielding a discretization interval of 0.05 m for the interior control volumes and 0.025 m for the control volumes on the boundary. Initial condition for the flow problem is hydraulic head zero for the whole domain. Boundary conditions for the flow problem

Validation report-page# 3-170

consist of a flux 1.20×10^{-6} m/s on the top boundary, hydraulic head zero on the left bottom boundary, and seepage for the left boundary.

3.2.6.3 Parameters

The physical parameters (material properties) used for the simulations are summarized in Table 3.17.

Table 3.17: Physical parameters for the demonstration example shlomot

Parameter	Symbol	Value	Unit
Width of domain	L	6.0	[m]
Height of domain	L	1.2	[m]
Porosity	ϕ	0.348	[-]
Hydraulic conductivity	K_{zz}, K_{xx}	6.43×10^{-5}	m s^{-1}
Specific storage coefficient	S_s	0.0	[-]
Residual saturation	S_{ra}	0.04954	[-]
Van Genuchten parameter α	α	3.43	$[\text{m}^{-1}]$
Van Genuchten parameter n	n	4.7068	[-]

3.2.6.4 Results

Water flow was simulated for a period of 8 days, and the simulated hydraulic head contours after 4 days are provided in Figure 3.13.

3.2.6.5 File locations

The input file is: *shlomot.dat* under folder:

.\benchmarks\benchmarks_standard\flow\shlomot

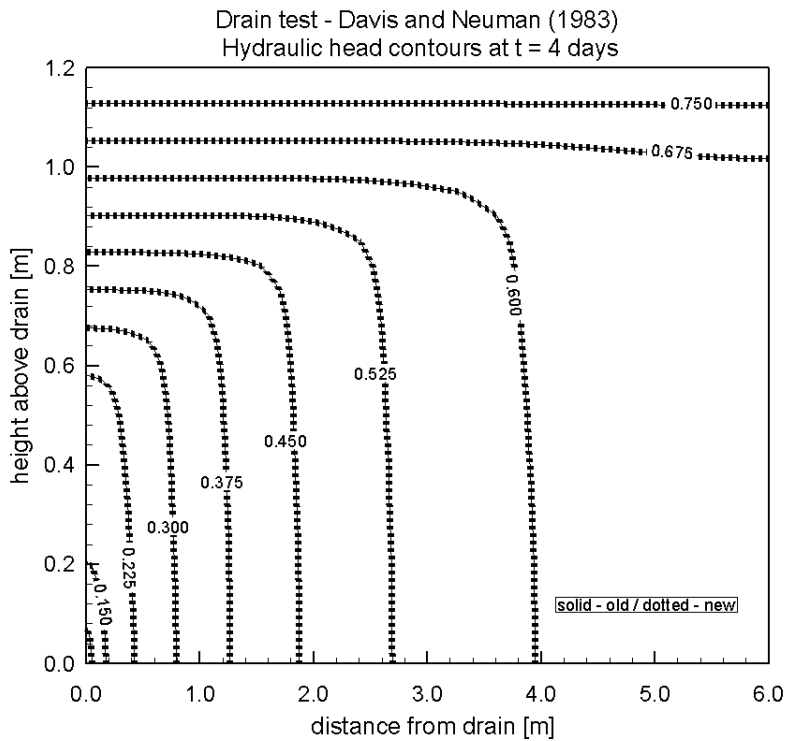


Figure 3.13: Simulated hydraulic head contours after 4 days.

3.2.7 3D VARIABLY-SATURATED FLOW

3.2.7.1 Problem definition

This demonstration example is a three-dimensional variably-saturated transient flow problem.

3.2.7.2 Model setup

A 3D model with 3.0 m in length, 1.0 m in width and 2.0 m in height is discretized into 13,981 control volumes yielding a discretization interval of horizontal 0.1 m and vertical 0.05 for the interior control volumes and horizontal 0.05 m and vertical 0.025 m for the control volumes on the boundary. Initial condition for the flow problem is hydraulic head 0.65 m for the entire domain. Boundary conditions for the flow problem consist of a flux 4.11×10^{-5} m/s on the top corner boundary (x 0.0-0.5 m, y 0.0-0.2 m, and z 2.0 m), and outflow boundary with hydraulic head 0.65 m on the right corner boundary (x 3.0 m, y 0.0-0.6 m and z 0.0-0.65 m).

3.2.7.3 Parameters

The physical parameters (material properties) used for the simulations are summarized in Table 3.18.

Validation report-page# 3-172

Table 3.18: Physical parameters for demonstration example clem3d

Parameter	Symbol	Value	Unit
Length of domain	L	3.0	[m]
Width of domain	L	1.0	[m]
Height of domain	L	2.0	[m]
Porosity	ϕ	0.3	[-]
Hydraulic conductivity	K_{xx}, K_{yy}, K_{zz}	9.72×10^{-5}	[m s ⁻¹]
Specific storage coefficient	S_s	0.0	[-]
Residual saturation	S_{ra}	0.01	[-]
Van Genuchten parameter α	α	3.3	[m ⁻¹]
Van Genuchten parameter n	n	4.1	[-]

3.2.7.4 Results

Water flow was simulated for a period of 48 hours, and the simulated hydraulic head contours after 8 hours are given in Figure 3.13.

3-dimensional transient water table mounding - Hydraulic head contours after T = 8 hrs.

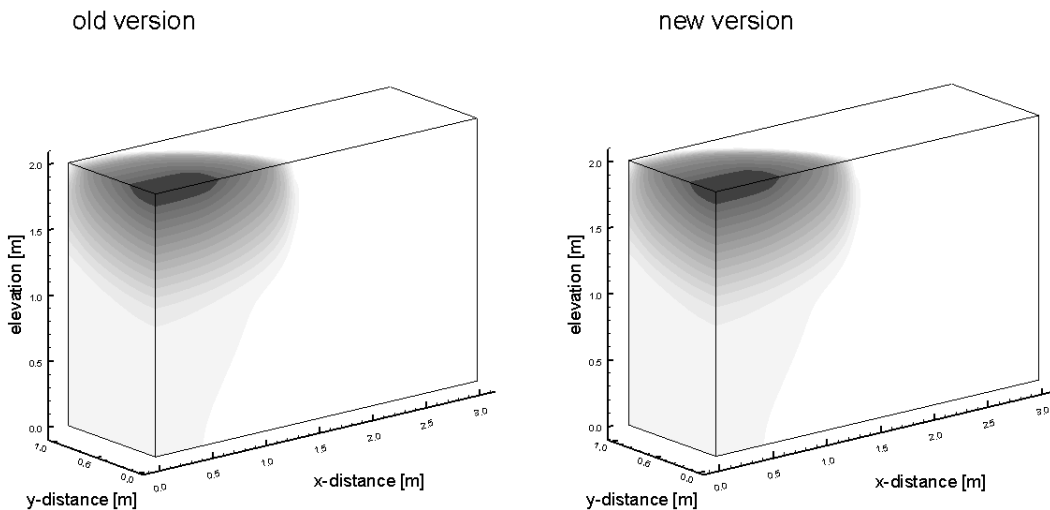


Figure 3.14: Simulated hydraulic head contours after 8 hours.

3.2.7.5 File locations

The input file is: *clem3d.dat* under folder:

.\benchmarks\benchmarks_standard\flow\clem3d

3.3 DENSITY DEPENDENT FLOW AND CONSERVATIVE SOLUTE TRANSPORT

Theoretical box problems were simulated to evaluate error-driven spreading of solutes in static and advecting fluids (Voss and Souza, 1987; Diersch and Kolditz, 2002).

3.3.1 BOX PROBLEMS – HYDROSTATIC BOX TEST (DIERSCH)

3.3.1.1 Problem definition

These simulations are designed to detect spurious numerical results which may be generated in the vicinity of freshwater-saltwater interfaces. Two box problems were benchmarked, investigating stable density stratifications under hydrostatic conditions and in advecting fluids. A stable density stratification satisfies the following condition throughout the model domain:

$$\frac{\partial P_a}{\partial z} \geq \rho |g| \quad \text{Equation 2-1}$$

where P_a is the aqueous fluid pressure [$M L^{-1} T^{-2}$], ρ is the fluid density [$M L^{-3}$], and $|g|$ is the magnitude of gravitational acceleration [$L T^{-2}$], and in this case, z [L] is positive downward.

The hydrostatic box test (Diersch and Kolditz, 2002) compares solute diffusion in variable density fluids, with solute diffusion in a freshwater system in which fluid density is not a function of solute concentration. The implementation of hydrodynamic dispersion in MIN3P-THCm should produce results for solute diffusion, from saltwater into freshwater, that are independent of the density contrast between the two fluids.

3.3.1.2 Model setup

The hydrostatic box test was simulated in a 20 m horizontal by 40 m vertical domain, with a saltwater layer located below a freshwater layer. The two fluids were initially separated by a sharp horizontal interface in the middle of the domain (Diersch and Kolditz, 2002). The domain was surrounded by no flow boundaries for flow and transport. The decoupled (reference) case was simulated by setting the coefficient of density variation, $\partial\rho/\partial c$, to zero, resulting in the freshwater density being assigned to both fluids. The coupled variable density scenario was simulated by setting the coefficient of density variation to 0.7, resulting in a three percent density contrast between the saltwater and freshwater layers. The model was discretized using a 40,200-node grid with $\Delta x = 1.0$ m and $\Delta z = 0.2$ m. The simulations were executed for a period of 1000 days.

3.3.1.3 Parameters

Key flow and transport parameters are summarized in Table 3.19.

Table 3.19: Parameters for Hydrostatic Box Problem (Bea et al., 2011)

Parameter	Symbol	Value	Units
Hydraulic conductivity	K	1.0×10^{-4}	[m s ⁻¹]
Porosity	ϕ	0.4	[-]
Specific storage	S_s	0.0	[m ⁻¹]
Longitudinal dispersivity	α_L	5.0	[m]
Transverse dispersivity	α_T	0.5	[m]
Molecular diffusion coefficient	D_0	1.0×10^{-8}	[m ² s ⁻¹]
Saltwater density	ρ_s	1030	[kg m ⁻³]
Freshwater density	ρ_0	1000	[kg m ⁻³]
Maximum density ratio	ρ_{max}	1.03	[-]
Coefficient of density variation	$\partial\rho/\partial c$	0.0/0.7	[-]
Saltwater concentration	C_s	43	[g l ⁻¹]

3.3.1.4 Results

Figure 3.15 compares the diffusive concentration distributions for the constant density and variable density cases at a simulation time of 1000 days. As shown in Figure 3.15, an excellent agreement was obtained for the two cases, indicating an absence of spurious fluid movement for the coupled case.

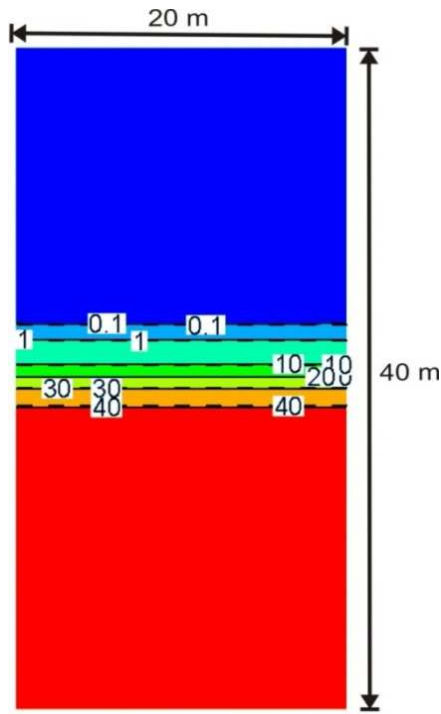


Figure 3.15: Concentration distributions at 1000 days for decoupled ($\partial\rho/\partial c = 0$; dashed lines) and coupled ($\partial\rho/\partial c = 0.7$; solid lines) hydrostatic simulations. Concentration contours have the unit g l⁻¹ (Bea et al., 2011)

3.3.1.5 File locations

The input file for coupled case can be found under

..\benchmarking_nwmo_report\nwmo_verification_examples\d311_hydrostatic_box_test\coupled\diirsch.dat

Database is a subfolder under the folder of the input file: *\database\kmno4_unix*

The input file for decoupled case can be found under

..\benchmarking_nwmo_report\nwmo_verification_examples\d311_hydrostatic_box_test\decoupled\diirsch.dat

Database is a subfolder under the folder of the input file: *\database\kmno4_unix*

3.3.2 HYDROSTATIC BOX PROBLEM (VOSS)

3.3.2.1 Problem definition

The second box problem was simulated to investigate the potential for numerically-induced smearing of sharp concentration gradients in the direction normal to the direction of fluid movement (Voss and Souza, 1987).

3.3.2.2 Model set-up

The domain dimensions were 2000 m in height and length, and the region was discretized using 21 control volumes in the x and z directions. Similar to the hydrostatic problem, a layer of freshwater was initially present above a layer of saltwater.

A constant groundwater seepage velocity of 5 m d⁻¹ in the positive x-direction was simulated by assigning hydrostatic pressure profiles to the left and right sides of the model domain. Fixed solute concentrations were assigned to the influent (left) boundary of the domain, and these were set equal to the initial concentrations assigned to the model domain. A free exit solute boundary condition was assigned to the right side of the model domain. The molecular diffusion coefficient and the transverse dispersivity were both set to zero (Table 3.20). Given these values, no mechanism was present to cause the vertical spreading of solutes, except for potential numerical errors. The simulation was run for a total of 4000 days.

Table 3.20: Parameters for Hydrodynamic Box Problem (Bea et al., 2011)

Parameter	Symbol	Value	Units
Hydraulic conductivity	K	1.16×10^{-3}	[m s ⁻¹]
Porosity	ϕ	0.01	[-]
Specific storage	S_s	0.0	[m ⁻¹]
Longitudinal dispersivity	α_l	100.0	[m]
Transverse dispersivity	α_t	0.0	[m]
Molecular diffusion coefficient	D_0	0.0	[m ² s ⁻¹]
Saltwater density	ρ_s	1025	[kg m ⁻³]
Freshwater density	ρ_0	1000	[kg m ⁻³]
Maximum density ratio	ρ_{max}	1.025	[-]
Coefficient of density variation	$\partial\rho/\partial c$	0.71	[-]
Saltwater concentration	C_s	35	[g l ⁻¹]

3.3.2.3 Results

As Figure 3.16 indicates, the solute iso-concentration lines at the conclusion of the 4000 day simulation were identical to those of the initial solute distribution. The results indicate no numerically-induced solute spreading, or smearing of the solute concentration gradient.

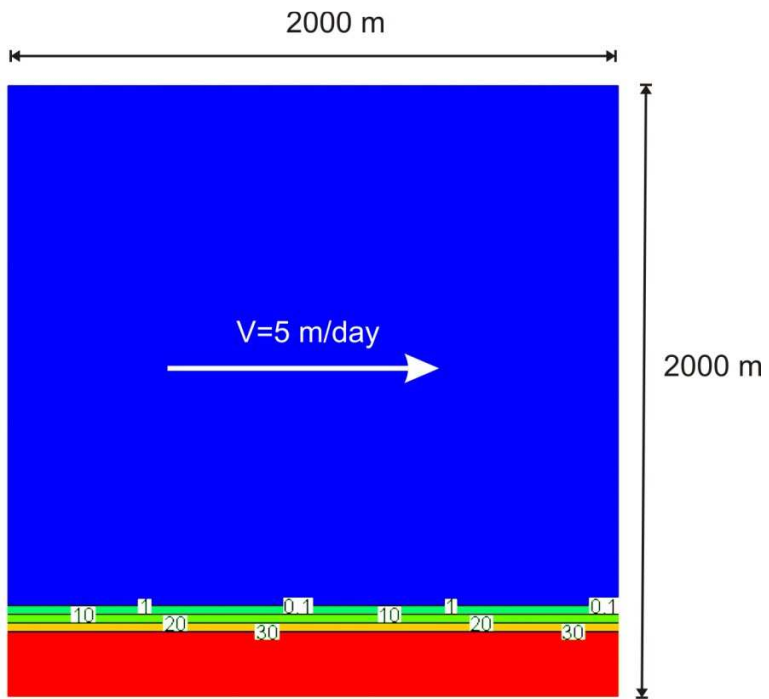


Figure 3.16: Concentration distributions for the hydrodynamic box simulations. Concentration contours (g L^{-1}) at 0 days (solid lines) and 4000 days (dashed lines) are coincident (Bea et al., 2011)

3.3.2.4 File locations

The input file can be found under

`..\benchmarking_nwmo_report\ nwmo_verification_examples\d312_hydrodynamic_box_problem\voss.dat`

Database is a subfolder under the folder of the input file: `\database\kmno4_unix`

3.4 MULTICOMPONENT REACTIVE TRANSPORT

MIN3P-THCm provides multicomponent reactive transport in saturated, unsaturated domain in 1D, 2D and 3D Cartesian and radial-coordinates. Some additional test examples to demonstrate code applications of MIN3P-THCm for reactive transport are listed in Table 3.21.

Table 3.21: List of reactive transport test examples

Example Name	Description of Main Features	Section
complex	1D advective-dispersive transport with aqueous complexation	3.4.1
hom_2D	2D advective-dispersive transport with aqueous complexation	3.4.2
diff_harmonic	Spatial averaging methods for diffusion coefficients	3.4.3
transrc	1D-advective-dispersive transport with transient boundary conditions	3.4.4
dissol	1D advective-dispersive transport with aqueous complexation and mineral dissolution-precipitation	3.4.5
het_2d	2D advective-dispersive transport with aqueous complexation and mineral dissolution-precipitation	3.4.6
weather	Mineral weathering in a soil column	3.4.7
ion-binary	1D advective-dispersive transport with binary monovalent ion exchange	3.4.8
comptran	1D advective-dispersive transport including Monod kinetics, degradation of organic contaminants	3.4.9
degas	1D advective-dispersive transport, degassing from a hydrocarbon spill	3.4.10
raoult	Dissolution and volatilization of an organic contaminant mixture in the vadose zone	3.4.11
surfa2	1D-advective-dispersive transport with anionic surface complexation reactions	3.4.12
surfme2	1D-advective-dispersive transport with cationic surface complexation reactions	3.4.13
prb	Groundwater remediation by a permeable reactive barrier	3.4.14
amd_ex	Generation and attenuation of acid mine drainage	3.4.15
waybrant	Isotope fraction	3.4.16
sulfur	Salinity dependent SRB reaction	3.4.17

3.4.1 1D ADVECTIVE-DISPERSIVE TRANSPORT WITH AQUEOUS

COMPLEXATION

3.4.1.1 Problem definition

This application example is intended to demonstrate how MIN3P-THCm simulates advective dispersive transport including aqueous complexation reactions. MIN3P-THCm calculates concentrations of secondary species according to the reactions defined in the database. Concentrations of components as species in solution and aqueous complexes are provided in the output files.

3.4.1.2 Model setup

A 1D model, 0.40 m in length, is discretized into 81 control volumes. The hydraulic head at the inflow boundary is constant at 0.0014 m, while the hydraulic head at the outflow boundary is set to 0.0 m. With the infiltration of a CaCO₃ rich solution into the column, the aqueous species composition changes over time. In this demonstration example, the primary species are H⁺, CO₃²⁻, and Ca²⁺, and the secondary species are OH⁻, HCO₃⁻, H₂CO₃(aq), CaOH⁺, CaHCO₃⁺ and CaCO₃(aq). The initial condition (IC) of the pore water and the boundary aqueous composition (BC) are listed in Table 3.22.

Table 3.22: Initial and boundary conditions (IC & BC) for demonstration example
complex

Parameter	Initial Condition	Boundary Condition	Unit
H ⁺	1.0×10 ⁻⁷	1.98×10 ⁻²	[mol l ⁻¹]
CO ₃ ²⁻	3.0×10 ⁻⁷	1.0×10 ⁻²	[mol l ⁻¹]
Ca ²⁺	1.0×10 ⁻⁷	1.0×10 ⁻⁴	[mol l ⁻¹]

3.4.1.3 Parameters

The parameters of the porous medium are: porosity is 0.35, hydraulic conductivity is 1.16×10⁻⁵ [m/s], longitudinal dispersivity is 0.005 m.

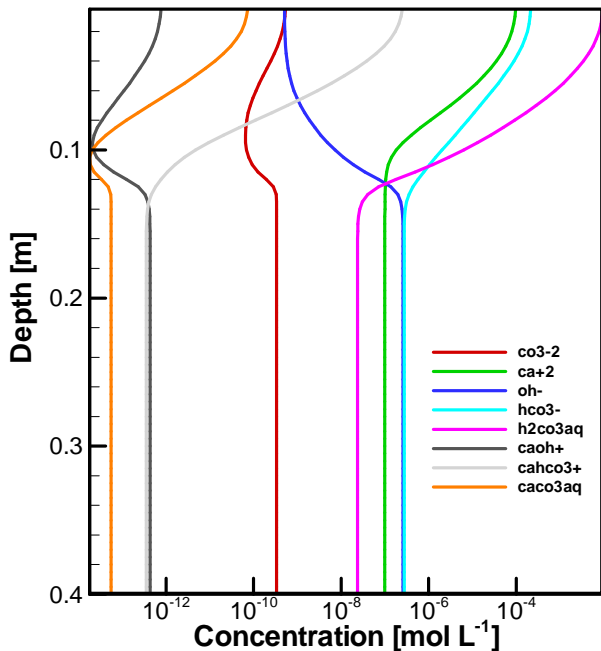


Figure 3.17: Profiles of concentrations of aqueous species at 3 days for benchmark *complex*

3.4.1.4 Results

Simulated results are shown in Figure 3.17. After 3 days, the dilute solution initially present in the porous media ($\text{pH} = 7.4$) is gradually replaced by the infiltrating solution with a pH 4.7. Figure 3.17 depicts the aqueous speciation along the flowpath.

3.4.1.5 File locations

The input file is: *complex.dat* under folder `.\benchmarks\benchmarks_standard\reactran\`
Database can be found under: `.\benchmarks\database\default`

3.4.2 2D ADVECTIVE-DISPERSIVE TRANSPORT WITH AQUEOUS COMPLEXATION

3.4.2.1 Problem definition

This 2D application example demonstrates the use of MIN3P-THCm for multi-dimensional reactive transport including complexation reactions.

3.4.2.2 Model setup

A 2D model, 0.1 m in width and 0.2 m in depth, is discretized into 21×41 control volumes (Figure 3.18). The hydraulic head for the top boundary is constant at 0.0 m, for the bottom

boundary, the hydraulic head is set at 0.0014 m. The remaining boundaries are no flow boundaries. The primary species H^+ and CO_3^{2-} , and the secondary species OH^- , HCO_3^- and $H_2CO_3(aq)$ are included in the geochemical system. The initial (IC) and boundary conditions (BCs) for flow and mass transport are listed in Table 3.23. A different solution with higher concentrations of H^+ and CO_3^{2-} enters from the bottom left corner (i.e. $x=0.0$ to 0.02 m, $Z=0.0$ m) (Figure 3.18). The chemical composition in the solution for the remainder of the bottom boundary is set to be the same as that defined in the initial solution of the domain by using the keyword 'use background chemistry for boundary zone' (see the user manual section BOUNDARY CONDITIONS - REACTIVE TRANSPORT). The BC for reactive transport on the top is set to be the second, free exit, type BC. The final simulation time is 4.0 days.

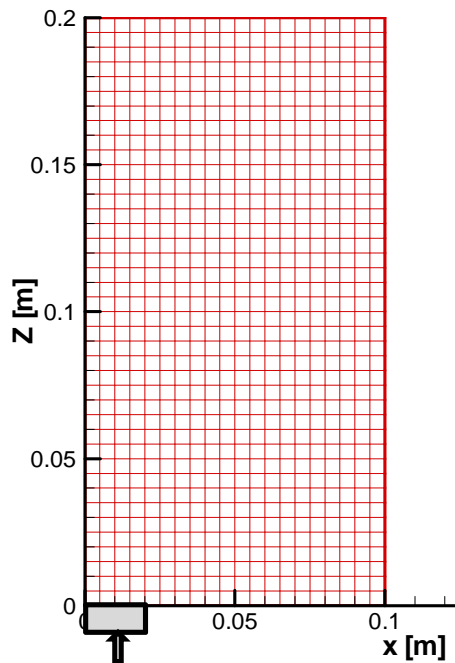


Figure 3.18: Boundary conditions: A carbonic acid solution enters from the bottom left, constant hydraulic head on the top ($h=0.0$ m) and bottom boundaries ($h=0.0014$ m).

Table 3.23: Initial and boundary conditions for flow and reactive transport

Parameter	Initial condition	Boundary conditions		Unit
<i>Aqueous phase</i>		Bottom left	Top	
H^+	2.0×10^{-7}	2.0×10^{-2}	(free exit)	[mol l ⁻¹]
CO_3^{2-}	1.0×10^{-7}	1.0×10^{-2}		[mol l ⁻¹]
<i>Hydraulic condition</i>				
Hydraulic head	0.0	0.0014 (first)	0.0 (first)	[m]

3.4.2.3 Parameters

The parameters of the porous medium are: porosity is 0.35, hydraulic conductivity is $1.16 \times 10^{-5} \text{ m s}^{-1}$, longitudinal dispersivity is 0.005 m, transverse dispersivity is $1.25 \times 10^{-4} \text{ m}$, and the diffusion coefficient is set to $0.0 \text{ m}^2 \text{ s}^{-1}$.

3.4.2.4 Results

The simulated contours of pH and calcite volume fractions at 4.0 days are shown in Figure 3.19. With the intrusion of the solution with higher concentrations of H^+ and CO_3^{2-} from the bottom left boundary upwards, the total CO_3^{2-} concentration increases accordingly (Figure 3.19 left). The concentration distribution of the secondary species (e.g. HCO_3^-) is depicted in Figure 3.19 (right).

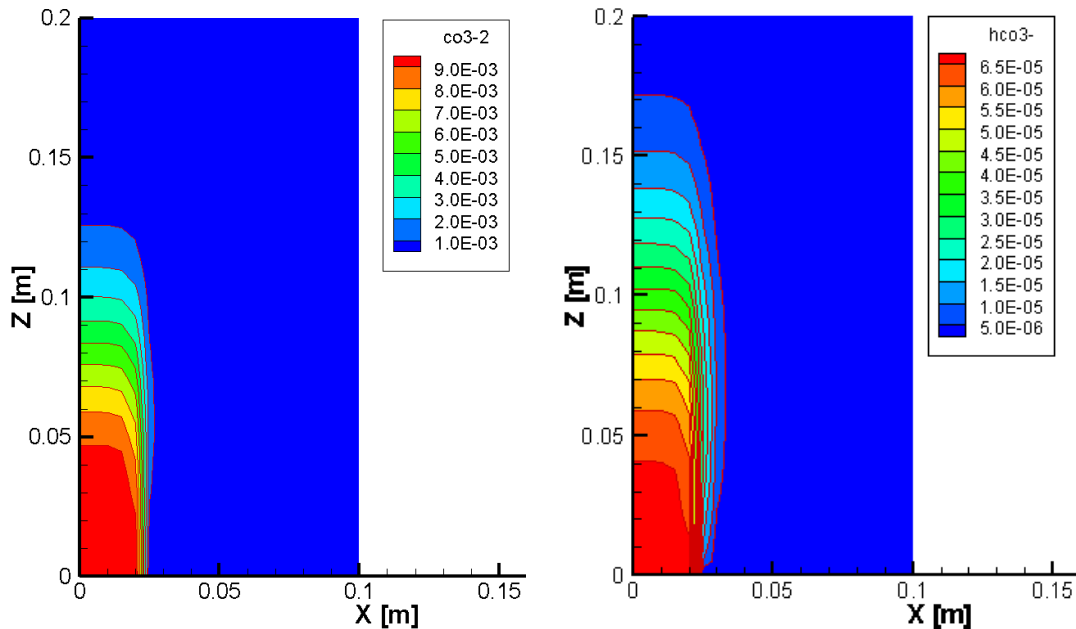


Figure 3.19: Simulated contours of the total CO_3^{2-} concentration (left) and the HCO_3^- concentration (right) at 4.0 days

3.4.2.5 File locations

The input file for the demonstration example can be found under

`.\benchmarks\benchmarks_standard\reactran\hom_2d\hom-2d.dat`

Database can be found under: `.\benchmarks\database\default`

3.4.3 SPATIAL AVERAGING METHODS FOR DIFFUSION COEFFICIENTS

3.4.3.1 Problem definition

This demonstration example is a 1D steady state diffusion problem to demonstrate the averaging methods implemented in MIN3P-THCm for calculating the effective diffusion coefficients between the centroids of two adjacent control volumes with different diffusion parameters, which is important for the accurate simulation of diffusion processes in heterogeneous materials (Patankar, 1980; Kadioglu et al. 2008).

3.4.3.2 Model setup

A 1D model with 1.0 m in length is divided into 3 zones: 0.0 –0.375 m (Zone1), 0.375–0.625m (Zone2) and 0.625– 1.0 m (Zone3). This model is discretized into 5 control volumes. The tracer HTO is the only component considered in the problem. Its initial concentration (IC), and the concentrations at left and right boundaries (BCs) are listed in Table 3.24.

Table 3.24: Initial and boundary conditions (IC & BC) for tracer HTO

Parameter	Initial Condition		Boundary Conditions		Unit
Aqueous phase	Zone 1 & 3	Zone 2	left	right	
HTO	1.0×10^{-100}	1.0×10^{-100}	1.0	1.0×10^{-100}	[mol l ⁻¹]

3.4.3.3 Parameters

The parameters of the porous medium are: porosity is 0.50 for Zone 1 and Zone3, and 0.04 for Zone 2. The free aqueous phase diffusion coefficient (D_0) is $3.75 \times 10^{-9} \text{ m}^2 \text{ s}^{-1}$. The effective diffusion coefficient (D_e) is calculated with the model of Millington and Quirk (1961):

$$D_e = \phi^{\frac{4}{3}} D_0$$

In which ϕ is the porosity.

3.4.3.4 Averaging methods for effective diffusion coefficient

In MIN3P-THCm, three different averaging methods to determine the effective diffusion coefficient D_e were implemented: two arithmetic averaging methods and the harmonic averaging methoda (see the user manual section ‘averaging diffusion’ for details).

3.4.3.5 Results

The simulated concentration profiles applying all three averaging methods mentioned above at steady-state were verified with hand calculations (Figure 3.20).

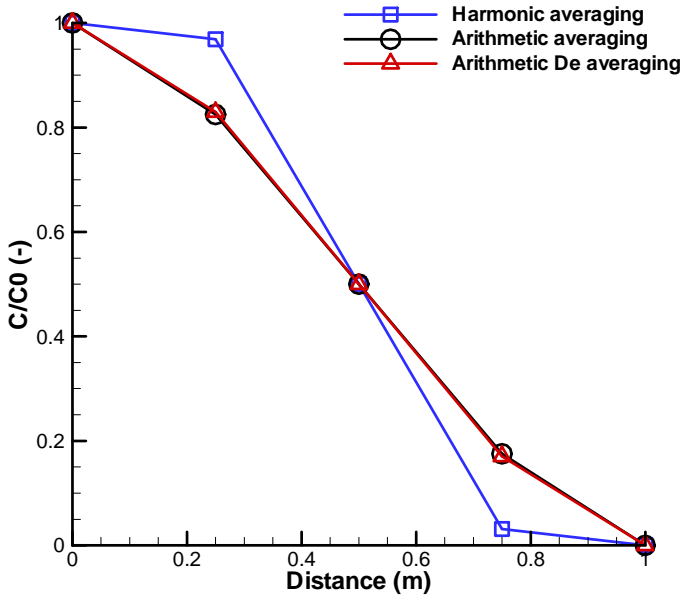


Figure 3.20: Comparison of simulated tracer concentration profiles by harmonic, arithmetic, and arithmetic De averaging methods

Simulated results indicate that the much lower porosity in Zone 2 causes sharper decrease of tracer concentration in the middle zone. This effect is even more apparent when the harmonic averaging method is used. The difference of the simulated results by both arithmetic averaging methods is very small and can be neglected with finer discretization. It is important to note that the simulated results in Figure 3.20 were obtained by using 5 control volumes only, so that the difference between different averaging methods can be easily recognized and can be compared with hand calculations. However, if the model is finer discretized, the difference will be reduced (Kadioglu et al., 2008).

3.4.3.6 File locations

The input file for the 1D steady-state diffusion using harmonic De averaging method can be found under

`.\benchmarks\benchmarks_standard\reactran\diff_harmonic\diffh_cc\diffh.dat`

The input file for the 1D steady-state diffusion using arithmetic averaging method can be found under

`.\benchmarks\benchmarks_standard\reactran\diff_harmonic\diff_h_cc_noHarm\diff.dat`

The input file for the 1D steady-state diffusion using arithmetic averaging method can be found under

`.\benchmarks\benchmarks_standard\reactran\diff_harmonic\diff_h_cc_de_ave\diff.dat`

Databases are the same and can be found under: `\benchmarks\database\default`

3.4.4 1D ADVECTIVE-DISPERSIVE TRANSPORT WITH TRANSIENT BOUNDARY CONDITIONS

3.4.4.1 Problem definition

This demonstration example is a one dimensional reactive transport problem with transient boundary conditions.

3.4.4.2 Model setup

A 1D model, 0.2 m in length is discretized into 141 control volumes yielding a discretization interval of 0.0014 m for the interior control volumes and 0.0007 m for the control volumes on the boundary. Transport simulations are conducted for steady-state saturated flow conditions. Boundary conditions for the flow problem are constant hydraulic heads of 0.0014 m at the inflow boundary and 0.0 m at the outflow boundary. The geochemical system includes two aqueous components (H^+ , CO_3^{2-}), 3 secondary aqueous species (OH^- , HCO_3^- , and $H_2CO_3(aq)$). The initial and boundary hydraulic and geochemical conditions are listed in Table 3.25. The concentrations of H^+ , CO_3^{2-} at the inflow boundary remain the same from 0.0 to 0.5 days with 2.0×10^{-2} mol L⁻¹ (H^+) and 1.0×10^{-2} mol L⁻¹ (CO_3^{2-}), after that, the concentrations at the boundary decrease to the initial concentrations (Table 3.25 and Figure 3.21 - upper panel).

Table 3.25: Initial & boundary hydraulic and reactive transport conditions for benchmark transrc

Parameter	Initial condition	Boundary conditions		Unit	
		inflow	outflow		
<i>Aqueous phase</i>		0 to 0.5 day	>0.5 day		
H^+	2.0×10^{-7}	2.0×10^{-2}	2.0×10^{-7}	(free exit)	[mol l ⁻¹]
CO_3^{2-}	1.0×10^{-7}	1.0×10^{-2}	1.0×10^{-7}		[mol l ⁻¹]
<i>Hydraulic condition</i>					
Hydraulic head	0.0	0.0014 (first)	0.0014 (first)	0.0 (first)	[m]

3.4.4.3 Parameters

The physical parameters (material properties) used for the simulations are summarized in Table 3.26.

Validation report-page# 3-186

Table 3.26: Physical parameters for demonstration example transrc

Parameter	Symbol	Value	Unit
Length of domain	L	0.20	[m]
Porosity	ϕ	0.35	[\cdot]
Hydraulic conductivity	K_{zz}	1.16×10^{-5}	[$m\ s^{-1}$]
Diffusion coefficient	De	0.0	[$m^2\ s^{-1}$]
Longitudinal dispersivity	α_l	0.0	[m]
Transverse horizontal dispersivity	α_t	0.0	[m]

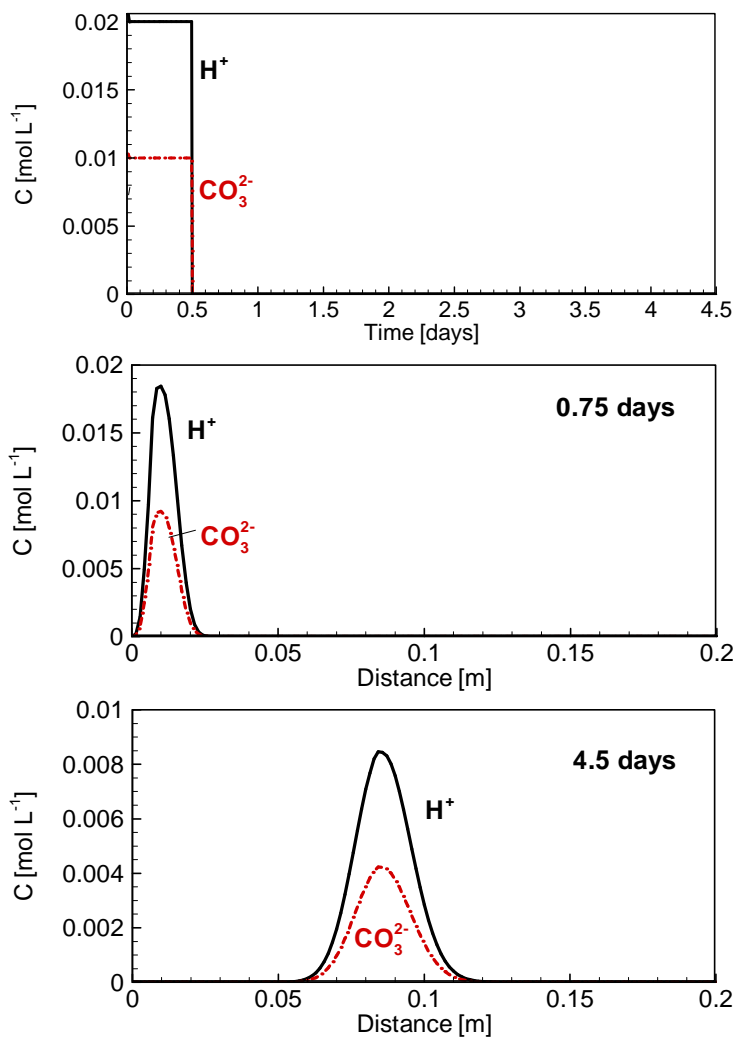


Figure 3.21: Transient boundary concentrations (upper panel), simulated concentration profiles of components H^+ and CO_3^{2-} at 0.75 days (middle panel) and 4.5 days (bottom panel) for benchmark *transrc*

3.4.4.4 Results

The simulated profiles at 0.75 and 4.5 days depicted the ingress of the high concentration pulse for both components Figure 3.21 (middle and lower panels).

3.4.4.5 File locations

The input file *transrc.dat* can be found in folder

.\benchmarks\benchmarks_standard\reactran\transrc

Database can be found under: *.\benchmarks\database\default*

3.4.5 1D ADVECTIVE-DISPERSIVE TRANSPORT WITH AQUEOUS COMPLEXATION AND MINERAL DISSOLUTION-PRECIPITATION

3.4.5.1 Problem definition

This application example demonstrates the use of MIN3P-THCm for simulating reactive transport including complexation and kinetically controlled dissolution-precipitation reaction of calcite.

3.4.5.2 Model setup

A 1D model, 0.4 m in length, is discretized into 81 control volumes, resulting in 79 inner control volumes with a length of 0.05 m and two half boundary control volumes with a length of 0.025 m. The initial concentration (IC) and boundary conditions (BC) for flow and mass transport are listed in Table 3.27. A solution with low pH enters from the left hand side. This solution causes the dissolution of calcite in the domain.

Table 3.27: Initial and boundary hydraulic and reactive transport conditions for demonstration example *dissol*

Parameter	Initial condition	Boundary conditions		Unit
<i>Aqueous phase</i>				
H ⁺	2.15400×10^{-4}	left	right	[mol l ⁻¹]
CO ₃ ²⁻	2.69512×10^{-4}	1.00×10^{-2}	(free exit)	[mol l ⁻¹]
Ca ²⁺	1.69512×10^{-4}	1.00×10^{-4}		[mol l ⁻¹]
<i>Mineral</i>				
Calcite	5.0×10^{-5}	-	-	[m ³ m ⁻³]
<i>Hydraulic condition</i>				
Hydraulic head	0.0	0.0014 (first)	0.0 (first)	[m]

3.4.5.3 Parameters

The parameters of the porous media are: porosity is 0.35, hydraulic conductivity is 1.16×10^{-5} m s⁻¹, longitudinal dispersivity is 0.005 m, and the diffusion coefficient is 0.0 m² s⁻¹. The kinetic reaction of calcite (i.e. ‘calcite-ch’ in database) is described by a model with three parallel reaction pathways as described in the user manual section “Surface-controlled rate expressions” (Chou et al. 1989). The update model for kinetic parameters is ‘geometric’ (see the user manual section “Initial condition – Batch reactions” sub section “mineral input”) and related parameters are listed in Table 3.28.

Table 3.28: Geometric update model parameters for calcite dissolution

Parameter	Symbol	Calcite-ch	Unit
Surface area	S	1.0	[m ² l ⁻¹ bulk]
Initial particle radius	r_i	1.5×10^{-4}	[m]
Particle radius	r_s	1.5×10^{-4}	[m]
Minimum particle radius	r_{min}	3.0×10^{-7}	[m]

3.4.5.4 Results

The simulated concentration profile after 6.0 days is shown in Figure 3.22. With the intrusion of the low pH solution from the left boundary, calcite dissolves and results in the increase of Ca²⁺, CO₃²⁻, CaHCO₃⁺ concentration in the solution.

3.4.5.5 File locations

The input file for this demonstration example can be found under:

`.\benchmarks\benchmarks_standard\reactran\dissol.dat`

Database can be found under: `.\benchmarks\database\default`

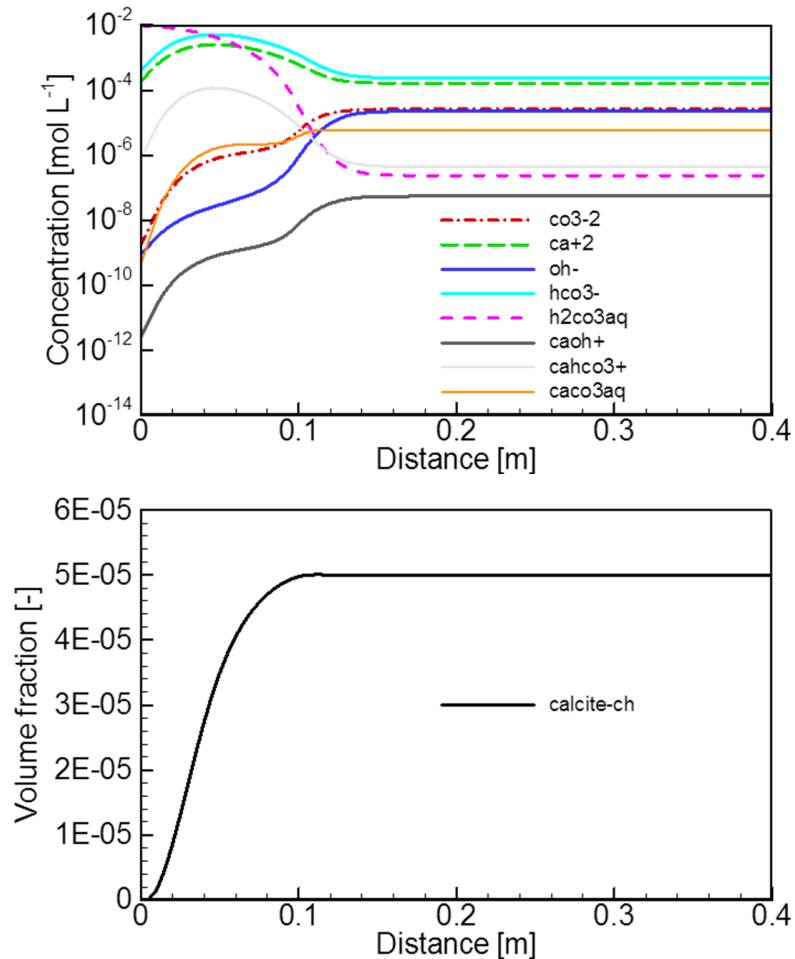


Figure 3.22: Profiles of aqueous species' concentrations (up) and mineral fraction of calcite at 6 days (down)

3.4.6 2D ADVECTIVE-DISPERSIVE TRANSPORT WITH AQUEOUS COMPLEXATION AND MINERAL DISSOLUTION-PRECIPITATION

3.4.6.1 Problem definition

This application example describes reactive transport including complexation and kinetically controlled dissolution- precipitation reaction of calcite for a 2D-system.

3.4.6.2 Model setup

The geometry, domain discretization and hydraulic conditions (IC, BC) are the same as for the corresponding 2D-example without mineral dissolution-precipitation (Figure 3.18). The primary species H⁺ and CO₃²⁻, the secondary species OH⁻, HCO₃⁻ and H₂CO₃(aq), and the mineral calcite are included in the geochemical system. The initial pore water

Validation report-page# 3-190

concentrations and mineral contents (IC) are shown in Table 3.29. A low pH solution flows into the domain from the bottom left (between $x=0.0$ to 0.02 m, $Z=0.0$ m) (Figure 3.18). The BC of chemical composition for the remainder of the bottom is set to be the same as that of IC. The reactive transport boundary on the top is set as a second (free exit) type BC.

Table 3.29 Initial and boundary conditions for flow and reactive transport – demonstration example *het_2d*

Parameter	Initial condition	Boundary conditions		Unit
<i>Aqueous phase</i>		Bottom left	Top	
H+	2.0×10^{-7}	2.0×10^{-4}		[mol l ⁻¹]
CO ₃ ²⁻	1.0×10^{-7}	1.0×10^{-4}	(free exit)	[mol l ⁻¹]
Ca ²⁺	1.0×10^{-8}	1.0×10^{-8}		[mol l ⁻¹]
<i>Mineral</i>				
Calcite	1.0×10^{-5}	-	-	[m ³ m ⁻³]
<i>Hydraulic condition</i>				
Hydraulic head	0.0	0.0014 (first)	0.0 (first)	[m]

3.4.6.3 Parameters

The parameters of the porous medium are: porosity is 0.35, hydraulic conductivity is 1.16×10^{-5} m s⁻¹, longitudinal dispersivity is 0.005 m, transverse dispersivity is 1.25×10^{-4} m, and the diffusion coefficient is 0.0 m² s⁻¹. The kinetic reaction of calcite (i.e. ‘calcite-ch’ in database) is described by a model with three parallel reaction pathways as described in the user manual section “Surface-controlled rate expressions” (Chou et al. 1989). The update model for kinetic parameters is ‘geometric’ (see the user manual section “Initial condition – Batch reactions” sub section “mineral input”) and related parameters are listed in Table 3.30.

Table 3.30: Geometric update model parameters for calcite for benchmark *het_2d*

Parameter	Symbol	Calcite-ch	Unit
Surface area	<i>S</i>	1.157×10^{-1}	[m ² l ⁻¹ bulk]
Initial particle radius	<i>r_i</i>	3.0×10^{-6}	[m]
Particle radius	<i>r_s</i>	3.0×10^{-6}	[m]
Minimum particle radius	<i>r_{min}</i>	3.0×10^{-7}	[m]

3.4.6.4 Results

The simulated contours of pH and calcite volume fractions at 10 days are shown in Figure 3.23. With the intrusion of the low pH solution at the bottom left corner, calcite dissolves (Figure 3.23 right) and results in the increase of Ca²⁺, CO₃²⁻, CaHCO₃⁺ concentration in the pore water solution, while pH decreases from 9.9 to 5.2 accordingly (Figure 3.23 left).

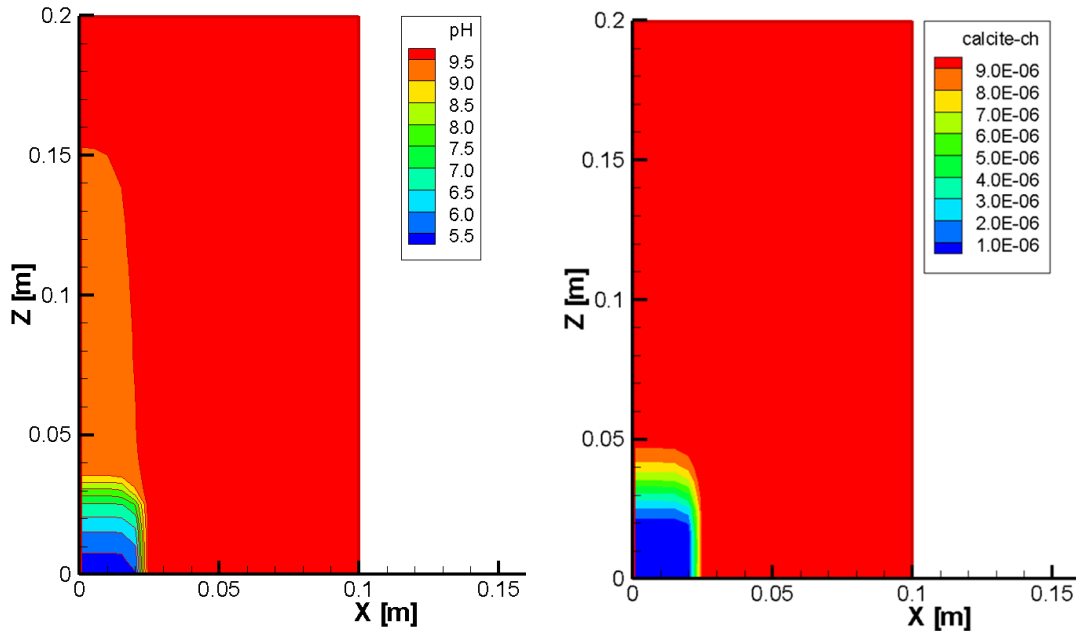


Figure 3.23: Simulated contours of pH (left) and calcite volume fraction (right) at 10 days

3.4.6.5 File locations

The input file for the demonstration example can be found under

`.\benchmarks\benchmarks_standard\reactran\het_2d\het-2d.dat`

Database can be found under: `.\benchmarks\database\default`

3.4.7 MINERAL WEATHERING IN A SOIL COLUMN

3.4.7.1 Problem definition

This demonstration example is a one-dimensional reactive transport problem with kinetically controlled mineral weathering at different rates.

3.4.7.2 Model setup

A 1D model with 0.4 m in length is discretized into 81 control volumes yielding a discretization interval of 0.005 m for the interior control volumes and 0.0025 m for the control volumes on the boundary. Steady-state saturated flow conditions are applied. A constant hydraulic head of 0.00014 m is specified at the inflow boundary and 0.0 m at the outflow boundary. The geochemical system includes six aqueous components (H^+ , Ca^{2+} , Na^+ , H_4SiO_4 , Al^{3+} , CO_3^{2-}), 14 secondary aqueous species (OH^- , HCO_3^- , $\text{H}_2\text{CO}_3(\text{aq})$, CaOH^+ , CaHCO_3^+ , $\text{CaCO}_3(\text{aq})$, $\text{H}_3\text{SiO}_4^{2-}$, NaCO_3^- , $\text{NaHCO}_3(\text{aq})$, Al(OH)^{2+} , Al(OH)_2^+ ,

Validation report-page# 3-192

$\text{Al(OH)}_3\text{(aq)}$ and Al(OH)_4^- , and two minerals (calcite and albite). The initial and boundary hydraulic and geochemical conditions are listed in Table 3.31. The chemical compositions of the initial solution are the same as those of the inflow solution with a pH of 5.6. This solution is, however, not in equilibrium with calcite and albite. The chemical initialization was calculated before the reactive transport at each control volumes. The calculated results show that the pH value of the initialized pore water solution is 9.5.

Table 3.31: Initial and boundary conditions for flow and reactive transport for demonstration example *weather*

Parameter	Initial condition	Boundary conditions		Unit
<i>Aqueous phase</i>				
Ca^{2+}	1.60×10^{-5}	top	bottom	$[\text{mol l}^{-1}]$
Na^+	1.30×10^{-5}	1.30×10^{-5}		$[\text{mol l}^{-1}]$
CO_3^{2-}	2.10×10^{-5}	2.10×10^{-5}	(free exit)	$[\text{mol l}^{-1}]$
H_4SiO_4	1.00×10^{-10}	1.00×10^{-10}		$[\text{mol l}^{-1}]$
Al^{3+}	1.00×10^{-10}	1.00×10^{-10}		$[\text{mol l}^{-1}]$
H^+	4.14×10^{-5}	4.14×10^{-5}		$[\text{mol l}^{-1}]$
<i>Mineral</i>				
Calcite	5.00×10^{-5}	-	-	$[\text{m}^3 \text{ m}^{-3}]$
Albite	5.00×10^{-3}	-	-	$[\text{m}^3 \text{ m}^{-3}]$
<i>Hydraulic condition</i>				
Hydraulic head	0.0	0.00014 (first)	0.0 (first)	[m]

3.4.7.3 Parameters

The physical parameters (material properties) for the simulations are summarized in Table 3.32.

Table 3.32: Physical parameters for benchmark transrc

Parameter	Symbol	Value	Unit
Length of domain	L	0.40	[m]
Porosity	ϕ	0.35	[\cdot]
Hydraulic conductivity	K_{zz}	1.16×10^{-5}	$[\text{m s}^{-1}]$
Diffusion coefficient	D_0^a	0.0	$[\text{m}^2 \text{ s}^{-1}]$
Longitudinal dispersivity	α_l	0.0025	[m]
Transverse horizontal dispersivity	α_t	0.0	[m]

The update model used for the simulation is the geometric model. Related parameters are listed in Table 3.33. The pH-dependent kinetic reaction of albite is described by a model with two parallel reaction pathways (corresponding to albite-ph_1 and albite-ph_2 with

Validation report-page# 3-193

different kinetic rates) as described in the user manual section “Minerla dissolution-precipitation reactions” (Wollast and Chou 1985).

Table 3.33: Geometric update model parameters for calcite and albite

Parameter	Symbol	Calcite	Albite	Unit
Surface area	S	1.157×10^{-6}	1.0×10^{-1}	[m ² l ⁻¹ bulk]
Initial particle radius	r_i	1.5×10^{-6}	3.0×10^{-6}	[m]
Particle radius	r_s	1.5×10^{-6}	3.0×10^{-6}	[m]
Minimum particle radius	r_{min}	3.0×10^{-7}	3.0×10^{-7}	[m]

3.4.7.4 Results

Due to the infiltration of the low pH solution from the top, calcite dissolves at a high rate (Figure 3.24 bottom left and right). The dissolution rate of albite increases under more alkaline conditions. As the dissolution rates of albite are low, the depletion of the total amount of albite is insignificant for the simulation period (Figure 3.24 bottom left). However, the changes of related dissolved components such as Na⁺, Al³⁺ and H₄SiO₄ are significant (Figure 3.24 top right).

3.4.7.5 File locations

The input file is: *weather.dat* under folder

.\\benchmarks\\benchmarks_standard\\reactran\\weather

Database can be found under: *.\\benchmarks\\database\\default*

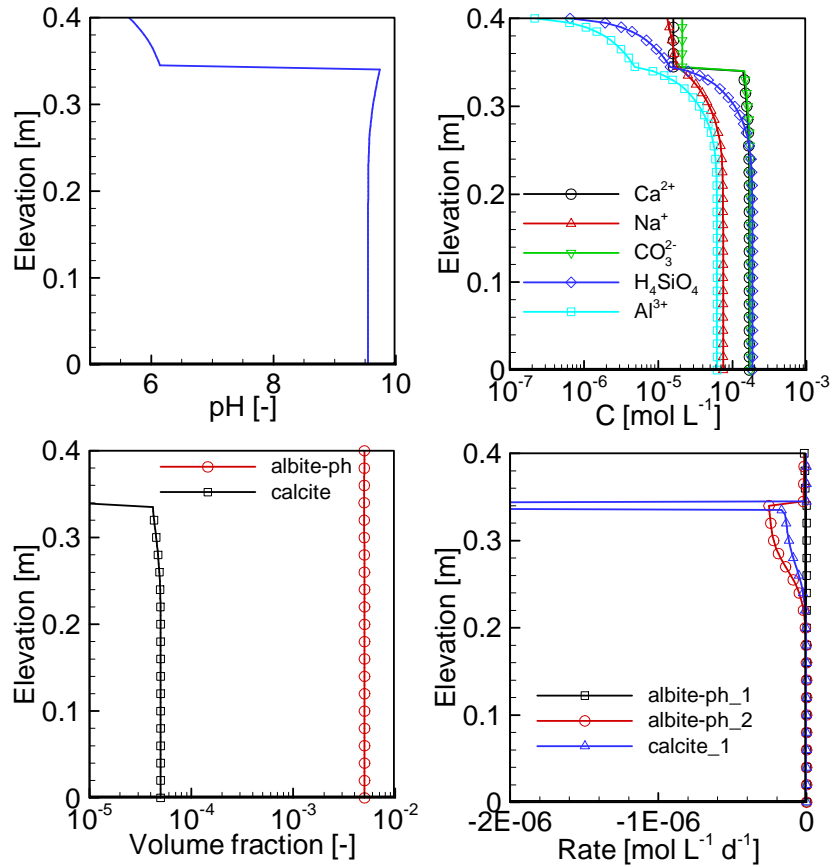


Figure 3.24: Simulated profiles of pH (top left), concentrations of selected components (top right), mineral volume fractions (bottom left) and dissolution rates (bottom right) for the demonstration example weather at 5.0 years

3.4.8 1D ADVECTIVE-DISPERSIVE TRANSPORT WITH BINARY MONOVALENT ION EXCHANGE

3.4.8.1 Problem definition

This demonstration example is designed to simulate 1D advective and dispersive mass transport in saturated porous media affected by homovalent ion exchange processes.

3.4.8.2 Model setup

A 1D model, 30.0 m in length, is discretized into 101 control volumes, in which the first and the last are half control volumes. The hydraulic head on the left boundary is constant at 30.0 m, while the hydraulic head on the right border is constant at 0.0 m. The infiltration of a Na-bearing-solution leads to the displacement of exchangeable K-X. The initial condition (IC) of the pore water and the chemical composition at the inflow boundary (BC)

are listed in Table 3.34.

Table 3.34: Initial and boundary conditions of solutions for demonstration example *ion-binary*

Parameter	Initial condition	Boundary condition	Unit
Na^+	20.0	9.5	$[\text{mg L}^{-1}]$
K^+	80.0	0.5	$[\text{mg L}^{-1}]$

3.4.8.3 Parameters

The parameters of the porous medium are: porosity is 0.50, hydraulic conductivity is $5.125 \times 10^{-5} \text{ m s}^{-1}$, the diffusion coefficient is $1.0 \times 10^{-9} \text{ m}^2 \text{ s}^{-1}$, longitudinal dispersivity is 0.187 m, dry bulk density is 1.325 g/cm^3 and the cation exchange capacity (CEC) is 0.45 meq/100 g solid.

3.4.8.4 Results

Simulated results are shown in Figure 3.25. The initial concentrations of components Na^+ and K^+ in the pore water of the domain are much higher than those in the inflow boundary solution; however, the ratio of Na/K is higher in the inflow solution than in the background water, leading to the displacement of K by Na (Figure 3.25).

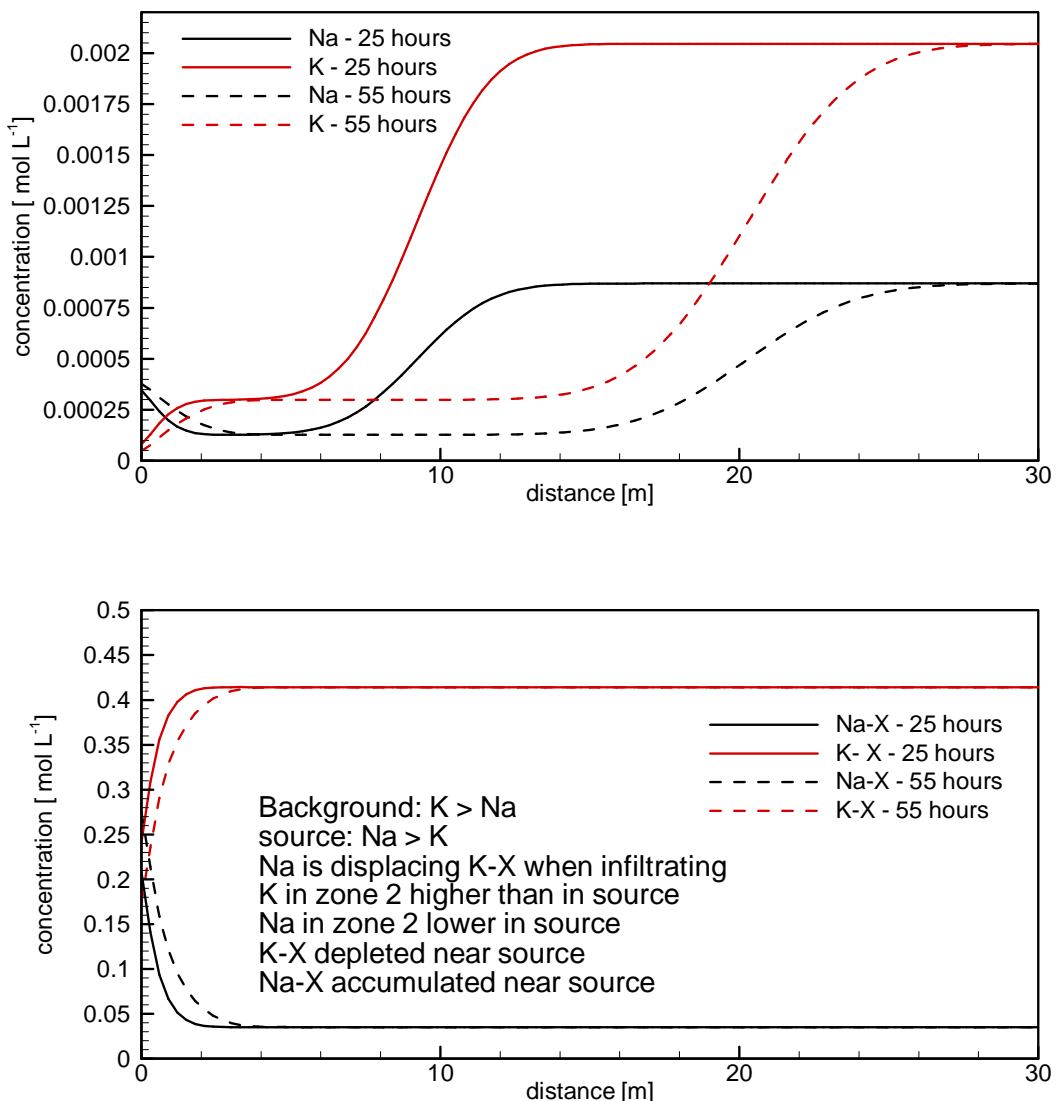


Figure 3.25: Simulated spatial profiles of total aqueous component concentrations (upper panel) and ion exchanged species (lower panel) at 25 hours (solid lines) and at 55 hours (dashed lines)

3.4.8.5 File locations

The input file is: *binary.dat* under folder
 .\benchmarks\benchmarks_standard\reactran\ion-binary
 Database can be found under: .\benchmarks\database\default

3.4.9 1D ADVECTIVE-DISPERSIVE TRANSPORT INCLUDING MONOD KINETICS, DEGRADATION OF ORGANIC CONTAMINANTS

3.4.9.1 Problem definition

This application example demonstrates the use of intra-aqueous and heterogeneous kinetic redox reactions based on the Monod equations for the degradation of organic contaminants through aerobic and anaerobic degradation processes.

3.4.9.2 Model setup

A 1D model, 1.0 m in length, is discretized into 41 control volumes. The domain is homogeneous. The hydraulic head on the left boundary is constant at 1.0 m, while the hydraulic head on the right boundary is constant at 0.0 m. The initial condition (IC) of the pore water and minerals, and the aqueous concentrations at the boundary (BC) are listed in Table 3.35.

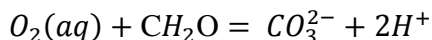
Table 3.35: Initial and boundary conditions for aqueous solutions and minerals for demonstration example *comptran*

Parameter	Initial Condition	Boundary Condition	Unit
<i>Aqueous phase</i>			
CH ₂ O	1.0×10 ⁻⁷	3.1×10 ⁻³	[mol l ⁻¹]
O ₂ (aq)	2.5×10 ⁻⁴	2.5×10 ⁻⁴	[mol l ⁻¹]
NO ₃ ⁻	1.0×10 ⁻⁷	2.3×10 ⁻⁴	[mol l ⁻¹]
Fe ²⁺	1.0×10 ⁻⁷	1.0×10 ⁻⁷	[mol l ⁻¹]
Mn ²⁺	1.0×10 ⁻⁷	1.0×10 ⁻⁷	[mol l ⁻¹]
N ₂ (aq)	1.0×10 ⁻⁷	1.0×10 ⁻⁷	[mol l ⁻¹]
CO ₃ ²⁻	5.0×10 ⁻⁴	5.0×10 ⁻⁴	[mol l ⁻¹]
H ⁺	5.51	5.51	pH
<i>minerals</i>			
Fe(OH) ₃	7.92×10 ⁻⁶	-	[m ³ m ⁻³]
MnO ₂	6.04×10 ⁻⁸	-	[m ³ m ⁻³]

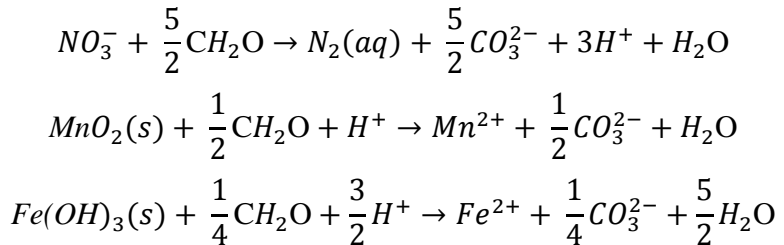
3.4.9.3 Parameters

The parameters of the porous medium are: porosity is 0.30, hydraulic conductivity is 8.68×10⁻¹⁰ [m s⁻¹], longitudinal dispersivity is 0.025 m. The geochemical reactions for the aerobic degradation of the organic contaminant and contaminant degradation coupled with denitrification are provided in the database redox.dbs based on Abrams et al. (1998). Effective rate coefficients for both reactions are 1.46×10⁻¹¹.mol l⁻¹ H₂O s⁻¹. The parameters for the surface-controlled reductive dissolution of the mineral phases FeOH₃ and MnO₂ are provided in the input file.

The main reactions considered in the simulation are:



Validation report-page# 3-198



3.4.9.4 Results

Simulated results are depicted in Figure 3.26 and Figure 3.27. Due to the infiltration of the organic substance CH₂O from the left boundary, aerobic degradation is initiated. The consumption of O₂(aq) and production of CO₃²⁻ results in the decrease of O₂(aq) and pH in the solution. At the same time, NO₃⁻ in the infiltrating solution reacts with the organic substance CH₂O, which results in additional increase of CO₃²⁻ and lowering of pH. Further intrusion of CH₂O reductively dissolves MnO₂(s) and Fe(OH)₃(s). Consequently, the concentration of Fe²⁺ and Mn²⁺, and the pH increase.

3.4.9.5 File locations

The input file is: *comptran.dat* under folder

.|benchmarks\benchmarks_standard\reactran\comptran

Database can be found under: *.|benchmarks\database\default*

Validation report-page# 3-199

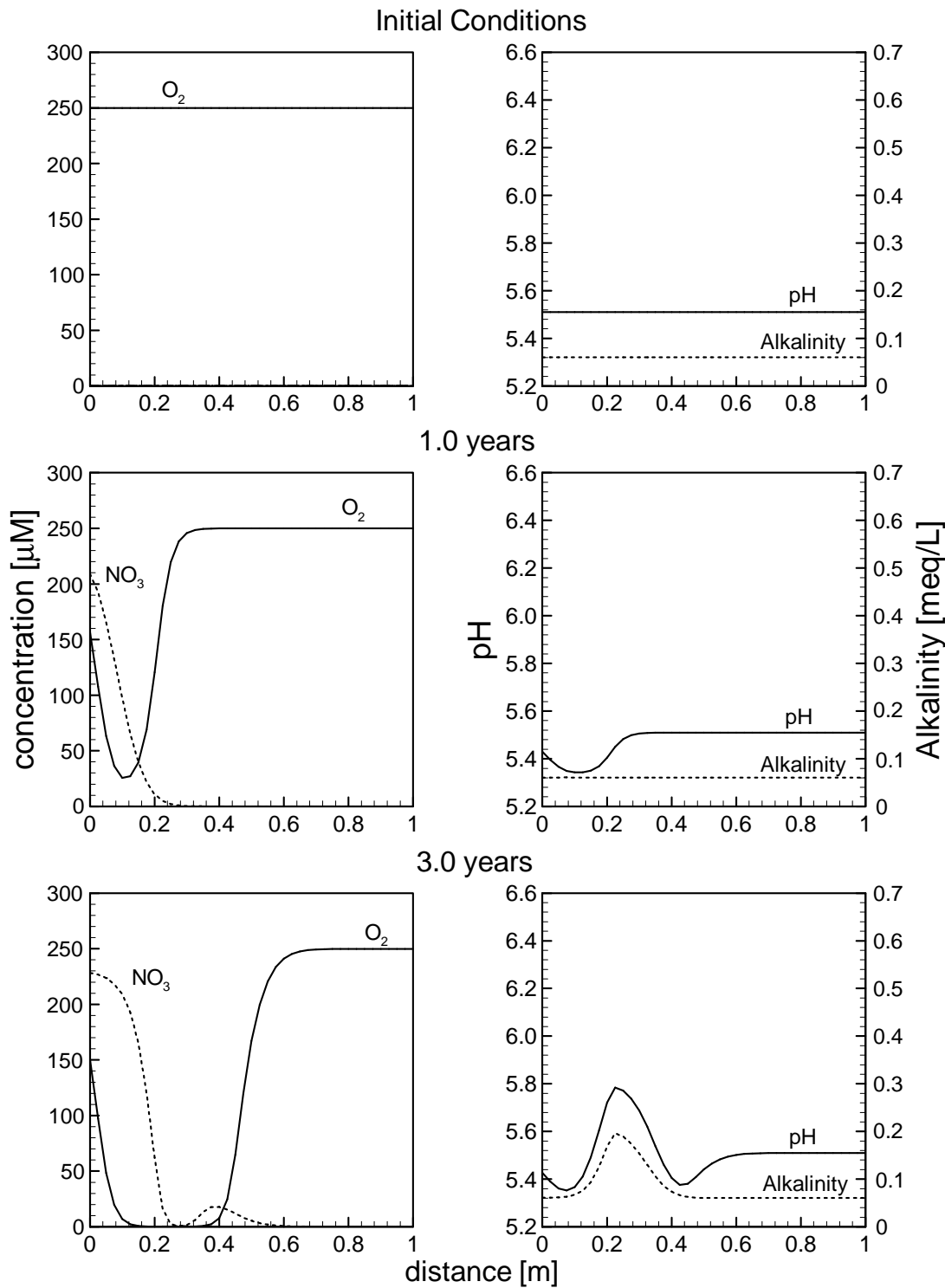


Figure 3.26: Spatial profiles of $O_2(\text{aq})$, NO_3^- , $\text{Fe}(\text{II})$, $\text{Mn}(\text{II})$ (left), and pH , alkalinity (right) at 0.0 years, 1.0 year, 3.0 years for demonstration example *comptran*

Validation report-page# 3-200

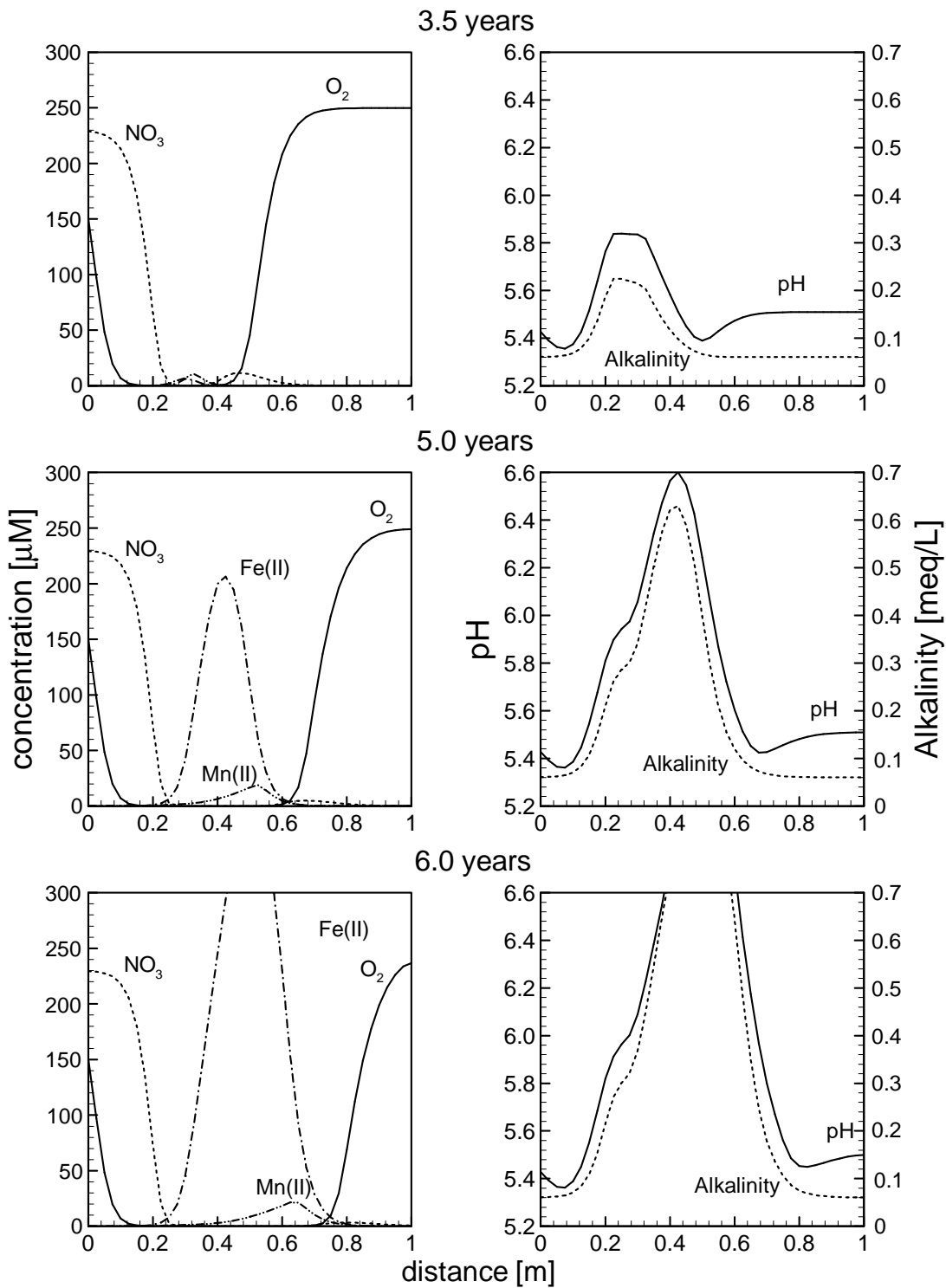


Figure 3.27: Spatial profiles of $\text{O}_2(\text{aq})$, NO_3^- , $\text{Fe}(\text{II})$, $\text{Mn}(\text{II})$ (left), and pH, alkalinity (right) at 3.5 years, 5.0 years, and 6.0 years for demonstration example comprtran

Validation report-page# 3-201

3.4.10 1D ADVECTIVE-DISPERSIVE TRANSPORT - DEGASSING FROM A HYDROCARBON SPILL

3.4.10.1 Problem definition

This application example demonstrates the simulation of gas release induced by biodegradation processes during reactive transport of organic contaminants. Processes affecting gas generation are aerobic degradation, denitrification and fermentation simulated as intra-aqueous kinetic reactions (see the theory manual section “Intra-aqueous kinetic reactions”). Consequently, the produced gases cause an increase in gas pressures in the subsurface. If the total gas pressure exceeds the hydrodynamic pressure, gas will tend to exsolve and degas.

3.4.10.2 Model setup

A 1D model, 300 m in length, is discretized into 3 zones: 0.0 – 10.0m (Zone 1), 10-15.0 m (Zone 2) and 15.0 – 300.0 m (Zone 3). The domain is homogeneous in terms of physical parameters. The hydraulic head at the inflow boundary is constant at 2.1 m, while the hydraulic head at the outflow boundary is constant at 0.3 m. The initial condition (IC) of the pore water concentrations and mineral contents, and the inflow boundary condition (BC) are listed in Table 3.36. The only difference of the three zones lies in the initial concentration of an organic contaminant, here described as benzene (C_6H_6) present as a immobile NAPL phase, which exists only in Zone 2 with a volume fraction of $0.01\text{ m}^3\text{ m}^{-3}$.

Table 3.36: Initial and boundary conditions (IC & BC) for solutions and minerals

Parameter	Initial Condition	Boundary Condition	Unit
<i>Aqueous phase</i>	Zone1 & 3	Zone2	
C_6H_6	1.0×10^{-10}	1.0×10^{-10}	$[\text{mg l}^{-1}]$
$O_2(\text{aq})$	0.21	0.21	$pO_2 [\text{atm}]$
NO_3^-	10.0	10.0	$[\text{mg l}^{-1}]$
$CH_4(\text{aq})$	1.0×10^{-10}	1.0×10^{-10}	$[\text{mg l}^{-1}]$
$N_2(\text{aq})$	0.79	0.79	$pN_2 (\text{atm})$
CO_3^-	373.8	373.8	$[\text{mg l}^{-1}]$
H^+	7.2	7.2	pH
<i>NAPL phase</i>			
$C_6H_6(n)$	0.0	0.01	$[\text{m}^3\text{ m}^{-3}]$

3.4.10.3 Parameters

The parameters of the porous media are: porosity is 0.30, hydraulic conductivity is $5.8 \times 10^{-5}\text{ m s}^{-1}$. The rate constant for the degassing of exsolved gas is $1.0 \times 10^{-8}\text{ mol l}^{-1}\text{ H}_2\text{O s}^{-1}$.

The NAPL dissolution of $C_6H_6(n)$ can be expressed analogous to a mineral dissolution-precipitation reaction:

Validation report-page# 3-202



The initial rate constant is set to $1.0 \times 10^{-7} \text{ mol l}^{-1} \text{ bulk s}^{-1}$.

The intra-aqueous kinetic reactions and the effective rate coefficients are listed in Table 3.37. The reaction C6H6-O2 represents the aerobic degradation, C6H6-NO3 defined contaminant degradation via denitrification and C6H6-CH4 is related to fermentation and methanogenesis of the contaminant. Monod-kinetics parameters are defined in database redox.dbs.

Table 3.37: Intra-aqueous kinetic reactions and effective ate coefficients for benchmark *degassing*

Name	Reaction	Effective rate coefficient [mol l ⁻¹ H ₂ O s ⁻¹]	Inhibiting species
C6H6-O2	$\text{C}_6\text{H}_6 + 7.5\text{O}_2(\text{aq}) \rightarrow 6\text{CO}_3^{2-} + 12\text{H}^+$	1.0×10^{-9}	-
C6H6-NO3	$\text{C}_6\text{H}_6 + 6\text{NO}_3^- \rightarrow 6\text{CO}_3^{2-} + 6\text{H}^+ + 3\text{N}_2(\text{aq})$	1.0×10^{-10}	O ₂ (aq)
C6H6-CH4	$\text{C}_6\text{H}_6 + 6.75\text{H}_2\text{O} \rightarrow 2.25\text{CO}_3^{2-} + 4.5\text{H}^+ + 3.75\text{CH}_4(\text{aq})$	1.0×10^{-11}	O ₂ (aq), NO ₃ ⁻

3.4.10.4 Results

Simulated profiles at 3.0 years are shown in Figure 3.28. C₆H₆ is degraded through aerobic degradation, denitrification and fermentation and results in the consumption of O₂(g), and NO₃⁻, and the production of N₂(g), CH₄(g) and CO₂(g), associated with a decrease of pH in Zone 2 and in the downgradient region. Total dissolved gas pressures become elevated in regions where active C₆H₆ degradation takes place, resulting in gas exsolution and degassing. The degassing rates of individual gases are depicted in Figure 3.28c. The C₆H₆ degradation rates by aerobic degradation, denitrification and fermentation are depicted in Figure 3.28d. The highest degradation rates for both aerobic degradation and denitrification processes are at x = 11.25 m near the inflow boundary (Figure 3.28d). This is due to the continuous supply of O₂(g) and NO₃⁻ through advective and diffusive transport. The degradation rate by fermentation and methanogenesis depends on the concentration of dissolved C₆H₆.

3.4.10.5 File locations

The input file is: *degas.dat* under folder:

.\benchmarks\benchmarks_standard\reactran\degas

Database can be found under: .\benchmarks\database\default

Validation report-page# 3-203

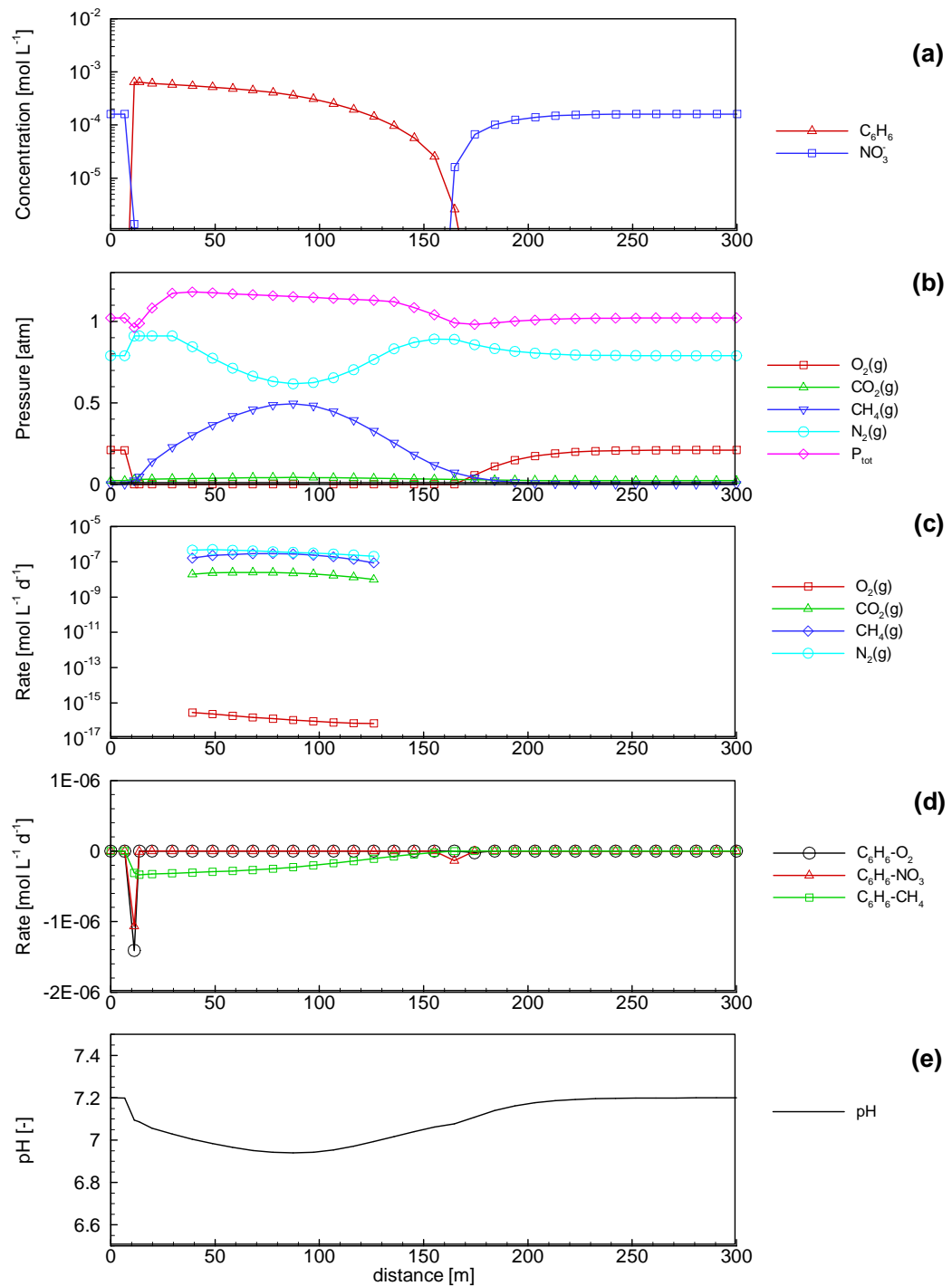


Figure 3.28: Profiles of simulated aqueous component concentration (a), gas partial pressure (b), degassing rate (c), degradation rates of organic contaminant (d) and pH (e) at 3 years

3.4.11 DISSOLUTION AND VOLATILIZATION OF AN ORGANIC CONTAMINANT MIXTURE IN THE VADOSE ZONE

3.4.11.1 Problem definition

This demonstration example is a one-dimensional problem simulating the dissolution and volatilization from an organic contaminant mixture in unsaturated porous media. The organic contaminants considered are PCE, MTBE, pentane, iso-octane, toluene and 1,3,5-TMB. The dissolution reactions are assumed to be reversible reaction and solubility follow Raoult's law.

3.4.11.2 Model setup

A 1D model, 0.58 m in depth, is discretized into 59 control volumes yielding a discretization interval of 0.01 m for the interior control volumes and 0.005 m for the control volumes on the boundary. Steady-state unsaturated flow conditions are assumed. Boundary conditions are constant hydraulic heads of -0.34 m at the top and 0.24 m at the bottom boundaries, implying a no flow condition. It is assumed that all organic contaminants can exist in aqueous, gaseous and the mixed NAPL phase without any degradation; and chemical reactions do not occur. The initial and boundary conditions for flow and reactive transport are listed in Table 3.38. The organic contaminants initially exist in the domain at a depth from 0.24 m to 0.243 m (corresponding to z=0.337 to 0.34 m in the input file).

Table 3.38: Initial and boundary conditions for flow and reactive transport – demonstration example raoult

Parameter	Initial condition	Boundary conditions		Unit
<i>Aqueous phase</i>				
PCE	1.0×10^{-10}	top	bottom	[mol l ⁻¹]
MTBE	1.0×10^{-10}	1.0×10^{-10}		[mol l ⁻¹]
Pentane	1.0×10^{-10}	1.0×10^{-10}	(free exit)	[mol l ⁻¹]
iso-octane	1.0×10^{-10}	1.0×10^{-10}		[mol l ⁻¹]
Toluene	1.0×10^{-10}	1.0×10^{-10}		[mol l ⁻¹]
1,3,5-TMB	1.0×10^{-10}	1.0×10^{-10}		[mol l ⁻¹]
<i>NAPL mixture</i>				
PCE	0.25	-	-	[m ³ m ⁻³]
MTBE	0.125	-	-	[m ³ m ⁻³]
Pentane	0.125	-	-	[m ³ m ⁻³]
iso-octane	0.05	-	-	[m ³ m ⁻³]
Toluene	0.25	-	-	[m ³ m ⁻³]
1,3,5-TMB	0.2	-	-	[m ³ m ⁻³]
<i>Hydraulic condition</i>				
Hydraulic head	0.24	-0.34 (first)	0.24 (first)	[m]

3.4.11.3 Parameters

The physical parameters (material properties) used for the simulation are summarized in Table 3.39.

Table 3.39: Physical parameters for demonstration example raoult

Parameter	Symbol	Value	Unit
Length of domain	L	0.58	[m]
Porosity	ϕ	0.287	[-]
Hydraulic conductivity	K_{zz}	1.21×10^{-3}	[m s ⁻¹]
Residual saturation	S_{ra}	0.125	[-]
Van Genuchten parameter α	α	20.0	[m ⁻¹]
Van Genuchten parameter n	n	5.0	[-]
Diffusion coefficient, aqueous	D_0^a	8.0×10^{-10}	[m ⁻² s ⁻¹]
Diffusion coefficient, gas	D_0^g	7.3×10^{-6}	[m ⁻² s ⁻¹]
longitudinal dispersivity	α_l	0.001	[m]

3.4.11.4 Results

Simulated results show that the domain below a depth of 0.33 remains saturated (Figure 3.29 – right panel). All organic contaminants initially exist just below the saturated line in the NAPL mixture. The contaminants dissolve and then volatilize. Volatilized organic contaminants migrate upwards by diffusion. At 50 years, the profiles of gas partial pressures of all organic contaminants and of the total gas pressure are depicted in Figure 3.29 (left panel). Figure 3.30 shows the temporal evolution of the NAPL mixture following Raoult's law.

3.4.11.5 File locations

The input file is: *raoult.dat* under folder:

.\benchmarks\benchmarks_standard\reactran\raoult

Database can be found under: .\benchmarks\database\ organic

Validation report-page# 3-206

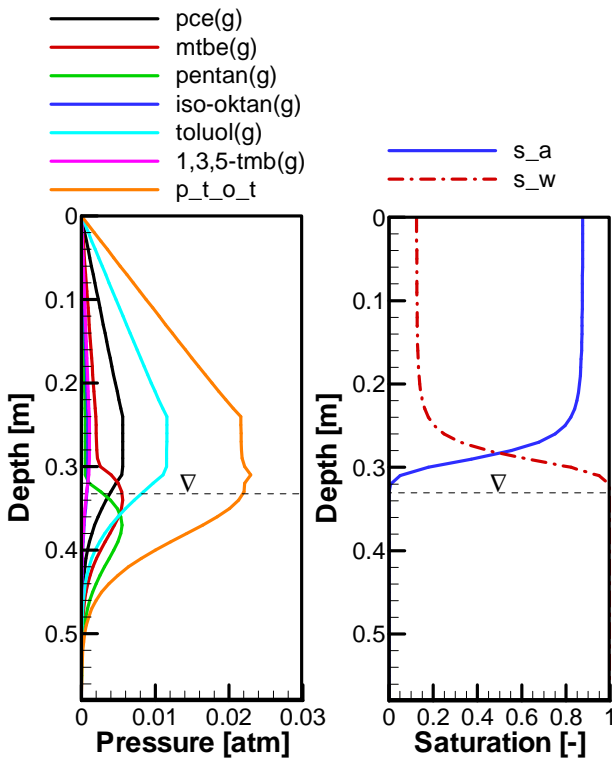


Figure 3.29: Simulated spatial profiles of partial pressures of the six organic contaminants and total gas pressures (p_{tot}) at 50 days (left), and saturation profiles of gas (S_g) and aqueous (S_a) phases at steady state (right)

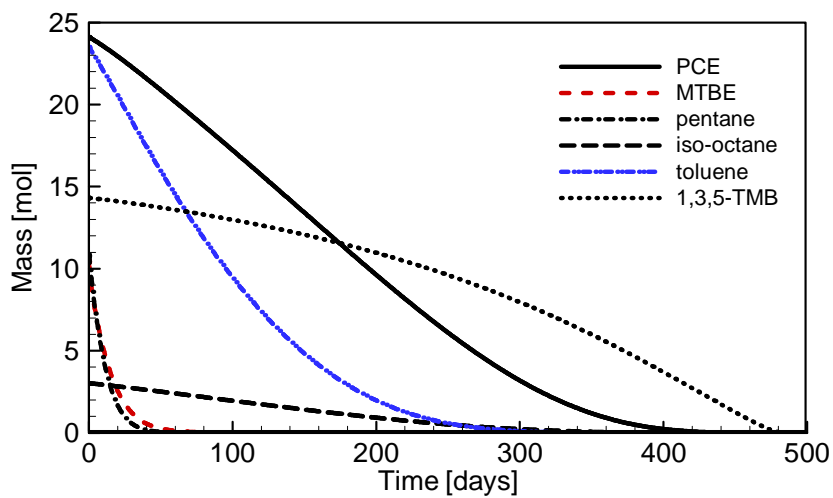


Figure 3.30: Simulated system mass evolution of the six organic components in the NAPL mixture

3.4.12 1D-ADVECTIVE-DISPERSIVE TRANSPORT WITH ANIONIC SURFACE COMPLEXATION REACTIONS

3.4.12.1 Problem definition

This demonstration example is a one-dimensional advective-dispersive reactive transport problem considering surface complexation in saturated porous media. This example simulates adsorption of a ligand (A^-) to a hydrous oxide using a non-electrostatic surface complexation model. The reaction parameters are based on Example 9.3b (page 545) in Stumm and Morgan (1996). The surface complexation reactions are highly pH dependent.

3.4.12.2 Model setup

A 1D model, 16.0 m in length, is discretized into 101 control volumes yielding a discretization interval of 0.16 m for the interior control volumes and 0.08 m for the control volumes on the boundary. Boundary conditions are constant hydraulic heads of 1.4 m at the inflow boundary and 0.0 m at the outflow boundary. The geochemical system includes three aqueous components (H^+ , HA and Na^+), one non-aqueous component ‘=SOH’, two secondary aqueous species (OH^- , A^-) and three surface-complexed species ($=SOH_2^+$, $=SO^-$ and $=SA$). The initial and boundary conditions for the flow and reactive transport problem are listed in Table 3.40.

Table 3.40: Initial and boundary conditions for flow and reactive transport – demonstration example - benchmark surfa2

Parameter	Initial condition	Boundary conditions		Unit
<i>Aqueous phase</i>		inflow	outflow	
H^+	6.0	2.0		pH
HA	1.0×10^{-7}	1.0×10^{-3}	(free exit)	[mol l ⁻¹]
Na^+	1.0×10^{-7}	1.0×10^{-3}		[mol l ⁻¹]
<i>Hydraulic condition</i>				
Hydraulic head	0.0	1.4 (first)	0.0 (first)	[m]

Table 3.41: Physical parameters for benchmark surfa2

Parameter	Symbol	Value	Unit
Length of domain	L	16.0	[m]
Porosity	ϕ	0.25	[-]
Hydraulic conductivity	K_{zz}	1.0×10^{-3}	[m s ⁻¹]
Diffusion coefficient	D_0^a	1.0×10^{-9}	[m ² s ⁻¹]
Longitudinal dispersivity	α_l	0.05	[m]
Mass of surface site ‘=SOH’	M	1.0	[g solid L ⁻¹ H ₂ O]
Surface area of ‘=SOH’	S	10.0	[m ² g ⁻¹ solid]
Site density	D	6.02228	[sites nm ⁻²]

3.4.12.3 Parameters

The physical parameters (material properties) and the parameters for the surface complexation reactions used for the simulations are summarized in Table 3.41.

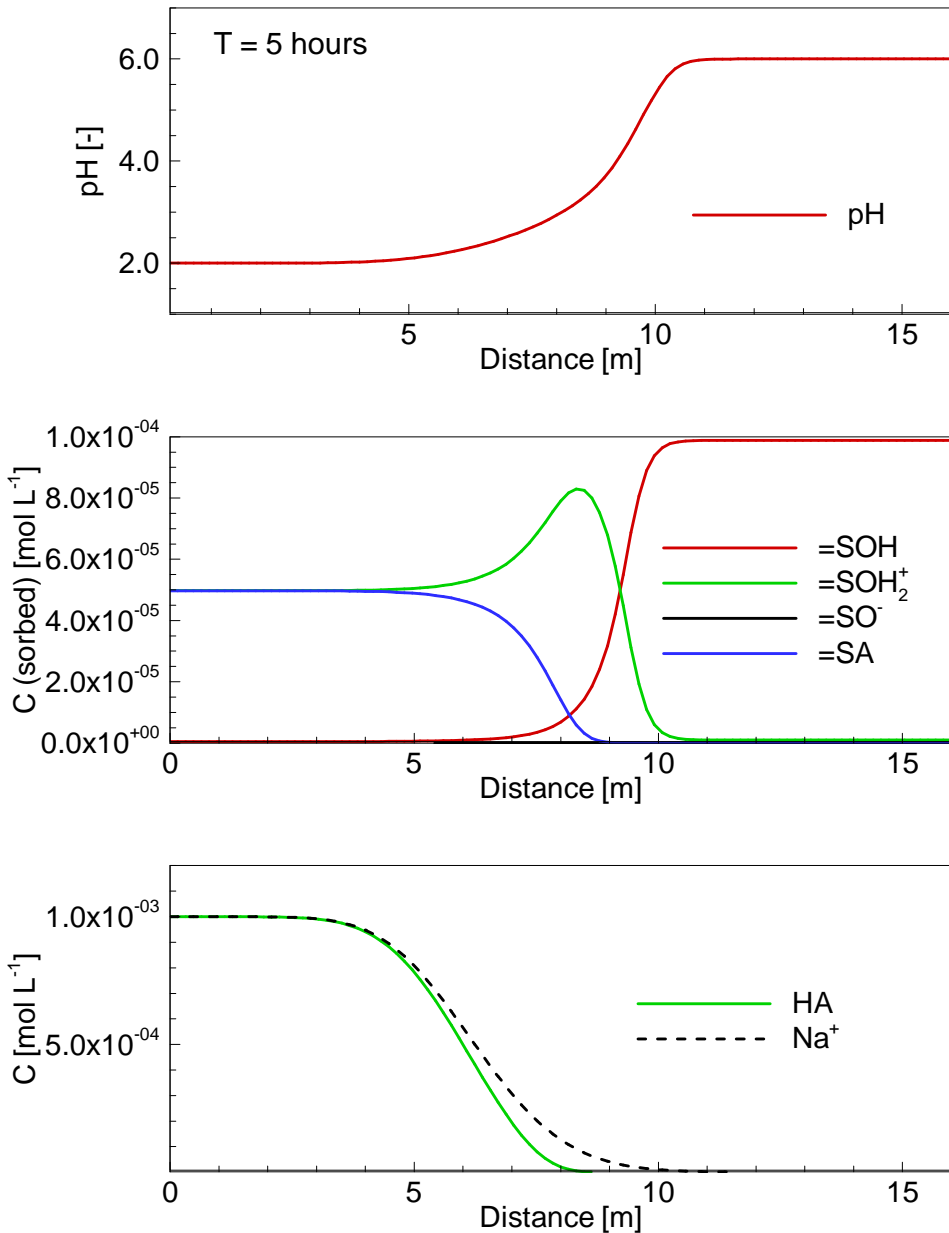


Figure 3.31: Simulated spatial profiles of pH (upper panel), concentrations of sorbed species (middle panel) and total aqueous component concentrations (lower panel) at 5 hours for demonstration example surfa2

3.4.12.4 Results

Simulated profiles of pH, sorbed species and total aqueous component concentrations at 5 hours are depicted in Figure 3.31. The results show that the infiltrating low-pH solution ($\text{pH}=2$) replaces the initial solution with $\text{pH}=6.0$ (Figure 3.31 upper panel). Because surface complexation reactions are pH-dependent, as described in the chemical batch reactions (see section 2.1.2), the concentration of the initially dominating sorbed species $=\text{SOH}$ decreases and the concentrations of $=\text{SOH}_2^+$ and $=\text{SA}$ increase. In comparison to Na^+ , which is not participating in surface complexation reactions, the component HA is lightly attenuated, owing to the sorption effect (Figure 3.31 bottom).

3.4.12.5 File locations

The input file is: *surfa2.dat* under folder:

.\benchmarks\benchmarks_standard\reactran\surfa2

Database can be found under: *.\benchmarks\database\surftest*

3.4.13 1D-ADVECTIVE-DISPERSIVE TRANSPORT WITH CATIONIC SURFACE COMPLEXATION REACTIONS

3.4.13.1 Problem definition

This demonstration example is a one-dimensional advective-dispersive reactive transport problem considering surface complexation in saturated porous media. This example simulates adsorption of a metal (Me^{2+}) to a hydrous oxide using a non-electrostatic surface complexation model. The reaction parameters are based on Example 9.3a (page 545) in Stumm and Morgan (1996). The surface complexation reactions are highly pH dependent.

3.4.13.2 Model setup

A 1D model, 16.0 m in length, is discretized into 101 control volumes yielding a discretization interval of 0.16 m for the interior control volumes and 0.08 m for the control volumes on the boundary. Boundary conditions are constant hydraulic heads of 1.4 m at the inflow boundary and 0.0 m at the outflow boundary.

Table 3.42: Initial and boundary conditions for flow and reactive transport – demonstration example surfme2

Parameter	Initial condition	Boundary conditions		Unit
<i>Aqueous phase</i>		inflow	outflow	
H^+	10.0	4.0		pH
Me^{2+}	1.0×10^{-7}	1.0×10^{-5}	(free exit)	[mol l ⁻¹]
Cl^-	1.0×10^{-10}	2.0×10^{-5}		[mol l ⁻¹]
<i>Hydraulic condition</i>				
Hydraulic head	0.0	1.4 (first)	0.0 (first)	[m]

The geochemical system includes three aqueous components (H^+ , Me^{2+} and Cl^-), one non-

Validation report-page# 3-210

aqueous component ‘=SOH’ as the sorption surface, one secondary aqueous species (OH^-) and three sorbed species ($=\text{SOH}_2^+$, $=\text{SO}^-$ and $=\text{SOMe}^+$). The initial and boundary hydraulic and geochemical conditions are listed in Table 3.42.

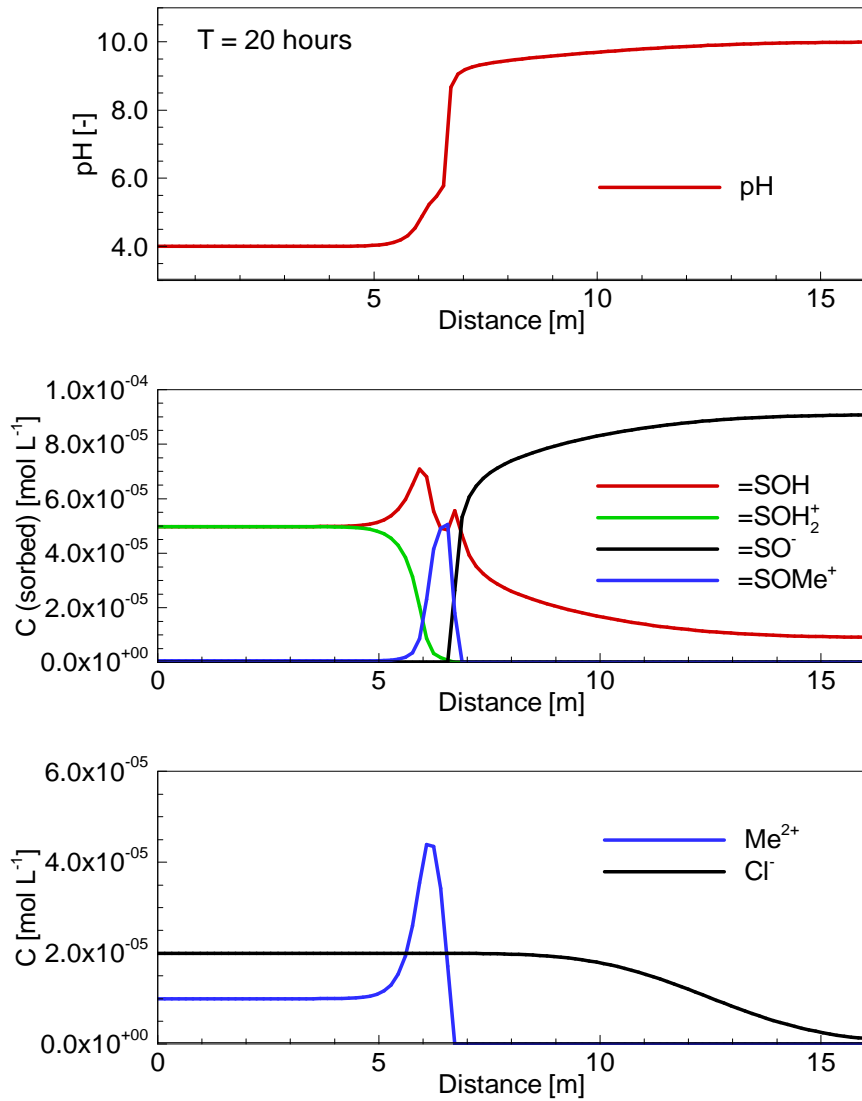


Figure 3.32: Simulated profiles of pH (upper panel), concentrations of sorbed species (middle panel) and total aqueous component concentrations (lower panel) at 20 hours for benchmark surfme2

3.4.13.3 Parameters

The physical parameters (material properties) and the parameters for the surface complexation reactions used for the simulations are the same as those for benchmark surfa2 as summarized in Table 3.41.

3.4.13.4 Results

Simulated results are depicted in Figure 3.32. The results show that the infiltrating solution with low pH (pH=2) replaces the initial solution (with pH of 10.0) (Figure 3.32 upper panel). Consequently, the concentration of the initially dominating sorbed species $=\text{SO}^-$ decreases and the concentrations of $=\text{SOH}_2^+$, $=\text{SO}^-$ and $=\text{SOMe}^+$ increase. In comparison to Na^+ , which does not undergo surface complexation, the component Me^{2+} is substantially attenuated owing to the sorption effect (Figure 3.32 bottom). Because $=\text{SOMe}^+$ is stable when $\text{pH}>6.0$, but unstable when $\text{pH}<6.0$ (Stumm and Morgan 1996), a peak concentration of $=\text{SOMe}^+$ is observed at the transition area of pH from 4.0 to 6.0.

3.4.13.5 File locations

The input file is: *surfme2.dat* under folder

.\benchmarks\benchmarks_standard\reactran\surfme2

Database can be found under: *.\benchmarks\database\surftest*

3.4.14 GROUNDWATER REMEDIATION BY A PERMEABLE REACTIVE BARRIER

3.4.14.1 Problem definition

This benchmark is to demonstrate the capability of MIN3P-THCm to simulate the treatment of contaminated groundwater by a permeable reactive barrier (PRB) (Mayer 1999; Mayer et al. 2001). All geochemical reactions can be expressed with 15 components H^+ , Cl^- , CO_3^{2-} , SO_4^{2-} , HS^- , Ca^{2+} , Fe^{3+} , Fe^{2+} , CrO_4^{2-} , $\text{Cr}(\text{OH})_2^+$, TCE (C_2HCl_3), cis-1,2-DCE ($\text{C}_2\text{H}_2\text{Cl}_2$), VC ($\text{C}_2\text{H}_3\text{Cl}$), ethane (C_2H_6), $\text{H}_2(\text{aq})$, 51 secondary species and 12 mineral reactions including $\text{Fe}_0\text{-H}_2\text{O}_3$, $\text{Fe}_0\text{-cr}$, $\text{Fe}_0\text{-TCE}$, $\text{Fe}_0\text{-CDCE}$, $\text{Fe}_0\text{-VC}$, $\text{Fe}_0\text{-SO}_4\text{-2}$, calcite, siderite(d), $\text{Fe}(\text{OH})_2(\text{s})$, $\text{Cr}(\text{OH})_3(\text{a})$, mackinawite, and ferrihydrite. The reaction stoichiometries of the first six minerals are reduction-corrosion reactions that are normalized with respect to zero valent iron reacting with different oxidants as shown in Table 3.43.

Table 3.43: Reaction stoichiometries of reduction-corrosion reactions (Mayer, 1999)

Mineral	Oxidant	Reaction
$\text{Fe}_0\text{-H}_2\text{O}_3$	water	$\text{Fe}^0(\text{s}) + 2\text{H}^+ \rightarrow \text{Fe}^{2+} + \text{H}_2(\text{aq})$
$\text{Fe}_0\text{-cr}$	Cr(VI)	$\text{Fe}^0(\text{s}) + \text{CrO}_4^{2-} \rightarrow \text{Fe}^{3+} + \text{Cr}(\text{OH})_2^+ + 2\text{H}_2\text{O}$
$\text{Fe}_0\text{-TCE}$	TCE	$\text{Fe}^0(\text{s}) + 0.3025 \text{C}_2\text{HCl}_3 + 1.2335\text{H}^+ \rightarrow \text{Fe}^{2+} + 0.07\text{C}_2\text{H}_2\text{Cl}_2 + 0.2325 \text{C}_2\text{H}_6 + 0.7675 \text{Cl}^-$
$\text{Fe}_0\text{-CDCE}$	Cis-1,2 DCE	$\text{Fe}^0(\text{s}) + \text{C}_2\text{H}_2\text{Cl}_2 + \text{H}^+ \rightarrow \text{Fe}^{2+} + \text{C}_2\text{H}_3\text{Cl} + \text{Cl}^-$
$\text{Fe}_0\text{-VC}$	VC	$\text{Fe}^0(\text{s}) + 0.5 \text{C}_2\text{H}_3\text{Cl} + 1.5 \text{H}^+ \rightarrow \text{Fe}^{2+} + 0.5 \text{C}_2\text{H}_6 + 0.5 \text{Cl}^-$
$\text{Fe}_0\text{-SO}_4\text{-2}$	sulfate	$\text{Fe}^0(\text{s}) + 0.25 \text{SO}_4^{2-} + 2.25 \text{H}^+ \rightarrow \text{Fe}^{2+} + 0.25 \text{HS}^- + \text{H}_2\text{O}$

3.4.14.2 Model setup

A 1D model, 4 m in length, is discretized into 68 control volumes. The domain is divided into three zones: Zone 1 – 0.0 to 1.8 m, Zone 2 – 1.8 to 2.4 m, and Zone 3 – 2.4 to 4.0 m. Zone 1 and Zone 3 represent the aquifer with identical material properties and initial conditions, while Zone 2 represents the reactive barrier including zero valent iron with a volume fraction of $0.5 \text{ m}^3 \text{ m}^{-3}$. The initial volume fractions of all minerals other than Fe(0) is set to 0.0. The initial chemical composition of the pore water in the entire domain and chemical composition at the inflow boundary are listed in Table 3.44. The infiltrating groundwater contains contaminants such as Cr(VI), TCE, which are to be treated by the permeable reactive barrier (Zone 2). Constant hydraulic heads at both boundaries are applied as listed in Table 3.44.

Table 3.44: Initial and boundary conditions for flow and reactive transport – demonstration example prb

Parameter	Initial condition	Boundary conditions		Unit
<i>Aqueous phase</i>		left	right	
Cl ⁻	4.04×10^{-3}	4.04×10^{-3}		[mol l ⁻¹]
CO ₃ ²⁻	1.95×10^{-3}	1.95×10^{-3}		[mol l ⁻¹]
SO ₄ ²⁻	1.44×10^{-3}	1.44×10^{-3}		[mol l ⁻¹]
HS ⁻	5.29×10^{-20}	5.29×10^{-20}		[mol l ⁻¹]
Ca ²⁺	5.32×10^{-4}	5.32×10^{-4}		[mol l ⁻¹]
Fe ²⁺	2.53×10^{-13}	2.53×10^{-13}		[mol l ⁻¹]
Fe ³⁺	4.72×10^{-12}	4.72×10^{-12}	(free exit)	[mol l ⁻¹]
CrO ₄ ²⁻	9.84×10^{-5}	9.84×10^{-5}		[mol l ⁻¹]
Cr(OH) ₂ ⁺	1.52×10^{-7}	1.52×10^{-7}		[mol l ⁻¹]
TCE	1.98×10^{-6}	1.98×10^{-6}		[mol l ⁻¹]
Cis-1,2-DCE	1.37×10^{-6}	1.37×10^{-6}		[mol l ⁻¹]
VC	1.73×10^{-7}	1.73×10^{-7}		[mol l ⁻¹]
ethane	2.99×10^{-6}	2.99×10^{-6}		[mol l ⁻¹]
H ₂ (aq)	1.98×10^{-31}	1.98×10^{-31}		[mol l ⁻¹]
H ⁺	6.29	3.0		pH
<i>Mineral</i>				
Fe_0	0.5	-	-	[m ³ m ⁻³]
Calcite	0.00	-	-	[m ³ m ⁻³]
siderite	0.00	-	-	[m ³ m ⁻³]
Fe(OH) ₂ (s)	0.00	-	-	[m ³ m ⁻³]
Cr(OH) ₃ (a)	0.00	-	-	[m ³ m ⁻³]
Mackinawite	0.00	-	-	[m ³ m ⁻³]
Ferrihydrite	0.00	-	-	[m ³ m ⁻³]
<i>Hydraulic condition</i>				
Hydraulic head	0.0	3.0088 (first)	3.0 (first)	[m]

3.4.14.3 Parameters

The physical parameters of the porous medium are given in Table 3.45. Geochemical parameters are mainly derived from MINTEQA2 (Allison et al., 1991). Details can be found in Mayer (1999) and Mayer et al. (2001).

Table 3.45: Physical parameters for demonstration example prb

Parameter		Value			Unit
		Zone 1	Zone 2	Zone 3	
Porosity	ϕ	0.38	0.50	0.38	[-]
Hydraulic conductivity	K_{xx}	8.10×10^{-5}	1.2×10^{-3}	8.10×10^{-5}	[m s ⁻¹]
Diffusion coefficient	D_0^a	0.0	0.0	0.0	[m ⁻² s ⁻¹]
longitudinal dispersivity	α_l	0.0	0.0	0.0	[m]

3.4.14.4 Results

The simulated profiles of pH, concentrations of contaminants and selected components, volume fraction of minerals and iron consumption rates at 240 are depicted in Figure 3.33. The reaction-corrosion reactions taking place in the reactive barrier zone lead to a pronounced pH-increase in the solution passing through the barrier (Figure 3.33 (a)). Simulated results show very rapid removal of the contaminant Cr(VI) (Figure 3.33 (b)), leading to the precipitation of Cr(OH)₃ in the barrier (Figure 3.33 (e)). Reductive dechlorination of the chlorinated organic compounds (such as TCE, cis-1,2 DCE and VC) across the barrier is not as rapid as the reduction of Cr(VI) and the transformation remains incomplete (Figure 3.33 (b)). Iron corrosion is most significant in the entry area of the barrier, decreases along the flow path and leads to the formation of Fe(II) and Fe(III), H₂(aq), HS⁻ in the aqueous phase (Figure 3.33 (c)) and precipitation of Fe(OH)₂(s), siderite, mackinawite, and ferrihydrite (Figure 3.33 (e)). The reaction rates of selected reduction-corrosion reactions are depicted in Figure 3.33 (f). Sulfate is the most important electron acceptor in the system, contributing most significantly to iron corrosion. The reduction of Cr(VI) has only a limited effect on iron corrosion. The simulated results showed generally good agreement with field test results by Bennett (1997) (Mayer, 1999, Mayer et al., 2001).

3.4.14.5 File locations

The input file for the benchmark can be found under

.\benchmarks\benchmarks_standard\reactran\prb

Database can be found under: .\benchmarks\database\default

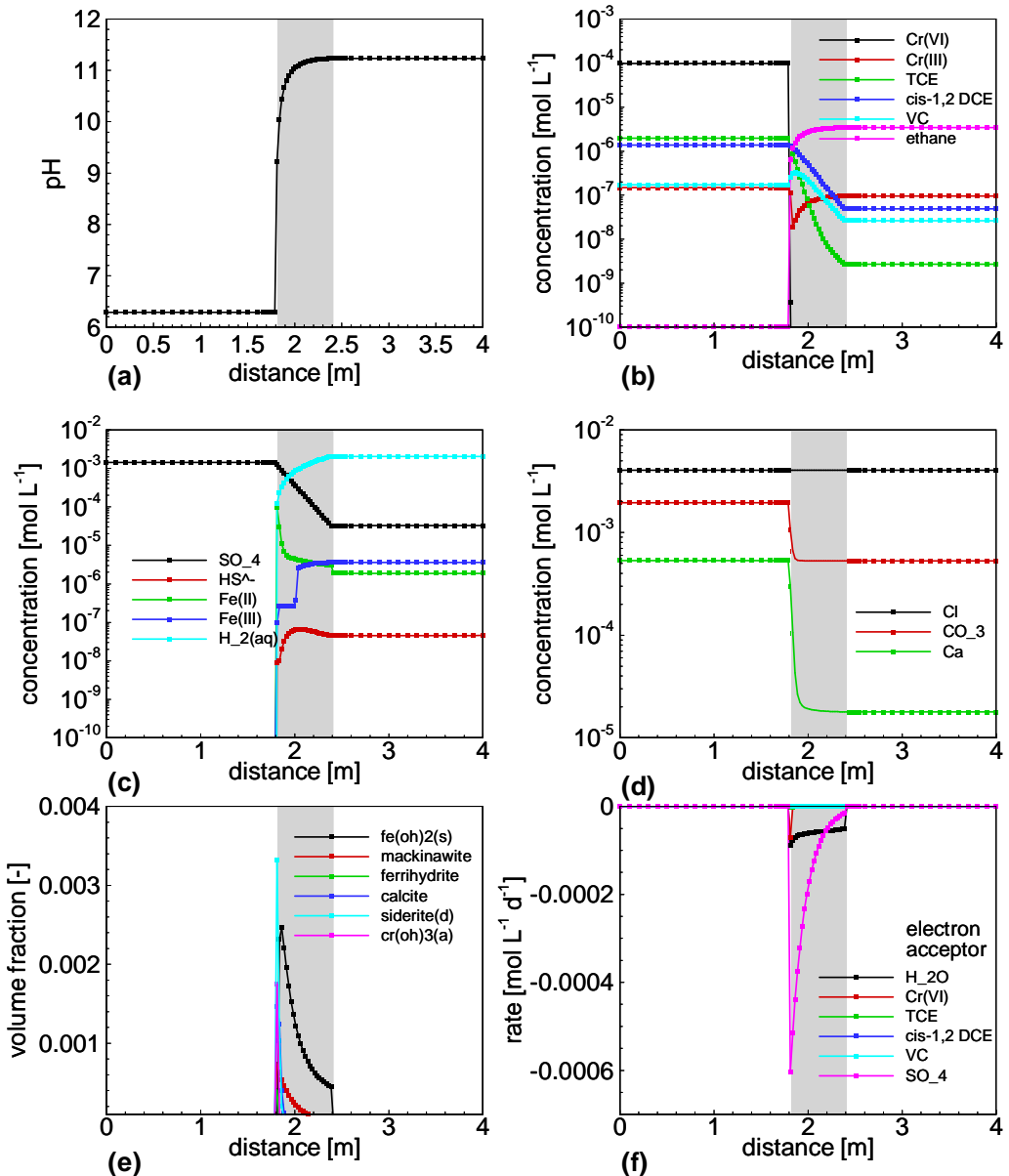


Figure 3.33: Simulated spatial profiles of pH (a), concentrations of contaminants (b) and selected components (c) and (d), volume fraction of minerals (e) and iron consumption rates (f) at 240 days. The gray background indicates the position of the reactive barrier (Zone 2).

3.4.15 ACID ROCK DRAINAGE GENERATION AND ATTENUATION

3.4.15.1 Problem definition

This demonstration example addresses the generation and attenuation of acid rock drainage in variably-saturated porous media. Atmospheric oxygen penetrates into the tailings material due to the existence of an unsaturated zone. Gaseous oxygen subsequently partitions into the aqueous phase, where it causes the oxidation of sulfide minerals such as pyrite. The oxidation of pyrite leads to an increase in acidity, dissolved iron, and sulfate concentrations. The low pH-water is buffered, as the pore water migrates downwards into the tailings impoundment, leading to a series of dissolution-precipitation reactions.

Table 3.46: Initial and boundary conditions for reactive transport – demonstration example *amd_ex*

Parameter	Initial Condition	Boundary Condition	Unit
<i>Aqueous phase</i>			
Ca ²⁺	1.6684×10 ⁻⁰²	2.9214×10 ⁻⁰³	[mol l ⁻¹]
K ⁺	9.0000×10 ⁻⁰³	9.0000×10 ⁻⁰³	[mol l ⁻¹]
Cl ⁻	1.1400×10 ⁻⁰³	1.1400×10 ⁻⁰⁴	[mol l ⁻¹]
H ₄ SiO ₄	1.9300×10 ⁻⁰³	1.9900×10 ⁻⁰⁴	[mol l ⁻¹]
Al ³⁺	2.5900×10 ⁻⁰⁸	1.2800×10 ⁻⁰⁸	[mol l ⁻¹]
CO ₃ ²⁻	2.4929×10 ⁻⁰³	3.1700×10 ⁻⁰⁴	[mol l ⁻¹]
H ⁺	7	5	pH
O ₂ (aq)	-2.5	0.21	pe/pO ₂
Fe ²⁺	1.4506×10 ⁻⁰⁴	1.2885×10 ⁻¹¹	[mol l ⁻¹]
SO ₄ ²⁻	1.9688×10 ⁻⁰²	7.4800×10 ⁻⁰³	[mol l ⁻¹]
Fe ³⁺	7.1614×10 ⁻¹²	5.3610×10 ⁻⁰⁵	[mol l ⁻¹]
HS ⁻	3.3137×10 ⁻¹²	2.5901×10 ⁻¹³⁹	[mol l ⁻¹]
<i>Minerals</i>			
Pyrite	1.37×10 ⁻⁰²		[m ³ m ⁻³]
Calcite	1.77×10 ⁻⁰³		[m ³ m ⁻³]
Siderite	3.49×10 ⁻⁰⁴		[m ³ m ⁻³]
Gibbsite	8.30×10 ⁻⁰⁴		[m ³ m ⁻³]
Gypsum	6.06×10 ⁻⁰³		[m ³ m ⁻³]
Ferrihydrite	0.0		[m ³ m ⁻³]
Jarosite	0.0		[m ³ m ⁻³]
K-feldspar	2.68×10 ⁻⁰²		[m ³ m ⁻³]
Muscovite	7.31×10 ⁻⁰²		[m ³ m ⁻³]
Silica(am)	0.0		[m ³ m ⁻³]

3.4.15.2 Model setup

A 1D model, 5.0 m in depth, is discretized into 101 control volumes yielding a discretization interval of 5 cm for the interior control volumes and 2.5 cm for the control volumes on the boundary. Boundary conditions for the flow problem consist of a specified flux boundary at the top of 300 mm yr^{-1} ($=9.51 \times 10^{-9} \text{ m s}^{-1}$), which represents recharge, and a fixed head boundary of $h = 2.5 \text{ m}$ at the bottom boundary. These boundary conditions lead to the development of an unsaturated zone, which extends from the surface to a depth of 2.45 m with variable moisture content.

In this demonstration example, the intra-aqueous reactions are treated as equilibrium reactions, while all minerals are assumed to be surface-controlled kinetic dissolution-precipitation. $\text{O}_2(\text{aq})$ has been used as the redox master variable. 10 minerals are considered: pyrite, calcite, siderite, gibbsite, gypsum, ferrihydrite, jarosite, k-feldspar, muscovite and silica(am). Detailed kinetic parameters for these minerals can be found in Mayer (1999).

The total chemical compositions of the initial background pore water (IC) and the inflow solution on the top boundary (BC), and the initial volume fraction of all minerals are listed in Table 3.46.

3.4.15.3 Parameters

The physical parameters used for the simulations are summarized in Table 3.47. The free phase diffusion coefficients are representative for oxygen at $T = 25^\circ\text{C}$ and were taken from the compilation of Glinski and Stepniewski [1985]. The key chemical reactions and kinetic parameters are given in Table 3.48.

Table 3.47: Physical parameters for demonstration example *amd_ex*

Parameter	Symbol	Value	Unit
Length of domain	L	5.0	[m]
Porosity	ϕ	0.5	[\cdot]
Infiltration rate	q_{in}	0.3	[m yr^{-1}]
Hydraulic conductivity	K_{zz}	1.0×10^{-6}	[m s^{-1}]
Residual saturation	S_{ra}	0.05	[\cdot]
van Genuchten parameter α	α	3.5	[m^{-1}]
van Genuchten parameter n	n	1.4	[\cdot]
Longitudinal dispersivity	α_l	5.0×10^{-4}	[m]
Free phase diffusion coefficient in gaseous phase	D_0^g	2.07×10^{-5}	[$\text{m}^{-2} \text{s}^{-1}$]
Free phase diffusion coefficient in aqueous phase	D_0^a	2.38×10^{-9}	[$\text{m}^{-2} \text{s}^{-1}$]

3.4.15.4 Results

The simulation results are shown in Figure 3.34. The results indicate a rapid decline of

Validation report-page# 3-217

gaseous oxygen concentrations versus depth. This is primarily due to the oxidation of pyrite, which becomes depleted in the zone where oxygen is present, as shown in Figure 3.34b. Figure 3.34a shows a pronounced decrease of pH and pe in the zone of pyrite oxidation. The pe decreases rapidly, when oxygen and ferric iron become depleted. The stepwise increase of pH at greater depth can be attributed to the dissolution of calcite ($\text{pH} \sim 6.4$), siderite ($\text{pH} \sim 4.8$) and gibbsite ($\text{pH} \sim 4.0$), which is depicted in Figure 3.34b). As a result of the dissolution of these primary mineral phases, secondary minerals such as jarosite, amorphous silica and gypsum form within the column. After 10 years, elevated concentrations of dissolved iron and sulfate have penetrated deep into the column, as shown in Figure 3.34c. Ferric iron dominates close to the ground surface where oxidizing conditions prevail, while dissolved ferrous iron dominates below the zone of active oxidation. The demonstration problem is characterized by steep geochemical gradients in the transition zone from oxic to anoxic conditions and in the zones of pH-buffering due to mineral dissolution.

Table 3.48: Mineral reaction and kinetic parameters for demonstration example *amd_ex*

Mineral	Reaction	$\log K_{25}$	$k_i^{m,0}$ [mol L ⁻¹ bulk s ⁻¹]
Pyrite	$\text{FeS}_2 + \text{H}_2\text{O} \leftrightarrow 0.5\text{O}_2(\text{aq}) + \text{Fe}^{2+} + 2\text{HS}^-$	-61.488	1.0×10^{-9}
Calcite	$\text{CaCO}_3 \leftrightarrow \text{Ca}^{2+} + \text{CO}_3^{2-}$	-8.4750	5.0×10^{-8}
Siderite	$\text{FeCO}_3 \leftrightarrow \text{Fe}^{2+} + \text{CO}_3^{2-}$	-10.4500	1.0×10^{-8}
Gibbsite	$\text{Al}(\text{OH})_3 + 3\text{H}^+ \leftrightarrow \text{Al}^{3+} + 3\text{H}_2\text{O}$	8.1100	1.0×10^{-8}
Gypsum	$\text{CaSO}_4 \cdot 2\text{H}_2\text{O} \leftrightarrow \text{Ca}^{2+} + \text{SO}_4^{2-} + 2\text{H}_2\text{O}$	-4.5800	1.0×10^{-7}
Ferrihydrite	$\text{Fe}(\text{OH})_3 + 3\text{H}^+ \leftrightarrow \text{Fe}^{3+} + 3\text{H}_2\text{O}$	4.8910	1.0×10^{-7}
Jarosite	$\text{KFe}_3(\text{SO}_4)_2(\text{OH})_6 + 6\text{H}^+ \leftrightarrow \text{K}^+ + 3\text{Fe}^{3+} + 2\text{SO}_4^{2-} + 6\text{H}_2\text{O}$	-9.2100	1.0×10^{-7}
K-feldspar	$4\text{H}_2\text{O} + 4\text{H}^+ + \text{KAlSi}_3\text{O}_8 \rightarrow \text{K}^+ + \text{Al}^{3+} + 3\text{H}_4\text{SiO}_4$	0.0800	5.0×10^{-11}
Muscovite	$\text{KAl}_2(\text{AlSi}_3\text{O}_{10})(\text{OH})_2 + 10\text{H}^+ \rightarrow \text{K}^+ + 3\text{Al}^{3+} + 3\text{H}_4\text{SiO}_4$	12.9900	1.0×10^{-11}
Silica(am)	$\text{H}_4\text{SiO}_4 \leftrightarrow \text{SiO}_2 + 2\text{H}_2\text{O}$	-2.7100	1.0×10^{-8}

→ stands for irreversible reaction, ↔ stands for reversible reaction

3.4.15.5 File locations

The input file is: *amd-ex.dat* under folder:

.\benchmarks\benchmarks_standard\reactran\amd_ex

Database can be found under: *.\benchmarks\database\default*

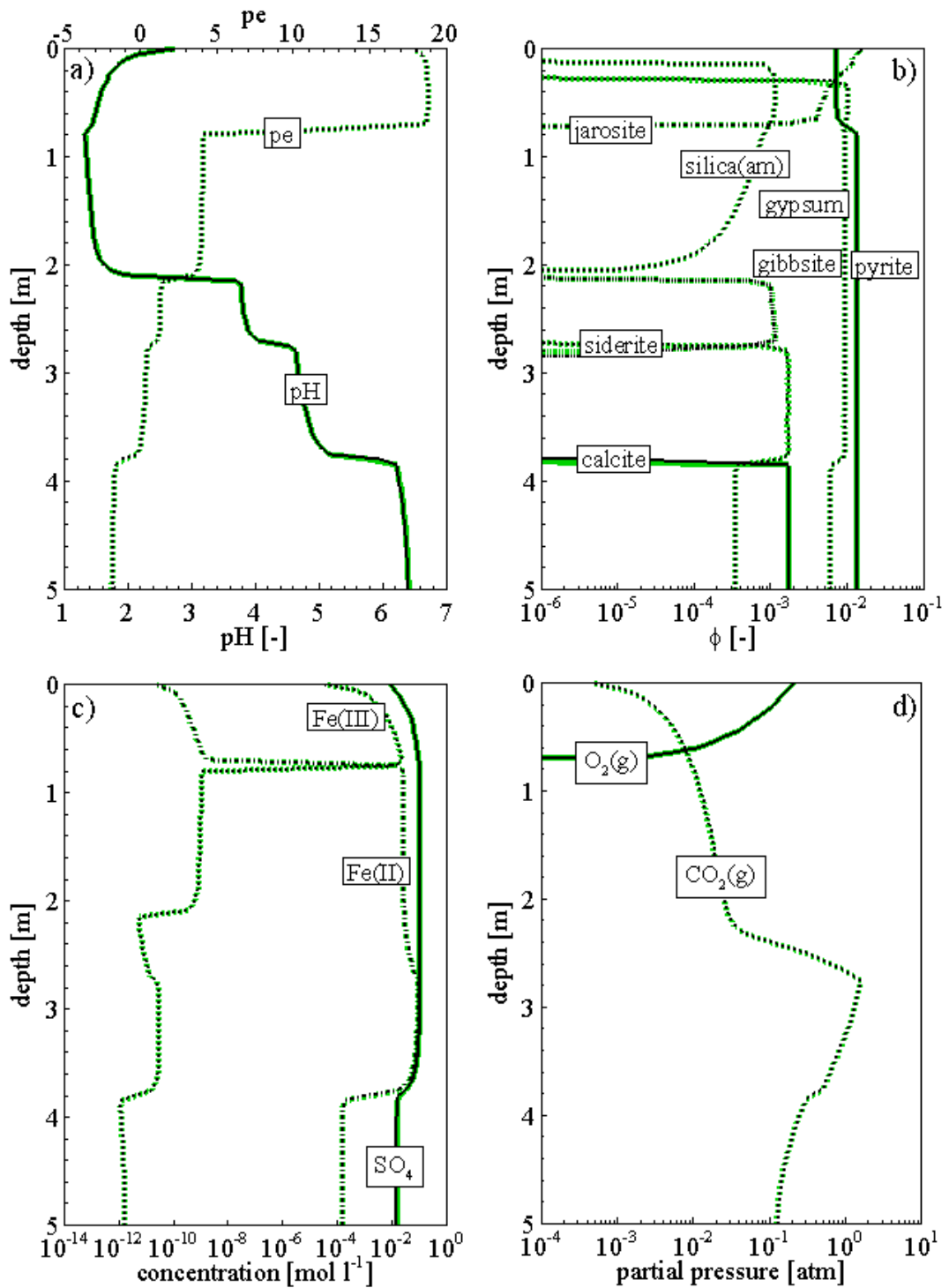


Figure 3.34: Simulated spatial profiles for the acid mine drainage generation problem at $T = 10$ years: a) pH and pe, b) mineral volume fractions, c) selected total aqueous component concentrations, d) partial gas pressures

3.4.16 ISOTOPE FRACTIONATION

3.4.16.1 Problem definition

This benchmark demonstrates the fractionation model used to evaluate sulfur isotope fractionation in a column experiment (Column I) designed to simulate treatment of contaminated water by microbially mediated sulfate reduction occurring within organic carbon-based and iron and carbon-based permeable reactive barriers (Waybrant et al. 2002; Gibson et al. 2011).

3.4.16.2 Model setup

The column in length 0.4 m is simulated by a 1D model discretized into 41 control volumes. The reactive zone locates in the middle from 0.05 m to 0.385 m. The bottom and top layers are composed of silica and sand without organic additives. The final simulation time is 429 days. The initial hydraulic head is set to 1.0 m for the whole domain. Boundary conditions for the flow problem consist of a specified flux boundary at the bottom in 1.1×10^{-7} m s⁻¹, which represents recharge, and a fixed head boundary of h = 1.0 m at the top boundary. The 18 primary components considered in the simulation are: Ca²⁺, Fe²⁺, SO₄²⁻, ³⁴SO₄²⁻, H⁺, CO₃²⁻, HS⁻, H³⁴S⁻, Ar(aq), Zn²⁺, Ni²⁺, Mn²⁺, Na⁺, K⁺, Mg²⁺, Br⁻, Cl⁻, and O₂(aq). The number of secondary components is 92. The minerals included in the simulation are: calcite, siderite, gypsum, ³⁴gypsum (i.e., gypsum that its sulfur is the heavier isotope ³⁴S). The same notation is used for other minerals including sulfur), mackinawite, ³⁴mackinawite, miller, ³⁴miller, sphaler, ³⁴sphaler, rhodochrosite and dolomite. These minerals are treated as kinetically controlled reversible dissolution/precipitation reactions. Additionally, the reduction of sulphate isotopes by organic substance are represented as minerals CH₂O-H₂S-m and CH₂O-H₂³⁴S-m and specified as irreversible, kinetically-controlled reactions. To model sulfur isotope fractionation in the laboratory column experiment, all instances of sulfur species in the databases (including all aqueous species and sulfur minerals) were modified to include separate entries for both heavy (³⁴S) and light (³²S) sulfur components.

The initial volume fraction of calcite in 3.1×10^{-3} was adjusted to fit the modeled data. Other minerals as listed above are considered to be secondary minerals. The other components of the column (including the silica and sand layers on the top and bottom of the column) were considered to be nonreactive and thus not included in the model. The initial volume fraction of organic carbon was arbitrarily set to 0.1 to account for an excess of available carbon for the sulfate reduction.

The reduction of sulfate by sulfate reducing bacteria through the addition of organic carbon as the electron donor is calculated as kinetically controlled irreversible reactions:



Both reactions were simulated with a simplified Monod-type rate expression dependent on the mass of sulfate for both heavy and light sulfur isotopes:

Validation report-page# 3-220

$$R_{CH_2O-^{32}SO_4} = -^{32}k_{SO_4} \left[\frac{[SO_4]}{K_s + [SO_4]} \right]$$

$$R_{CH_2O-^{34}SO_4} = -^{34}k_{SO_4} \left[\frac{[SO_4]}{K_s + [SO_4]} \right]$$

where $R_{CH_2O-^{32}SO_4}$ and $R_{CH_2O-^{34}SO_4}$ are rates of the overall reaction progress, K_s is the half saturation constant, and $[SO_4]$ is the total sulfate concentration (i.e. including both heavy and light isotopes).

The initial concentrations of the aqueous components are the same in the domain as listed in Table 3.49. The injected solutions were replaced eight times during the experiment and were simulated as time dependent boundary condition. The chemical compositions of the injected solutions are listed in Table 3.50.

Table 3.49: Initial concentrations [mg/L] of the aqueous components in the domain

Component	concentration	Remark	Component	concentration	Remark
Ca²⁺	425	'free'	Zn ²⁺	1.0×10^{-10}	'free'
Fe²⁺	1.0×10^{-10}	'free'	Ni ²⁺	1.0×10^{-10}	'free'
SO₄²⁻	965.316	'free'	Mn ²⁺	1.0×10^{-10}	'free'
³⁴SO₄²⁻	44.423	'free'	Na ⁺	3.6	'free'
H⁺	7.8	'pH'	K ⁺	1.0×10^{-10}	'free'
CO₃²⁻	22.4	'free'	Mg ²⁺	1.0×10^{-10}	'free'
HS⁻	1.0×10^{-10}	'free'	Br ⁻	1.0×10^{-10}	'free'
H³⁴S⁻	1.0×10^{-10}	'free'	Cl ⁻	1.0×10^{-10}	'free'
Ar(aq)	50.4	'fixed'	O ₂ (aq)	0.0	'Eh'

Table 3.50: Time dependent boundary concentrations [mg/L] of the aqueous components representing eight replacements of injection solutions

t _{in} [d]	0	95.9	135	163.6	205.6	254.6	298.1	344.6	395.6
Comp.	Concentration [mg/L]								
Ca²⁺	425	506	99	92	83	205	214	220	220
Fe²⁺	tiny	694.5	1181	875.7	956.3	443.7	379.4	333.8	316.3
SO₄²⁻	965.3	3068.0	3721.7	3302.1	3498.1	1911.5	1551.2	1293.0	1338.1
³⁴SO₄²⁻	44.42	141.19	171.27	152.01	160.98	87.97	71.39	59.69	61.58
pH	7.8	6.4	5.85	6.41	6.46	6.6	6.16	6.61	6.43
CO₃²⁻	22.4	88.62	32.88	27	20.4	15.54	6.72	16.68	14.28
HS⁻	tiny	tiny	tiny	tiny	tiny	tiny	tiny	tiny	tiny
H³⁴S⁻	tiny	tiny	tiny	tiny	tiny	tiny	tiny	tiny	tiny
Ar(aq)	50.4	50.4	50.4	50.4	50.4	50.4	50.4	50.4	50.4
Zn²⁺	tiny	0.72	0.95	0.58	0.97	1.22	0.85	0.57	0.57
Ni²⁺	tiny	0.94	1.4	1.31	12.28	2.34	1.6	3.36	3.36

Validation report-page# 3-221

Mn²⁺	tiny	9.75	12.87	12.75	19.8	14.12	8.96	8.62	8.62
Na⁺	3.6	46.8	50	48.8	48.8	19.8	14.1	13	13
K⁺	tiny	27.4	31.7	32.3	29.2	11.8	7.9	7.2	7.2
Mg²⁺	tiny	242	320	317	288	121	83	77	77
Br⁻	tiny	26	tiny	tiny	tiny	tiny	tiny	tiny	tiny
Cl⁻	tiny	14.19	4.82	8.16	7.71	0.91	15.43	17.55	14.43
Eh	10	16	74	142	179	2	23	307	180

t_{in} – injection time in [days], tiny = 1.0×10^{-10} mg/L

3.4.16.3 Parameters

The kinetic parameters of the minerals are listed in Table 3.51. K_s for the sulfate reduction is 1.62 mmol/L as used by Gibson et al. (2011).

Table 3.51: Mineral reaction and kinetic parameters for demonstration example *waybrant*

Mineral	Reaction	logK ₂₅	$k_i^{m,0}$ [mol L ⁻¹ bulk s ⁻¹]
Calcite	$\text{Ca}^{2+} + \text{CO}_3^{2-} \leftrightarrow \text{CaCO}_3$	8.4750	4.0×10^{-8}
Siderite	$\text{Fe}^{2+} + \text{CO}_3^{2-} \leftrightarrow \text{FeCO}_3$	10.4500	4.0×10^{-8}
Gypsum	$\text{Ca}^{2+} + \text{SO}_4^{2-} + 2\text{H}_2\text{O} \leftrightarrow \text{CaSO}_4 \cdot 2\text{H}_2\text{O}$	4.5800	4.0×10^{-9}
34Gypsum	$\text{Ca}^{2+} + {}^{34}\text{SO}_4^{2-} + 2\text{H}_2\text{O} \leftrightarrow \text{Ca}^{34}\text{SO}_4 \cdot 2\text{H}_2\text{O}$	4.5800	4.0×10^{-9}
Mackinawite	$\text{Fe}^{2+} + \text{HS}^- \leftrightarrow \text{FeS} + \text{H}^+$	4.6480	1.16×10^{-11}
34Mackinawite	$\text{Fe}^{2+} + \text{H}^{34}\text{S}^- \leftrightarrow \text{Fe}^{34}\text{S} + \text{H}^+$	4.6480	1.16×10^{-11}
Millerite	$\text{Ni}^{2+} + \text{HS}^- \leftrightarrow \text{NiS} + \text{H}^+$	8.0420	1.16×10^{-12}
34Millerite	$\text{Ni}^{2+} + \text{H}^{34}\text{S}^- \leftrightarrow \text{Ni}^{34}\text{S} + \text{H}^+$	8.0420	1.16×10^{-12}
Sphalerite	$\text{Zn}^{2+} + \text{HS}^- \leftrightarrow \text{ZnS} + \text{H}^+$	11.6180	1.16×10^{-12}
34Sphalerite	$\text{Zn}^{2+} + \text{H}^{34}\text{S}^- \leftrightarrow \text{Zn}^{34}\text{S} + \text{H}^+$	11.6180	1.16×10^{-12}
Rhodochrosite	$\text{Mn}^{2+} + \text{CO}_3^{2-} \leftrightarrow \text{MnCO}_3$	10.4100	1.16×10^{-8}
Dolomite	$\text{Ca}^{2+} + \text{Mg}^{2+} + 2\text{CO}_3^{2-} \leftrightarrow \text{CaMg}(\text{CO}_3)_2$	17.0900	1.16×10^{-8}

\leftrightarrow stands for reversible reaction, K_{25} is the equilibrium constant at 25°C, $k_i^{m,0}$ is the initial kinetic rate constant

Key modeling parameters used in the simulations are listed in Table 3.52.

Table 3.52: General parameters for the circulation chamber, filter, gap and OPA

Parameter	Bottom	Reactive	Top
Porosity [-]	0.53	0.53	0.53
Hydraulic conductivity [m/d]	1.20×10^{-5}	1.20×10^{-5}	1.20×10^{-5}
Longitudinal dispersivity [m]	0.019	0.019	0.019

3.4.16.4 Results

The calcite initially in the column dissolves with the injection of boundary solutions (Figure 3.35). The concentration of CO_3^{2-} in the pore solution increases accordingly, which reacts with the injected Fe^{2+} and thus siderite precipitates. In the meanwhile, the sulfate concentration increase in the pore water results in the precipitation of gypsum. The sulfate reduction by biodegradation produces $\text{H}_2\text{S}(\text{aq})$ and reacts with ions such as Fe^{2+} , and thus mackinawite precipitates.

Breakthrough curves of modeled SO_4^{2-} and $\delta^{34}\text{S}$ for the Column experiment were compared to measured effluent values (Figure 3.36). Periods of decreasing SO_4^{2-} correspond to periods of increasing $\delta^{34}\text{S}$. According to the model, when the SO_4^{2-} concentration approaches a very low level, the $\delta^{34}\text{S}$ value increases substantially. This phenomena is especially obvious at the early stage within 100 days, during which there was no isotope measurements to verify the prediction of the $\delta^{34}\text{S}$ values. Nevertheless, predicted $\delta^{34}\text{S}$, $\text{Fe}(\text{II})$ and SO_4^{2-} values showed good agreement to the measured data in the effluent.

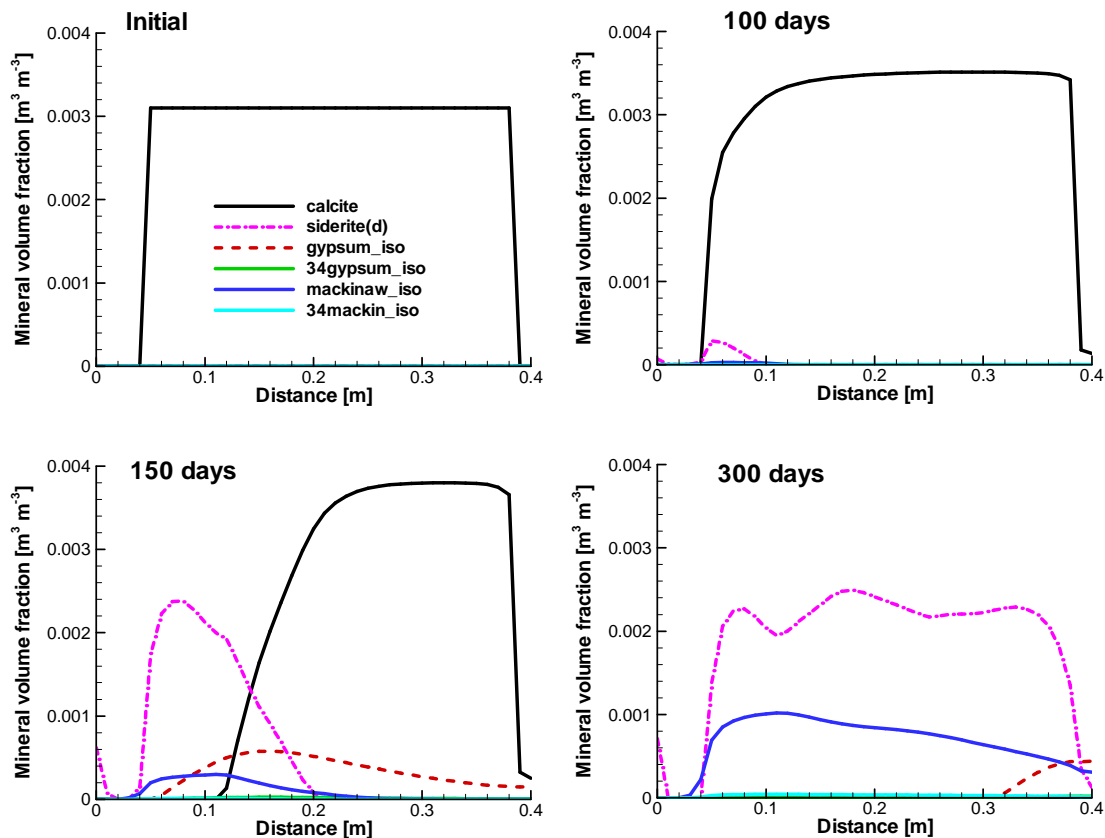


Figure 3.35: Simulated profiles of mineral volume fractions

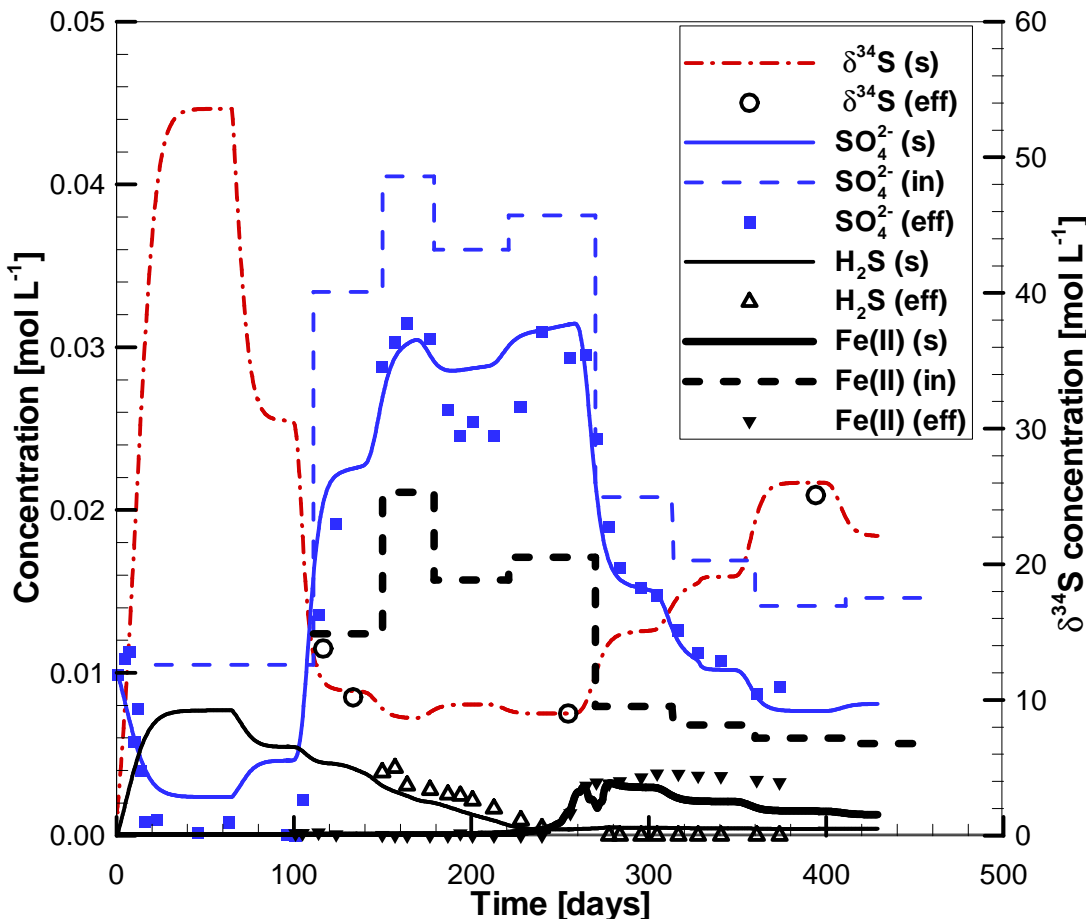


Figure 3.36: Comparison of concentration time curves of simulated (s) to measured $\delta^{34}\text{S}$, SO_4^{2-} and Fe(II) in the influent (in) and effluent (eff) (Gibson et al. 2011).

3.4.16.5 File locations

The input file is: *waybrant.dat* under folder:

```
.\benchmarks\benchmarks_new_add\isotope\isotope_examples\Gibson et al  
2011\Waybrant_2 - new\
```

Database can be found under:

```
.\benchmarks\benchmarks_new_add\isotope\isotope_examples\Gibson et al  
2011\Waybrant_2 - new\database
```

3.4.17 1D SALINITY DEPENDENT SRB REACTION

3.4.17.1 Problem definition

This application example demonstrates the application of the salinity dependent sulfur reducing bacteria (SRB) reaction model.

3.4.17.2 Model setup

A 1D model, 400.0 m in length, is discretized into 81 control volumes. The domain consists of three material groups – naming the ‘inflow’ from 0 to 20 m, ‘reactive’ from 20 to 180 m and ‘outflow’ from 180 to 400 m. The initial hydraulic head is 1.0 across the domain. A flux at the inflow boundary is constant at 1.0×10^{-9} m s⁻¹, while the hydraulic head at the outflow boundary is set to 1.0 m. Initially, the column was filled with highly saline solutions based on Hobbs et al. (2011), Table A-3 (Table 3.53). With the infiltration of a fresh water solution (i.e. rain water according to Bea et al. 2011) into the column, the aqueous species composition changes over time. The geochemical system includes 10 primary species (Ca^{2+} , Na^+ , Mg^{2+} , K^+ , Cl^- , SO_4^{2-} , H^+ , CO_3^{2-} , HS^- and $\text{O}_2(\text{aq})$), and 22 secondary species. The initial condition (IC) of the pore water and the boundary aqueous composition (BC) are listed in Table 3.53.

Table 3.53: Initial and boundary conditions (IC & BC) of the aqueous and mineral compositions for the example *sulfur*

Parameter	IC (inflow, reactive) [#]	IC (outflow) ^{\$}	BC (inflow) ^c	Unit
Aqueous component concentration				
Ca^{2+}	6000.00	9600.00	8.40	[mg l ⁻¹]
Na^+	10900.00	94000.00	189.00	[mg l ⁻¹]
Mg^{2+}	2800.00	3400.00	0.097	[mg l ⁻¹]
K^+	450.00	2600.00	72.00	[mg l ⁻¹]
Cl^-	31000.00	193000.00	164.00	[mg l ⁻¹]
SO_4^{2-}	1240.00	600.00	1.0×10^{-10}	[mg l ⁻¹]
pH	5.95	5.95	7.0	[-]
CO_3^{2-}	303.00	76.00	164.00	[mg l ⁻¹]
HS^-	1.0×10^{-10}	1.0×10^{-10}	1.0×10^{-10}	[mg l ⁻¹]
Eh	-200.00	-200.00	200.00	[mV]
Mineral volume fraction				
Parameter	IC (inflow)	IC (reactive)	IC (outflow)	Unit
ch2o-h2s	1.0×10^{-10}	0.10	0.10	[m ³ m ⁻³]
Calcite	1.0×10^{-10}	0.31	0.10	[m ³ m ⁻³]
Anhydrite	1.0×10^{-10}	5.0×10^{-6}	0.32	[m ³ m ⁻³]
Halite	1.0×10^{-10}	1.0×10^{-10}	0.30	[m ³ m ⁻³]

- From Hobbs et al. (2011), Table A-3, Sample ID: CFN-161

\$ - From Hobbs et al. (2011), Table A-5, Sample ID: SF-3

C - Bea et al. (2011)

3.4.17.3 Parameters

The parameters of the porous medium are: porosity is 0.13 for the material ‘inflow’ and ‘reactive’, 0.11 for the material ‘outflow’; hydraulic conductivity is 1.20×10^{-5} [m/s], longitudinal dispersivity is 0.0019 m.

Sulfate reduction reaction by SRB and its dependence on salinity are described in section

2.5.22.

Other parameters applied are: k_s is 1.62×10^{-3} and k_{sulf} $6.9 \times 10^{-9} \text{ m}^2 \text{ mineral L}^{-1}$ bulk (Gibson et al. 2011). $K_{H_2S}^{in}$ and $K_{O_2}^{in}$ are not found in the literature, therefore used the value 3.125×10^{-6} for reductive dissolution of goethite by benzene according to MINTEQA2 database (Allison et al., 1991).

3.4.17.4 Results

Simulated results are depicted in Figure 3.37. Due to the higher concentration of anhydrite in the lower part of the column, the sulfate concentration of the lower part is higher than the upper parts (Figure 3.37 top left). Nevertheless, the concentration of $\text{H}_2\text{S}(\text{aq})$ is much lower in the lower part than that in the upper part. This is because of the higher salinity in the lower part (i.e. significantly higher concentrations of Na^+ and Cl^-) (Figure 3.37 top right). Consequently, the SRB reaction in the lower part is significantly inhibited. Infiltration of the rain water from the top results in dilution of the pore water along the column downwards. Therefore, significant peaks of SO_4^{2-} and $\text{H}_2\text{S}(\text{aq})$ (Figure 3.37 top left) occur around the depth at 180 m (i.e. the boundary of ‘reactive’ and ‘outflow’).

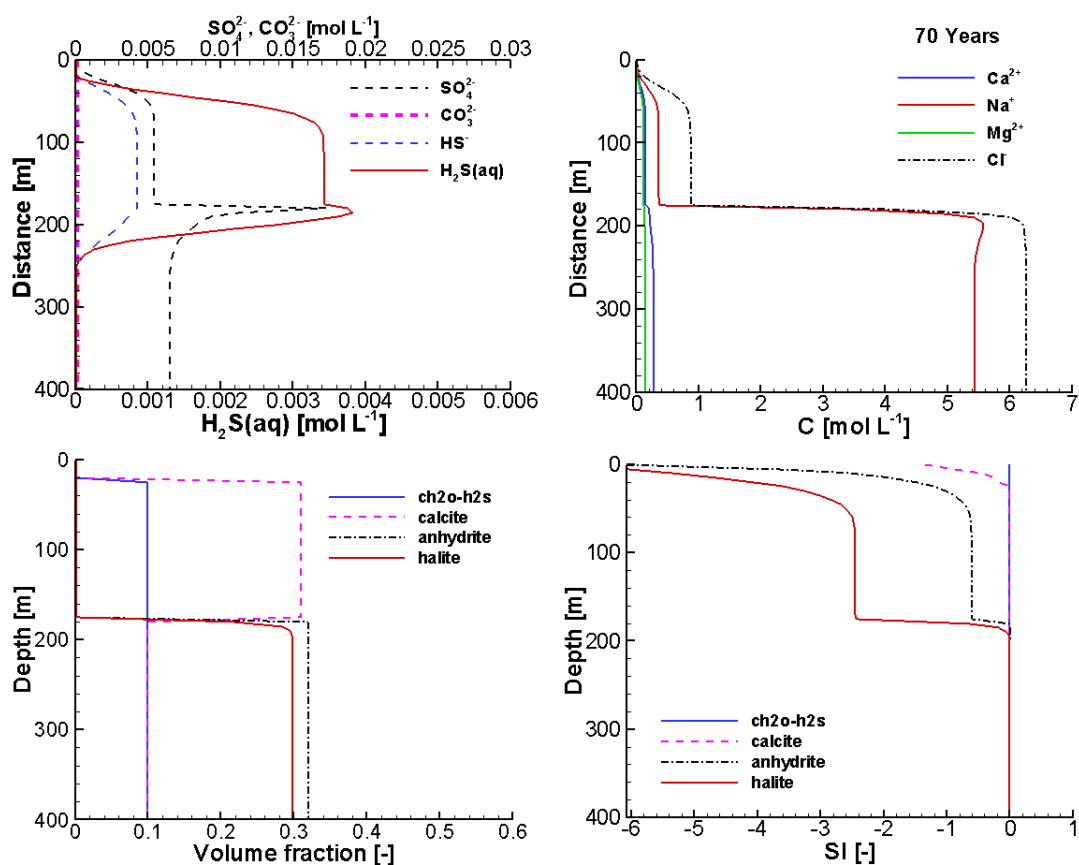


Figure 3.37: Profiles of total concentrations of SO_4^{2-} , CO_3^{2-} , HS^- and $\text{H}_2\text{S}(\text{aq})$ (Top left), and of other main ions (top right), and of the volume fractions of minerals (bottom left) and of the mineral saturation indexes (bottom right) at 70 years

Validation report-page# 3-226

3.4.17.5 File locations

The input file is: *sulfur.dat* under folder `.\benchmarks\benchmarks_new_added\sulfur\`

Database can be found under: `.\benchmarks_new_add\sulfur-V1.0.431\database\default\`

4 VALIDATION EXAMPLES AGAINST EXPERIMENTS

4.1 MONT TERRI IN-SITU DIFFUSION EXPERIMENTS

MIN3P-THCm has been used to simulate/predict DR-A in-situ diffusion experiments at Mont Terri Underground Rock Laboratory (Switzerland), a chemical perturbation (replacement of the initial synthetic porewater in the borehole with a high-salinity solution) to study the effects on solute transport and retention (Xie et al. 2014). The experiments were performed in three phases: Phase I, Phase II and overcoring. The Phase I in-situ diffusion experiment was performed with an artificial porewater with the same chemical compositions for the major ions in the Opalinus clay (OPA) porewater. In addition, a mixture of tracers (HTO , I^- , Br^- , Cs^+ , $^{85}\text{Sr}^{2+}$ and $^{60}\text{Co}^{2+}$) were added and observed during for 189 days (Xie et al. 2013). Phase II experiment was conducted immediately after the Phase I by changing the circulation solution to a solution with much higher concentrations of Cl^- , Na^+ and K^+ , and a much lower concentration of SO_4^{2-} (to create a chemical perturbation). The concentrations of both tracers and major ions were analyzed before the overcoring at 728 days. The OPA samples obtained through overcoring were systematically analyzed and the chemical compositions dissolved in the pore water and sorbed on the solid materials along the radial directions were obtained. The readers are referred to the technical report NWMO-TR-2014-25 by Xie et al. (2014) for detailed information of the experiments. Due to the fact that Co and Sr are mainly retarded through strong sorption (with K_d sorption model), while the retardation of Cs is dominated by multisite ion exchange model (MIE), two separate simulations were undertaken for each experiment using K_d sorption model or MIE model, respectively.

A selection of six numerical simulations for the experiments are listed in Table 4.1.

Table 4.1: List of validation cases in Mont Terri in-situ diffusion experiments

Example Name	Description of Main Features	Section
mtterri01	In-situ diffusion experiment in clay	4.1.1
mtterri01Cs	In-situ diffusion experiment in clay (MIE model)	4.1.2
mtterri02	Effect of chemical perturbation on diffusion and retardation in clay	4.1.3
mtterri02Cs	Effect of chemical perturbation on diffusion and retardation in clay (MIE model)	4.1.4
mttoc	Back diffusion during overcoring	4.1.5
mttocCs	Back diffusion during overcoring (MIE model)	4.1.6

The concentration profiles of all aqueous species consistently showed a signal of back diffusion from the OPA towards the borehole, which was caused by the presence of

porewater in the space above the packer, which could not be removed before the overcoring. Consequently, this water gathered at the bottom of the borehole after retrieving the equipment. Most probably, this water was original formation water as listed in Table 4.3 (Xie et al. 2014). Water of this composition was used to simulate the impact of the overcoring process on the concentration distributions.

4.1.1 IN-SITU DIFFUSION EXPERIMENT IN CLAY

4.1.1.1 Problem definition

This example is to validate tracer diffusion and retardation in low permeable porous media through the comparison of the simulated results to the in-situ diffusion experiment data (Phase I).

4.1.1.2 Model setup

The diffusion of the tracers from the injection solution into the surrounding media can be represented by a 1D axial symmetric model, as shown in Figure 4.1.

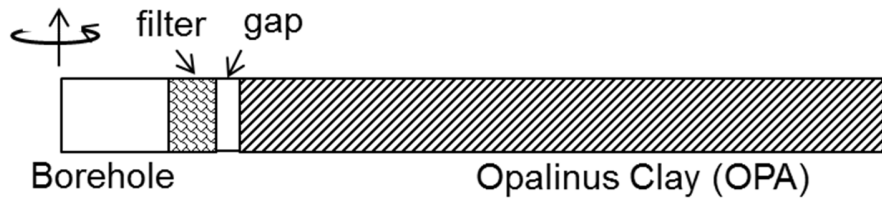


Figure 4.1: Schematic Diagram of the Simulation Domain Representing the Experimental Set-up Including the Inner Borehole (Radius= 3.1 cm) that Contains the Tracers in Solution, Filter (4 mm in Thickness), Gap (3 mm in Thickness), and OPA up to a Radius of 61.5 cm. The Thickness of the Test Chamber is $h = 1.04$ m. A Radial Coordinate System was Used for the Simulations.

The anisotropic diffusion properties of the Opalinus Clay (OPA) at Mont Terri with a dip angle of 30 - 35° (averaging 32.5°) can be accounted through a geometric transformation (Xie et al. 2014). The equivalent outer radius of each segment in the borehole (i.e., r'_{iBH} for circulation chamber, r'_F for filter, and r'_{Gap} for gap) as well as the equivalent borehole capacity (α') can be calculated for the cases including a filter and gap (Table 4.2). In MIN3P-THCm, the borehole capacity is described by an effective porosity that represents the total tracer mass in the circulation chamber and tracer circulation system. Physically, α' is equivalent to the ratio between the total circulation solution volume and the volume of the circulation chamber.

The problem was simulated in a 0.615 m long, one-dimensional in radial coordinate, horizontal domain, including borehole, filter, gap and Opalinus Clay (OPA). The domain

Validation report-page# 4-229

was discretized into 165 control volumes. The geometry and discretization are used for the following five examples to simulate the in-situ diffusion and retardation experiments at Mont Terri test site.

Table 4.2: Calculated Equivalent Outer Radius of Circulation Chamber (r'_{iBH}), Filter (r'_F), and Gap (r'_{Gap}) and Borehole Capacity of the Circulation Chamber (α')

r_{iBH}	r'_{iBH}	r'_F	r'_{Gap}	α'
[m]	[m]	[m]	[m]	[-]
0.031	0.0339	0.0383	0.0416	3.567

r_{iBH} – actual radius of the circulation chamber

The flow field is set as a pure diffusion condition without advection. The initial geochemical concentrations of the major ions for the entire domain are set as listed in Table 4.3. The initial concentrations of the tracers HTO, Cs⁺, ⁸⁵Sr²⁺, ⁶⁰Co²⁺, I⁻ and Br⁻ in the borehole are as listed in Table 4.4 at time 0.0. For the rest of the domain, the tracers are assumed non-existing at the beginning of the experiment.

Table 4.3: Composition of the Synthetic OPA Porewater Used in the DR-A Diffusion and Sorption Experiment - Phase I (van Loon et al. 2003)

Element	Total concentration [mol L ⁻¹]
Na ⁺	2.40×10 ⁻⁰¹
K ⁺	1.60×10 ⁻⁰³
Mg ²⁺	1.70×10 ⁻⁰²
Ca ²⁺	2.60×10 ⁻⁰²
Sr ²⁺	5.10×10 ⁻⁰⁴
Cl ⁻	3.00×10 ⁻⁰¹
SO ₄ ²⁻	1.40×10 ⁻⁰²
CO ₃ ²⁻ /HCO ₃ ⁻	4.76×10 ⁻⁰⁴
pH	7.6
Sum of cations	0.328 eq L ⁻¹
Sum of anions	0.328 eq L ⁻¹
Ionic strength	0.39 mol L ⁻¹

4.1.1.3 Experimental data

The concentrations of all tracers in the tank were analyzed at designated intervals. The

Validation report-page# 4-230

measured results, after making any necessary corrections for decay, are listed in Table 4.4. The concentrations of major ions were measured at the beginning of the experiment and at 168.8 days only, because they were in equilibrium with the OPA and thus expected to be unchanged, which was confirmed by the test results (Xie et al. 2014).

Table 4.4: Measured Tracer Concentrations [mol L⁻¹] during the DR-A In-situ Diffusion Experiment - Phase I (Xie et al. 2014)

Time	Cs ⁺	HTO	⁸⁵ Sr ²⁺	⁶⁰ Co ²⁺	I ⁻	Br ⁻
0.0	2.09×10 ⁻⁰⁴	1.20×10 ⁻¹⁰	5.88×10 ⁻¹⁴	2.18×10 ⁻¹³	1.11×10 ⁻⁰²	1.11×10 ⁻⁰²
0.1	1.81×10 ⁻⁰⁴	1.11×10 ⁻¹⁰	5.81×10 ⁻¹⁴	1.92×10 ⁻¹³	1.04×10 ⁻⁰²	1.05×10 ⁻⁰²
0.3	1.45×10 ⁻⁰⁴	1.08×10 ⁻¹⁰	5.27×10 ⁻¹⁴	1.55×10 ⁻¹³	1.00×10 ⁻⁰²	1.01×10 ⁻⁰²
0.9	1.15×10 ⁻⁰⁴	1.05×10 ⁻¹⁰	5.19×10 ⁻¹⁴	1.23×10 ⁻¹³	1.00×10 ⁻⁰²	1.02×10 ⁻⁰²
1.2	1.02×10 ⁻⁰⁴	1.05×10 ⁻¹⁰	5.00×10 ⁻¹⁴	1.10×10 ⁻¹³	9.95×10 ⁻⁰³	1.00×10 ⁻⁰²
2.0	8.73×10 ⁻⁰⁵	1.06×10 ⁻¹⁰	4.95×10 ⁻¹⁴	9.04×10 ⁻¹⁴	9.94×10 ⁻⁰³	1.00×10 ⁻⁰²
3.0	7.67×10 ⁻⁰⁵	1.04×10 ⁻¹⁰	4.92×10 ⁻¹⁴	7.92×10 ⁻¹⁴	9.81×10 ⁻⁰³	9.98×10 ⁻⁰³
4.0	6.74×10 ⁻⁰⁵	1.04×10 ⁻¹⁰	4.81×10 ⁻¹⁴	7.04×10 ⁻¹⁴	9.88×10 ⁻⁰³	9.95×10 ⁻⁰³
5.0	6.11×10 ⁻⁰⁵	1.03×10 ⁻¹⁰	4.68×10 ⁻¹⁴	6.23×10 ⁻¹⁴	9.79×10 ⁻⁰³	9.90×10 ⁻⁰³
7.0	5.08×10 ⁻⁰⁵	1.01×10 ⁻¹⁰	4.70×10 ⁻¹⁴	5.39×10 ⁻¹⁴	9.77×10 ⁻⁰³	9.87×10 ⁻⁰³
10.0	4.27×10 ⁻⁰⁵	9.92×10 ⁻¹¹	4.40×10 ⁻¹⁴	4.71×10 ⁻¹⁴	9.63×10 ⁻⁰³	9.71×10 ⁻⁰³
14.0	3.52×10 ⁻⁰⁵	9.77×10 ⁻¹¹	4.25×10 ⁻¹⁴	3.87×10 ⁻¹⁴	9.58×10 ⁻⁰³	9.66×10 ⁻⁰³
21.0	2.84×10 ⁻⁰⁵	9.61×10 ⁻¹¹	4.01×10 ⁻¹⁴	2.87×10 ⁻¹⁴	9.56×10 ⁻⁰³	9.65×10 ⁻⁰³
29.0	2.20×10 ⁻⁰⁵	9.49×10 ⁻¹¹	3.76×10 ⁻¹⁴	2.11×10 ⁻¹⁴	9.46×10 ⁻⁰³	9.55×10 ⁻⁰³
43.0	1.74×10 ⁻⁰⁵	9.28×10 ⁻¹¹	3.49×10 ⁻¹⁴	1.02×10 ⁻¹⁴	9.43×10 ⁻⁰³	9.50×10 ⁻⁰³
63.0	1.28×10 ⁻⁰⁵	8.92×10 ⁻¹¹	3.14×10 ⁻¹⁴	7.96×10 ⁻¹⁵	9.19×10 ⁻⁰³	9.24×10 ⁻⁰³
85.4	-	-	2.93×10 ⁻¹⁴	u.d.	9.07×10 ⁻⁰³	9.05×10 ⁻⁰³
113.0	-	8.67×10 ⁻¹¹	2.77×10 ⁻¹⁴	-	8.87×10 ⁻⁰³	8.94×10 ⁻⁰³
168.8	6.66×10 ⁻⁰⁶	8.17×10 ⁻¹¹	2.37×10 ⁻¹⁴	-	8.46×10 ⁻⁰³	8.69×10 ⁻⁰³

- Not measured, u.d. – under detection limit

Validation report-page# 4-231

4.1.1.4 Parameters

Key modeling parameters used in the simulations are listed in Table 4.5. The final simulation time was 189 days.

Table 4.5: General parameters for the circulation chamber, filter, gap and OPA

Parameter	Borehole	Filter	Gap	OPA
Porosity [-]	3.262 ^a	0.45	1.0	0.15
Solid dry bulk density [kg/m ³]	-	-	-	2310.0 ^b

^a borehole capacity ^b Bossart (2013)

The free aqueous diffusion coefficients D_0 listed in Table 4.6 were used; these were obtained from the CRC Handbook of Chemistry and Physics (Lide et al., 1994). The effective tortuosity of OPA in 0.12 is a fitted parameter based on the measured HTO concentration time curve. Selected effective porosity correction factor ($f_{\phi,j}^c$) and effective tortuosity factor ($f_{\tau,j}^c$) for the primary species are listed in Table 4.6, in which the $f_{\phi,j}^c$ factors for I^- and Br^- are the measured effective porosity values for I^- (0.08) and Br^- (0.10) divided by the effective porosity measured through uncharged HTO (0.15) (van Loon et al., 2003). The effective porosity correction factors for all secondary species $f_{\phi,j}^x$ are set to 0.667 for all anions and 1.0 for other species. The effective tortuosity correction factors $f_{\tau,j}^x$ for secondary species are 1.0.

Table 4.6: Free aqueous phase diffusion coefficients (D_0) (Lide et al., 1994), correction factors $f_{\phi,j}^c$ and $f_{\tau,j}^c$ (Xie et al. 2014)

Species	$D_0 \times 10^{-9}$ m ² s ⁻¹	$f_{\phi,j}^c$	$f_{\tau,j}^c$	Species	$D_0 \times 10^{-9}$ m ² s ⁻¹	$f_{\phi,j}^c$	$f_{\tau,j}^c$
H^+	9.311	1.0	1.0	SO_4^{2-}	1.065	0.667	0.30
Na^+	1.334	1.0	1.0	CO_3^{2-}	0.923	0.667	1.0
K^+	1.957	1.0	1.0	I^-	2.045	0.533	0.50
Mg^{2+}	0.706	1.0	1.0	Br^-	2.08	0.533	0.30
Ca^{2+}	0.792	1.0	1.0	HTO	2.23#	1.0	1.0
$^{85}\text{Sr}^{2+}$	0.791	1.0	3.5	Cl^-	2.032	0.667	1.0
$^{60}\text{Co}^{2+}$	0.732	1.0	10.0	Cs^+	2.056	1.0	5.4

from O'Reilly & Peterson 1971

The linear sorption coefficients (K_d) of tracers $^{85}\text{Sr}^{2+}$ and $^{60}\text{Co}^{2+}$ are 1.0 kg L⁻¹ and 200.0 kg L⁻¹, respectively (Wersin et al. (2008)).

4.1.1.5 Results

Simulated results showed that all tracers diffuse through the filter, gap and into the Opalinus Clay. After 189 days, the moving fronts of all tracers are less than 0.3 m. The uncharged HTO diffuses the fastest, while other tracers were retarded through anion exclusion (I^- and Br^-) or sorption ($^{60}\text{Co}^{2+}$ and $^{85}\text{Sr}^{2+}$). Simulated concentration time curves of tracers showed good agreement to the measured data (Figure 4.2).

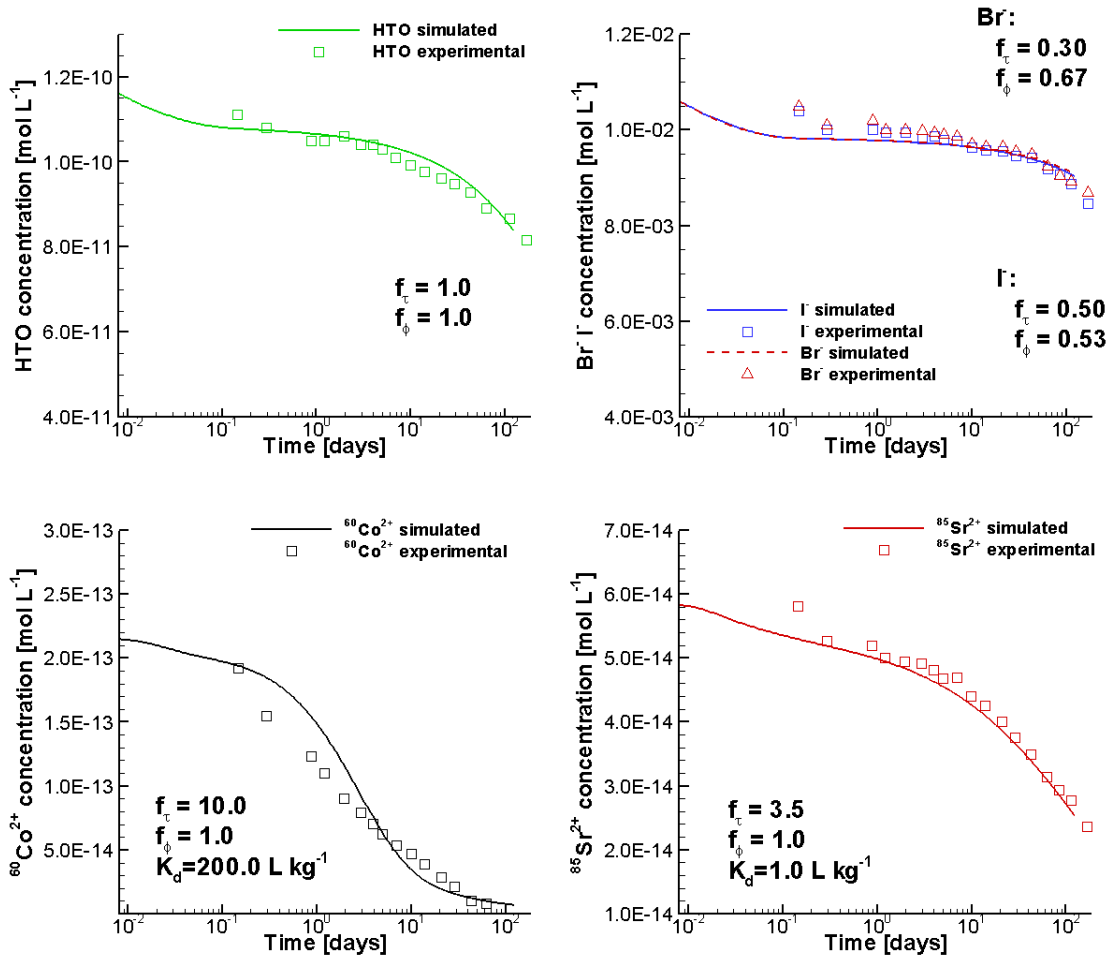


Figure 4.2: Comparison of Simulated (Lines) and Experimental (Symbols) Concentration Time Curves for HTO, Br^- , I^- , $^{60}\text{Co}^{2+}$ and $^{85}\text{Sr}^{2+}$ in the Borehole Solution during the DR-A Field Diffusion Experiment Phase I (Xie et al. 2014)

4.1.1.6 File location

Input file: .\Benchmark\ benchmarks_new_add\MtTerri-V1.0.409\mtterri01.dat

Databases: .\Benchmark\ benchmarks_new_add\MtTerri-V1.0.409\database\

4.1.2 IN-SITU DIFFUSION EXPERIMENT IN CLAY (MIE MODEL)

4.1.2.1 Problem definition

This example is to validate tracer diffusion and retardation (multisite ion exchange model for Cs) in low permeable porous media through the comparison of the simulated results to the in-situ diffusion experiment data (Phase I).

4.1.2.2 Model setup

The model set up, including the geometry, initial and boundary conditions for flow and reactive transport, is exactly the same as the example ‘in-situ diffusion experiment in clay’ in section 4.1.1. The only difference is the use of multisite ion exchange model to simulate the retardation process instead of the linear sorption model (Xie et al. 2014).

4.1.2.3 Parameters

The key parameters for the simulation are the same as described in section 4.1.1.4. Additional parameters for the multisite ion exchange model are listed in Table 4.7 (van Loon et al. 2009 with modification by Gimmi 2012). Illite in the OPA provides different types of ion exchange sites that control the retardation of Cs⁺ along with associated cations while diffusing through the OPA clay (van Loon et al. 2009). Three sites are taken into accounts including the strong sorbing sites (Frayed edge sites) with the highest selectivity coefficient but the least in quantity (i.e. 0.101% of the total CEC), the weak sorbing sites (planar sites) with the lowest selectivity coefficient but the most abundant (i.e. 91.779% of the CEC), and the intermediate sorbing site (Type II).

Table 4.7: Parameters for the Generalized Cs⁺ Cation Exchange Model for Illite (van Loon et al. 2009; as Modified by Gimmi 2012)

Site types	Site capacity
Frayed edge sites (FES)	0.101% of the CEC
Type II sites (II)	8.12% of the CEC
Planar sites (PS)	91.779% of the CEC
<i>CEC of illite</i>	<i>0.1035 eq kg⁻¹ (=10.35 meq (100g)⁻¹)</i>
Cation exchange reactions	Selectivity coefficients (log K _s)
Na-FES + Cs ⁺ ⇌ Cs-FES + Na ⁺	7.0
Na-FES + K ⁺ ⇌ K-FES + Na ⁺	2.4
K-FES + Cs ⁺ ⇌ Cs-FES + K ⁺	4.6
Na-II + Cs ⁺ ⇌ Cs-II + Na ⁺	3.2
Na-II + K ⁺ ⇌ K-II + Na ⁺	2.1
K-II + Cs ⁺ ⇌ Cs-II + K ⁺	1.1
Na-PS + Cs ⁺ ⇌ Cs-PS + Na ⁺	1.6
Na-PS + K ⁺ ⇌ K-PS + Na ⁺	1.1
K-PS + Cs ⁺ ⇌ Cs-PS + K ⁺	0.5
2Na-PS + Ca ²⁺ ⇌ Ca-PS ₂ + 2Na ⁺	0.67
2Na-PS + Mg ²⁺ ⇌ Mg-PS ₂ + 2Na ⁺	0.59
2Na-PS + Sr ²⁺ ⇌ Sr-PS ₂ + 2Na ⁺	0.59

4.1.2.4 Results

When the Cs⁺ in the borehole reaches the OPA clay, it is partially sorbed on the three ion exchange sites. The higher the Cs⁺ concentration, the more will be sorbed on the clay. At 10 days the diffusion front of Cs⁺ reached about 0.045m (Figure 4.3 left). The concentration of sorbed Cs on Type-II sites (Cs-II) in the OPA clay on the borehole wall is the highest with up to 0.103 meq/100g bulk and decreasing along the radial axis outwards. Similarly, the concentration of Cs-PS is up to 0.03 meq/100g bulk and deceasing along the radial axis outwards. The concentration of sorbed Cs-FES is up to 0.01 meq/100g bulk but decreasing only slightly along the radial axis and then drops sharply until approaching the diffusion front. This is because FES sites have the highest selectivity coefficient and thus tend to sorb the Cs even at a lower Cs⁺ concentration in the porewater and thus FES sites can easily reach their maximum sorption capacity. With the on-going diffusion process, the concentration of Cs⁺ in the borehole decreases and the diffusion front moves outwards (Figure 4.3 right). Consequently, the concentrations of the sorbed Cs species in the OPA clay at the borehole wall decrease as well. By the end of the Phase I experiment at 189 days, the maximum concentrations of sorbed Cs-II and Cs-PS are 0.02 and 0.005 meq/100g bulk, respectively. However, the maximum concentrations of sorbed Cs-FES drops only slightly.

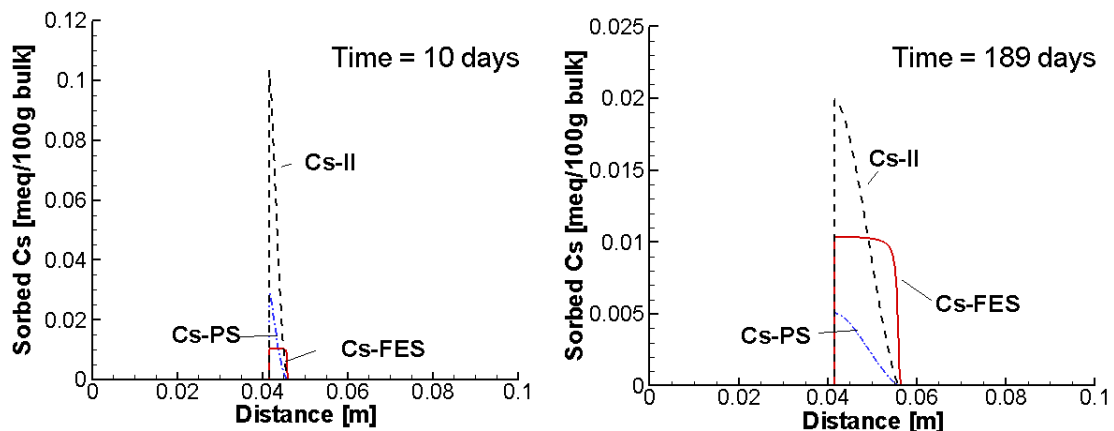


Figure 4.3: Concentration profiles of sorbed Cs on three sites at 10 days (left) and 189 days (right) (solid red line – Cs-FES, dashed black line – Cs-II, dash dot blue line – Cs-PS) (Xie et al. 2014)

The measured data showed that the concentration of Cs⁺ in the borehole drops very fast within the first day. Simulated concentration time curves of Cs⁺ showed good agreement to the measured data (Figure 4.4).

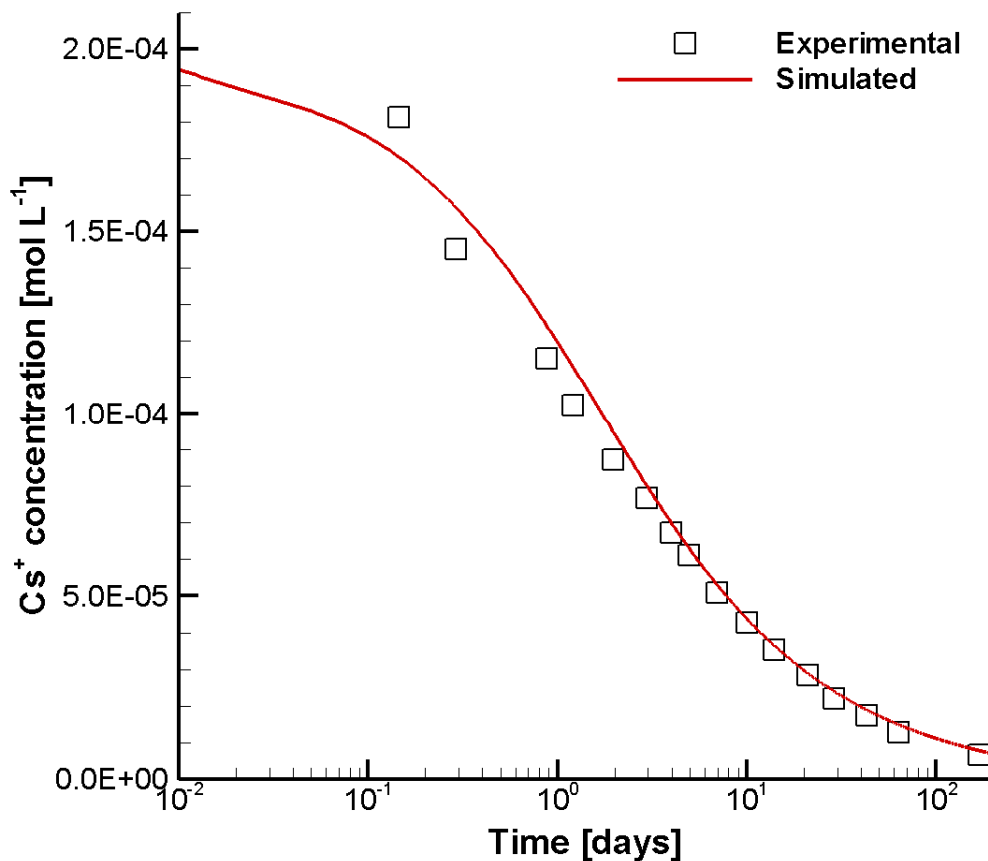


Figure 4.4: Comparison of Simulated (Lines) and Experimental (Symbols) Concentration Time Curve for Cs⁺ in the Borehole Solution during the DR-A Field Diffusion Experiment Phase I (Xie et al. 2014)

4.1.2.5 File location

Input file:

.\Benchmark\ benchmarks_new_add\MtTerri-V1.0.409\mtterri01Cs.dat

Databases:

.\Benchmark\ benchmarks_new_add\MtTerri-V1.0.409\database\

Validation report-page# 4-236

4.1.3 EFFECT OF CHEMICAL PERTURBATION ON DIFFUSION AND RETARDATION IN CLAY

4.1.3.1 Problem definition

This example is to validate the effect of chemical perturbation on tracer diffusion and retardation in low permeable porous media through the comparison of simulated and in-situ diffusion experiment data (Phase II).

4.1.3.2 Model setup

The diffusion of the tracers from the injection solution into the surrounding media can be represented by a 1D axial symmetric model, as shown in Figure 4.1 and Table 4.2.

The problem was simulated in a 0.615 m long, one-dimensional in radial coordinate, horizontal domain, including borehole, filter, gap and Opalinus Clay (OPA) (detailed information see section 4.1.1.2).

Phase II of the DR-A in-situ diffusion test was conducted immediately after the first phase, beginning at 189 days, by changing the circulation solution to a solution with much higher concentrations of Cl^- , Na^+ and K^+ , and a much lower concentration of SO_4^{2-} (to create a higher ionic strength solution perturbation) (Table 4.8). A spike of 3.64 Bq/g was also added for $^{85}\text{Sr}^{2+}$. All other tracers remained at the same concentrations as measured just before the exchange of the solution.

Table 4.8: Composition of the Synthetic OPA Porewater Used in the DR-A Diffusion and Sorption Experiment - Phase II (Xie et al. 2014)

Element	Total concentration [mol L ⁻¹]
Na^+	5.00×10^{-1}
K^+	5.60×10^{-1}
Mg^{2+}	1.47×10^{-2}
Ca^{2+}	2.30×10^{-2}
Sr^{2+}	4.49×10^{-4}
Cl^-	1.15
SO_4^{2-}	2.37×10^{-4}
$\text{CO}_3^{2-}/\text{HCO}_3^-$	4.76×10^{-4}
pH	7.6
Sum cations	1.14 eq L ⁻¹
Sum anions	1.15 eq L ⁻¹
Ionic strength	1.18 mol L ⁻¹

To simulate the replacement of the solution in the borehole, a restart file restart.dat is generated using the restart.tmp2 file at 189 days for the Phase I simulation (section 4.1.1) and replaced the chemical compositions of the ions in the control volumes within the borehole (for major ions with the data in Table 4.8, for tracers with the data at 168.8 in Table 4.4).

4.1.3.3 Experimental data

The concentrations of the major ions and all tracers in the tank were analyzed at designated intervals. The measured results until 728.9 days, after making any necessary corrections for decay, are listed in Table 4.9 and Table 4.10, respectively.

Table 4.9: Measured Major Ion Concentrations [mol L⁻¹] in the Circulation Solution during the DR-A In-situ Diffusion Experiment Phase II until Overcoring (Xie et al. 2014)

Time [days]	Ca ²⁺	Mg ²⁺	Na ⁺	K ⁺	Cl ⁻	SO ₄ ²⁻	Sr ²⁺
189.2	2.30×10 ⁻⁰²	1.47×10 ⁻⁰²	5.05×10 ⁻⁰¹	5.60×10 ⁻⁰¹	1.16	2.37×10 ⁻⁰⁴	4.50×10 ⁻⁰⁴
189.3	-	-	5.00×10 ⁻⁰¹	5.60×10 ⁻⁰¹	1.15	2.37×10 ⁻⁰⁴	4.50×10 ⁻⁰⁴
189.9	-	-	-	-	-	1.00×10 ⁻⁰³	-
190.1	-	-	-	-	-	1.09×10 ⁻⁰³	-
190.2	-	-	-	-	-	1.41×10 ⁻⁰³	-
190.9	-	-	4.78×10 ⁻⁰¹	4.83×10 ⁻⁰¹	1.05	1.49×10 ⁻⁰³	5.19×10 ⁻⁰⁴
191.2	2.99×10 ⁻⁰²	2.07×10 ⁻⁰²	-	-	-	1.58×10 ⁻⁰³	-
192.9	2.55×10 ⁻⁰²	1.72×10 ⁻⁰²	4.92×10 ⁻⁰¹	4.65×10 ⁻⁰¹	1.05	1.72×10 ⁻⁰³	6.55×10 ⁻⁰⁴
195.9	3.19×10 ⁻⁰²	2.14×10 ⁻⁰²	-	-	-	1.90×10 ⁻⁰³	-
200.0	2.77×10 ⁻⁰²	1.88×10 ⁻⁰²	4.78×10 ⁻⁰¹	4.09×10 ⁻⁰¹	1.02	2.03×10 ⁻⁰³	6.54×10 ⁻⁰⁴
204.2	2.84×10 ⁻⁰²	1.95×10 ⁻⁰²	4.78×10 ⁻⁰¹	3.96×10 ⁻⁰¹	1.01	2.20×10 ⁻⁰³	6.84×10 ⁻⁰⁴
206.9	-	-	-	-	-	2.35×10 ⁻⁰³	-
213.9	2.94×10 ⁻⁰²	2.00×10 ⁻⁰²	4.78×10 ⁻⁰¹	3.81×10 ⁻⁰¹	1.02	2.56×10 ⁻⁰³	7.02×10 ⁻⁰⁴
220.8	-	-	-	-	-	2.68×10 ⁻⁰³	-
234.8	3.37×10 ⁻⁰²	2.51×10 ⁻⁰²	5.00×10 ⁻⁰¹	3.53×10 ⁻⁰¹	1.01	3.29×10 ⁻⁰³	8.16×10 ⁻⁰⁴
291.1	3.94×10 ⁻⁰²	2.99×10 ⁻⁰²	5.09×10 ⁻⁰¹	2.92×10 ⁻⁰¹	9.79×10 ⁻⁰¹	3.82×10 ⁻⁰³	1.15×10 ⁻⁰³
322.9	3.54×10 ⁻⁰²	2.26×10 ⁻⁰²	3.85×10 ⁻⁰¹	2.74×10 ⁻⁰¹	1.06	4.82×10 ⁻⁰³	9.64×10 ⁻⁰⁴
353.2	3.94×10 ⁻⁰²	3.18×10 ⁻⁰²	5.13×10 ⁻⁰¹	2.49×10 ⁻⁰¹	8.63×10 ⁻⁰¹	4.02×10 ⁻⁰³	1.09×10 ⁻⁰³
385.8	3.92×10 ⁻⁰²	3.45×10 ⁻⁰²	5.31×10 ⁻⁰¹	2.33×10 ⁻⁰¹	8.52×10 ⁻⁰¹	3.95×10 ⁻⁰³	1.14×10 ⁻⁰³
412.9	4.17×10 ⁻⁰²	3.43×10 ⁻⁰²	5.05×10 ⁻⁰¹	2.06×10 ⁻⁰¹	8.57×10 ⁻⁰¹	4.65×10 ⁻⁰³	1.15×10 ⁻⁰³
535.1	4.54×10 ⁻⁰²	3.45×10 ⁻⁰²	4.52×10 ⁻⁰¹	1.44×10 ⁻⁰¹	7.93×10 ⁻⁰¹	4.89×10 ⁻⁰³	1.24×10 ⁻⁰³
563.9	4.49×10 ⁻⁰²	3.71×10 ⁻⁰²	5.26×10 ⁻⁰¹	1.54×10 ⁻⁰¹	7.62×10 ⁻⁰¹	5.02×10 ⁻⁰³	1.42×10 ⁻⁰³
597.1	4.44×10 ⁻⁰²	3.83×10 ⁻⁰²	5.00×10 ⁻⁰¹	1.37×10 ⁻⁰¹	8.26×10 ⁻⁰¹	5.29×10 ⁻⁰³	1.48×10 ⁻⁰³
662.1	4.54×10 ⁻⁰²	3.95×10 ⁻⁰²	5.22×10 ⁻⁰¹	1.29×10 ⁻⁰¹	7.31×10 ⁻⁰¹	4.98×10 ⁻⁰³	1.52×10 ⁻⁰³
692.1	4.32×10 ⁻⁰²	4.01×10 ⁻⁰²	5.31×10 ⁻⁰¹	1.24×10 ⁻⁰¹	7.50×10 ⁻⁰¹	5.26×10 ⁻⁰³	1.54×10 ⁻⁰³
717.9	4.77×10 ⁻⁰²	4.03×10 ⁻⁰²	5.18×10 ⁻⁰¹	1.17×10 ⁻⁰¹	7.19×10 ⁻⁰¹	5.12×10 ⁻⁰³	1.54×10 ⁻⁰³
728.9	4.28×10 ⁻⁰²	3.92×10 ⁻⁰²	4.87×10 ⁻⁰¹	1.09×10 ⁻⁰¹	7.71×10 ⁻⁰¹	5.01×10 ⁻⁰³	1.49×10 ⁻⁰³

Not measured. Note: The major ions were analyzed by Bachema AG (Fierz and Rosli 2012).

Validation report-page# 4-238

Table 4.10: Measured Tracer Concentrations [mol L⁻¹] in the Circulation Solution during the DR-A In-situ Diffusion Experiment - Phase II until Overcoring (Xie et al. 2014)

Time [days]	HTO	⁸⁵ Sr ²⁺	⁶⁰ Co ²⁺	I ⁻	Br ⁻
189.2	-	-	-	-	-
189.3	-	-	-	-	-
e	7.80×10 ⁻¹¹	5.42×10 ⁻¹⁴	n.d.	8.60×10 ⁻⁰³	8.86×10 ⁻⁰³
189.9	-	-	-	-	-
189.8	7.93×10 ⁻¹¹	5.08×10 ⁻¹⁴	n.d.	8.63×10 ⁻⁰³	8.91×10 ⁻⁰³
190.1	7.72×10 ⁻¹¹	4.99×10 ⁻¹⁴	n.d.	8.50×10 ⁻⁰³	8.87×10 ⁻⁰³
190.2	-	-	-	-	-
190.3	7.80×10 ⁻¹¹	4.89×10 ⁻¹⁴	n.d.	8.48×10 ⁻⁰³	8.80×10 ⁻⁰³
190.9	-	-	-	-	-
190.8	8.04×10 ⁻¹¹	4.82×10 ⁻¹⁴	n.d.	8.65×10 ⁻⁰³	8.87×10 ⁻⁰³
191.2	-	-	-	-	-
e	7.82×10 ⁻¹¹	4.81×10 ⁻¹⁴	n.d.	8.68×10 ⁻⁰³	8.88×10 ⁻⁰³
192.9	-	-	-	-	-
192.9	7.73×10 ⁻¹¹	4.78×10 ⁻¹⁴	n.d.	8.68×10 ⁻⁰³	8.86×10 ⁻⁰³
195.9	7.64×10 ⁻¹¹	4.64×10 ⁻¹⁴	n.d.	8.50×10 ⁻⁰³	8.90×10 ⁻⁰³
199.9	7.54×10 ⁻¹¹	4.69×10 ⁻¹⁴	n.d.	8.60×10 ⁻⁰³	8.63×10 ⁻⁰³
200.0	-	-	-	-	-
204.2	7.67×10 ⁻¹¹	4.62×10 ⁻¹⁴	n.d.	-	-
206.9	-	-	-	-	-
206.9	7.57×10 ⁻¹¹	4.71×10 ⁻¹⁴	n.d.	8.71×10 ⁻⁰³	8.72×10 ⁻⁰³
213.9	-	-	-	-	-
214.0	7.43×10 ⁻¹¹	4.70×10 ⁻¹⁴	n.d.	7.89×10 ⁻⁰³	8.61×10 ⁻⁰³
220.8	-	-	-	-	-
221.2	7.29×10 ⁻¹¹	4.66×10 ⁻¹⁴	n.d.	8.08×10 ⁻⁰³	8.74×10 ⁻⁰³
234.8	-	-	-	-	-
234.9	7.05×10 ⁻¹¹	4.43×10 ⁻¹⁴	n.d.	7.87×10 ⁻⁰³	8.31×10 ⁻⁰³
291.1	6.73×10 ⁻¹¹	4.12×10 ⁻¹⁴	n.d.	8.02×10 ⁻⁰³	8.16×10 ⁻⁰³
322.9	6.13×10 ⁻¹¹	4.12×10 ⁻¹⁴	n.d.	7.72×10 ⁻⁰³	7.84×10 ⁻⁰³
353.1	6.00×10 ⁻¹¹	3.96×10 ⁻¹⁴	n.d.	7.27×10 ⁻⁰³	7.63×10 ⁻⁰³
353.2	-	-	-	-	-
385.8	5.81×10 ⁻¹¹	3.53×10 ⁻¹⁴	n.d.	7.00×10 ⁻⁰³	7.27×10 ⁻⁰³
412.9	5.67×10 ⁻¹¹	3.70×10 ⁻¹⁴	n.d.	6.79×10 ⁻⁰³	7.39×10 ⁻⁰³
535.1	5.03×10 ⁻¹¹	3.75×10 ⁻¹⁴	n.d.	6.27×10 ⁻⁰³	7.56×10 ⁻⁰³
563.9	4.82×10 ⁻¹¹	3.18×10 ⁻¹⁴	n.d.	6.05×10 ⁻⁰³	7.51×10 ⁻⁰³
597.1	4.75×10 ⁻¹¹	2.99×10 ⁻¹⁴	n.d.	6.72×10 ⁻⁰³	6.80×10 ⁻⁰³
662.1	4.48×10 ⁻¹¹	3.83×10 ⁻¹⁴	n.d.	5.96×10 ⁻⁰³	6.34×10 ⁻⁰³
692.1	4.32×10 ⁻¹¹	2.87×10 ⁻¹⁴	n.d.	5.85×10 ⁻⁰³	6.00×10 ⁻⁰³
717.9	4.20×10 ⁻¹¹	2.82×10 ⁻¹⁴	n.d.	6.15×10 ⁻⁰³	6.41×10 ⁻⁰³
728.9	-	-	-	6.39×10 ⁻⁰³	6.26×10 ⁻⁰³

- Not measured, n.d. - not detected. Note: The tracers were analyzed by PSI (Fierz and Rosli 2012).

4.1.3.4 Parameters

Key modeling parameters used in the simulations are listed in Table 4.11. The simulation time was from 189 to 728 days.

Table 4.11: General parameters for the circulation chamber, filter, gap and OPA

Parameter	Borehole	Filter	Gap	OPA
Porosity [-]	3.262 ^a	0.45	1.0	0.19
Solid dry bulk density [kg/m ³]	-	-	-	2310.0 ^b

^a borehole capacity ^b Bossart (2013)

The free aqueous diffusion coefficients D₀ listed in Table 4.6 were used; these were obtained from the CRC Handbook of Chemistry and Physics (Lide et al., 1994). The effective tortuosity of OPA in 0.19 is a fitted parameter based on the measured HTO concentration time curve. This value increases from 0.12 (Phase I) to 0.19 (Phase II) due to the increase of the ionic strength increase from 0.39 (Phase I, Table 4.3) to 1.18 (Phase II, Table 4.8). Selected effective porosity correction factor ($f_{\phi,j}^c$) and effective tortuosity factor ($f_{\tau,j}^c$) for the primary species in OPA are listed in Table 4.12. The effective porosity correction factors for all secondary species $f_{\phi,j}^x$ are set to 0.667 for all anions and 1.0 for other species. The effective tortuosity correction factors $f_{\tau,j}^x$ for secondary species are 1.0.

Table 4.12: Free aqueous phase correction factors $f_{\phi,j}^c$ and $f_{\tau,j}^c$

Species	$f_{\phi,j}^c$	$f_{\tau,j}^c$	Species	$f_{\phi,j}^c$	$f_{\tau,j}^c$
H ⁺	1.0	1.0	SO ₄ ²⁻	0.67	0.38
Na ⁺	1.0	1.0	CO ₃ ²⁻	0.67	0.38
K ⁺	1.0	1.0	I ⁻	0.53	0.55
Mg ²⁺	1.0	1.0	Br ⁻	0.67	0.38
Ca ²⁺	1.0	1.0	HTO	1.0	1.0
⁸⁵ Sr ²⁺	1.0	1.0	⁶⁰ Co ²⁺	1.0	10.0

The linear sorption coefficients (K_d) of tracers ⁸⁵Sr²⁺ and ⁶⁰Co²⁺ are 1.0 kg L⁻¹ and 200.0 kg L⁻¹, respectively (Wersin et al. 2008).

4.1.3.5 Results

Experimental results showed that the tracer ⁸⁵Sr²⁺ with elevated concentration, similar to Phase I experiment, drops sharply within the first day of the Phse II experiment (Figure 4.5). Even tracer HTO showed also a rapid drop shortly after the solution exchange in the borehole (Figure 4.5). The concentration of ⁶⁰Co²⁺ couldn't be detected during the Phse II experiment. The concentration of all detectable tracers showed a gentle decrease with time but with a decreasing rate. Simulated concentration time curves of tracers

Validation report-page# 4-240

using elevated effective porosity and tortuosity for the OPA clay showed good agreement to the measured data (Figure 4.5).

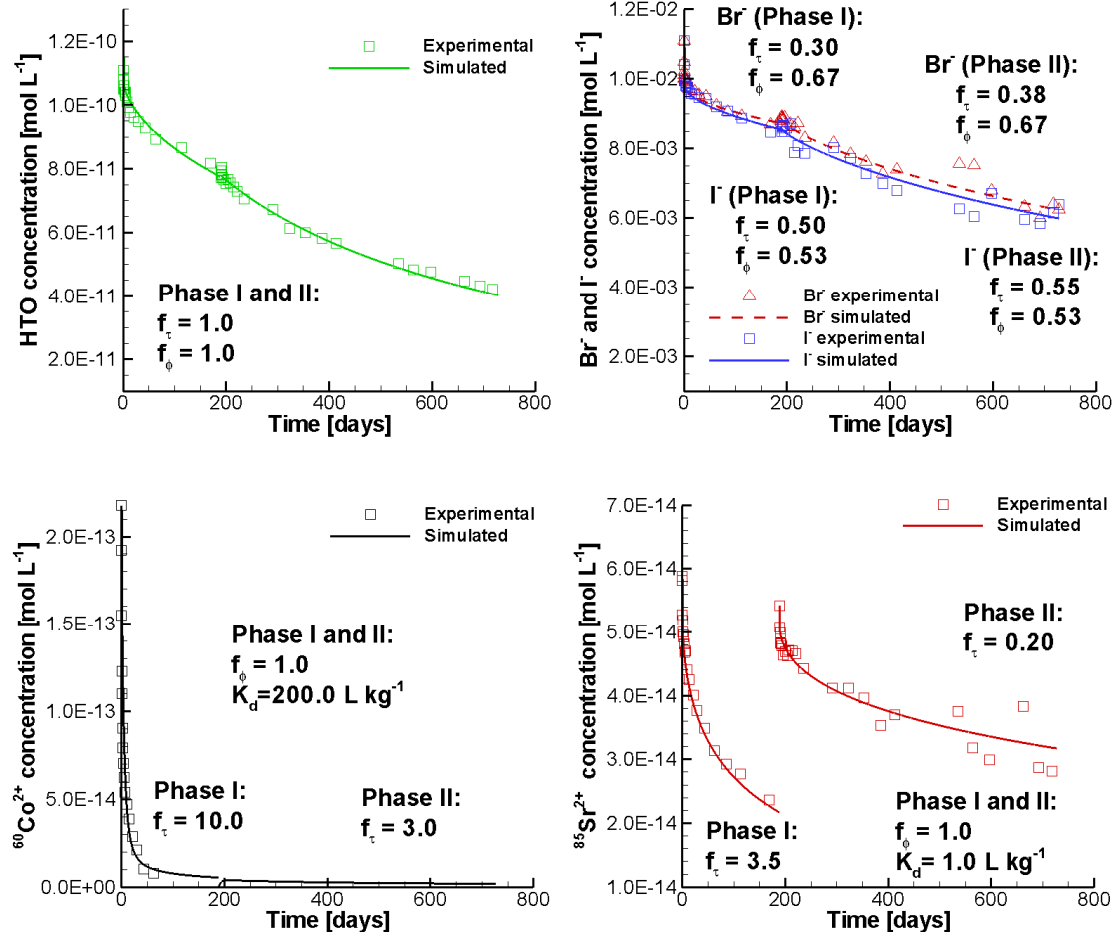


Figure 4.5: Comparison of Simulated (Lines) and Experimental (Symbols) Concentration Time Curves for HTO, Br^- , I^- , $^{60}\text{Co}^{2+}$ and $^{85}\text{Sr}^{2+}$ in the Borehole Solution during the DR-A Field Diffusion Experiment Phase II (Xie et al. 2014)

4.1.3.6 File location

Input file:

.\Benchmark\ benchmarks_new_add\MtTerri-V1.0.409\mtterri02.dat

Databases:

.\Benchmark\ benchmarks_new_add\MtTerri-V1.0.409\database\

4.1.4 EFFECT OF CHEMICAL PERTURBATION ON DIFFUSION AND RETARDATION IN CLAY (MIE)

4.1.4.1 Problem definition

This example is to validate the effect of chemical perturbation on Cs⁺ diffusion and retardation in low permeable porous media through the comparison of simulated using the multisite ion exchange model and the in-situ diffusion experiment data (Phase II).

4.1.4.2 Model setup

The model set up, including the geometry, initial and boundary conditions for flow and reactive transport, is exactly the same as the example in section 4.1.3.2. The difference is the use of the multisite ion exchange model (Xie et al. 2014).

To simulate the exchange of the solution in the borehole, a restart file restart.dat is generated using the restart.tmp2 file at 189 days for the Phase I simulation (section 4.1.2) and replaced the chemical compositions of the ions in the control volumes within the borehole (for major ions with the data in Table 4.8, for tracers with the data at 168.8 in Table 4.4).

4.1.4.3 Experimental data

The concentrations of the major ions and all tracers in the tank were analyzed at designated intervals. The measured results until 728.9 days, after making any necessary corrections for decay, are listed in Table 4.9 and Table 4.13, respectively.

Table 4.13: Measured Cs⁺ Concentrations [mol L⁻¹] in the Circulation Solution during the DR-A In-situ Diffusion Experiment - Phase II until Overcoring (Calculated Based on NAGRA 2012)

Time		Time		Time		Time	
[days]	Cs ⁺						
189.2	6.37×10 ⁻⁰⁶	192.9	2.42×10 ⁻⁰⁵	234.8	3.03×10 ⁻⁰⁵	563.9	1.05×10 ⁻⁰⁵
189.3	6.23×10 ⁻⁰⁶	195.9	2.81×10 ⁻⁰⁵	291.1	2.70×10 ⁻⁰⁵	597.1	1.06×10 ⁻⁰⁵
189.9	7.75×10 ⁻⁰⁶	200.0	3.18×10 ⁻⁰⁵	322.9	2.30×10 ⁻⁰⁵	692.1	7.60×10 ⁻⁰⁶
190.1	1.05×10 ⁻⁰⁵	204.2	3.44×10 ⁻⁰⁵	353.2	2.06×10 ⁻⁰⁵	717.9	7.15×10 ⁻⁰⁶
190.2	1.48×10 ⁻⁰⁵	206.9	3.53×10 ⁻⁰⁵	385.8	1.85×10 ⁻⁰⁵	728.9	7.28×10 ⁻⁰⁶
190.9	1.78×10 ⁻⁰⁵	213.9	3.37×10 ⁻⁰⁵	412.9	1.57×10 ⁻⁰⁵		
191.2	1.86×10 ⁻⁰⁵	220.8	3.35×10 ⁻⁰⁵	535.1	1.10×10 ⁻⁰⁵		

Note: The tracer Cs⁺ was analyzed by Bachema AG (Fierz and Rosli 2012).

4.1.4.4 Parameters

The key parameters for the simulation are the same as described in section 4.1.1.4. Additional parameters for the multisite ion exchange model are listed in Table 4.7 (section

4.1.2.3).

4.1.4.5 Results

Experimental results showed that the concentration of Cs^+ increases significantly shortly after the solution replacement in the borehole even though the concentration of Cs^+ was kept the same in both solutions (the solution in the borehole before replacement and the synthetic one with elevated ionic strength) (Figure 4.6). This is because of the sorbed Cs on OPA clay during Phase I is now replaced by other cations through ion exchange due to the increased concentrations of Na^+ , Ca^+ , K^+ in the borehole solution. The Cs^+ in the clay porewater diffuses back into the borehole. Consequently, the total sorbed Cs on the clay decreases with the time and the ion exchange process slows down. After about 24 days, the Cs^+ concentration in the borehole began to decrease again for the rest of the Phase II experiment. Comparison of the simulated results to the experimental data are depicted in Figure 4.6 and Figure 4.7.

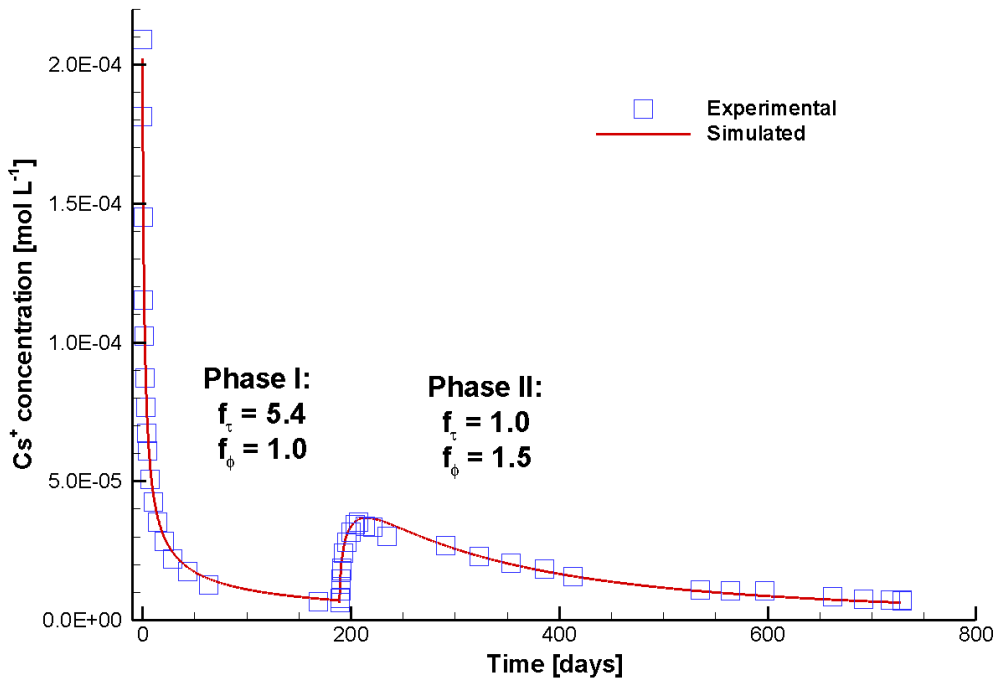


Figure 4.6: Comparison of Simulated (Lines) and Experimental (Symbols) Cs^+ Concentration Time Curves for Phase I and Phase II of the DR-A In-situ Diffusion Experiment after Diffusion Parameter Calibration (Xie et al. 2014)

The predicted Cs^+ time curve shows very good agreement with the experimental observations (Figure 4.6). The simulated concentration time curves for the major ions also show good agreement to the experimental data (Figure 4.7) with the exception of Ca^{2+} , which is slightly over predicted compared to the experimental observations. The

predicted concentration time curves of Cs^+ , Na^+ , K^+ , Cl^- and SO_4^{2-} in the borehole from 420 to 735 days are in very good agreement to the experimental data.

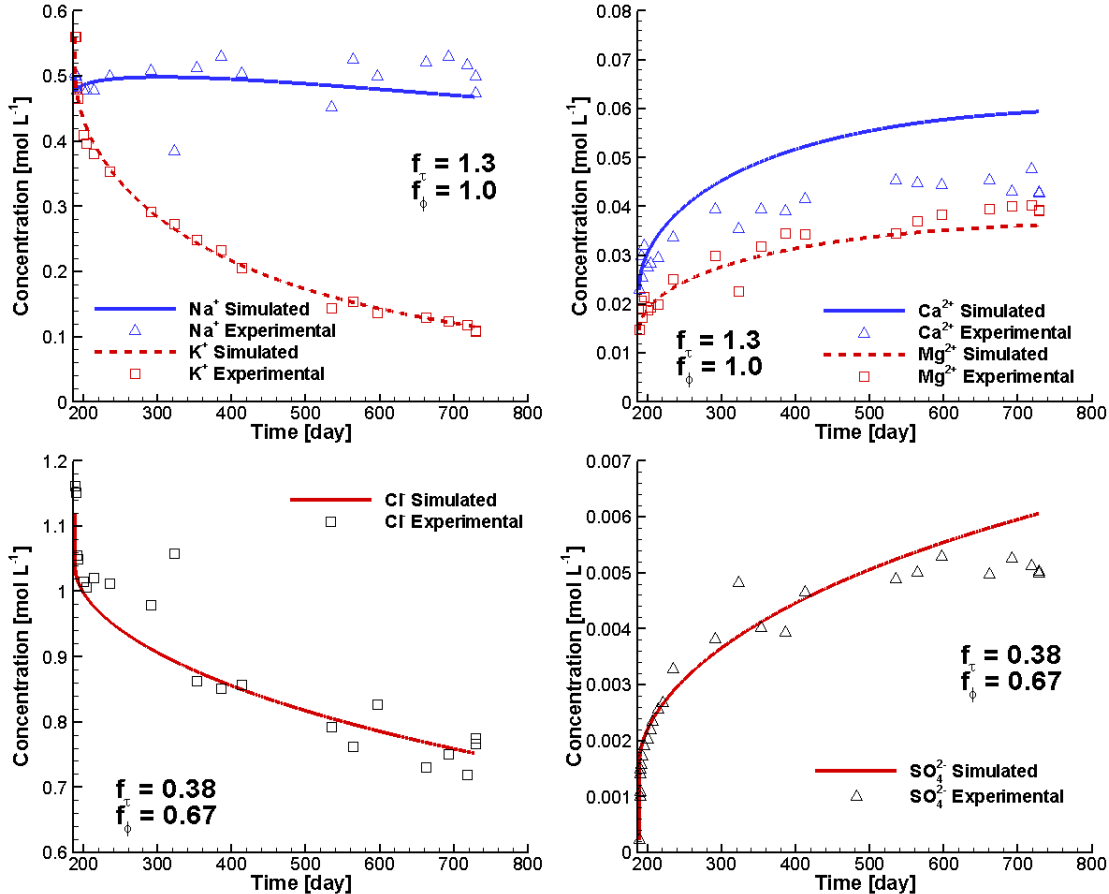


Figure 4.7: Comparison of Simulated (Lines) and Experimental (Symbols) Concentration Time Curves of Major Ions during the DR-A In-situ Diffusion Experiment Phase II after Diffusion Parameter Calibration (Xie et al. 2014)

The predicted profiles for the aqueous species HTO , Br^- , Cl^- and I^- also exhibit good agreement with the experimental data except for the region close to the borehole wall (Figure 4.8). The discrepancies near the borehole wall are the result of back diffusion from the clay towards the borehole during overcoring, which is further discussed in the following two sections.

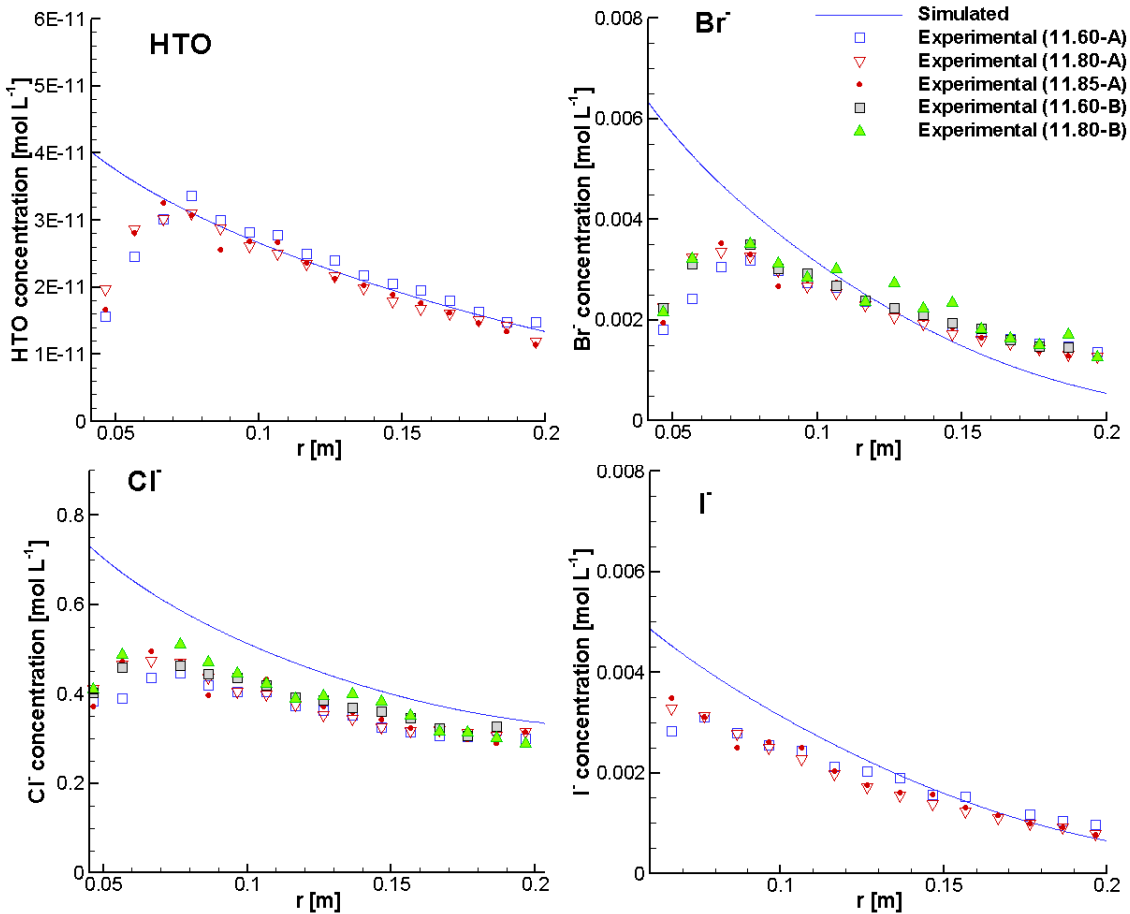


Figure 4.8: Simulated Total Concentration Profiles for HTO, Br⁻, Cl⁻ and I⁻ and Comparison to the Experimental Results in the Porewater of the Overcored Samples at 728 Days (Xie et al. 2014)

The predicted total concentration profiles (i.e. including both aqueous and sorbed species) of the major elements Na, Ca, Mg and K in the Opalinus Clay agree well with the general trends observed in the experimental data (Figure 4.9). The total concentrations of K far from the clay-borehole interface are in very good agreement to the experimental data, but the predicted background total concentrations of Ca are higher than the observed data, and concentrations for Mg are lower than the measured data. This might be occurring because the ion exchange sites for both Ca and Mg are limited to PS sites only (see Table 4.7 and Figure 4.10). This could lead to underestimation of the total sorbed amount of both species.

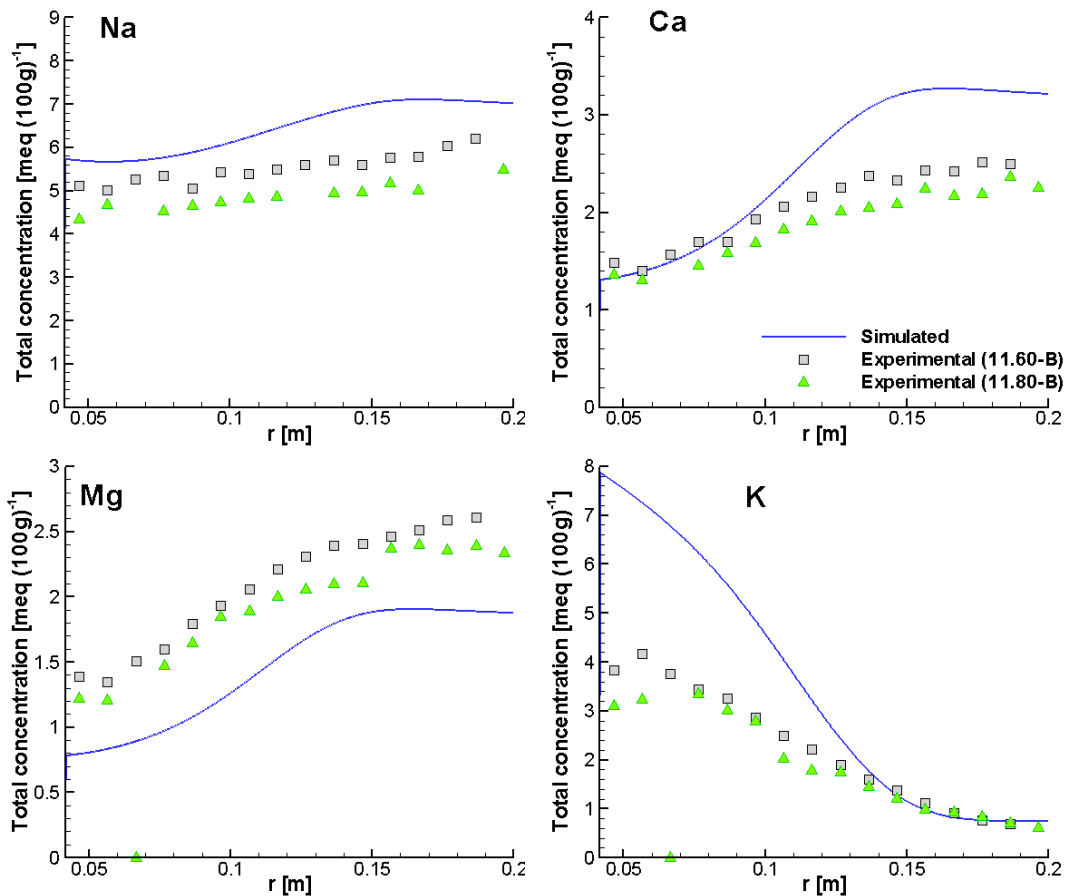


Figure 4.9: Simulated Total Concentration Profiles for Na^+ , Ca^{2+} , Mg^{2+} and K^+ and Comparison to the Experimental Results in the Porewater of the Overcored Samples at 728 Days

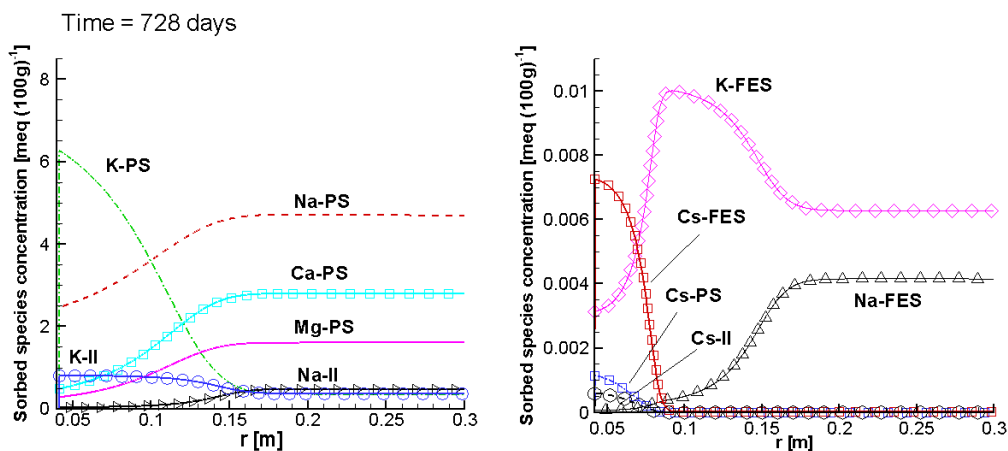


Figure 4.10: Simulated Profiles of Sorbed Species on Three Ion Exchange Sites (-PS, -FES and -II) at 728 Days (Xie et al. 2014)

4.1.4.6 File location

Input file:

.\Benchmark\ benchmarks_new_add\MtTerri-V1.0.409\mtterri02Cs.dat

Databases:

.\Benchmark\ benchmarks_new_add\MtTerri-V1.0.409\database\

4.1.5 BACK DIFFUSION DURING OVERCORING

4.1.5.1 Problem definition

This example simulates the observed back diffusion process during overcoring using a linear sorption model for $^{60}\text{Co}^{2+}$ and $^{85}\text{Sr}^{2+}$ retardation.

4.1.5.2 Model setup

The 1D axial symmetric model, as shown in Figure 4.1 and Table 4.2 is used without filter and gap (detailed information see section 4.1.1.2).

For this simulation, the circulation chamber and the filter are no longer present. The porewater gathered in the borehole was assumed to be Opalinus Clay formation water with the chemical composition as listed in Table 4.3, characterized by much lower concentrations in comparison to the borehole solution during the chemical perturbation for most major ions except SO_4^{2-} , and no tracers. To simulate the solution gathered after pulling out the assembly in the borehole, a restart file restart.dat is generated using the restart.tmp2 file at 728 days for the Phase II simulation (section 4.1.3) and replaced the chemical compositions of the ions in the control volumes within the borehole (for major ions with the data in Table 4.3, and no tracers).

4.1.5.3 Parameters

Key modeling parameters used in the simulations are listed in Table 4.14. The simulation time was from 728 to 735 days.

Table 4.14: General parameters for the circulation chamber, filter, gap and OPA

Parameter	Borehole	OPA
Porosity [-]	1.0	0.19
Tortuosity [-]	1.0	0.15
Solid dry bulk density [kg/m ³]	-	2310.0 ^a

^a Bossart (2013)

All other parameters such as the D_0 , porosity and tortuosity correction factors for individual species are the same as described in section 4.1.3.4.

4.1.5.4 Results

Experimental data consistently showed back diffusion in the OPA clay adjacent to the borehole. Simulated total concentration profiles for HTO, Br⁻, I⁻, Cl⁻ and Co²⁺ in the Opalinus Clay are depicted in Figure 4.11.

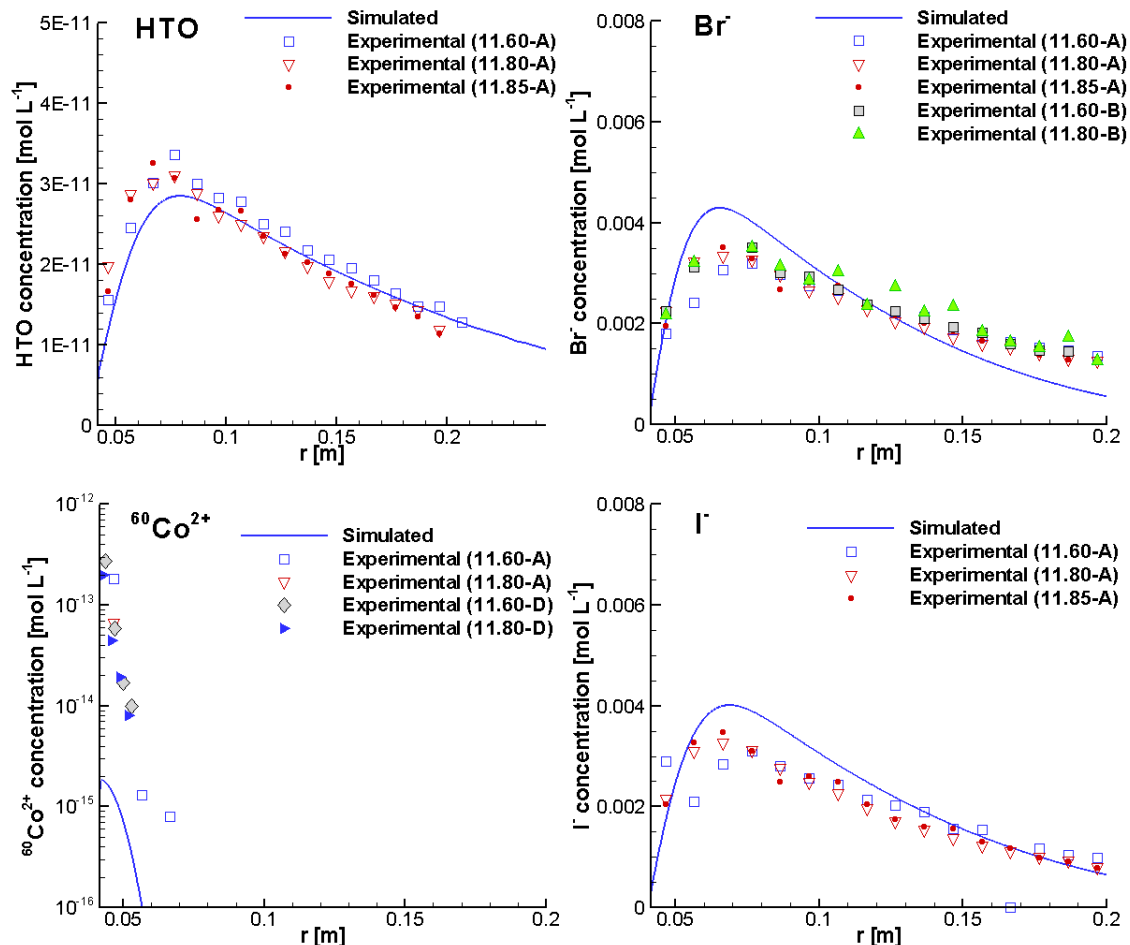


Figure 4.11: Comparison of the Simulated Total Concentration Profiles for HTO, ⁶⁰Co²⁺, Br⁻ and I⁻ in the Opalinus Clay at 735 days and in the Porewater of the Overcored Opalinus Clay Samples (Xie et al. 2014)

The simulation results show good agreement to the experimental data for all dissolved species (note that no experimental data for Sr²⁺ in the porewater were available and thus not plotted). The simulated concentrations of dissolved Co²⁺ are slightly lower than observed, which can be considered very good agreement considering analysis uncertainties in the range of 5% to 80% (NAGRA 2014).

4.1.5.5 File location

Input file:

.\Benchmark\ benchmarks_new_add\MtTerri-V1.0.409\mttoc.dat

Databases:

.\Benchmark\ benchmarks_new_add\MtTerri-V1.0.409\database\

4.1.6 BACK DIFFUSION DURING OVERCORING (MIE)

4.1.6.1 Problem definition

This example simulates the observed back diffusion process during overcoring using the multisite ion exchange model for Cs⁺ retardation.

4.1.6.2 Model setup

The 1D axial symmetric model, as shown in Figure 4.1 and Table 4.2 is used without filter and gap (detailed information see section 4.1.1.2 and section 4.1.5.2).

To simulate the solution gathered after pulling out the assembly in the borehole, a restart file restart.dat is generated using the restart.tmp2 file at 728 days for the Phase II simulation (section 4.1.4) and replaced the chemical compositions of the ions in the control volumes within the borehole (for major ions with the data in Table 4.3, and no tracers).

4.1.6.3 Parameters

Key modeling parameters used in the simulations are listed in Table 4.14. The simulation time was from 728 to 735 days.

All other parameters such as the D₀, porosity and tortuosity correction factors for individual species are the same as described in section 4.1.4.4.

4.1.6.4 Results

Experimental data consistently showed back diffusion in the OPA clay adjacent to the borehole. Simulated total concentration profiles for HTO, Br⁻, I⁻, Cl⁻ and Co²⁺ in the Opalinus Clay are depicted in Figure 4.11.

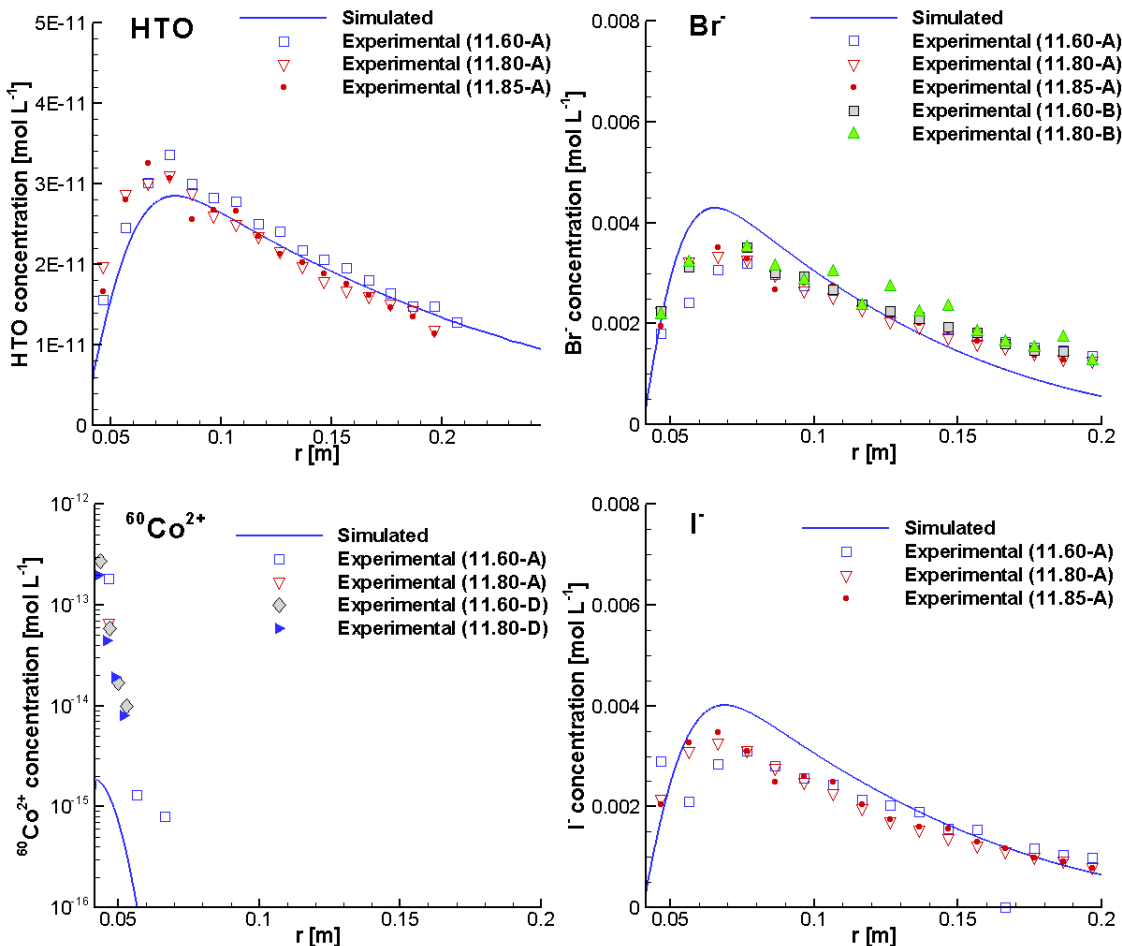


Figure 4.12: Comparison of the Simulated Total Concentration Profiles for HTO, $^{60}\text{Co}^{2+}$, Br⁻ and I⁻ in the Opalinus Clay at 735 days and in the Porewater of the Overcored Opalinus Clay Samples (Xie et al. 2014)

The simulation results show good agreement to the experimental data for all dissolved species (note that no experimental data for Sr²⁺ in the porewater were available and thus not plotted). The simulated concentrations of dissolved Co²⁺ are slightly lower than observed, which can be considered very good agreement considering analysis uncertainties in the range of 5% to 80% (NAGRA 2014).

4.1.6.5 File location

Input file:

.\Benchmark\ benchmarks_new_add\MtTerri-V1.0.409\mttoc.dat

Databases: .\Benchmark\ benchmarks_new_add\MtTerri-V1.0.409\database\

4.2 EBS-TF EXPERIMENTS

MIN3P-THCm has been applied to simulate the benchmarks defined in the framework of the EBS-TF (Engineered Barrier Systems – Task Forces). There are four benchmarks defined within the framework of the EBS TF-C project. All benchmarks are based on laboratory diffusion experiments on compacted bentonite or purified montmorillonite undertaken by Clay Technology AB (Sweden) or the University of Bern (Switzerland) (Birgersson 2011). Readers are referred to the technical report Xie et al. (2014a) for detailed description of the experiments and numerical simulations. In the following subsections, four selected benchmarks were included (Table 4.15).

Table 4.15: List of validation cases in EBS-TF experiments

Example Name	Description of Main Features	Section
B2.1	CaSO ₄ solution diffusion through compacted Ca-montmorillonite	4.2.1
B2.2a	Gypsum dissolution and diffusion through Ca-montmorillonite	4.2.2
B2.2b	Gypsum dissolution, diffusion and ion exchange through Na-montmorillonite	4.2.3
B4b	Multicomponent transport through a compacted and saturated MX-80 bentonite	4.2.4

The first three experiments corresponding to the Benchmark II in the EBS TF-C project (Xie et al. 2014a). Two types of diffusion experiments are included: through-diffusion (i.e. B2.1 in Table 4.15); mineral dissolution in the central of the samples and diffusion towards the top and bottom reservoirs (i.e. B2.2a, B2.2b in Table 4.15). Sample dimensions and soil properties are listed in Table 4.16.

Table 4.16: Sample dimensions and soil properties for Benchmark II (Birgersson, 2011)

Parameters	Unit	B2.1	B2.2a	B2.2b
Montmorillonite height *)	[mm]	5	5	5
Diameter	[mm]	35	35	35
Water-to-solid mass ratio w	[-]	0.35	0.38	0.32
Dry density (calc. from w)	[g cm ⁻³]	1.40	1.34	1.46
Total porosity (from w)	[-]	0.49	0.51	0.47

*) These are nominal heights; in the case of B2.2a and B2.2b the sample height on either side of the gypsum was approximately equal

The B4b is based on a flow-through experiment on a bentonite core carried out in a Rock-Water-Interaction group at the University of Bern, Switzerland.

4.2.1 DIFFUSION THROUGH COMPACTED CA-MONTMORILLONITE

4.2.1.1 Problem definition

This example is to validate ion diffusion in compacted purified Ca-montmorillonite through the comparison of the simulated results to the diffusion experiment data. Figure 4.13 depicted the experimental set-up according to Birgesson (2011). Highly compacted purified Ca-montmorillonite is placed in an isovolumetric cylindrical cell connecting with two reservoirs. The source reservoir (bottom) contains 250 ml 0.016 mol L⁻¹ CaSO₄ solution that is in equilibrium with pure gypsum. The target reservoir includes pure H₂O. The accumulated amount of CaSO₄ (mol) was regularly recorded during the 31.8 days' experiment (Birgersson 2011).

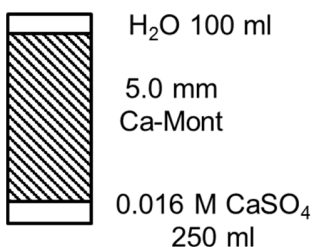


Figure 4.13: Schematic Diagram of the Simulation Domain Representing the Experimental Set-up Including the Source Reservoir (Bottom), Compacted Ca-montmorillonite (5 mm in Thickness) and Target Reservoir (Top)

4.2.1.2 Model setup

The experiment is represented by a 1D model including the montmorillonite (5 mm) and both reservoirs with a model cell thickness of 1 mm each as shown in Figure 4.13. To account for the actual volume of the reservoirs, porosities of 259.8 and 103.9 were applied to the source and target reservoir cells, respectively. The tortuosity values of the reservoir cells were set to 1.0 to ensure complete mixing occurred within these cells. The steel filters on either side of the samples were not included in the model discretization due to the lack of detailed information such as the thickness, porosity and diffusion parameters of the filters. The advantage of this treatment is that the mixing effect through the circulation of the solutions in both reservoirs can be better represented. The 1D model was discretized into 58 control volumes. No flux boundary conditions were applied at both boundaries. Multicomponent diffusion model is applied in the modelling.

4.2.1.3 Parameters

Key modeling parameters used in the simulations are listed in Table 4.16. The diffusion coefficients of Ca²⁺ and SO₄²⁻ are listed in Table 4.6. The final simulation time was 31.8 days. The effective porosity and tortuosity of the compacted Ca-montmorillonite have to be determined by fitting the model to the results from diffusion experiments using MIN3P-THCm and PEST (Parameter ESTimation; Doherty 2010). PEST is an

internationally recognized, state-of-the-art software package for model-independent non-linear parameter estimation and predictive uncertainty analysis (Doherty 2010).

4.2.1.4 Results

The numerical analysis results of the through-diffusion using MIN3P-THCm and PEST for adjusting the effective porosity and tortuosity are shown in Figure 4.14 and Table 4.17. The simulated results of the accumulated mass of CaSO_4 agree to the experimental data (Figure 4.14) when the effective porosity is 0.079 and tortuosity is 0.037 (Table 4.17). The derived effective diffusion coefficients (D_e) of Ca^{2+} and SO_4^{2-} are $2.32 \times 10^{-12} \text{ m}^2 \text{ s}^{-1}$ and $3.12 \times 10^{-12} \text{ m}^2 \text{ s}^{-1}$, respectively.

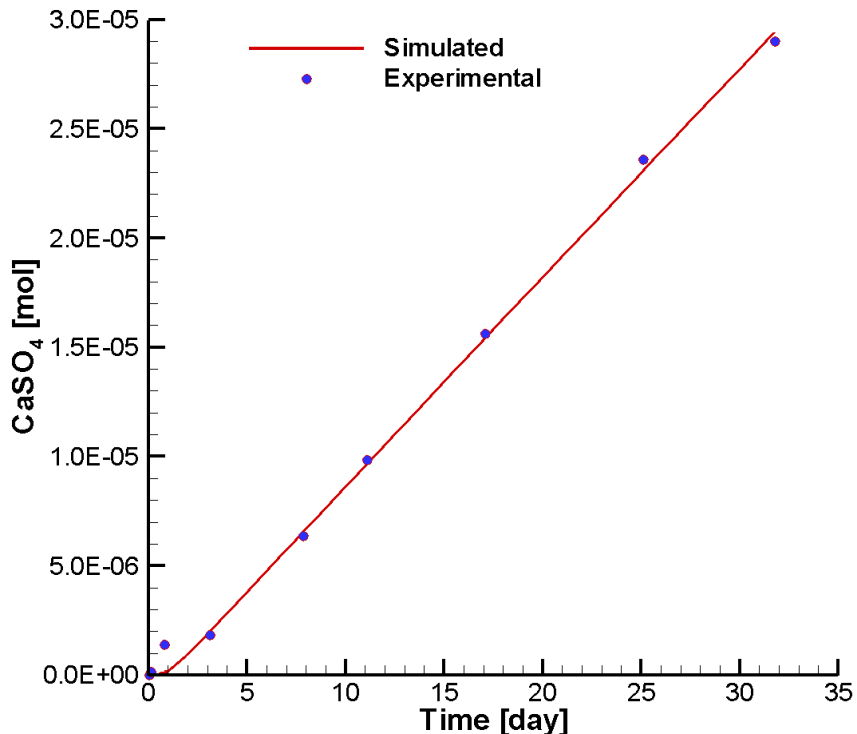


Figure 4.14: Comparison of simulated results and experimental data for accumulated CaSO_4 mass in the target reservoir for case B2.1

4.2.1.5 File location

Input file:

.\Benchmark\ benchmarks_new_add\EBS-V1.0.446\B2\B2.1\B2.1a.dat

Databases: .\Benchmark\ benchmarks_new_add\EBS-V1.0.446\database\

Table 4.17: Experimental data and simulated results for the accumulated mass of CaSO₄ for case B2.1

Time [day]	Accumulated CaSO ₄ mass [mol]		
	Measured	Simulated	Residual
0.13	1.49×10 ⁻⁷	1.07×10 ⁻¹¹	1.49×10 ⁻⁷
0.82	1.39×10 ⁻⁶	1.16×10 ⁻⁷	1.27×10 ⁻⁶
3.12	1.81×10 ⁻⁶	2.00×10 ⁻⁶	-1.88×10 ⁻⁷
7.89	6.36×10 ⁻⁶	6.58×10 ⁻⁶	-2.19×10 ⁻⁷
11.10	9.84×10 ⁻⁶	9.68×10 ⁻⁶	1.66×10 ⁻⁷
17.08	1.56×10 ⁻⁵	1.54×10 ⁻⁵	1.94×10 ⁻⁷
25.10	2.36×10 ⁻⁵	2.31×10 ⁻⁵	5.18×10 ⁻⁷
31.81	2.90×10 ⁻⁵	2.95×10 ⁻⁵	-5.03×10 ⁻⁷
Correlation coefficient	0.999		
Estimated parameters	Value	95% confidence limits	
Effective porosity	0.079	0.04 – 0.15	
Tortuosity	0.037	0.02– 0.07	
Calculated parameter			
D _e for Ca ²⁺ in [m ² s ⁻¹]	2.32×10 ⁻¹²		
D _e for SO ₄ ²⁻ in [m ² s ⁻¹]	3.12×10 ⁻¹²		

4.2.2 GYPSUM DISSOLUTION AND DIFFUSION THROUGH CA-MONTMORILLONITE

4.2.2.1 Problem definition

This example is to validate mineral dissolution and ion diffusion in compacted purified Ca-montmorillonite through the comparison of the simulated results to the experiment data. Figure 4.15 depicted the experimental set-up according to Birgesson (2011). Highly compacted purified Ca-montmorillonite is first saturated with pure water, then cut in half and sandwiched with a thin layer of gypsum powder. The sandwich is then recompacted and placed in an isovolumetric cylindrical cell connecting with two reservoirs (i.e. 100 ml pure water each). Gypsum dissolves and results in the increase of Ca²⁺ and SO₄²⁻ concentration in the middle gypsum layer. Consequently, Ca²⁺ and SO₄²⁻ diffuse towards both reservoirs. The accumulated amounts of CaSO₄ (mol) in both reservoirs were regularly recorded during the 77.9 days' experiment (Birgersson 2011; Xie et al. 2014a).

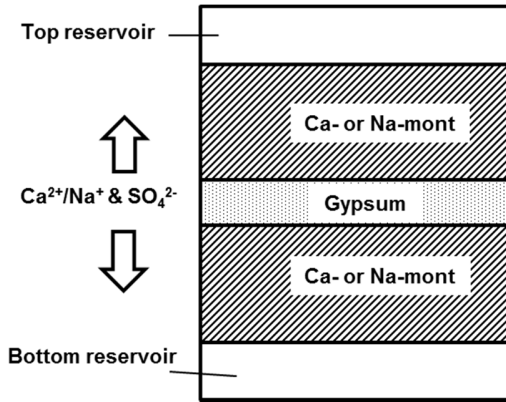


Figure 4.15: Concept of Benchmark II: Gypsum Dissolution and CaSO_4 Diffusion Including the Reservoirs (Top and Bottom), Compacted Ca-montmorillonite (B2.2a) or Na-montmorillonite (B2.2b) and Thin Gypsum Powder Layer (Middle)

4.2.2.2 Model setup

The model setup for B2.2a is the same as B2.1 except for adding a 0.5 mm layer of gypsum powder as shown in Figure 4.15. To account for the actual volume of the reservoirs, porosities of 103.9 were applied to both reservoir cells. The 1D model was discretized into 79 control volumes.

4.2.2.3 Parameters

Key modeling parameters used in the simulations are listed in Table 4.16. The diffusion coefficients of Ca^{2+} and SO_4^{2-} are listed in Table 4.6. The final simulation time was 77.9 days. The effective porosity and tortuosity of the compacted Ca-montmorillonite have to be determined by fitting the model to the averaged concentrations of CaSO_4 in both reservoirs using MIN3P-THCm and PEST (Parameter ESTimation; Doherty 2010).

4.2.2.4 Results

The numerical analysis results are shown in Figure 4.16. The simulated results of the accumulated mass of CaSO_4 agree to the experimental data (Figure 4.16).

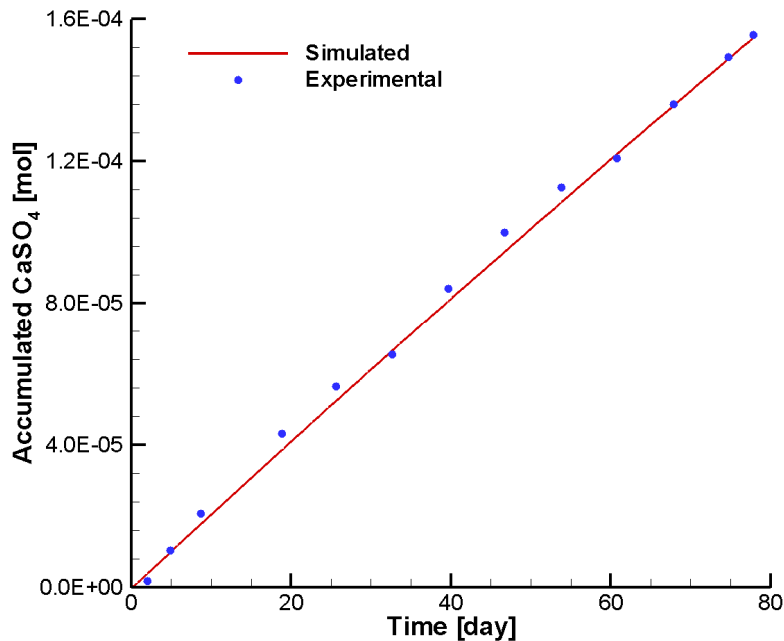


Figure 4.16: Comparison of simulated results and experimental data for accumulated CaSO₄ mass in the target reservoir for case B2.2a

Table 4.18: Experimental data and simulated results for the accumulated mass of CaSO₄ for case B2.2a

Time [day]	Accumulated CaSO ₄ mass [mol]		
	Measured	Simulated	Residual
2.00	1.76×10 ⁻⁶	3.84×10 ⁻⁶	-2.08×10 ⁻⁶
4.87	1.03×10 ⁻⁵	9.79×10 ⁻⁶	4.76×10 ⁻⁷
8.72	2.07×10 ⁻⁵	1.77×10 ⁻⁵	2.94×10 ⁻⁶
18.85	4.32×10 ⁻⁵	3.85×10 ⁻⁵	4.67×10 ⁻⁶
25.64	5.63×10 ⁻⁵	5.23×10 ⁻⁵	4.04×10 ⁻⁶
32.66	6.54×10 ⁻⁵	6.64×10 ⁻⁵	-1.06×10 ⁻⁶
39.69	8.40×10 ⁻⁵	8.05×10 ⁻⁵	3.46×10 ⁻⁶
46.70	9.99×10 ⁻⁵	9.44×10 ⁻⁵	5.51×10 ⁻⁶
53.85	1.13×10 ⁻⁴	1.08×10 ⁻⁴	4.14×10 ⁻⁶
60.76	1.21×10 ⁻⁴	1.22×10 ⁻⁴	-1.15×10 ⁻⁶
67.86	1.36×10 ⁻⁴	1.36×10 ⁻⁴	2.62×10 ⁻⁷
74.75	1.49×10 ⁻⁴	1.49×10 ⁻⁴	3.39×10 ⁻⁷
77.87	1.55×10 ⁻⁴	1.55×10 ⁻⁴	6.96×10 ⁻⁷
Correlation coefficient		0.999	
Estimated parameters	Value	95% confidence limits	
Effective porosity	0.046	0.0008 – 2.77	

Validation report-page# 4-256

Tortuosity	0.069	0.001– 4.14
Calculated parameter		
D _e for Ca ²⁺ in [m ² s ⁻¹]	2.49×10 ⁻¹²	
D _e for SO ₄ ²⁻ in [m ² s ⁻¹]	3.35×10 ⁻¹²	

4.2.3 GYPSUM DISSOLUTION, DIFFUSION AND ION EXCHANGE THROUGH NA-MONTMORILLONITE

4.2.3.1 Problem definition

This example is to validate mineral dissolution, ion diffusion and cation exchange in compacted purified Na-montmorillonite through the comparison of the simulated results to the experiment data. The experimental set-up is depicted in Figure 4.15. The procedure for this experiment was the same as for experiment B2.2a (see section 4.2.2.1). The only difference lies in the use of Na-montmorillonite instead of Ca-montmorillonite, which results in ion exchange during Ca²⁺ diffusion through the montmorillonite. The Na⁺ that is initially adsorbed on the montmorillonite is partially replaced by Ca²⁺ and enters into the pore water solution, which results in an increase of the local Na⁺ concentration. Consequently, both Na⁺ and Ca²⁺ diffuse towards the top and bottom reservoir. The accumulated amounts of Na₂SO₄ and CaSO₄ (mol) in both reservoirs were regularly recorded during the 40.6 days' experiment (Birgersson 2011; Xie et al. 2014a).

4.2.3.2 Model setup

The model setup for B2.2b is the same as B2.2a as shown in Figure 4.15. The only difference is the consideration of the cation exchange reaction (Appelo 2005):



According to the Equation 4-1, the absorption of one mol Ca²⁺ results in two mol Na⁺.

4.2.3.3 Parameters

Key modeling parameters used in the simulations are listed in Table 4.16 Similar to the simulation of Case B2.2a as described in section 4.2.2 and depicted in Figure 4.15, a 1D numerical analysis of reactive transport processes was undertaken, but with the additional consideration of ion exchange. The cation exchange capacity (CEC) of the Na-bentonite is 92 meq (100g soil)⁻¹ (Birgersson et al., 2009).

4.2.3.4 Results

The numerical analysis results are shown in Figure 4.16. The simulated results of the accumulated mass of CaSO_4 agree to the experimental data (Figure 4.16).

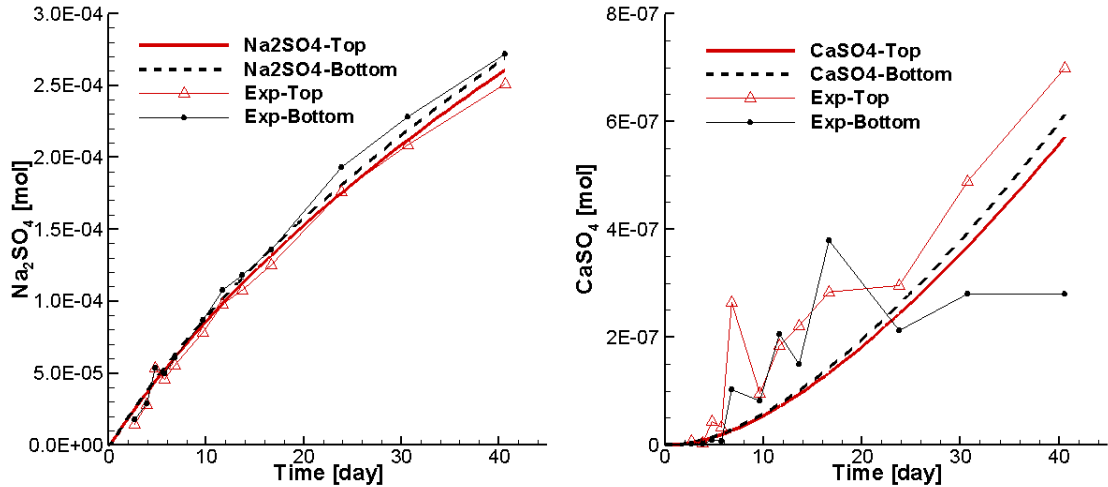


Figure 4.17: Comparison of simulated results and experimental data for accumulated Na_2SO_4 (left) and CaSO_4 (right) mass in the Top and Bottom reservoirs for case B2.2b

Table 4.19: Experimental data and simulated results for the averaged accumulated CaSO_4 and Na_2SO_4 mass in [mol] for case B2.2b

Time [day]	Accumulated CaSO_4 at top reservoir			Accumulated Na_2SO_4 at top reservoir		
	Experimental	Simulated	Residual	Experimental	Simulated	Residual
2.66	7.72×10^{-9}	4.12×10^{-9}	3.60×10^{-9}	2.92×10^{-5}	5.00×10^{-5}	-2.08×10^{-5}
3.88	3.24×10^{-9}	8.92×10^{-9}	-5.68×10^{-9}	5.60×10^{-5}	7.24×10^{-5}	-1.64×10^{-5}
4.80	4.40×10^{-8}	1.37×10^{-8}	3.04×10^{-8}	1.07×10^{-4}	8.88×10^{-5}	1.82×10^{-5}
5.75	3.39×10^{-8}	1.93×10^{-8}	1.46×10^{-8}	9.13×10^{-5}	1.05×10^{-4}	-1.36×10^{-5}
6.80	2.64×10^{-7}	2.67×10^{-8}	2.37×10^{-7}	1.11×10^{-4}	1.22×10^{-4}	-1.13×10^{-5}
9.64	9.63×10^{-8}	5.11×10^{-8}	4.52×10^{-8}	1.57×10^{-4}	1.67×10^{-4}	-9.62×10^{-6}
11.65	1.85×10^{-7}	7.21×10^{-8}	1.12×10^{-7}	1.96×10^{-4}	1.96×10^{-4}	-3.80×10^{-9}
13.66	2.21×10^{-7}	9.58×10^{-8}	1.26×10^{-7}	2.15×10^{-4}	2.24×10^{-4}	-9.17×10^{-6}
16.69	2.84×10^{-7}	1.36×10^{-7}	1.48×10^{-7}	2.50×10^{-4}	2.64×10^{-4}	-1.42×10^{-5}
23.82	2.96×10^{-7}	2.47×10^{-7}	4.90×10^{-8}	3.53×10^{-4}	3.50×10^{-4}	2.79×10^{-6}
30.70	4.89×10^{-7}	3.71×10^{-7}	1.17×10^{-7}	4.18×10^{-4}	4.25×10^{-4}	-6.64×10^{-6}
40.64	7.00×10^{-7}	5.78×10^{-7}	1.22×10^{-7}	5.03×10^{-4}	5.22×10^{-4}	-1.90×10^{-5}
Time [day]	Accumulated CaSO_4 at bottom reservoir			Accumulated Na_2SO_4 at bottom reservoir		
	Experimental	Simulated	Residual	Experimental	Simulated	Residual
2.66	1.61×10^{-9}	4.43×10^{-9}	-2.82×10^{-9}	3.57×10^{-5}	5.17×10^{-5}	-1.60×10^{-5}

Validation report-page# 4-258

3.88	1.76×10^{-9}	9.58×10^{-9}	-7.82×10^{-9}	5.83×10^{-5}	7.49×10^{-5}	-1.66×10^{-5}
4.80	8.43×10^{-9}	1.47×10^{-8}	-6.22×10^{-9}	1.07×10^{-4}	9.19×10^{-5}	1.51×10^{-5}
5.75	7.08×10^{-9}	2.07×10^{-8}	-1.36×10^{-8}	9.90×10^{-5}	1.08×10^{-4}	-9.48×10^{-6}
6.80	1.03×10^{-7}	2.86×10^{-8}	7.44×10^{-8}	1.21×10^{-4}	1.26×10^{-4}	-5.44×10^{-6}
9.64	8.13×10^{-8}	5.48×10^{-8}	2.65×10^{-8}	1.73×10^{-4}	1.72×10^{-4}	8.67×10^{-7}
11.65	2.06×10^{-7}	7.73×10^{-8}	1.29×10^{-7}	2.16×10^{-4}	2.02×10^{-4}	1.35×10^{-5}
13.66	1.49×10^{-7}	1.03×10^{-7}	4.63×10^{-8}	2.37×10^{-4}	2.31×10^{-4}	5.50×10^{-6}
16.69	3.79×10^{-7}	1.45×10^{-7}	2.34×10^{-7}	2.72×10^{-4}	2.73×10^{-4}	-8.27×10^{-7}
23.82	2.12×10^{-7}	2.64×10^{-7}	-5.20×10^{-8}	3.85×10^{-4}	3.61×10^{-4}	2.36×10^{-5}
30.70	2.80×10^{-7}	3.98×10^{-7}	-1.18×10^{-7}	4.57×10^{-4}	4.38×10^{-4}	1.89×10^{-5}
40.64	2.80×10^{-7}	6.20×10^{-7}	-3.40×10^{-7}	5.45×10^{-4}	5.38×10^{-4}	6.74×10^{-6}
Correlation coefficient						0.998
Estimated parameters				Value	95% confidence limits	
Effective porosity				8.93×10^{-2}	$1.18 \times 10^{-2} - 0.67$	
Tortuosity				5.54×10^{-2}	$5.85 \times 10^{-3} - 0.523$	
Calculated parameter						
D _e for Ca ²⁺ in [m ² s ⁻¹]				3.91×10^{-12}		
D _e for Na ⁺ in [m ² s ⁻¹]				6.59×10^{-12}		
..D _e for SO ₄ ²⁻ in [m ² s ⁻¹]				5.26×10^{-12}		

4.2.3.5 File location

Input file:

.\Benchmark\ benchmarks_new_add\EBS-V1.0.446\B2\B2.2\ B2.2b\B2.2b.dat

Databases: .\Benchmark\ benchmarks_new_add\EBS-V1.0.446\database\

4.2.4 MULTICOMPONENT TRANSPORT THROUGH A COMPACTED AND SATURATED MX-80 BENTONITE

4.2.4.1 Problem definition

This example is to simulate a flow-through experiment on a bentonite core carried out in the Rock-Water-Interaction Group at the University of Bern, Switzerland. This multicomponent transport experiment was performed on a compacted and saturated MX-80 bentonite sample using the core infiltration technique developed by Mäder (2002, 2004, 2005); Mäder et al. 2004).

The flow-through experiment involved the injection of synthetic pore water similar in composition to the natural pore water of the field experiment. A tracer (deuterium) was added to monitor the breakthrough of the injected fluid and to assess the degree of mixing between the initial (natural) pore water and the injected fluid. The experimental period was 10 months. The reader is referred to the report for detailed information (Xie et al. 2014a).

4.2.4.2 Model setup

The model setup for this example is depicted in Figure 4.18. The compacted bentonite

Validation report-page# 4-259

column has a length of 0.05 m and was discretized into 25 cells. The total duration of the experiment was 300 days. A constant influx of $2.3 \times 10^{-9} \text{ m}^3 \text{ m}^{-2} \text{ s}^{-1}$ was assigned to the left-hand boundary. The flow rate is fairly low such that diffusion remains the dominant transport mechanism.

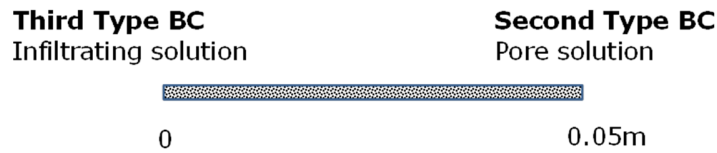


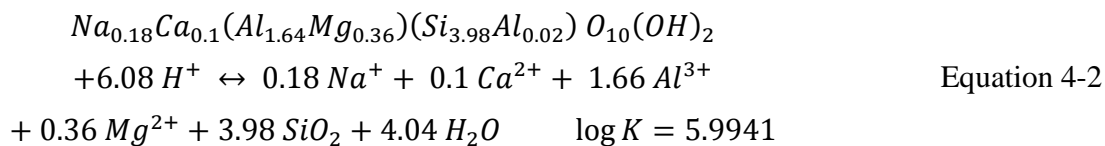
Figure 4.18: Model setup for multicomponent reactive transport experiment in bentonite

The chemical reaction system included 11 primary and 5 minerals as shown in Table 4.20 and 1 gas (Xie et al. 2014a). The secondary species are 32. This resulted in a reactive transport problem with 21 primary unknowns (11 components, 1 gas, 5 minerals and 4 adsorbed species).

Table 4.20: Components (i.e. primary species) and minerals used in the Benchmark IV simulations

Primary species	Primary species	Primary species
H ⁺	Na ⁺	SO ₄ ²⁻
Ca ²⁺	Cl ⁻	HCO ₃ ⁻
Mg ²⁺	SiO _{2,aq}	Tracer (deuterium)
K ⁺	Al ³⁺	
Minerals		logK (25 °C)
Calcite	CaCO ₃ + H ⁺ = Ca ²⁺ + HCO ₃ ⁻	1.8487
Gypsum	CaSO ₄ = Ca ²⁺ + SO ₄ ²⁻ + 2H ₂ O	-4.4823
Quartz	SiO ₂ = SiO _{2(aq)}	-3.9993
K-feldspar	KAlSi ₃ O ₈ + 4 H ⁺ = K ⁺ + Al ³⁺ + 3 SiO _{2(aq)} + 2 H ₂ O	-0.2753
MX-80	see Equation 4-2	5.9941

Bentonite is composed primarily of montmorillonite (MX-80), and its composition and dissociation reaction are as follows (Tournassat *et al.*, 2003):



Validation report-page# 4-260

The infiltrating solution composition shown in Table 4.21 served as boundary condition for the inflow side of the column.

Table 4.21: Composition of the infiltrating fluid (left-hand reactive transport boundary condition) and the initial conditions

Species Name	Boundary Concentration (mol/kg)	Initial Concentration (mol/kg)	Constraint
pH	7.2	8.5	
Ca ²⁺	5.84×10 ⁻²	3.5×10 ⁻²	
Mg ²⁺	1.52 ×10 ⁻³	2.5×10 ⁻²	
K ⁺	2.5×10 ⁻⁴	5.0×10 ⁻³	
Na ⁺	9.2×10 ⁻²	4.757×10 ⁻¹	Charge balance
Cl ⁻	2.0793×10 ⁻¹	5.0×10 ⁻¹	
SiO _{2,aq}	1.0×10 ⁻⁵	1.0×10 ⁻⁵	
Al ³⁺	1.0×10 ⁻⁵	1.0×10 ⁻⁵	
SO ₄ ⁻²	2.02×10 ⁻³	5.0303×10 ⁻²	Gypsum eq.
HCO ₃ ⁻	1.2×10 ⁻⁴	7.7024×10 ⁻⁵	Calcite eq.
Tracer	2.0×10 ⁻¹	1.4616×10 ⁻¹	

The initial pore water composition within the bentonite was constrained by the measured composition of the exchanger and by gypsum and calcite equilibrium (Table 4.21). The initial condition for the pore water within the bentonite also served as the boundary condition on the outflow side of the column.

4.2.4.3 Parameters

Material properties are assumed uniform throughout the column, and the total porosity was 0.4048 with an effective porosity for all species equal to 0.0714. The bentonite has a dry bulk density of 1.4 kg L⁻¹, the specific surface area is 788 m² g⁻¹ mineral (Alt-Epping et al, 2012, Fernandez et al., 2011).

Montmorillonite has a molar volume and weight of 134.88 cm³ mol⁻¹ and 368.44 g mol⁻¹ (Alt-Epping et al, 2012), respectively. Montmorillonite is not expected to dissolve in significant quantities and therefore it was assumed that it affects the pore water composition only via surface reactions. The total exchange capacity of montmorillonite (CEC) was fixed at 73.66 meq/100g_bulk. Selectivity coefficients for the ion exchange reactions were taken from Bradbury and Baeyens (2003) (Table 4.22). The diffusion coefficients of individual species are as listed in Table 4.6.

Table 4.22: Selectivity coefficients for ion exchange reactions (from Bradbury and

Baeyens 2003)

Exchange reaction	K_s
$\text{Na-montmor} + \text{K}^+ = \text{K-montmor} + \text{Na}^+$	4.0
$2 \text{ Na-montmor} + \text{Mg}^{2+} = \text{Mg-montmor} + 2 \text{ Na}^+$	2.2
$2 \text{ Na-montmor} + \text{Ca}^{2+} = \text{Ca-montmor} + 2 \text{ Na}^+$	2.6

4.2.4.4 Results

The numerical analysis results are shown in Figure 4.19. The agreement between MIN3P-THCm and CrunchFlow is very good. Gypsum dissolution increases SO_4^{2-} concentrations in the effluent and facilitates the uptake of Ca^{2+} onto the exchanger. Therefore, the Ca^{2+} and SO_4^{2-} concentrations agree quite well with the experimental data. Sorption reactions combined with gypsum and calcite dissolution/precipitation reactions reproduce the cations in the effluent and on the exchanger as well as the distinct shape of the sulphate breakthrough curve. However, there are still differences between the simulated and observed Na^+ and Cl^- at early time. The composition of effluent is affected by ion exchange where Ca^{2+} substitutes for Na^+ and Mg^{2+} on the exchange sites.

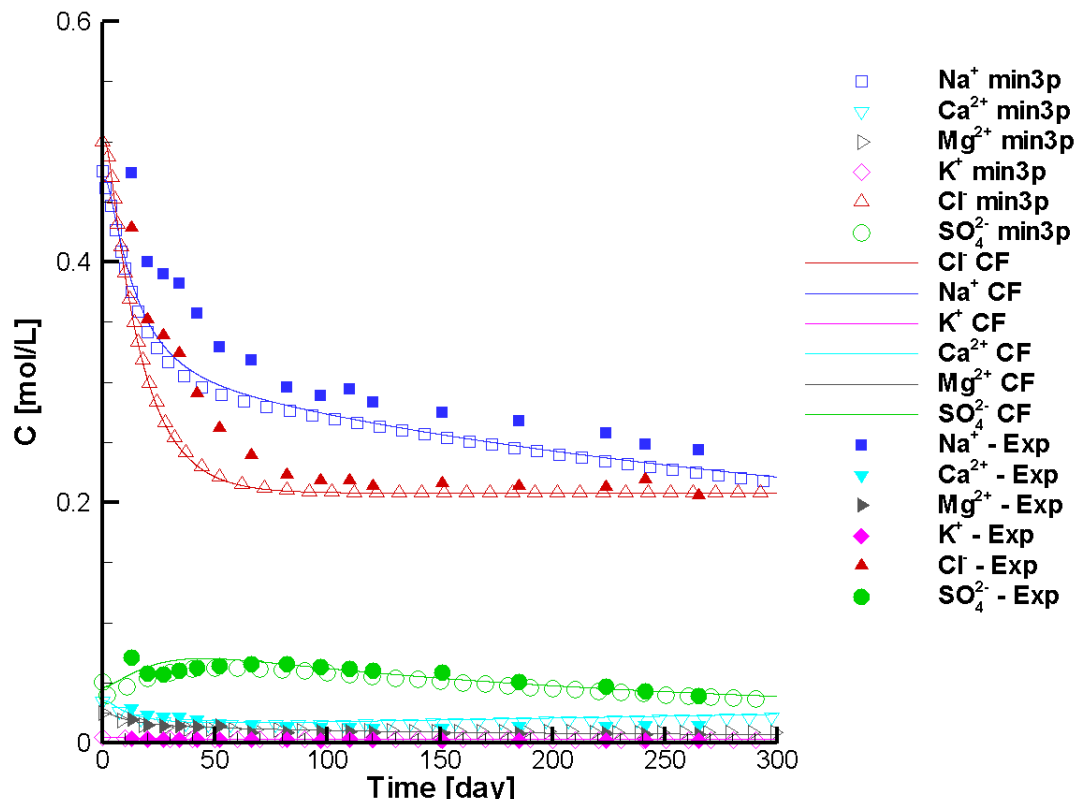


Figure 4.19: Time series of the simulated effluent composition and measured concentrations (min3p – results simulated by MIN3P-THCm; CF – results simulated by CrunchFlow)

4.2.4.5 File location

Input file:

.\Benchmark\ benchmarks_new_add\EBS-V1.0.446\B4\min3p\B4MCD\step3b.dat

Databases: .\Benchmark\ benchmarks_new_add\EBS-V1.0.446\database\

5 SSBENCH BENCHMARKING

MIN3P-THCm team has participated in the annual Subsurface Environmental Simulation Benchmarking workshop series (SSBench) benchmarking activities since 2012. SS Bench is an initiative for benchmarking subsurface environmental simulation methods with a current focus on reactive transport processes. A special issue in the journal ‘Computational Geosciences’ volume 19 issue 3, 2015 has been published including 10 benchmarking papers, nine out of them with the contribution of MIN3P-THCm team. Each paper documents detailed descriptions of problems, geochemical systems and the comparison of simulated results obtained by at least three reactive transport codes. Each paper includes several levels of well-defined benchmarks in various complexities. For some benchmarks, the input files and databases for the participating codes are available online. The related papers are attached in the Appendix II.

REFERENCES

- Appelo, C.A.J., and D. Postma. 2005. Geochemistry, groundwater and pollution, 2nd ed. Amsterdam, the Netherlands.
- Appelo, C.A.J. and Wersin, P., 2007. Multicomponent diffusion modeling in clay systems with application to the diffusion of Tritium, Iodide, and Sodium in Opalinus Clay. Environ. Sci. Technol. 41, 5002-5007. DOI: 10.1021/es0629256
- Appelo, C.A.J., Van Loon, L.R. and Wersin, P., 2010. Multicomponent diffusion of a suite of tracers (HTO, Cl, Br, I, Na, Sr, Cs) in a single sample of Opalinus Clay. Geochim. Cosmochim. Acta 74, 1201-1219
- Bossart, P. 2013. Characteristics of the Opalinus Clay at Mont Terri, <http://www.mont-terri.ch/>.
- Brandt, K., F. Vester, A.N. Jensen and K. Ingvorsen. 2001. Sulfate reduction dynamics and enumeration of sulfate-reducing bacteria in hypersaline sediments of the Great Salt Lake (Utah, USA). Microbial Ecology, 41(1):1-11.
- Calderhead, A.I. and K.U. Mayer. 2004. Comparison of the suitability of the global implicit method and the sequential non-iterative approach for multicomponent reactive transport modeling. 57th Canadian Geotechnical Conference. October 24-28, 2004. Quebec City. Canada
- Doherty, J. 2010. PEST, Model-independent parameter estimation—User manual (5th ed.): Brisbane, Australia, Watermark Numerical Computing. (<http://www.pesthomepage.org>).
- Fierz, T. and U. Rösli. 2012. DR-A Experiment: Instrumentation of BDR-A3 and tracer injection, TECHNICAL NOTE 2011-21, Solexperts AG, Switzerland.
- Foti M., D.Y. Sorokin, B. Lomans, M. Mussman, E.E. Zakharova, N.V. Pimenov, J.G. Kuenen and G. Muyzer G. 2007. Diversity, activity and abundance of sulfate-reducing bacteria in saline and hypersaline soda lakes. Applied and Environmental Microbiology 73: 2093–2100.
- Gelhar, L. W. and M. A. Collins. 1971. General Analysis of Longitudinal Dispersion in Nonuniform Flow, Water Resour. Res., 7(6), 1511–1521, doi:10.1029/WR007i006p01511.
- Geiger, S., T. Driesner, C. A. Heinrich, and S. K. Matthäi (2006b), Multiphase thermohaline convection in the Earth's crust: II. Benchmarking and application of a finite element–finite volume solution technique with a NaCl -H₂O equation of state, Transp. Porous Media, 63, 435–461, doi:10.1007/s11242-005-0109-y
- Gibson, B., R.T. Amos and D.W. Blowes. 2011. ³⁴S/³²S fractionation during sulfate reduction in groundwater treatment systems: Reactive transport modeling.

Validation report-page# 5-264

- Environmental Science & Technology* 45, 2863–2870.
- Gimmi, T., J. Soler and O. Leupin. 2012. Cs sorption parameters for the modeling the DR-A experiment (Task 1.3), (email communication).
- Kipp, K.L. 1986. HST3D: A computer code for simulation of heat and solute transport in three-dimensional ground-water flow systems, U.S. Geological Survey, Water-Resources Investigations Report 86-4095.
- Lide, D. R. 1994. CRC Handbook of chemistry and physics: a ready-reference book of chemical and physical data 74th Edition, CRC Press/The chemical Rubber Co., Boca Raton, FL. U.S.A.
- MacInnes, D.A., (1919). The activities of the ions of strong electrolytes: Journal American Chemical Society, 41, 1086-1092.
- Mäder, U.K. 2002. GTS-HPF: Hyperalkaline fluid infiltration experiment through a drill core of a shear zone from the Grimsel Test Site. NAGRA Internal Report NIB 02-43. (Wettingen) 23 pp.
- Mäder, U. 2004. Porewater Chemistry (PC) Experiment: A new method of porewater extraction from Opalinus Clay with results for a sample from borehole BPC-A1. Mont Terri Technical Note TN 2002-25.
- Mäder, U.K. 2005. Porewater chemistry, porosity and hydraulic conductivity of Callovian Oxfordian claystone at the EST-322 deep drilling site sampled by the method of advective displacement (Laboratoire de Recherche Souterrain de Meuse / Haute-Marne). Nagra Working Report NAB 05-04, Nagra, Wettingen, Switzerland.
- Mäder, U.K., Waber, H.N. and A. Gautschi 2004. New method for porewater extraction from claystone and determination of transport properties with results for Opalinus Clay (Switzerland). In: R.B. Wanty & R.R. Seal II (eds) Proceedings of the 11th International Symposium on Water-Rock Interaction, WRI-11, 2004, Saratoga Springs (N.Y.) Balkema, 445-448.
- NAGRA. 2012. Mont Terri DR-A field diffusion experiment results (unpublished, internal data exchange). NAGRA.
- NAGRA. 2014. Mont Terri DR-A field diffusion experiment results (continued until overcoring) and chemical analysis of the porewater and sorbed species of the overcored samples (unpublished, internal data exchange).
- O'Reilly, D.E. and E.M. Peterson. 1971. Self - Diffusion Coefficients and Rotational Correlation Times in Polar Liquids. II, *The Journal of Chemical Physics*, 55, 2155-2164.
- Parkhurst, David L. and C.A.J. Appelo. 1999. User's guide to PHREEQC (Version 2): a computer program for speciation, batch-reaction, one-dimensional transport, and

Validation report-page# 5-265

- inverse geochemical calculations. U.S. Geological Survey : Earth Science Information Center, Open-File Reports Section [distributor], Water-Resources Investigations Report 99-4259, xiv, 312 p. :ill.;28 cm.
- Parkhurst, D.L. and C.A.J. Appelo 2013, Description of input and examples for PHREEQC version 3--A computer program for speciation, batch- reaction, one-dimensional transport, and inverse geochemical calculations: U.S. Geological Survey Techniques and Methods, book 6, chap. A43, 497 p
- Pitzer, K.S. 1973. Thermodynamics of electrolytes. I. Theoretical basis and general equations, *J. Phys. Chem.*, 77, pp. 268–277
- Pitzer, K. S. 1991. Ion interaction approach: theory and data correlation. In Activity Coefficients in Electrolyte Solutions (ed. K. S. Pitzer). CRC Press, Boca Raton.
- Pitzer, K.S., J.-J. Kim. 1974. Thermodynamics of electrolytes. IV. Activity and osmotic coefficients for mixed electrolytes. *J. Am. Chem. Soc.*, 96, p. 5701
- Steefel C.I. (2008) CrunchFlow. Software for Modeling Multicomponent Reactive Flow and Transport. Lawrence Berkeley National Laboratory, Berkeley, CA, USA.
- USDOE (United States Department of Energy). 2007. In-drift precipitates/salts model. Argonne National Laboratory Report EBS-MD-000045 REV 03. Chicago, USA.
- van Loon, L.R., J.M. Soler and M.H. Bradbury. 2003. Diffusion of HTO, ^{36}Cl and ^{125}I in Opalinus Clay samples from Mont Terri – effect of confining pressure. *Journal of Contaminant Hydrology*, **61**, 73–83.
- van Loon, L.R., B. Baeyens and M.H. Bradbury. 2009. The sorption behaviour of caesium on Opalinus Clay: A comparison between intact and crushed material. *Applied Geochemistry*, 24, 999-1004.
- Waybrant, K. R.; Ptacek, C. J.; Blowes, D. W. 2002. Treatment of mine drainage using permeable reactive barriers: column experiments. *Environmental Science and Technology*, **36**, 1349–1356.
- Wersin, P., J.M. Soler, L.V. Loon, J. Eikenberg, B. Baeyens, D. Grolimund, T. Gimmi and S. Dewonck. 2008. Diffusion of HTO, Br-, I-, Cs+, 85-Sr $^{2+}$ and 60-Co $^{2+}$ in a clay formation: Results and modelling from an in-situ experiment in Opalinus Clay. *Applied Geochemistry*, 23, 678-691.
- Wolery, T.J. 1992. EQ3/6, A Software Package for Geochemical Modeling of Aqueous Systems: Package Overview and Installation Guide (Version 7.0). UCRL-MA-110662 PT I. Livermore, California: Lawrence Livermore National Laboratory. TIC: 205087.
- Xie, M., P. Rasouli, K.U. Mayer and K.T.B. MacQuarrie 2014. Reactive Transport Modelling of In-situ Diffusion Experiments for the Mont Terri Project, MIN3P-

Validation report-page# 5-266

THCm Code Enhancements and Numerical Simulations, NWMO Technical Report NWMO TR-2014-25, December 2014.

Xie, M., P. Rasouli, K.U. Mayer and K.T.B. MacQuarrie 2014a. Reactive Transport Modelling of Diffusion in Low Permeable Media – MIN3P-THCm Simulations of EBS TF-C Compacted Bentonite Diffusion Experiments, NWMO Technical Report, NWMO TR-2014-23, December 2014.

APPENDIX I: PITZER VIRIAL COEFFICIENTS DATA BASE FOR MODEL VERIFICATION

This section presents the Pitzer virial coefficients used in the reactive transport verification example described in **section 2.1.4**. The coefficients are based on the work from Harvie et al. (1984) and Greenberg and Möller (1989).

Table III. 1: Pitzer Virial Coefficients Used for Model Verification – Part 1

Cation	Anion	$\beta^{(0)}$	$\beta^{(1)}$	$\beta^{(2)}$	C^Φ
Na ⁺	Cl ⁻	0.07456	0.27524	-	0.00077
K ⁺	Cl ⁻	0.04778	0.21551	-	-0.00037
Mg ²⁺	Cl ⁻	0.35114	1.65325	-	0.00231
Ca ²⁺	Cl ⁻	0.30382	1.70143	-	0.00042
CaCl ⁺	Cl ⁻	0.35684	4.81235	-	-0.00339
MgOH ⁺	Cl ⁻	-0.10000	1.65800	-	-
H ⁺	Cl ⁻	0.17700	0.29292	-	0.00018
Na ⁺	SO ₄ ²⁻	0.01206	1.11538	-	0.00232
K ⁺	SO ₄ ²⁻	0.05554	0.79638	-	-0.00665
Mg ²⁺	SO ₄ ²⁻	0.22282	3.37713	35.25878	0.00609
Ca ²⁺	SO ₄ ²⁻	0.15000	3.00000	-	-
H ⁺	SO ₄ ²⁻	0.09862	0.00000	-	0.02097
Na ⁺	HSO ₄ ⁻	0.07343	0.29994	-	-0.00231
K ⁺	HSO ₄ ⁻	-0.00030	0.17350	-	-
Mg ²⁺	HSO ₄ ⁻	0.47460	1.72880	-	-
Ca ²⁺	HSO ₄ ⁻	0.21450	2.52750	-	-
H ⁺	HSO ₄ ⁻	0.20909	0.44092	-	-
Na ⁺	OH ⁻	0.08834	0.24442	-	0.00200
K ⁺	OH ⁻	0.12980	0.32000	-	0.00205
Ca ²⁺	OH ⁻	-0.17470	-0.23030	-5.72000	-
Na ⁺	HCO ₃ ⁻	0.02800	0.04401	-	-
Mg ²⁺	HCO ₃ ⁻	0.03300	0.84980	-	-
K ⁺	HCO ₃ ⁻	-0.01070	0.04780	-	-
Ca ²⁺	HCO ₃ ⁻	0.40000	2.97700	-	-
Na ⁺	CO ₃ ²⁻	0.03620	1.51207	-	0.00184
K ⁺	CO ₃ ²⁻	0.12880	1.43330	-	0.00018

Validation report-page# 5-268

Table III. 2: Pitzer Virial Coefficients Used for Model Verification – Part 2

Ion	Ion	θ	Ion	Ion	θ
K ⁺	Na ⁺	-0.0032	K ⁺	CaCl ⁺	0.0000
Mg ²⁺	Na ⁺	0.0700	K ⁺	MgHCO ₃ ⁺	0.0000
Ca ²⁺	Na ⁺	0.0500	K ⁺	CaOH ⁺	0.0000
H ⁺	Na ⁺	0.0360	Na ⁺	MgOH ⁺	0.0000
Ca ²⁺	K ⁺	0.1156	Na ⁺	CaCl ⁺	0.0000
H ⁺	K ⁺	0.0050	Na ⁺	MgHCO ₃ ⁺	0.0000
Ca ²⁺	Mg ²⁺	0.0070	Na ⁺	CaOH ⁺	0.0000
H ⁺	Mg ²⁺	0.1000	Ca ²⁺	MgOH ⁺	0.0000
H ⁺	Ca ²⁺	0.0920	Ca ²⁺	CaCl ⁺	0.0000
SO ₄ ²⁻	Cl ⁻	0.0703	Ca ²⁺	MgHCO ₃ ⁺	0.0000
HSO ₄ ⁻	Cl ⁻	-0.0060	Ca ²⁺	CaOH ⁺	0.0000
HSO ₄ ⁻	SO ₄ ²⁻	-0.1168	CO ₃ ²⁻	HSO ₄ ⁻	0.0000
OH ⁻	Cl ⁻	-0.0500	Mg ²⁺	MgOH ⁺	0.0000
HCO ₃ ⁻	Cl ⁻	0.0359	Mg ²⁺	CaCl ⁺	0.0000
CO ₃ ²⁻	Cl ⁻	-0.0920	Mg ²⁺	MgHCO ₃ ⁺	0.0000
OH ⁻	SO ₄ ²⁻	-0.0130	Mg ²⁺	CaOH ⁺	0.0000
HCO ₃ ⁻	SO ₄ ²⁻	0.0100	HSO ₄ ⁻	OH ⁻	0.0000
CO ₃ ²⁻	SO ₄ ²⁻	0.0200	HSO ₄ ⁻	HCO ₃ ⁻	0.0000
CO ₃ ²⁻	OH ⁻	0.1000	OH ⁻	HCO ₃ ⁻	0.0000
CO ₃ ²⁻	HCO ₃ ⁻	-0.0400	MgOH ⁺	CaCl ⁺	0.0000
H ⁺	MgOH ⁺	0.0000	MgOH ⁺	MgHCO ₃ ⁺	0.0000
H ⁺	CaCl ⁺	0.0000	MgOH ⁺	CaOH ⁺	0.0000
H ⁺	MgHCO ₃ ⁺	0.0000	CaCl ⁺	MgHCO ₃ ⁺	0.0000
H ⁺	CaOH ⁺	0.0000	CaCl ⁺	CaOH ⁺	0.0000
K ⁺	Mg ²⁺	0.0000	MgHCO ₃ ⁺	CaOH ⁺	0.0000
K ⁺	MgOH ⁺	0.0000			

Table III. 3: Pitzer Virial Coefficients Used for Model Verification – Part 3

Ion	Neutral species	λ
Cl ⁻	CO ₂ (aq)	-0.0050
Na ⁺	CO ₂ (aq)	0.11544
K ⁺	CO ₂ (aq)	0.11544
Ca ²⁺	CO ₂ (aq)	0.23088
Mg ²⁺	CO ₂ (aq)	0.23088
SO ₄ ²⁻	CO ₂ (aq)	0.09386
HSO ₄ ⁻	CO ₂ (aq)	0.00300

Validation report-page# 5-269

Table III. 4: Pitzer Virial Coefficients Used for Model Verification – Part 4

Ion	Ion	Ion	ψ	Ion	Ion	Ion	ψ
Na ⁺	K ⁺	Cl ⁻	-0.0037	Cl ⁻	SO ₄ ²⁻	Mg ²⁺	-0.008
Na ⁺	K ⁺	SO ₄ ²⁻	0.00732	Cl ⁻	HSO ₄ ⁻	Na ⁺	-0.006
Na ⁺	K ⁺	HCO ₃ ⁻	-0.003	Cl ⁻	HSO ₄ ⁻	H ⁺	0.013
Na ⁺	K ⁺	CO ₃ ²⁻	0.003	Cl ⁻	OH ⁻	Na ⁺	-0.006
Na ⁺	Ca ²⁺	Cl ⁻	-0.003	Cl ⁻	OH ⁻	K ⁺	-0.006
Na ⁺	Ca ²⁺	SO ₄ ²⁻	-0.012	Cl ⁻	OH ⁻	Ca ²⁺	-0.025
Na ⁺	Mg ²⁺	Cl ⁻	-0.012	Cl ⁻	HCO ₃ ⁻	Na ⁺	-0.0143
Na ⁺	Mg ²⁺	SO ₄ ²⁻	-0.015	Cl ⁻	HCO ₃ ⁻	Mg ²⁺	-0.096
Na ⁺	H ⁺	Cl ⁻	-0.004	Cl ⁻	CO ₃ ²⁻	Na ⁺	0.016
Na ⁺	H ⁺	HSO ₄ ⁻	-0.0129	Cl ⁻	CO ₃ ²⁻	K ⁺	0.004
K ⁺	Ca ²⁺	Cl ⁻	-0.0432	SO ₄ ²⁻	HSO ₄ ⁻	Na ⁺	0.01437
K ⁺	Mg ²⁺	Cl ⁻	-0.022	SO ₄ ²⁻	HSO ₄ ⁻	K ⁺	-0.0677
K ⁺	Mg ²⁺	SO ₄ ²⁻	-0.048	SO ₄ ²⁻	HSO ₄ ⁻	Mg ²⁺	-0.0425
K ⁺	H ⁺	Cl ⁻	-0.011	SO ₄ ²⁻	HSO ₄ ⁻	H ⁺	0.02781
K ⁺	H ⁺	SO ₄ ²⁻	0.197	SO ₄ ²⁻	OH ⁻	Na ⁺	-0.0091
K ⁺	H ⁺	HSO ₄ ⁻	-0.0265	SO ₄ ²⁻	OH ⁻	K ⁺	-0.05
Ca ²⁺	Mg ²⁺	Cl ⁻	-0.012	SO ₄ ²⁻	HCO ₃ ⁻	Na ⁺	-0.005
Ca ²⁺	Mg ²⁺	SO ₄ ²⁻	0.024	SO ₄ ²⁻	HCO ₃ ⁻	Mg ²⁺	-0.161
Ca ²⁺	H ⁺	Cl ⁻	-0.015	SO ₄ ²⁻	CO ₃ ²⁻	Na ⁺	-0.005
Mg ²⁺	MgOH ⁺	Cl ⁻	0.028	SO ₄ ²⁻	CO ₃ ²⁻	K ⁺	-0.009
Mg ²⁺	H ⁺	Cl ⁻	-0.011	OH ⁻	CO ₃ ²⁻	Na ⁺	-0.017
Mg ²⁺	H ⁺	HSO ₄ ⁻	-0.0178	OH ⁻	CO ₃ ²⁻	K ⁺	-0.01
Cl ⁻	SO ₄ ²⁻	Na ⁺	-0.0091	HCO ₃ ⁻	CO ₃ ²⁻	Na ⁺	0.002
Cl ⁻	SO ₄ ²⁻	K ⁺	-0.0016	HCO ₃ ⁻	CO ₃ ²⁻	K ⁺	0.012
Cl ⁻	SO ₄ ²⁻	Ca ²⁺	-0.018				

APPENDIX II: LIST OF BENCHMARKING PAPERS

- Mayer, K.U. and K. T. B. MacQuarrie. 2010. Solution of the MoMaS reactive transport benchmark with MIN3P - Model formulation and simulation results, *Computational Geosciences*, 14(3):405-419, doi:10.1007/s10596-009-9158-6
- Molins, S., J. Greskowiak, C. Wanner and K.U. Mayer. 2015. A benchmark for microbially mediated chromium reduction under denitrifying conditions in a biostimulation column experiment, *Computational Geosciences* 19(3): 479. doi:10.1007/s10596-014-9432-0
- Rasouli, P., C.I. Steefel and K.U. Mayer. 2015. Benchmarks for multicomponent diffusion and electrochemical migration, *Computational Geosciences* 19(3): 523. doi:10.1007/s10596-015-9481-z
- Alt-Epping, P., C. Tournassat, P. Rasouli, C. I. Steefel, K. U. Mayer, A. Jenni, U. Mäder, S. S. Sengor and R. Fernández. 2015. Benchmark reactive transport simulations of a column experiment in compacted bentonite with multispecies diffusion and explicit treatment of electrostatic effects, *Computational Geosciences* 19(3): 535. doi:10.1007/s10596-014-9451-x.
- Greskowiak, J., J. Gwo, D. Jacques, J. Yin and K. U. Mayer. 2015. A benchmark for multi-rate surface complexation and 1D dual-domain multi-component reactive transport of U(VI), *Computational Geosciences* 19(3): 585. doi: 10.1007/s10596-014-9457-4
- Mayer, K.U., P. Alt-Epping, D. Jacques, B. Arora and C. I. Steefel. 2015. Benchmark problems for reactive transport modeling of the generation and attenuation of acid rock drainage, *Computational Geosciences* 19(3): 599. doi:10.1007/s10596-015-9476-9.
- Marty, N.C.M., O. Bildstein, P. Blanc, F. Claret, B. Cochebin, E.C. Gaucher, D. Jacques, J.-E. Lartigue, S. Liu, K.U. Mayer, J.C.L. Meeussen, I. Munier, I. Pointeau, D. Su, C.I. Steefel. 2015. Benchmarks for multicomponent reactive transport across a cement/clay interface, *Computational Geosciences* 19(3): 635. doi:10.1007/s10596-014-9463-6
- Şengör, S.S., K.U. Mayer, J. Greskowiak, C. Wanner, D. Su and H. Prommer. 2015. Benchmarks for multicomponent reactive transport across a cement/clay interface, *Computational Geosciences* 19(3): 569. doi: 10.1007/s10596-015-9480-0
- Xie, M., K.U. Mayer, F. Claret, P. Alt-Epping, D. Jacques, C.I. Steefel, Ch. Chiaberge and J. Simunek. 2015. Benchmark of implementation and evaluation of permeability-porosity relationships linked to mineral dissolution-precipitation, *Computational Geosciences* 19(3): 655 doi:10.1007/s10596-014-9458-3.
- Perko, J., K.U. Mayer, G. Kosakowski, L. De Windt, J. Govaerts, D. Jacques, D. Su and J.C.L. Meeussen. 2015. Decalcification of cracked cement structures, *Computational Geosciences* 19(3): 673 doi:10.1007/s10596-014-9467-2.